OPTIMISATION OF PERFORMANCE IN RUNNING JUMPS

by

CASSIE WILSON

A Doctoral Thesis

Submitted in partial fulfilment of the requirements for the award of
Doctor of Philosophy of Loughborough University

April 2003

ABSTRACT

OPTIMISATION OF PERFORMANCE IN RUNNING JUMPS

Cassie Wilson, Loughborough University, April 2003

Running jumps such as the high jump and the long jump involve complex movements of the human body. The factors affecting performance include approach conditions, strength of the athlete and the muscle activation timings at each joint. In order to investigate the mechanics of jumping performances and the effect of these factors, an eight-segment, subject specific, torque-driven computer simulation model of running jumps was developed, evaluated and used to optimise performances of jumps for height and distance.

Wobbling masses within the shank, thigh and trunk segments, and the ground-foot interface were modelled as non-linear spring-damper systems. The values for the stiffness and damping constants were determined through optimisation. The inertia data were obtained from anthropometric measurements on the subject using the inertia model of Yeadon (1990b). Joint torques predicted by the simulation model were expressed as a function of angular velocity and angle using data collected from an isovelocity dynamometer. The simulation model was evaluated by comparing the actual performances with simulations using kinematic and kinetic data collected.

Movement of the wobbling masses was found to be in the region of 40 mm in the shank and thigh and 90 mm in the trunk. This movement resulted in a lower, more realistic initial peak in the ground reaction force. Co-contraction was found to occur at the joints during impact in order to increase the initial level of eccentric activation and also the rise time to maximum eccentric activation. Differences of 2% and 1% in the height and distance achieved were obtained between actual performances and simulations.

An optimisation procedure was used to maximise the height reached and distance travelled by the mass centre, in simulations of jumps for height and distance respectively, by varying the torque generator activation time histories at each joint. An increase of 12% in the height reached by the mass centre in the jump for height and 14% in the distance reached by the mass centre in the jump for distance were achieved.

PUBLICATIONS

Conference presentations

Wilson, C., Yeadon, M.R. and King, M.A. (2001). The use of simple models of high jumping. Journal of Sports Sciences 19 (1): 8.

Wilson, C., Yeadon, M.R. and King, M.A. (2001). The use of simple models in high jumping. In F. Casalo, V. Lorenzi and B. Zappa (Eds). Computer Simulation in Biomechanics (pp. 19-22). Libreria Clup. Milan.

ACKNOWLEGEMENTS

I wish to express my thanks to:

- My supervisors Professor Fred Yeadon and Dr. Mark King for their continued advice and encouragement,
- Ben Challenger for his time and effort during the data collection sessions,
- The Biomechanics group (Matt, Mike, Lesley, Grant, Veni, Chris and Jo) for their friendship, assistance and support,
- Johan Kotze and the Department of Manufacturing Engineering for their help in using Coda,
- David Bentley for his technical assistance,
- The Faculty of Social Sciences and Humanities, and the School of Sport and Exercise Sciences, Loughborough University for their financial support,

  and
- My family and friends for their constant support and encouragement, in particular Susan Backhouse and Nicholas Gant.

DEDICATION

Mum & Dad

And

Keith xxx

TABLE OF CONTENTS

LIST OF FIGURES

LIST OF TABLES

CHAPTER 1

INTRODUCTION

Many sports at elite level involve different types of dynamic jumps which generally comprise an approach phase, a contact phase, and a flight phase. In track and field athletics the long jump and the high jump are two classic examples of dynamic or running jumps. Many researchers have collected data on high jumping (Dapena, McDonald and Cappaert, 1990; Greig and Yeadon, 2000) and long jumping (Koh and Hay, 1990; Lees, Graham-Smith and Fowler, 1994) but relatively little is known about the mechanics governing optimum performance.

High jumpers try to maximise the height reached by the mass centre during the flight phase whereas long jumpers attempt to maximise the distance travelled. They are, however, limited by factors which control the outcome of and which are most important during one critical phase: the takeoff. It is not surprising therefore that Dapena (1988) believes that the most important phase of the jump is the takeoff, the preparation for which is achieved in the approach phase.

In high jumping, the performance of an athlete is determined primarily by the vertical velocity at the instant the athlete leaves the ground. The bar height which an athlete clears may be considered to be the sum of three separate heights: (a) the height of the mass centre at takeoff, (b) the height the mass centre is raised during flight, and (c) the height of the bar minus the peak height attained by the mass centre (Hay, 1975). In the long jump both the vertical and horizontal velocities at takeoff are of prime importance to the performance of a jump. In a similar way to the high jump, the total distance achieved by a long jumper consists of three components: (a) the horizontal distance between the front edge of the takeoff board and the jumper's centre of mass at the instant of takeoff, (b) the distance the mass centre travels during the aerial phase and (c) the horizontal distance between the centre of mass at the instant at which contact is made with the sand and the mark left in the sand closest to the takeoff board (Ward-Smith, 1983).

Previous research

Previous research on dynamic jumping has been descriptive, experimental and theoretical in nature. Krazhev, Strizhah, Popov and Bobrovnik (1990) analysed the technique of two of the world's top female high jumpers. The performances were filmed at an elite international competition. It was concluded that to break the women's world record, athletes need their mass centre at a height of about 140 cm from the ground at the point of lift-off from the support, the horizontal speed at the start of the takeoff to be about 7 ms^{-1} and at the end of takeoff to be 4 ms^{-1}, with the support time lasting between 140-150 ms.

Another study investigating the optimum approach speed in high jumping was completed by Bruggeman and Lock (1992). Trials in the final of an international high jump competition were recorded using two synchronised cameras. The mean approach speed used by the jumpers was close to 7 ms^{-1}. In general, within the group of finalists the height of the centre of mass at touchdown was not related to the height reached by the centre of mass during the jump.

Greig and Yeadon (2000) conducted a study during a training session of an elite male high jumper. Direct intervention was used to induce a change in technique so that a greater range in approach speed was obtained than was observed in competition. They found the optimum approach speed to be 7 ms^{-1} with the leg planted away from the vertical at 34° and with minimum knee flexion. It was concluded that the jump height was most sensitive to changes in the leg plant angle and knee angle at touchdown and not as sensitive to the approach speed.

Theoretical work on dynamic jumping has been undertaken by Alexander (1990) who developed a two-segment model with a knee torque generator in order to determine the optimum approach speed and plant angle in high jumping and long jumping. Although the model is grossly simplified, it nevertheless identifies the principles that govern optimum approach speed and plant angle for the takeoff of both the long jump and the high jump, and is insensitive to the values assigned to the series elasticity and the curvature parameter of the Hill force-velocity equation. 'The advantage of using such a simple model is that complexity tends to obscure basic principles' (Alexander, 1990). It was concluded, in high jumping, that the optimum approach speed should be close to 6.7 ms^{-1} and the

plant angle close to 45°, whereas in the long jump the athlete should run up as fast as possible and set the leg down at a steeper angle. Both of these are in reasonable agreement with actual performances.

King (1998) developed more complex models, consisting of five segments, to simulate tumbling and vaulting. The models help in understanding the contributions to the performance of dynamic jumps. They showed that approach characteristics at touchdown can have a large effect on overall jumping performance. Small changes in approach characteristics resulted in completely different performances. It was concluded that for those jumps where the athlete is trying to achieve a maximal performance (such as in high jumping and long jumping) it might be expected that there is a small range of approach characteristics at touchdown that could result in a near optimal performance.

Ramey (1981) used a planar 9-segment, hinge-connected model of the human body to simulate actions of athletes using the three most widely used styles of long jumping – the sail, hang, and hitch kick. He determined that in order to obtain an acceptable landing position in a long jump the angular momentum required is different for each technique, and concluded that provided that the amount of angular momentum at takeoff is commensurate to the style of jumping, one style is as good as another.

It is the intention of this research project to develop a computer simulation model of dynamic jumping, which will be used to optimise technique in running jumps for height and distance.

Statement of purpose

The purposes of this study are summarised below:

(i) To gain an understanding of the mechanics of dynamic jumping

(ii) To identify what elements are needed in a computer simulation model of jumping in order to provide an accurate representation

(iii) To apply such a model to the optimisation of jumping

Questions

Having realised the aims it will be possible to address questions such as:

(i) How do muscle activation timings affect performance?

Jumping performance can be optimised by varying the sequence and timing of muscle activation (Bobbert and de Bruin, 1994). The sensitivity of the model to such changes will be determined.

(ii) How do the initial conditions affect performance?

The approach velocity, leg plant angle and knee angle all have a significant effect on dynamic jumps (Alexander, 1990; Greig and Yeadon, 2000). These three parameters and their effect on performance will be investigated in jumps for both height and distance.

Methods

Both experimental and theoretical studies have their strengths and their limitations. A combination of the two approaches could be most profitable.

Various experimental studies have been carried out on high jumping; some are discussed above. These experimental studies result in the acquisition of real data. They are, however, very limited in what they can tell us about the result of any change in variables or conditions.

The major problems in experimental studies have been identified as systematic errors and extraneous variance (Yeadon and Challis, 1994). In a study such as this one systematic error may arise due to errors in the calibration procedure. Extraneous variance may arise due to a variable such as the hip angle which may not be accounted for in the study. In experimental studies the researcher attempts to control one or more variables, in order to investigate their effect on the dependent variable (e.g. the height jumped). By changing one variable, however, additional changes may also occur, reducing the internal validity of the experiment. Ensuring good internal validity (imposing control on the experimental setting) may however result in a reduced applicability of findings (low external validity). It would seem that by improving one part of the experiment another part has to suffer.

Theoretical studies have the advantage over experimental studies in that they are able to simulate different movements with different conditions or parameter values without changing other variables in the study.

'The importance and strength of simulation models is not only in providing a general insight into the movement, but particularly in making it possible to predict the movement quantitatively for any other combination of body characteristics or initial conditions, without recourse to 'in vivo' experiments' (Van Gheluwe, 1981).

The weakness of a purely theoretical study is that the model may not provide a reasonable representation of the movement being studied. This can be avoided by evaluating models in the areas where they are applied and basing simulations and comparing predictions on appropriate experimental data. Once a model has been developed and evaluated it may be used to answer questions which are difficult to tackle experimentally.

Chapter organisation

Chapter 2

This chapter comprises a review of relevant literature for the present study. This includes literature on dynamic jumping, techniques of investigation, data collection methods, simulation models and the determination of model parameter values.

Chapter 3

Chapter 3 contains investigations on simple one and two-segment models. The models investigated include a one-segment rigid body model with an elastic ground contact (spring), a two-segment rigid body model based on Alexander's (1990) model which employs a knee extensor containing contractile and series elastic components, and a two-segment rigid body model with elastic ground contact.

Chapter 4

Three eight-segment models are developed in Chapter 4. These models include two angle-driven models and one torque-driven model. The models are

developed using the symbol manipulation package Autolev^{TM}3 and are then customised to this study.

Chapter 5

This chapter presents the procedures used to collect and analyse kinematic and kinetic data from jumping trials. These data are then used in Chapter 6 and Chapter 7 to evaluate the simulation models and provide initial conditions for each of the simulations.

Chapter 6

Chapter 6 describes the methods used to calculate subject specific inertia and muscle parameters. The inertia parameters are calculated from the anthropometric measurements on the subject using the inertia model of Yeadon (1990b). Muscle parameters are determined from data collected using an isokinetic dynamometer based on the method of King and Yeadon (2002). The simulations performed using the angle-driven models are matched to the actual performances in this chapter using the kinematic and kinetic data from Chapter 5 and the inertia parameters obtained in this chapter. Optimised spring parameters are then obtained from the models.

Chapter 7

The torque-driven model is evaluated in Chapter 7 using the kinematic and kinetic data from Chapter 5, the inertia and strength parameters calculated in Chapter 6 and the spring parameters obtained from the angle-driven simulation models.

Finally, optimisations are run to obtain simulations which result in maximum height and distance reached / travelled by the mass centre using the evaluated torque-driven model. This is achieved by varying the muscle activation time histories.

Chapter 8

Chapter 8 addresses the aims and questions posed in this study using results and findings from the previous Chapters, followed by a general discussion

of the limitations of, and improvements to the study. Finally, future applications and directions are addressed.

CHAPTER 2

REVIEW OF LITERATURE

Jumping

Many sports involve dynamic jumps which are all based upon the same mechanical principles (Jacoby and Fraley, 1995). The following section will describe these mechanical principles with particular reference to the long jump and the high jump.

All jumpers try to extend their flight by either length or distance. They are however limited by vital factors which control the outcome and which are important during one critical phase, the takeoff. According to Lease (1994) these factors are:

-The amount of forward or horizontal force

-The amount of upward force

-The angle of takeoff

Others (Dapena et al., 1990) believe that while technique does influence performance it is genetic factors which primarily determine the overall performance. Technique and genetic factors can, however, be considered as not being independent as technique determines how effectively the genetic factors such as dynamic strength of the athlete are used.

The total height or distance achieved by an athlete during a running jump can be considered to consist of three separate components. In the high jump these are: (a) the height of the mass centre at takeoff, (b) the height the mass centre is raised to during flight and (c) the height of the bar minus the peak height attained by the mass centre (Hay, 1975). In the long jump they are: (a) the horizontal distance between the front edge of the takeoff board and the jumper's centre of mass at the moment of takeoff, (b) the distance the centre of mass travels during the aerial phase, and (c) the horizontal distance between the centre of mass at the instant at which contact is made with the sand and the mark left in the sand closest to the takeoff board (Ward-Smith, 1983).

Elite male high jumpers clear heights above 2.30 m close to the World Record of 2.45 m. Elite male long jumpers reach distances in excess of 8.00 m,

with the World Record currently at 8.95 m. In studying high jumping and long jumping performances, there are generally considered to be three main phases; the approach, the takeoff and the flight (Greig and Yeadon, 2000; Dapena, 1988; Dapena and Chung, 1988). All three phases are important for the completion of a successful jump, and each needs to be considered separately in the analysis of the whole jump.

The approach

The main purpose of the approach is to place the athlete in the optimum position from which to begin the takeoff in order to maximise either height or distance. The takeoff is considered to be the most important of the three phases and the approach is vital preparation for this phase (Dapena, 1988).

Approach speed

A high jumper tries to maximise vertical velocity at takeoff whereas a long jumper seeks to obtain a high horizontal velocity which is controllable and allows the development of vertical velocity.

High jumpers enter the final steps of the approach at much lower speeds than long jumpers (Alexander, 1990). Alexander (1990) found the relationship between approach speed and height jumped in high jumping to be non-linear. In agreement with this, Greig and Yeadon (2000) reported that for an elite male high jumper, the peak height reached by the mass centre during flight is significantly correlated with a quadratic function of approach speed, with the optimum speed being 7 ms^{-1}. On a study of experienced jumpers, Dapena (1980) recorded velocities at touchdown of between 6.3 and 7.9 ms^{-1}, which was in good agreement with values reported previously.

The importance of achieving a high sprinting speed on approach is well known to be an important factor in long jumping performances. Ward-Smith (1984) found there to be a relationship with a high linear correlation between approach speed and distance. In agreement with this, the linear correlation of the horizontal velocity and the distance of the jump have consistently yielded coefficients in the 0.7 – 0.9 range (Hay and Nohara , 1990; Hay, Miller and Canetrna, 1986). In a study by Hay et al. (1986) on twelve finalists in the men's

long jump in the US National Championships, the maximum horizontal velocity recorded for each subject ranged from 10.1 ms^{-1} to 11.4 ms^{-1}.

Leg plant angle

Greig and Yeadon (2000) reported an optimum value for the leg plant angle in high jumping, defined as the angle between the vertical and a line passing through the ankle and hip joints, of 33.7°. The peak height reached by the mass centre during the flight phase was found to be correlated with a quadratic function of the leg plant angle. Using a simple two-segment model of jumping, Alexander (1990) found high jumpers use a fairly shallow approach angle in the region of 45°. This shallow plant angle facilitates the production of vertical velocity.

Long jumpers generally use a steeper plant angle than those used in high jumping (Alexander, 1990). In order to gain vertical velocity whilst maintaining a fast horizontal velocity a plant angle, defined as the angle made by the line from the centre of mass to the ankle joint and the downward vertical, of the order of 18-22° is required (Hay, 1981). In agreement with this, it was found that the projection angle in elite male long jumpers, defined as the trajectory of the centre of gravity from the ground, ranges from 18° to 24° (IAAF, 1990). Alexander (1990) found using a simple two-segment model of jumping that the longest jumps were obtained using a leg plant angle of 20°.

In summary, coaches of the high jump advocate a relatively fast and low approach and this is reiterated in much of the literature (Dapena, 1988; Dapena and Chung, 1988). Although the research suggests that a fast, low approach is preferable, this approach should be utilised with caution. In the long jump a compromise between loss in horizontal and gain in vertical velocity needs to be maintained and this is achieved using a relatively steep leg plant angle. The high approach speed needed in the long jump needs to be controllable otherwise at takeoff it may be detrimental to performance.

Knee angle

Optimium knee angles at touchdown in the high jump may be expected to be close to 180° (Greig and Yeadon, 2000). If the knee is too flexed at touchdown

this may cause the knee to collapse in the same way as if the leg plant angle is too small. This is true in both the long jump and the high jump.

The takeoff

The takeoff phase is considered to be the most important of the phases and is defined as the period of time between the instant when the takeoff foot first touches the ground and the instant when it loses contact with the ground (Dapena, 1993). During this period the takeoff leg flexes at the knee in the eccentric phase and subsequently extends in the concentric phase. As already stated, during this phase the high jumper tries to maximise the gain in vertical velocity while the long jumper tries to develop vertical velocity whilst limiting the inevitable loss in horizontal velocity. Cavagna, Dusman and Margaria (1968) have shown that the maximum force that a muscle can exert in isometric and concentric conditions is larger if the muscle has been subjected previously to a stretch. This is one of the reasons why in jumping activities the concentric phase is preceded by a flexion of the knee. 'The degree of flexion of the knee of the takeoff leg during the takeoff phase is generally considered to be one of the factors that strongly influences the production of vertical velocity' (Dapena, 1980).

In order to maximise the gain in vertical velocity in high jumping, the net impulse must be as large as possible (Dapena, 1993; Dapena and Chung, 1988). This net impulse is maximised by exerting a large force while the mass centre travels through a large range (Dapena, 1996). A faster approach speed can increase the force exerted and an initially low position of the centre of mass can increase its range of motion, however, as already stated a fast, low approach must be applied with caution. If the approach is too fast or low, the takeoff leg may be forced to flex excessively during the takeoff phase and may not be able to make a forceful extension. Few high jumpers, however, use approaches that will result in a buckling of the takeoff leg. Frequently they approach at speeds below optimum, as they are not skilled enough to use higher speeds (Dapena et al., 1990).

During the takeoff in the long jump the two important tasks of developing vertical velocity and limiting the loss in horizontal are vital for the success of the performance. In a study of elite male long jumpers, Hay et al.(1986) found there was a pronounced loss in horizontal velocity during the takeoff that ranged from

1.1-2.1 ms^{-1}. This loss in horizontal velocity was, however, associated with a corresponding gain in vertical velocity of between 3.4 and 4.3 ms^{-1}.

The flight

During the flight phase in both high jumping and long jumping it is not only the height or distance gained by the mass centre that is of importance but also how the body is positioned.

All elite high jumpers use the Fosbury flop. One reason Fosbury flop jumpers are able to clear greater heights in competition than athletes using other techniques is not necessarily because they jump higher, but because they have perfected their clearance. The most usual reasons for ineffective bar clearance are: taking off too close or too far from the bar, insufficient somersaulting angular momentum, insufficient twist rotation, poor arching and bad timing of the arching process (Dapena, 1996).

An optimal landing position in the long jump is one which: (a) extends the flight path of the centre of mass as far as possible, (b) provides the greatest possible horizontal distance between the heels and the centre of mass at touchdown, and (c) permits the athlete to avoid falling back on landing (Dyson, 1977). This statement is in conflict, however, as two variables which are interdependent are trying to be optimised. All the factors influencing the performance of a jump need to be addressed in a compromising manner.

Contribution of free limbs

In sports such as the high jump and the long jump where an athlete wants to get every last centimetre out of a jump, the use of arms is clearly called for (Harman, Rosenstein, Frykman and Rosenstein, 1990). According to Dapena (1996) the actions of the arms and of the lead leg during the takeoff phase are important for the outcome of a jump. It would appear from the literature that there is general agreement that the use of the free limbs does positively affect performance. An upward force produced by the trunk on the arms evokes a downward reaction force. This might suggest a simple transmission of force through the trunks and the legs to the ground. This is what happens if the arms accelerate upwards while a person stands on the ground with straight legs or if the

knees are flexed at a constant angle (Dapena, 1999). If however, as in a high jumping performance, the arms accelerate upward as the knees flex and then extend, how do we explain this enhanced performance through use of free limbs? At any given instant, for a given vertical velocity of the centre of mass, a larger vertical velocity of the arms results in a smaller vertical velocity of the hips, slower concentric conditions of the leg muscles and therefore a potentially larger force exerted by the feet on the ground (Dapena, 1999). For a good arm action, both the arms should be used, but neither should be too flexed during the swing. A good elbow angle should be somewhere between full extension and 90° of flexion (Dapena, 1996). The athletes with the strongest arm actions usually bring both arms back during the final one or two strides of the run up, as this allows the arm nearest to the bar to swing more actively during the takeoff phase (Dapena, 1992).

In the long jump, according to Teel (1981) the key to height is the free leg and it must be brought from behind the body to the front very quickly. During the flight phase of the long jump, the free limbs are also used to help stop the body rotating too much so that the athlete is able to get his feet well forward for landing.

Summary of jumping

In both the high jump and the long jump a compromise between optimum technique in all three of the phases and the optimum combination of the phases will result in a maximal performance. The literature suggests that it is the approach and the takeoff phases that are most crucial to the performance (Dapena, 1996), and several studies have looked at these two phases in the optimisation of performance (Lees et al., 1994; Dapena et al, 1990). The specific variables which have been investigated are the approach speed and the plant angle of the takeoff leg (Alexander, 1990; Greig and Yeadon, 2000).

Techniques of investigation

Studies which have looked at jumping, and in particular the approach characteristics discussed in the previous section, have been both experimental and

theoretical in nature. The following section will look at these methods and discuss their relative strengths and weaknesses.

Experimental research

'A true experiment may be defined as a study in which certain independent variables are manipulated and their effect on one or more dependent variables is determined' (Hicks, 1982).

The experimental approach may take the form of direct intervention in a sporting situation. However, more often the experiment is invisible to the athlete and is purely a matter of the way in which the biomechanist selects the data (Yeadon and Challis, 1994). Using the latter approach may be useful in highlighting techniques which are associated with good performances.

Any experiment should first involve a statement of the problem to be solved. The statement of the problem should include reference to one or more dependent variables to be used in assessing the results of the study. The independent variables to be used in the experiment need to be defined and how they are to be manipulated needs to be stated. John and Quenouille (1977) consider the three main considerations which enter into the design of experiments as: (i) the conclusions drawn from an experiment must have validity, (ii) the conclusions drawn from an experiment must have precision and (iii) the experimental conclusions must have wide application. In order to minimise the systematic error occurring in an experiment, it must be ensured that experimental conditions differ in no systematic way from each other. In an ideal experiment, the conditions should differ only in the independent variable, and so experiments should be designed to eliminate totally systematic differences which are considered to be threats to internal validity. Once the experiment has been designed to minimise systematic error and maximise precision, the external validity of the study must be considered - that is how applicable the results are. The wider the range of conditions investigated in the experiment, the greater the confidence there is in the extrapolation of the conclusions. However, there must be a compromise between the internal and external validity of the experiments. An ideal experiment would examine a wide range of conditions without losing accuracy.

In a competition environment there is only a small range of data available from experimental studies due to limitations. One widely used approach is to gather data on a number of athletes and see how the characteristics of their techniques compare. Hay (1985) refers to this as the cross-sectional approach and comments that this approach has been used in a large number of research investigations in sports biomechanics and might well be regarded as a standard research design in the field. This approach is also commonly known as an inter-individual study. A second approach is one in which data is obtained on multiple performances by the same individual in order to determine which characteristics of the technique are related to success in the event. Hay (1985) refers to this as a longitudinal study. This approach has been used very sparingly. Studies using this approach are frequently referred to as intra-individual studies. Both cross-sectional and longitudinal approaches have their advantages and disadvantages. In some cases cross-sectional approaches suggest that a factor is an important determinant of success, whereas longitudinal studies may suggest that it is not. In other cases the cross-sectional approach fails to identify a factor of importance which the longitudinal approach suggests is important. Whichever approach is decided upon, caution should be exercised in interpreting the results. Caution is especially indicated when the results suggest that a given factor is of little importance in determining the outcome. When a factor is optimised there may be little correlation between variability of this factor and the subsequent performance, but this may be due to the fact that the factor has already been optimised and only within the bounds that it is then varied is there little correlation.

A number of experimental studies have been conducted which have looked at the approach characteristics in high jumping and long jumping. One such study performed by Greig and Yeadon (2000), which adopted the longitudinal approach, was conducted during a training session with an elite male high jumper. Direct intervention was used to induce a change in technique so that a greater range in approach speed was obtained than could be observed in competition. The influence on the jump height of the approach characteristics was considered. It was shown that peak height of the mass centre during the flight over the bar was significantly correlated with quadratic functions of both the approach speed and leg plant angle. Dapena at al. (1990) performed a regression analysis of high

jumping technique in which 77 elite high jumpers were filmed using 3-D filming methods at various American national level competitions. The main application of this cross-sectional study was in the diagnosis of jumpers who were using techniques that were less demanding than their muscles could withstand. The study found that a function fitted to the points that mark the theoretical optimum jumps on a graph of approach speed against vertical velocity at takeoff was roughly linear. More information on an individual jumper might be expected to be gained from an intra-individual study such as the one by Greig and Yeadon (2000).

The majority of research into the mechanics of dynamic jumping has taken the form of descriptive studies as opposed to experiments designed to answer specific questions. The majority of descriptive studies have provided quantitative data on jumping performances by athletes, but few have attempted to explain the mechanics of the technique. Purely experimental studies result in the acquisition of real data, they are however very limited in what they can tell us regarding any change in variables or conditions. The problems associated with experimental and data based studies have been identified as those of control, experimental design, small samples, choice of variables and statistical analysis (Yeadon and Challis, 1994). Extraneous variance is another major problem in experimental studies, however, ensuring good internal validity (imposing control on the experimental setting) may result in a reduced applicability of findings (low external validity).

Theoretical research

Another method of investigation is to use a theoretical approach. This may involve using a theoretical model to simulate human motion. The term model can be defined as an attempt to represent reality. The construction of a model relies on two types of information: knowledge of the system being modelled and experimental data that constitute system inputs or expected outputs.

Modelling of the human body, its segments and tissues is one of the methods currently utilised to study specific problems. Mathematical modelling, which is often used in sports biomechanics, makes the link between the performer or sports object and its motions. It involves representing one or more of the characteristics of a system or object using mathematical equations. In sports

biomechanics, the motions of the mechanical systems studied are governed by Newton's Laws of Motion and so most models are mathematical formulations of Newtonian systems (Yeadon and Challis, 1994). Every model is an approximation that neglects certain features of the system or object.

Modelling is required when a physical experiment is not possible due to it being destructive or potentially dangerous to an individual. In addition modelling is appropriate when the system under study cannot be adequately represented physically so that its behaviour throughout a range of conditions can be examined (Miller, 1979). Such an approach in which one or more factors are varied individually or in combination is impossible to do experimentally. Whereas experiments measure what happens in the real world to real objects, a mathematical model forms a similar basis for a computer experiment (Bartlett, 1999). Simulation can be defined as the carrying out of experiments under carefully controlled conditions on a model of the real world system (Vaughan, 1984). There are many different types of mathematical model using different representations of the human body.

Theoretical work on dynamic jumping has been undertaken by Alexander (1990) who developed a two-segment model to calculate optimum approach characteristics. Although grossly simplified the model nevertheless enables us to identify the principles that govern optimum speed and plant angle for the takeoff of both the long jump and the high jump.

Theoretical models have the advantage over experimental studies in that they are able to simulate actions with different conditions or variable values without affecting other variables in the study, they therefore have the potential to predict performances. Theoretical models also have the advantage over experimental models in the time that can be saved. Once the model has been developed, many simulations can be performed in a relatively short period of time. Finally, as already mentioned there is the safety aspect, by using a model the athlete does not have to perform potentially hazardous experiments.

The limitations of the theoretical approach include the problem of model validation or evaluation (Vaughan, 1984), the need to use realistic input values, the need to use realistic model parameter values, and the need to make the model subject specific. The weakness of purely theoretical studies needs to be avoided by evaluating models in the areas where they are applied and basing simulations

on appropriate experimental data. Once a model has been selected and evaluated it may be used to answer questions which are difficult to tackle experimentally.

Summary of techniques of investigation

Both experimental and theoretical approaches have their strengths and weaknesses. Theoretical studies are most profitable when they are combined with an experimental approach and vice versa.

Data collection techniques

3-D movement analysis

The human skeletal system is composed of a series of jointed links which can be approximated as a system of rigid bodies with two adjacent bodies sharing a common joint centre. In order to describe the location and orientation of such links in space, three independent parameters are required for each link, with six parameters being required for the position and orientation of the reference body. Kinesiological measurements describe the spatial motion of the body segments and the movements of the joints connecting these segments. Biomechanical analysis involves the use of these measurements in the determination of the kinematics and the calculation of the kinetics: the forces (internal and external) and moments determined by the forces. For the recording and analysis of three-dimensional (3-D) human movement a diverse array of measurement equipment is available including, manual and automatic film and video systems, accelerometers, force platforms, pressure sensors and electromyography systems. The selection of a measurement system for studying human motion requires a careful match between the nature of the movement, the environment in which it is performed and the properties of the measurement system (Allard, Stokes and Blanchi, 1995).

Kinematic data collection

Many biomechanical three-dimensional analyses of human movement start with data capture by an imaging device. Still or high-speed cameras, video

cameras, or radiographic systems are the most common of these data capture systems.

Synchronisation of force and video data

The image formed by a camera represents a two-dimensional (2-D) projection of a 3-D object. The challenge in 3-D motion analysis is to calculate the position and orientation of the 3-D object which produced the 2-D projections. This process of the calculation of the co-ordinates of the 3-D object is called 3-D reconstruction.

Three-dimensional reconstruction of a single point requires image co-ordinates for that point simultaneously from at least two camera views (Yeadon and Challis, 1994). Synchronising data from the two or more camera views can therefore be achieved. One way to achieve this is to physically synchronise the video cameras or cine cameras by gen-locking or phase-locking them. If gen-locking or phase-locking is not possible then synchronous data can be obtained by interpolating the separately recorded data over the same time base (Yeadon and Challis, 1994). This can be achieved by placing a timing device, such as a set of timing lights, in the fields of view of both camera so the times for each field can be identified. Another way in which data sets can be synchronised is by identifying common events from the two camera views (Yeadon, 1989). This method can be improved by using several such events and fitting a regression line to the corresponding field number (Dapena and Chung, 1988). Yeadon and King (1999) presented a more general method of synchronisation using the direct linear transformation (DLT) reconstruction that uses the digitised data of all body landmarks. This method can be used to synchronise digitised data sets of any sports movements. Quintic splines are fitted to the time histories of the digitised data from the two camera views. The digitised data sets are synchronised by varying the time offset between them until the root mean square (RMS) difference is minimised. This method has numerous advantages over other methods (Yeadon and King, 1999). It does not require a timing device in the field of view so it is more convenient to use in competition, it can be used with a wide range of movements since it uses all the digitised data to synchronise views and finally it is more accurate than previous methods which used digitised data for

synchronisation. For data collections which are not performed during competition, timing lights are sufficient and may be considered one of the more robust methods.

As well as synchronisation of video or film data from multiple cameras views, biomechanical analyses frequently involve combining ground reaction force data and kinematic data in order to determine joint forces moments and powers (O'Connor, Yack and White, 1995). The accuracy of this combined data depends to some degree on how well the two sets of data are synchronised, and errors in synchronisation can lead to further errors in the analysis. O'Connor et al. (1995) demonstrated that using an LED to synchronise force and video data can result in errors as great as one field which can result in large errors in joint moments and joint powers. Using an event to trigger the force data collection and to produce a visible record of when this event occurred would allow the force and video data to be synchronised to within half the time for one field of the image recording. O'Connor et al. (1995) developed a synchronisation strategy that made it possible to align kinematic and ground reaction force data with a much greater accuracy than provided by conventional techniques. The process ensures that the force data that occur when the video image is captured are assigned to the correct video frame. Another method to synchronise the data involves the use of sequential timing lights, where the force data capture is triggered by the illumination of the first light. This allows the video and force data to be synchronised to within the time between sequential lights. Timing lights can therefore be used for both the synchronisation of video, and video and force together.

Three-dimensional reconstruction

Using the image coordinates from two or more camera views, 3-D coordinates can be determined. An essential requirement of 3-D motion analysis is that it is possible to determine real-space co-ordinates from image co-ordinates. Equations are used to determine the object point co-ordinates from their image co-ordinates. In order to solve these equations the external and internal parameters of the camera as well as the image co-ordinates from the camera views from the cameras are required.

According to Allard et al. (1995), among the 3-D reconstruction methods, the most widely applicable and discussed is probably the Direct Linear Transformation (DLT) technique (Abdel-Aziz and Karara, 1971). This method allows cameras to be placed at arbitrary positions, but requires that points with known locations are distributed throughout the whole activity space. This usually takes the form of a calibration frame. The DLT method is expressed by the following equations:

$$u = \frac{L_1X + L_2Y + L_3Z + L_4}{L_9x + L_{10}Y + L_{11}Z + 1}$$

$$v = \frac{L_5X + L_6Y + L_7Z + L_8}{L_9x + L_{10}Y + L_{11}Z + 1}$$

where u and v are the image co-ordinates, X, Y and Z are the object point co-ordinates and the constants L_1 to L_{11} are the DLT parameters, which define the camera position and orientation as well as the camera/digitiser internal parameters.

Correction for lens distortion

A number of researchers have identified the effects of non-linear lens distortion in the DLT procedure and have accounted for this by using extra parameters in the DLT equations (Karara, 1980; Challis, 1991). This correction for lens distortion has improved the reconstruction accuracy for video systems (Tan, 1997). Karara (1980) suggests that corrections Δu and Δv for the symmetrical distortion can be expressed as:

$$\Delta u = (u-u_0)r^2L_{12}, \qquad \Delta v = (v-v_0)r^2L_{12},$$

where L_{12} is the lens distortion parameter and r is the distance between the digitised point and the principal point (u_0, v_0) which should be close to the centre of the video image. DLT parameters can therefore be written as:

$$u + \Delta u = \frac{L_1x + L_2y + L_3z + L_4}{L_9x + L_{10}y + L_{11}z + 1}$$

$$v + \Delta v = \frac{L_5x + L_6y + L_7z + L_8}{L_9x + L_{10}y + L_{11}z + 1}$$

Manual motion analysis

Manual digitisation involves the use of video or cine along with digital computer hardware and appropriate software. The reconstruction method described above is then employed to provide estimates of the 3-D points, which have been digitised, in order to describe the position and orientation of the object.

Cinematography

The photographic technique is a low cost uncomplicated method of broad applicability (Atha, 1984). The information inherent in a photographic record is more extensive than can be provided by many of the more up to date techniques. Such films provide useful records of events. Viewing of the records can be repeated and this may be useful in gaining insight into performance. Furthermore, information can be gained by measurements within separate frames. Slow motion cine-photography is used for camera framing rates lower than 300 Hz, which although sufficient for dynamic analyses of fast movement of most activities is less suitable for some impact sports. High-speed cine-photography in which the framing rate is higher than 300 Hz may be required for the analysis of impacts, measurements of tissue shock waves and other transients (Atha, 1984). Cinematography has been used to study a variety of sports movements, including the tennis serve (Elliot, Marsh and Blanksby, 1986) and the penalty corner hit in hockey (Elliot and Chivers, 1988).

According to Atha (1984), however, there are at least three major disadvantages to using cine-photography: (i) time consuming, (ii) results are never immediately available for inspection and (iii) measurement errors tend to be significant. Cine-photography may use higher framing rates than standard video, but the disadvantages outweigh the advantages. Cine-photography is a very dated method of collecting kinematic data and one which is used less and less frequently.

Video

A common technique for collecting kinematic data is video. Its flexibility and real-time capabilities make it an excellent choice for biomechanical analysis, in particular for 3-D human movement determination (Gruen, 1997). Advantages

of video over cinematography include the fact that the images are available immediately, which allows control of the image quality during the recording session itself, thus helping to prevent errors with lighting conditions, the low cost of tapes (Angulo and Dapena, 1992), and the ease with which it can be used. Despite these major advantages, one negative features may be the low framing rate of standard video cameras (50 Hz in the UK). In this study time histories of body landmarks during the contact phase of running jumps are required. The duration of the contact times for these activities is short (100 ms -200 ms). Using video cameras operating at 50 Hz would result in few fields during this contact phase. A high speed video camera which operates at 200 Hz or above is required in order to obtain enough fields for accurate analysis.

Video systems, like cine, have the problem that digitisation of body landmarks is required, and this process is very time consuming. The need for faster information from the image, which thus provides potential for increasing the number of trials that can be analysed, has led to the development of automatic systems.

Automatic motion analysis

Automatic systems for collecting 3-D data involve taking an image and automatically obtaining 2-D data, from which 3-D coordinates which define the position and orientation of the body can be determined, using a version of the DLT method. There are two categories of commercial automatic instrumentation commonly used to measure whole body motion (Richards, 1999). The first category utilises equipment that provides a visual record of body segment positions while the second category utilises magnetic sensors to determine the position and orientation of segments in space. Image-based devices can be further divided into categories of passive and active systems depending on the type of marker that the system uses. Passive systems use markers that reflect light back to the sensor while active systems utilise markers that contain the source of light for the sensors. Active markers need an energy supply. This is usually used to power a low-powered light-emitting diode (LEDs). Passive markers are generally made from retro-reflective material. These markers reflect light back in the direction from which it comes, demonstrating a similar principle to the one used by bicycle

rear reflectors. The light comes from near the camera and is hence reflected back in the camera direction.

Video-based systems use passive markers such as those described above. Examples of such systems are VICON, ELITE and Motion Analysis. The advantages of these passive markers are that no wires and batteries are needed, they have small/negligible mass, and the fact that they are relatively inexpensive to replace. The disadvantage of passive marker systems are the limited image resolution, interference caused by sunlight and the difficulty in automatically identifying markers (Yeadon and Challis, 1994).

LED or active marker based measurement systems work by the LEDs flashing in a given sequence. The sequencing of the LED activity allows automatic identification of the markers, which is a great advantage over the passive marker based systems discussed above. Another advantage is the good resolution at high framing rates. Disadvantages include the constraint of the subject's freedom because of the wires connecting the markers attached to the body to the power supply (Allard et al., 1995), and interference caused by reflections (Yeadon and Challis, 1994). Probably the main disadvantage, however, is the fact that the markers move. This is a result of movement of the human tissue but more detrimentally due to the markers having a significant mass.

Richards (1999) conducted field tests to assess the performance characteristics of six passive marker based and one active marker based systems. The CODA system, the only active marker based system which was assessed, averaged an error for the marker position of approximately 2 mm. This was greater than the majority of the other systems assessed. Vicon's 370 system, Qualysis's ProReflex system and Motions Analysis' HiRes system typically kept the error of the marker position under 1mm. The Aerial system, however, averaged just under 4mm of error. Although the accuracy of Coda maybe slightly worse than many of the other systems, Coda does not require the user to edit the data, since the active markers are always correctly identified by the system, unlike the other systems (Richards, 1999).

All automatic systems have the advantage that the data are available much quicker than when digitising manually. All the automatic systems, however, are limited by the requirement for markers to be attached to the subject. They also can only give joint centre locations of the surface placed markers, whereas when

using a manual system locations can be estimated by the operator. Finally, no visual record of the recorded movement can be provided. Due to these limitations manual digitising will continue to be used when data has to be collected at major sporting events (Yeadon and Challis, 1994). For data collections not performed during competition, automatic systems can still provide a very useful technique of collecting kinematic data.

Kinetic data collection

Force plate

The most common force measurement device used in biomechanics is the force plate (Yeadon and Challis, 1994). Force plates are commonly used in biomechanics laboratories to measure ground reaction forces produced by human movement. The measurement of these ground reaction forces has been extremely important in the study of human motion. A force plate is simply a metal plate with four sensors attached to give an electrical output proportional to the forces on the plate. The sensors can be either strain gauges or piezoelectric elements (Cross, 1999). Hall, Flemming, Dolan, Millbank and Paul (1996) reported a series of methods for calibrating a Kistler piezo-electric force plate in its normal operating position. Three calibration procedures were performed. In two procedures vertical forces were applied using calibrated weights. Where required, horizontal forces were applied using a purpose built rig. The procedures allowed the output channels of the force plate to be accurately calibrated with the minimum amount of specialist equipment and disturbance.

In addition to the measurement of the ground reaction forces, the point of application of the ground reaction force vector is calculated from the measured distribution of the total force among the individual force transducers. By combining this information with the kinematic data in biomechanical models, intersegmental forces and moments can be calculated (Bobbert and Schamhardt, 1990). Bobbert and Schamhardt (1990) investigated the accuracy of determining the point of force application with a Kistler force plate. They found the errors ranged from –20 to +20 mm. This implies that if measurements of the point of force application are used in research on running, for example, the readings can vary by ± 20 mm from trial to trial.

The force plate has been used in jumping studies either on its own or in combination with other recording equipment (Kerwin, 1997). Studies on dynamic jumping involving the use of a force plate have included the study by Bedi and Cooper (1977) on the determination of angular momentum in the long jump takeoff, and the study on high jumping by Dessureault and Lafortune (1981).

Electromyography

Sports movement techniques and skills, and training apparatus methods have amongst other factors a highly specialised muscular activity in common (Clarys and Cabri, 1993). Knowledge of this muscular activity can lead to insight into what is happening in the muscles during performances and also how muscle activity affects performance.

Electromyography (EMG) is unique in revealing how a muscle is acting at any moment during various movements. It also provides information about the coordination of muscles (Basmajian, 1974). Electromyography offers the only method of objectively assessing when a muscle is active. It is a very convenient and sensitive piece of equipment, but is an indirect indicator of muscle tension (Grieve, 1975). An electromyogram is a record of the fluctuations of potential that occur between two conducting surfaces, placed on the surface of the body or within it, due to the electrical activity of the muscles.

Currently there are three common applications of the EMG signal: (i) to determine the activation timings of the muscle, that is, when the excitation to muscle begins and ends, (ii) to estimate the force produced by a muscle, (iii) to obtain an index at the rate at which a muscle fatigues through the analysis of the frequency spectrum of the signal (De Luca, 1997).

Within EMG, in particular sports science, a specific approach has been developed wherein EMG is used for studying muscular function and coordination. This approach is usually called kinesiological EMG (Clarys and Cabri, 1993).

Many factors, both intrinsic and extrinsic, influence the EMG signal. The intrinsic factors include physiological factors such as firing rates of motor units, type of fibre and conduction velocity of the muscle fibres, and anatomical factors such as muscle fibre diameters and relative positions of the muscle fibres. The extrinsic factors include the location of the electrodes with respect to the motor

end plates and the electrical characteristics of the recording system (Bartlett, 1992). Two main issues of concern that influence the fidelity of the EMG signal recorded are: (i) the signal to noise ratio and (ii) the distortion of the signal (de Luca, 1997). Sources of noise include noise in the electronic components, noise in the detection and recording equipment and ambient noise. Only signals with energy above the electrical noise level are usable.

In order to eliminate a potentially much greater noise signal from power line sources a differential detecting configuration may be employed (De Luca, 1997). The signal is detected at two sites, the two signals are subtracted from each other and the difference is amplified. As a result, any signal which is common to both detection sites will be removed.

Electrodes

Position

The electrodes used in electromyography are of a wide variety of types and combinations. The two main types of the electrodes used for the study of muscle are surface electrodes and inserted (wire and needle) electrodes. Although the use of inserted electrodes has been shown to have superiority over surface electrodes (Grieve, 1975), surface electrodes are most widely used in sports kinesiology research. This is due that fact that inserted electrodes are invasive (Clarys and Cabri, 1993) and utterly unsuited for studies of movement (Grieve, 1975). Grieve (1975) comments that surface electrodes are not only safer, easier to use, and more acceptable to the subject, but for superficial muscles at least provide a degree of qualitative repeatability that compares favourably with wire electrodes. Basmajian (1974), however, condemns the exclusive use of surface electrodes stating not only can they only be used with superficial muscles but that their pick up is generally too widespread which may result in cross-talk being an issue.

The placement of surface electrodes is both an art and a science and has been investigated considerably (Clarys and Cabri, 1993; De Luca, 1997; Clarys, 2000). In localising the site of detection of the electrode on the skin, a variety of approaches have been applied. It has been noted (Clarys and Cabri, 1993) that caution must be taken when selecting the position for the placement of the electrode on the skin. Muscles do not stay in the same place during complex

dynamic movement and the entire muscle belly may not be fully under the skin at all times. It is therefore uncertain which muscles have contributed to the EMG pattern presented. It was concluded that the best position to place the electrodes is over the visual midpoint of the contracted muscle (Clarys and Cabri, 1993). A reference (or ground) electrode is necessary for providing a common reference to the differential input of the pre-amplifier in the electrode. For this purpose, the reference electrode should be placed as far away as possible and on electrically neutral tissue. However, often this arrangement is inconvenient because the separation of the detecting electrode and reference electrode leads requires two wires between the electrode and the amplifier (De Luca, 1997).

Orientation

In addition to positioning the electrode in the correct place on the skin above a muscle, it is also important to pay attention to the orientation of the electrodes with respect to each other (inter-detection surface distance) and to the muscle fibres. Bi-polar surface electrodes have two detection surfaces. According to Clarys and Cabri (1993), for optimal results, the two detection surfaces should be oriented so that the line between them is parallel to the muscle fibres. In order to achieve this arrangement it is assumed that the orientation of the muscle fibres is linear and that muscle fibres are arranged parallel to each other. The distance between these two detection surfaces is a further contentious issue. De Luca (1997) believes this distance should be fixed so that qualitative recordings can be made between muscles and individuals. De Luca (1997) comments that it is not necessary to separate the two detection surfaces by a large space in order to obtain a representative sample of the EMG signal from a muscle. Large inter-detection surface distances result in cross-talk.

Because of the known variability of the EMG signal, not only between subjects but also between trials, different normalisation techniques to reduce this variability have been developed. Generally the EMG of maximum effort or the highest EMG value has been selected as the normalising factor (Clarys and Cabri, 1993; Clarys, 2000).

Processing EMG is often performed in biomechanics both to enable correlation with other biomechanical and physiological variables and to facilitate comparisons within and between different laboratories (Clarys and Cabri, 1993).

There are two main processing methods which are currently used in kinesiological EMG. Temporal processing (time domain analysis) is used to investigate the amount of activity in relation to time. Frequency domain analysis is used in the investigation of muscle fatigue. The former method is more important in this particular study.

Time domain analysis is usually preceded by rectification of the signal. Either half-wave rectification (removal of negative voltages), or more commonly full-wave rectification (inverting the negative voltages) is used. Following rectification of the signal there are many different methods of time domain analysis which are used, including:

Average rectified EMG (AREMG)

This is simply the time average of the full-rectified EMG over a specified time ($t_2 - t_1$).

$$AREMG = \frac{1}{(t_2 - t_1)} \int_{t_1}^{t_2} |E(t)| dt$$

Moving average

A moving average is commonly used to yield the time course of the EMG. A new average is calculated each time the time window is moved along the rectified EMG.

Root mean square EMG (RMSEMG)

This represents the square root of the average power of the signal in a given time.

$$RMSEMG = \sqrt{\left(\frac{1}{t_2 - t_1} \int_{t_1}^{t_2} E(t)^2 dt\right)}$$

Integrated EMG (IEMG)

This is simply the area under the rectified EMG, measured as for any integral.

$$IEMG = \int_{t_1}^{t_2} E(t)dt$$

Traditionally the IMEG has been the most commonly used method of processing the EMG. However, it has widely been miscalculated, and the resulting data misinterpreted. Due to this, the AREMG is becoming a more popular method (Burden and Bartlett, 1997).

In conclusion, the EMG and choice of processing method, including the choice of the best normalisation technique, depend on the specific demands of the type of subjects and circumstances (Clarys, 2000).

Summary of data collection

The advantages and disadvantages of many different data collection techniques have been discussed in this section. The choice of techniques to be used in this study was made after considering certain factors; the data required to successfully evaluate and utilise a simulation model, the suitability of the techniques and the equipment available.

Simulation models

Introduction

The techniques used in simulation modelling can be divided into four sections: (i) the development of the model, (ii) the evaluation of the model, (iii) the optimisation of a performance and (iv) sensitivity analysis (King, 1998). 'Modelling, simulation and optimisation encapsulate, in a unified structure, the process involved in seeking values of a set of variables or functional relationships that will optimise a performance.' (Bartlett, 1999).

Development

Model complexity

Many different computer simulation models have been developed for the analysis of sports movements. The complexity of the model depends on the proposed use of the model.

'Many models have been built with the intention of imitating the relevant features of the human body in as much detail as possible' (Alexander, 1995), such as the model of jumping developed by Hatze (1981). A complex model is, however, both difficult to develop and apply since the derivation of equations of motion can be extremely complicated and determination of model parameters can be very difficult . Other models that have been developed have been much simpler. Some of the literature highlights the advantages of using simple models, for example, Alexander (1995) states that scientists who have built these simple models have not kept them simple merely to avoid difficulty but see advantages in it. The simpler the model, the easier it is to discover which of its features are essential to the observed effect (Alexander, 1992). The most fundamental understanding often comes from the simplest models (Hubbard, 1993). Many of the basic principles of walking, running, jumping and throwing have been highlighted by simple models (Alexander, 1995). Alexander (1995) does, however, recognise that models that are too simple can be misleading and that for some purposes more complex models may be needed.

Muscle models

The simulation of movements where large forces are exerted on the body such as movements which involve ground contact, involve more complex equations of motion. When modelling such movements it is necessary to model the forces exerted by muscles within the simulation model (Yeadon and Challis, 1994). As with most computer simulation models, muscle models range from very simple to incredibly complicated.

The way the muscle is represented in simulation models is at present a very contentious issue. 'One of the major problems in modelling large scale problems of musculo-skeletal motion is that of describing actuators i.e. the muscles with appropriate models' (Audu and Davy, 1985).

There are two types of muscle model; those which are mechanical analogues of muscle, which are phemonogical in nature such as the model of Hill (1938), and those which model events at a microscopic level such as the kinetic model of Huxley (1957). Bobbert (1988) identified the 'lumped parameter' models based on the structural model of Hill (1938) and the 'distributed parameter' models based on the sliding filament concept of muscle contraction (Huxley, 1957). The model developed by Bobbert (1988) belongs to the category of lumped parameter models.

Mechanical models consist of a series elastic component (SEC), a contractile component (CC), and sometimes a parallel elastic component (PEC). Models based on the sliding filament theory provide a theoretical framework for considering the actual mechanisms underlying muscle action and provide a more detailed approach than that given by a Hill-type model. Hill-type models of muscle dynamics, however, yield a satisfactory description of muscle behaviour in the context of simulations of gross motor behaviour (van Soest, Schwab, Bobbert and van Ingen Schenau, 1993).

Regardless of the complexity of the model, most of them are derived from the muscle model of Hill (1938). In a large majority of muscle models the control of the skeletal muscle is discontinuous, that is the models assume the control of the muscle is bang-bang, where the muscles are off and then maximally on with a fixed ramp time. This is a feature of a single muscle fibre but not of skeletal muscle as a whole. Caldwell and Selbie (1996) developed a four-segment model of vertical jumping. The torque generators at each joint were controlled using the bang-bang principle. The rate of torque onset was determined using an exponential function which resulted in a fixed ramp time to 99% of maximum torque of 100ms. The only variable was the time of initial torque onset. The advantage of bang-bang control is that it minimises the number of parameters needed to describe muscle activation and hence reduces the time required to optimise movements (Yeadon and Challis, 1994). Having the ability to vary the ramp times and whether the muscle reaches full activation or not would, however, be a distinct advantage.

A range of muscle models have been described, and a question which is regularly addressed is how complex they need to be in order for them to be used successfully to simulate human movements. As already stated, the required

complexity of a model is dependent on the use of the model and the questions which are to be addressed. Winters (1995) developed principles underlying model design, and suggests the quality of current descriptive muscle models is reasonably high and that the primary limitation is more related to the need for additional experimental data than any fundamental problems with utilising muscle models to study multi-joint behaviour.

Torque generators 'v' individual muscles

The majority of muscle models are derived from the model of Hill (1938). Within this group of models there is a further subdivision. Some of the models previously discussed use a torque generator to represent the net effect of all the muscles crossing a joint (Alexander, 1990), whereas others model individual muscles (Bobbert, Huijing and van Ingen Schenau, 1986). Alexander's (1990) model represents the extensor muscles at the knee with a torque generator which exerts a torque at the knee joint, during foot contact. The model of Bobbert et al. (1986) consists of two units, one representing the muscle-tendon complex of the soleus and the other representing that of the gastrocnemius. The model of Nagano and Gerritsen (2001) consists of four rigid segments, three joints and six Hill-type muscles representing the six major muscle groups in the lower extremity. Each muscle consists of a series elastic component and a contractile element.

A model needs to be complex enough to be able to answer the questions it has been developed to investigate. The model of Nagano and Gerritsen (2001) was developed to answer questions regarding specific muscles, it would therefore be redundant if the model contained joint torque generators and not individual muscles.

Bi-articular muscles

One of the advantages of modelling individual muscles is that bi-articular muscles can be incorporated. The model developed by Bobbert et al. (1986) includes a representation of the soleus and the gastrocnemius muscles. The gastrocnemius crosses both the knee and the ankle joints. This model therefore raises the issue of the use of bi-articular muscles in models. Bobbert and Van Ingen Schenau (1988) performed a study to gain insight into the relationship

between muscle actions, movement pattern and achievement in vertical jumping. They claim that the human musculo-skeletal system would be equipped with larger knee extensors and ankle plantar flexors in the absence of bi-articular muscles. Bi-articular muscles play a crucial role in movements such as jumping (Bobbert and van Ingen Schenau, 1988). In disagreement with this Pandy and Zajac (1991) oppose the notion that jumping performance is increased by the unique bi-articular action of the gastrocnemius. Their results showed that replacing the gastrocnemius with a mono-articular muscle had very little affect on jump height reached. This result by Pandy and Zajac (1991) can be explained from the fact that they modelled the gastrocnemius by a straight line connecting the origin and insertion (van Soest et al., 1993). As a result, the moment arm of the gastrocnemius at the knee approaches zero as the knee approaches full extension. Since a moment arm equalling zero denotes a mono-articular gastrocnemius, and considering that the gastrocnemius is only active in the last phase of the push off, where the knee is close to full extension, the gastrocnemius in the model by Pandy and Zajac (1991) is essentially acting as a mono-articular muscle. Therefore, when the muscle was made mono-articular the jump height was hardly affected. The results by van Soest et al. (1993) support the hypothesis of Bobbert and Van Ingen Schenau (1988) on the special role of the gastrocnemius. They also conclude, however, that subtle differences in modelling methods can lead to very different results when applied to design questions.

There may be an argument that when modelling running jumps as in this study, where the time of contact is short and the majority of the energy is generated during the approach, that the modelling of bi-articular muscles is not as important as in say a vertical jump where the time of contact is longer and the majority of the energy is generated during this contact.

Advantages of torque generators over individual muscles include the ability to determine subject specific model parameters. This can be achieved by collecting torque data from an isokinetic dynamometer (King and Yeadon, 2002) or from an inverse dynamics analyses of jumps. When modelling individual muscles it is not possible to obtain a complete set of subject specific parameters.

Models with representations of muscles

Alexander (1990) developed a simplified but useful two-segment model of jumping. The model comprises a shank and a thigh with a single knee extensor torque generator between the two segments. The knee extensor muscle consists of only contractile and elastic components in series. The model was used to predict optimum takeoff techniques for the high jump and the long jump. Although the model is extremely simple and it is doubtful if the model could be used in investigating specific elite performances, it is very valuable in highlighting the general mechanical principles involved in dynamic jumps. Linthorne and Kemble (1998) attempted to tune Alexander's model to the performance of an elite athlete by altering the model parameter values. They found that by simply increasing the maximum knee extensor torque the model could jump heights similar to those reached by elite athletes using realistic optimum approach characteristics.

Pandy, Zajac, Sim and Levine (1990) modelled the human body as a four-segment planar model in order to study leg muscle activity in jumping. The model contains eight muscles each modelled as three components using a Hill-type muscle model. Qualitative comparisons of model predictions with published experimental results indicate that the model can reproduce the major features of a maximum-height squat jump.

A more detailed muscle model than those already described was developed by Hatze (1981). This model simulates in detail the controlled excitation and contraction dynamics of the muscles in the model. The model comprises 17 segments and 46 muscles and is used to simulate the long jump takeoff phase. The model employs a very complex muscle model to represent each muscle and requires activation parameters for each of the 46 muscle groups along with segment configurations and orientations. Hatze (1981) claimed the parameters were determined for an individual which allowed an evaluation of the model for a long jump takeoff. However, It is hard to believe that accurate values for each of the muscles were determined without a high reliance on data from the literature and a lot of assumptions.

Inverse dynamics models

An inverse dynamics model is one in which the kinematics of the system are known and it is the applied forces and moments which are determined (Chao and Rim, 1973).

Inverse dynamics models are very powerful tools in gaining insight into the net summation of all muscle activity at each joint. Inverse dynamics models have several advantages over forward dynamics models. These are: (i) the number of computations required for inverse dynamics is typically fewer than for forward dynamics solutions and (ii) when inverse dynamics techniques are used to calculate inputs (i.e. joint torques), small changes in the kinematics correspond to small changes in the inputs and therefore result in small changes in the objective cost function (Schutte and Risher, 1994).

They do, however, have some inherent limitations, including: (i) they can only determine the net moment and power, and (ii) they cannot differentiate between different muscles (Winter, 1990). Further disadvantages include the modelling of the joints and simple frictionless pin joints and the use of rigid segments. Inverse dynamics models do not include wobbling masses, the importance of which when modelling impacts is discussed in the following section.

Wobbling mass models

The majority of simulation models used for biomechanical analysis comprise rigid body segments such as the model of Gerritsen, van den Bogert and Nigg (1995). In reality the body is not composed of a set of rigid bodies, rather each body segment consists of a rigid part (bone) and a non-rigid part (soft tissue). During an impact such as a heel strike in running or landing in a drop jump, the skeletal structures of the body experience high accelerations whereas the soft tissue's acceleration is delayed (Nigg, Cole and Bruggeman, 1995). The approximation of the human body with rigid segments is only justified for movements which are not too rapid (Denoth, Gruber, Ruder and Keppler, 1985). The use of rigid body models in investigating activities involving impacts is therefore not recommended. More recently, wobbling mass models in which each segment of the model is represented by a combination of both a rigid part and a

soft part have been developed (Gruber, Ruder, Denoth and Schneider, 1998; Pain, 1999).

Two factors which have been identified as being affected by the inclusion of wobbling masses in a model are the vertical ground reaction force during the impact phase (Pain, 1999) and the internal joint forces and torques (Denoth et al., 1985).

Gruber et al. (1998) studied a drop jump from a height of 0.4 m with a heel landing. The passive or impact force peak was found to be much larger and longer for the rigid body model. Dramatic differences were found to occur during the impact phase i.e within the first 10 – 30 ms. Pain (1999) found for a drop jump from a height of 43 cm, the calculated peak vertical ground reaction force decreased from 33800 N for the rigid body model to about 13500 N when wobbling masses were introduced.

The differences in the joint forces and the torques when using the two models is again most obvious during the impact phase. Denoth et al. (1985) presented results for a vertical jump from a height of about 0.2 m and landing on the heel. During this impact phase neglecting wobbling masses resulted in the calculated forces and torques being wrong by more then a factor of 6. The reasons for these differences are explained by Gruber et al. (1998). During the impact phase the wobbling mass of the trunk shifts downwards resulting in the centre of mass of the trunk moving downwards more quickly than the centre of mass of the rigid part. In order to achieve this in the rigid body the trunk is bent more quickly at the hip. This movement causes the unrealistically high declining peak torque and the corresponding declining vertical component of the joint torque of the hip. After the wobbling masses have slowed down, the motion of the trunk must be decelerated. This causes an upward over-shooting torque and a peak in the joint torques to assist in the trunk's deceleration.

Small changes in the mechanical properties of the model have an enormous effect on the joint torques and forces during the impact phase (Gruber et al., 1998). Gruber et al. (1998) employed a planar three-linked model with the wobbling masses coupled quasi-elastically and strongly damped to each skeletal part. The wobbling masses were modelled as rigid bodies and were able to move and rotate relative to the segment.

Pain (1999) developed a 2-D, four-link wobbling mass model to simulate landings from a drop of 43 cm. With the exception of the foot, the segments had a soft tissue mass attached to them via two translational non-linear spring damper systems.

Modelling the soft tissue movement when simulating dynamic movements such as running jumps is very important and will be done in this study.

Software packages

The simulation models presented in this section have used a number of methods to obtain the equations of motion. Some researchers develop their models from first principles (e.g. Alexander, 1990) and others use computer software packages to develop them (e.g. Sorenson, Simonsen and van den Bogert, 1999 using DADS). The formulation and numerical solution of the equations of motion of a multi-segment mechanical system is not an easy task. Software packages are extremely useful in reducing the difficulty of producing a complex model and also in reducing the chances of making mistakes in the code. Additionally such packages allow the researcher to focus on the biomechanical problem instead of on the numerical methods used (Van Soest, 1992). 'The need for general purpose software packages with which the equations of motion can be derived automatically and solved numerically is growing' (Van Soest, 1992). These simulation packages, however, cannot help with the selection of the structure of the model (Yeadon and Challis, 1994). The following criteria should be used when assessing general purpose software packages for simulation (van Soest, 1992):

- Flexibility
- Accuracy
- User-friendliness
- Calculation speed and numerical effectiveness

Van Soest (1992) compared the packages SPACAR and DADS. Although the two packages are comparable in their general characteristics a number of differences were found to exist between them. SPACAR was used by Van Soest (1992) in the development of a four-segment, planar, rigid body muscle model which was used to investigate the effect of the bi-articularity of the gastrocnemius

muscle on vertical jumping performance. Sorenson et al. (1999) used DADS to calculate the equations of motion for a six-segment 2-D musculo-skeletal model for studying long jump takeoff dynamics and optimisation of performance. It was concluded both packages were accurate.

A further package which is commercially available is Autolev, a symbol manipulation program created to facilitate analysis based on Kane's method (Kane and Levinson, 1996). Autolev can produce Fortran programs in a ready to use format. This relieves the researcher of routine programming tasks. Autolev cannot handle extremely large systems, but it accommodates relatively large systems consisting of ten to twenty bodies without difficulty (Schaechter, Levinson and Kane, 1991). Autolev has been used by, among others, King (1998) in the development of five-segment models of vaulting and tumbling.

Evaluation

The weakness of some simulation models is that the level of accuracy of the model is unknown (Yeadon and Challis, 1994). In order to overcome this, models can be evaluated to test the accuracy and hence gain confidence in the model's capabilities. Many models, however, are not fully evaluated (Pandy et al., 1990; Bobbert, 1988) and this maybe one of their weaknesses. Although the model developed by Pandy et al. (1990) was not quantitatively evaluated, qualitative comparisons between the predictions of the model and previously reported experimental findings were performed. These indicated that the model reproduced the major features of a maximum height squat jump. Van Gheluwe (1981) used computer graphics as a visual comparison between simulation and reality to conclude that simulated and real movement patterns of the body in space were quite similar. This was reinforced by comparing the somersault, tilt and twist angles for the simulated and real movements of a backward twist somersault and a jack-knife backward twist somersault. Hatze (1981) used a planar model to simulate the long jump. The evaluation procedure consisted of the comparison of forces acting on the body during takeoff. The model gives good agreement for the reaction forces, however, the body configurations do not appear to resemble a long jump takeoff (Yeadon and Challis, 1994). Overall, there is little quantitative evaluation of muscle models. In order to thoroughly evaluate muscle models the

model needs to be customised to an athlete, with the simulated performance of the model compared with the same athlete's actual performance. Yeadon and King (2002) evaluated a torque-driven, subject-specific simulation model of tumbling. The model was evaluated using an objective function which represented the difference between the actual performance of the subject and the simulations in terms of strategy and takeoff conditions. The strategy component consisted of configuration and orientation angles at takeoff, and the takeoff components were horizontal and vertical velocity of the centre of mass and the whole body angular momentum. Weightings for each variable in this objective function were set proportional to the inverse of each variable from the actual performance. Simulated Annealing (Corana et al., 1987) was used to vary parameters until the best match between actual performances and simulations was found. These parameters included initial segmental angular velocities and 12 parameters defining the activation time histories of the four torque generators. The objective function used by Yeadon and King (2002) only compares the kinematics. Comparison of the ground reaction forces is not included. A more thorough evaluation would involve the comparison of kinematic and kinetic data.

Optimisation

Optimisation is the maximising or minimising of a function. Optimising the performance of a simulation model can be divided into three parts: (i) formulation of an objective function, (ii) setting of realistic limits for the parameters to be optimised and (iii) deciding upon an algorithm which is capable of minimising or maximising an objective function and finding the global optimum rather than a local optimum.

In simulation models of jumping the objective (or cost) function may simply be the height jumped with the input variables being the kinematics at touchdown and the activation profile of each muscle. Alexander (1990) optimised the approach speed and plant angle using a two-segment model of jumping, in order to achieve maximum height and distance in the high jump and long jump respectively. This was achieved by varying the input values for the simulation. The optimal double layout somersault simulation in the study by Yeadon and King (2002) was defined as the simulation with the correct amount of rotation potential

that maximised the peak height during the flight phase, and was found by varying parameters defining the initial conditions and the muscle activation time histories.

With only two parameters to vary, such as the approach speed and the leg plant angle, it is feasible to consider simulations over a range of values in each parameter and produce contour maps of heights as a function of speed and angle (Yeadon and Challis, 1994). With more parameters, however, the number of simulations required to find the optimal solution increases and mathematical techniques or algorithms need to be employed. Many algorithms capable of maximising or minimising a function are available. The problem with them is that the user has no confidence in them converging at a global and not a local optimum (Goffe, Ferrier and Rogers, 1994). The effectiveness of three popular algorithms will be considered. These are:

- The Simplex method (Nelder and Mead, 1965)
- The Simulated Annealing algorithm (Corana et al., 1987)
- The genetic method (Casius and Van Soest, 1999)

The Simplex method

The Simplex method is an efficient, robust and reliable method for minimising functions (Corana et al., 1987). It is a way of organising the procedure so that (i) a series of combinations is tried for which the objective function increases at each step and (ii) the optimal feasible vector is reached after a number of iterations (Press, Flannery, Teukolsky and Vetterling, 1986). The simplex algorithm uses N + 1 (N = number of unknowns) initial guesses to start the algorithm. The Simplex method is able to follow the gross behaviour of the function despite many local minima (Corana et al., 1987). A problem of the Simplex algorithm that has been identified (Corana et al., 1987; Nelder and Mead, 1965), however, is that due to accepting only downhill solutions there is a risk of getting stuck in a local minimum.

The Simulated Annealing algorithm

The Simulated Annealing algorithm is essentially an iterative random search procedure. It has been identified as a technique suitable for optimisation problems of a very large scale (Press et al., 1986). The Simulated Annealing algorithm starts

at some temperature given by the user. A sequence of points is then generated until equilibrium is approached (Corana, Marchesi, Martini and Ridella, 1987). The process continues until a temperature is reached whereby no more useful improvement can be expected.

The Simulated Annealing method explores the function's entire surface and tries to optimise whilst moving both uphill and downhill (Goffe et al., 1994). At higher temperatures only the gross behaviour of the cost function is relevant to the search. As temperature decreases, further details can be developed to get a good final point (Corana et al., 1987). An advantage of the Simulated Annealing method over most other optimisation methods is that due to the fact the Simulated Annealing method explores the functions entire surface, it is largely independent of the starting value (Goffe et al., 1994). The Simulated Annealing method is much more costly compared to the Simplex algorithm because of the number of function evaluations required (Corana et al., 1987). This greater number of function evaluations is for a single run of an algorithm. When compared to multiple runs needed by other algorithms to test different starting values, the Simulated Annealing method becomes competitive (Goffe et al., 1994). The most beneficial advantage of the Simulated Annealing method is that it is able to find the global optima of functions with an extremely high number of local optima (Corana et al., 1987). Yeadon and Hiley (2000) successfully used the Simulated Annealing algorithm to manipulate the start and end times of the flexion and extension actions in order to investigate why gymnasts flex after passing through the lowest point of a giant circle.

Genetic algorithms

Genetic algorithms find their inspiration in the notion that evolution tends to optimise the genetic material with respect to the environmental demands through a process of variation and selection (Casius and van Soest, 1999). The simulated evolutionary process is started by randomly producing a population of chromosomes (the genetic material) and evaluating the "fitness" of each of these on the basis of the corresponding value of the objective function. An intermediate population is then formed in which the fitter chromosomes appear more often than the less fit ones. A new population is then created through recombination of the

chromosomes in the intermediate population. As these steps are repeated over many generations, the quality of the genetic material is likely to improve, leading to a set of values for the optimisation parameters that (are near) optimal (Casius and van Soest, 1999). In work on maximum squat jumping, Casius and van Soest (1999) found both a simplex and a quadratic programming method were successful in identifying a (near) optimal solution providing reasonable initial guesses were given for the optimisation parameters. However, they found that these algorithms failed on the more complicated problem of counter-movement jumping. Genetic algorithms, which do not need initial guesses did, however, converge to a near optimal solution (Casius and van Soest, 1999). As with the Simulated Annealing method, the genetic algorithm has the disadvantage that it requires many evaluations of the objective function.

Sensitivity analysis

When an optimum solution is found using a simulation model, there is always some uncertainty associated with the values given to the model parameters not included in the optimisation procedure (Yeadon and Challis, 1994). Alexander (1990) found that the optimum techniques for high jumping and long jumping were not sensitive to model parameter values used in the torque generator and was thus able to have confidence in the results obtained.

If a model is not sensitive to model parameter values, this means there is confidence in the model's ability to account for differences in technique. If the model is sensitive to changes in parameter values then a small deviation from the optimum technique may result in a performance which is considerably less than optimum. A sensitivity analysis is therefore of great importance in simulation modelling.

Summary of simulation models

The development, evaluation and optimisation of simulation models has been discussed in this section. A simulation model with torque generators to represent the muscles at each joint would appear to be the best approach for the successful development and evaluation of a subject specific muscle-driven simulation model of jumping. Torque generators which allow co-contraction

would be most suitable in this study. The next section will discuss the parameters required in such a simulation model and the techniques used to obtain them.

Parameter determination

Inertia parameters

Introduction

The accuracy of biomechanical modelling depends upon the extent to which the approximation of the body represents the true anatomical structure. One important set of mechanical properties is body segment parameters (Pearsall and Reid, 1994). In many applications such as the analysis of individual sports performance it is desirable to have a parameter set for the particular individual under study (Yeadon, Challis and Ng, 1993). A number of different methods have been employed to calculate these segmental inertia parameters.

Cadaver studies

First attempts at obtaining body segment inertia parameters began with cadaver studies. These studies consisted of sectioning cadavers into segments and measuring the parameters experimentally: One of the first of these studies was undertaken by Dempster et al. (1955) who used eight male cadavers. After dissecting the body into segments and weighing each one, segment mass centres were determined using a balance plate and moments of inertia were measured using the pendulum method. Other researchers performing cadaver studies include Clauser, McConville and Young (1969) and Chandler, Clauser, McConville, Reynolds and Young (1975). Cadaver studies have the advantage of permitting direct measurement of segment inertia parameters and the moments of inertia can be used to check the accuracy of parameter values determined from other techniques. Disadvantages of cadaver studies are that the samples are generally small and not representative of the population under investigation (Pearsall and Reid, 1994). This type of study has largely been restricted to adult males of caucasian race (Vaughan, 1989).

The use of cadaver data to obtain segmental inertia parameters is not appropriate in this study, as the data would not be subject specific.

Measurement

Measurements of the masses, mass centres and moments of inertia of body segments is quite difficult, particularly in the case of moment of inertia. Several different methods have been proposed, each having limitations.

Researchers have measured segmental volumes using water immersion (Clauser et al., 1969; Drillis, Contini and Bluestein 1964), mass centre locations using reaction boards (Williams and Lissner, 1977), and moments of inertia using techniques such as the quick release method (Drillis et al., 1964). Some methods are restricted in application to only a few body segments; others require an excessive amount of time for the data collection, need expensive equipment or are not administratively feasible (Vaughan, 1989). Difficulties in calculating the moments of inertia of central body segments have been identified (Yeadon and Challis, 1994). Determing inertia parameters experimentally would therefore appear to be impractical for these reasons.

Models

Various models have been used to estimate personalised body segment inertia parameters and can be divided into two main catergories:

- Statistical models
- Geometric models

Statistical models

Statistical models attempt to relate moments of inertia to anthropometric measurements in the form of either ratios or regression equations based on cadaver data (Challis and Kerwin, 1992). Dempster (1955) calculated segment mass as a percentage of subject mass and segment centre of mass location as a percentage of segment length. Linear regression equations developed by Hinrichs (1975) utilised the data of Chandler et al. (1975) to estimate segmental moments of inertia in living subjects. Yeadon and Morlock (1989) used non-linear regression equations, again utilising the data of Chandler et al. (1975). They compared both linear and non-linear approaches for estimating segmental moments of inertia, and concluded that non-linear equations are superior to linear equations and that non-linear equations can provide reasonable estimates of

segmental inertia values even when the anthropometric measurements lie outside the sample range.

Geometric models

Mathematical models which represent the body segments using a number of geometric solids are capable of estimating values of all segmental inertia parameters (Yeadon, 1990b). In general mathematical models require the anthropometric measurements of the subject being modelled. The number of measurements taken depends on the number of solids that the model is constructed from. Hatze (1980) developed a model which consists of 17 segments and computes the parameter values of anthropometric segments from 242 anthropometric measurements taken directly from the subject, this process takes approximately 80 minutes to complete. Using the model, the maximum total body mass error for the subjects tested was found to be 0.32%. Hatze (1980) concluded that, owing to its accuracy, versatility and easy implementation, the model provides a good method of calculating segmental parameter values which would otherwise have to be gained experimentally by a very time consuming process. The inertia model of Yeadon (1990b) comprises 40 geometric solids which are specified by 95 anthropometric measurements. These measurements comprise 34 lengths, 41 perimeter, 17 widths and 3 depths. The time taken to record these measurements is less than 25 minutes for an experienced operator. Using the model, the maximum error of the total body mass estimates was found to be 2.3%. Yeadon (1990b) considered this error to be quite reasonable. The model was designed to produce personalised segmental values for input into a simulation model and it was considered adequate for this purpose providing there is good agreement between simulations and actual performance. The two models described require the direct acquisition of anthropometric measurements from the subject to be modelled. Jensen (1978) however, used an alternative method. He obtained the dimensions of the solids by digitising images of the subject from photographs. This method is known as photogrammetry. Photogrammetry has been demonstrated to be both a practical and reliable method for determining the shape and volumes of body segments from which mass and inertia properties may be estimated (Pearsall and Reid, 1994). Baca (1996) developed a method for the

precise determination of anthropometric dimensions from the video analysis of four different body configurations. An automated system was used to estimate 220 of the 242 measurements required for the geometric model of Hatze (1980). The parameter values computed did not differ much from those based on direct anthropometric measurements. Although it is possible to obtain anthropometric measurements by digitising video images, it is preferable to obtain direct measurements of the athlete where possible, as it is more accurate.

Gamma mass scanning

Gamma mass scanning is based on the principle that a gamma radiation beam becomes less strong as it passes through a substance. If the intensity of the beam before and after it passes through the substance is measured one can calculate the mass of the material. This method has been used by, among others Brooks and Jacobs (1975) and Zatsiorsky and Seluyanov (1983). Brooks and Jacobs (1975) passed gamma radiation from a cobalt-60 source through the object in ¼ inch segments. Legs of lamb were selected as the specimens, and the mass, centre of mass and moment of inertia were all calculated. Validation of the gamma mass scanner was performed by comparing results obtained by the scanner with results obtained by the reaction board and pendulum techniques. The results for the mass, centre of mass and moment of inertia were found to be within 1%, 1.7% and 2.1% respectively of values calculated using scales and the reaction board and pendulum techniques. Zatsiorsky and Seluyanov (1983) performed this technique on living subjects, in order to calculate the inertia parameters of 10 segments of the body. Although accurate this method is difficult to employ due to its requirements and is therefore not suitable for this study.

Computed tomography/magnetic resonance imaging

Computed tomography (CT) provides a method for obtaining criterion density and inertial measurements in vivo. Aukland, Henson and Bailey (1988) established the validity of the uniform density assumption for the leg segment and the ramifications for the subsequent computation of segment inertial parameters. Estimates for leg segmental parameters obtained using a modelling procedure based on the method of Jensen (1978) and employing either cadaver derived or

CT measured values were compared. The study showed that density is not uniform throughout the leg segment. However, the adoption of this assumption when modelling the human body was shown to produce only minor errors in the estimation of inertial parameters for the leg segment. A different result may however have been recorded for other body segments.

Mungiole and Martin (1990) used magnetic resonance imaging (MRI) to provide accurate estimates of segmental inertia parameters. It has been suggested that MRI may offer a greater contrast between various soft tissues than CT scanning can. This may be useful in determing subject specific parameters for wobbling masses included in models. A further advantage of MRI over both CT and gamma scanning is that it is not based on radiation. However, such techniques as CT and MRI are not widely available and are expensive. In addition there may be potential ethical and medical problems associated with such techniques.

Another method of determining body inertia parameters is the method of dual-energy x-ray absorptiometry (DEXA). Compared to earlier dual-radiation absorptiometers (DPA), DEXA makes use of x-ray tubes to enable greater precision, resolution and speed (Fuller, Laskey and Elia, 1992). In addition to this DEXA is safe because the radiation dose for a whole body scan is < 5 mrem, it is also quick (20-35 minutes for a whole body scan) and requires little co-operation from the subject (Roubenoff, Kehayias, Dawson-Hughs and Heymsfield, 1993; Blake and Fogelman, 1997). DPA were developed originally to assess skeletal muscle mass in vivo, whole body and segmental. In addition to this, however, DEXA can also determine bone and soft tissue composition (Fuller et al., 1992). This may be useful in the determination of wobbling mass parameters values (e.g. the ratio of soft tissue to bone) for the use in wobbling mass models.

The fundamental physical principle behind DEXA is the measurement of the transmission through the body of x-rays with high and low photon energies. Because of the dependence of the x-ray attenuation coefficient on atomic number and photon energy, measurement of the transmission factors at two different energies enables the area densities (i.e mass per unit projected area) of two different types of tissue to be inferred. In DEXA these are taken to be bone mineral and soft tissue (Blake and Fogelman., 1997).

Disadvantages / limitations of DEXA include measurements of the soft tissue being sensitive to hydration and measurements of the bone being sensitive to the anterior posterior thickness of the body. In addition it is not known whether DEXA instruments from different manufacturers offer directly comparable measurement of soft tissue.

The geometric models which have been looked at allow the inertia parameters to be customised to the individual. The use of the model of Yeadon (1990b) to calculate segmental inertia parameters from measurements taken on the subject has been shown to be accurate at predicting whole body masses and requires less than 25 minutes of contact time with the subject. As contact with the subject is possible, this method would appear to be the most appropriate. The use of CT and MRI although appearing to be successful in predicting accurate parameters is less practical at present.

Wobbling mass inertia parameters

The values for the lengths, masses and moment of inertias of both the rigid and wobbling mass parts in wobbling mass models have been obtained from experimental and theoretical estimations by matching simulation ground reaction force curves to the actual vertical ground reaction force curves obtained from a subject. The method used by Gruber et al. (1998) for calculating anthropometric parameters resulted in ratios of bone mass to soft tissue mass much greater than would be found in an actual human (Pain, 1999). Pain (1999) calculated subject-specific anthropometric parameters to be used in a simulation model in several ways. The mass of the shank and thigh were divided into the bone mass and the soft tissue mass for each link using data from Clarys and Marfell-Jones (1986) and Clarys, Martin and Drinkwater (1984). The moments of inertia for the bone and the soft tissue were calculated by modelling the bone and the soft tissue as geometric shapes. The model was found to successfully reproduce the vertical ground reaction force for the first 80 ms of the landing. The joint torques and forces calculated in the model were lower than in rigid body models and this was considered to be more accurate. This decrease in forces and torques in the joints was not found to be as drastic as that found by Gruber et al. (1998).

Spring parameters

Wobbling mass

The forces and torques between the skeletal and wobbling parts of a segment have been modelled in a variety of different ways. Cole, van den Bogert, Herzog and Gerritsen (1996) used a linear spring to connect the wobbling mass to the rest of the body. More recently however it has been argued that a non-linear spring is a more realistic representation (Gruber et al., 1998). Denoth et al. (1985) modelled the forces and torques between the two bodies using a quasi-elastic damped interaction of the form:

$$F_{sw} = a(\Delta r_{sw})^3 + b(\Delta r_{sw})(\Delta \dot{r}_{sw})$$

Where:

r_{sw} = displacement of the skeletal and wobbling parts

Pain and Challis (2001) also used non-linear springs to connect the wobbling masses to the rigid segments. They determined the stiffness and damping parameter values through optimisation. This involved matching the movement of the wobbling masses, in terms of magnitude and frequency, as closely as possible to actual wobbling mass movement determined experimentally. Non-linear springs of this form would appear to be a good representation of how wobbling masses move in a simulation model.

Ground/Surface

Contact forces can often be included by modelling the contact as a kinematic connection, similar to a joint. It may, however, be more realistic to model the contact by a force deformation model, especially when simulation results are compared to experimental force measurements (Van den Bogert and Nigg, 1999) as in this study. Experimental measurements from drop tests with a human heel (Misevich and Cavanagh, 1984) suggest that the force acting on the heel depends on the deformation, x(t) and on the velocity of deformation $\dot{x}(t)$. The heel pad therefore has visco-elastic properties.

A very simplistic mathematical description of human tissue is,

$F = -kx(t) - r\dot{x}(t)$. Where k and r are constants.

Yeadon and King (2002) modelled the foot-ground interface in this way, where both the vertical and horizontal forces were proportional to the spring displacement in that direction. Yeadon and King (2002) determined stiffness and damping parameters (k and r) of the elastic interface between the simulation model and tumbling track for a layout somersault performance by minimising the difference between actual and simulated performances in terms of strategy, elasticity of the track and takeoff components, as used in the procedure used to evaluate the model using the Simulated Annealing Algorithm (Corana et al., 1987). The stiffness and damping parameters obtained were then fixed and used as independent estimates for evaluating the simulation model.

In real life, contact between two surfaces can rarely be described using a linear spring (Nigg, 1999). Usually two materials do not behave like linear springs. A more sophisticated non-linear approach to modelling the foot-ground interface was employed by Nigg and Liu (1999):

$$F = A_c[ax(t)^b + cx(t)^d \dot{x}(t)^e]$$

Nigg and Liu (1999) determined the values of the parameters a, b, c, d and e using a least squares fit procedure to fit the simulated force-deformation curves to experimental data.

A multiplicative surface model in which the vertical force-deformation characteristics of heel-pad, shoe and ground were modelled by one non-linear visco-elastic element by Gerritsen et al. (1995) (Figure 2.1).

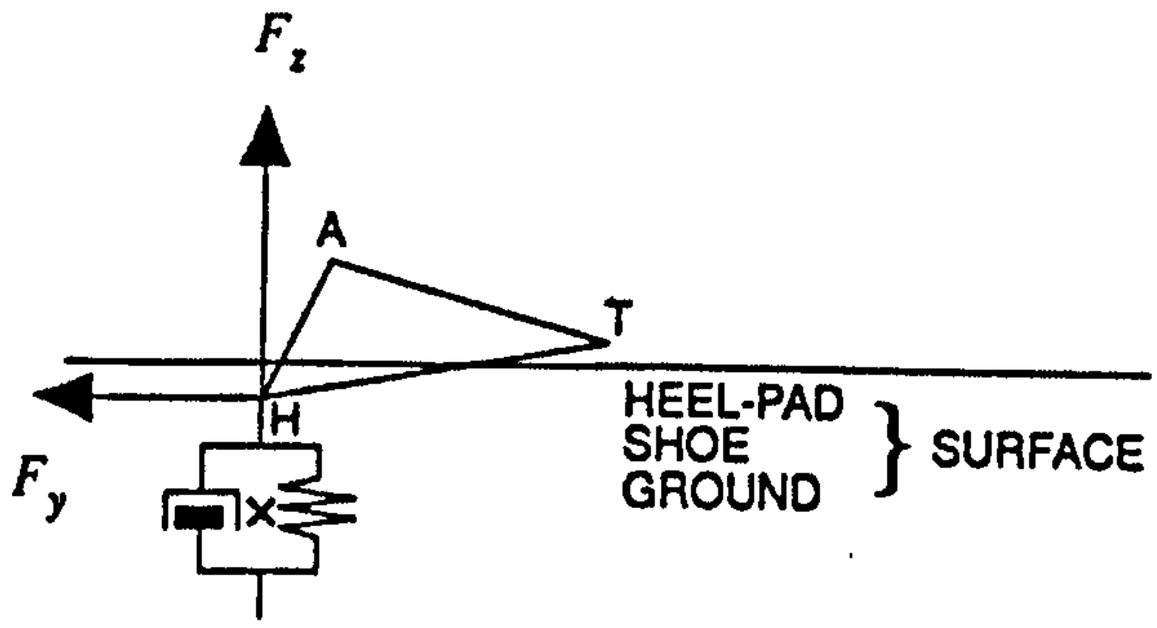

Figure 2.1. Schematic representation of the multiplicative surface model (taken from Gerritsen et al., 1995).

As with the wobbling mass, a non-linear spring equation would appear to be most realistic.

Muscle parameters

Introduction

According to Chapman (1985), the mechanical components of muscle include the contractile component (CC), the series elastic component (SEC) and the parallel elastic component (PEC). The contractile component represents the behaviour of the force generating process in the muscle described by the characteristic force-velocity and force-length relationships (Hill, 1938; Wilkie, 1968). The series elastic component and the parallel elastic component represent the behaviour of groups of anatomically distributed elastic structures according to their geometric relationship with the contractile component. Structures in series with the contractile component transmit the force of a muscular contraction. Structures in parallel are not brought under tension by contractile forces but carry passive tension across a joint whether the muscle is active or inactive.

Current evidence suggests that the system can be represented by two components, a contractile and series elastic component. The contractile component is the component which produces force as a function of its degree of activation, its velocity of shortening, its instantaneous length and the history of events preceding the time when the force is observed. The series elastic component behaves as a linear spring-like element which is lightly damped. The series elastic component is composed of tendinous tissues, which includes the tendon and other elastic structures such as the aponeurosis. A maximal stretch of 4% of the tendon under isometric conditions has been reported (Dixon, 1996; Bobbert, 1988). This stretch, however, does not take into account the other elastic structure with the series elastic component, which may have a considerable effect. Several studies have reported that elastic strain of the tendon and aponeurosis differs (Ettema and Huijing, 1989). More recently, Muramatsu, Muraoka, Takeshita, Kawakami, Hirano and Fukanaga (2001) found the maximal strain of the tendon and aponeurosis in the human gastrocnemius, estimated separately from the elongation data was 5.1 ± 1.1% and 5.9 ± 1.6% respectively. Muraoka, Kawakami and Fukunaga (2001) reported values of between 3 and 5% for

maximal tendon strain and 6 and 7% for maximal aponeurosis strain during isometric conditions. There is little support for the inclusion of a PEC in a model of human muscular contraction within the normal working ranges of the joints. However, if movement is outside this range a parallel elastic element maybe necessary.

Series elastic component parameters

Different methods have been employed to determine the stiffness of the series elastic components within the human body. These methods have included experimental approaches (Shorten, 1987; Hof, 1998) and those which have relied on data from the literature (King, 1998). Hof (1998) measured the force-extension characteristics of the series elastic components of the human triceps surae muscle in vivo by means of a hydraulic-release ergometer. The average maximum stiffness value was estimated to be 430 $Nmrad^{-1}$. King (1998) modelled the series elastic components as a linear spring with a natural length of zero. Lengths of muscles, tendons and moment arms were estimated from the literature. Maximum joint torques were estimated from the experimental testing using an isokinetic dynamometer. A 4% stretch of the tendon was assumed and this was equivalent to an angle extension. The stiffness was then calculated from this extension and the maximum joint torques. An ankle plantar flexion stiffness of 469 $Nm.rad^{-1}$ was calculated. King (1998) performed a sensitivity analysis that showed the model was not sensitive to the stiffness of the series elastic component.

The method used by King (1998) is less complex and time consuming than the experimental approaches, but still gives similar results. This approach is most suited to the present study.

Contractile component parameters

Force-velocity relationship

'The variation in muscle force as a function of shortening (concentric) or lengthening (eccentric) velocity, the so-called force-velocity relationship, is a fundamental characteristic of skeletal muscle' (Westing, Seger and Thorstensson, 1990).

Fenn and Marsh (1935) were the first to demonstrate that there exists a relationship between active force and velocity of shortening of a muscle. Hill (1938) further characterised the force-velocity relationship and he emphasised the importance of it in the study of muscle function. It has been demonstrated (Huxley, 1957) that this relationship is consistent with the cross-bridge mechanism of muscle contraction. Different equations have been used for the concentric phase of the force-velocity curve. One equation is that proposed by Hill (1938) which fits part of a hyperbola to the curve:

$$V = (Po - P)b / (P + a)$$

Where:

V = velocity, P = force, Po = isometric force, a, b = constants

Wilkie (1968).

The maximum speed of shortening (V_{max}) occurs when the load is zero. The maximum force is developed during the eccentric phase, that is, when the muscle is lengthening. The force developed during concentric contraction is defined by a hyperbolic curve (Figure 2.2.) The ratio of maximum eccentric torque to isometric torque is essentially constant, at a value of between 1.2 and 1.5 (Harry, Ward, Norman, Heglund, Morgan and McMahon, 1990). Alexander (1990) assumed the ratio between these two values to be 1.5.

Hill (1938) found there to be a discontinuity of slope in the force-velocity curve at the point where the velocity goes from positive to negative i.e from concentric to eccentric. The increase of tension above isometric required to produce a given small speed of lengthening is much greater than the drop in tension which allows an equal speed of shortening. Katz (1939) investigated this further and his curves show that the slope of the force velocity curve is about six times greater for lengthening than for slow shortening. Harry et al., (1990) performed a relatively simple set of force-velocity experiments on isolated, whole frog sartorius muscle in order to compare experimental force-velocity data at high velocities to that obtained from models of cross-bridge cycling. During the experiments they found this discontinuity in the slope at zero velocity was apparent. They measured a slope 3.9 times greater for slow lengthening than for slow shortening. These two experimentally obtained values can be compared to

the theoretical value of 4.3 which Huxley (1957) predicted with his original model.

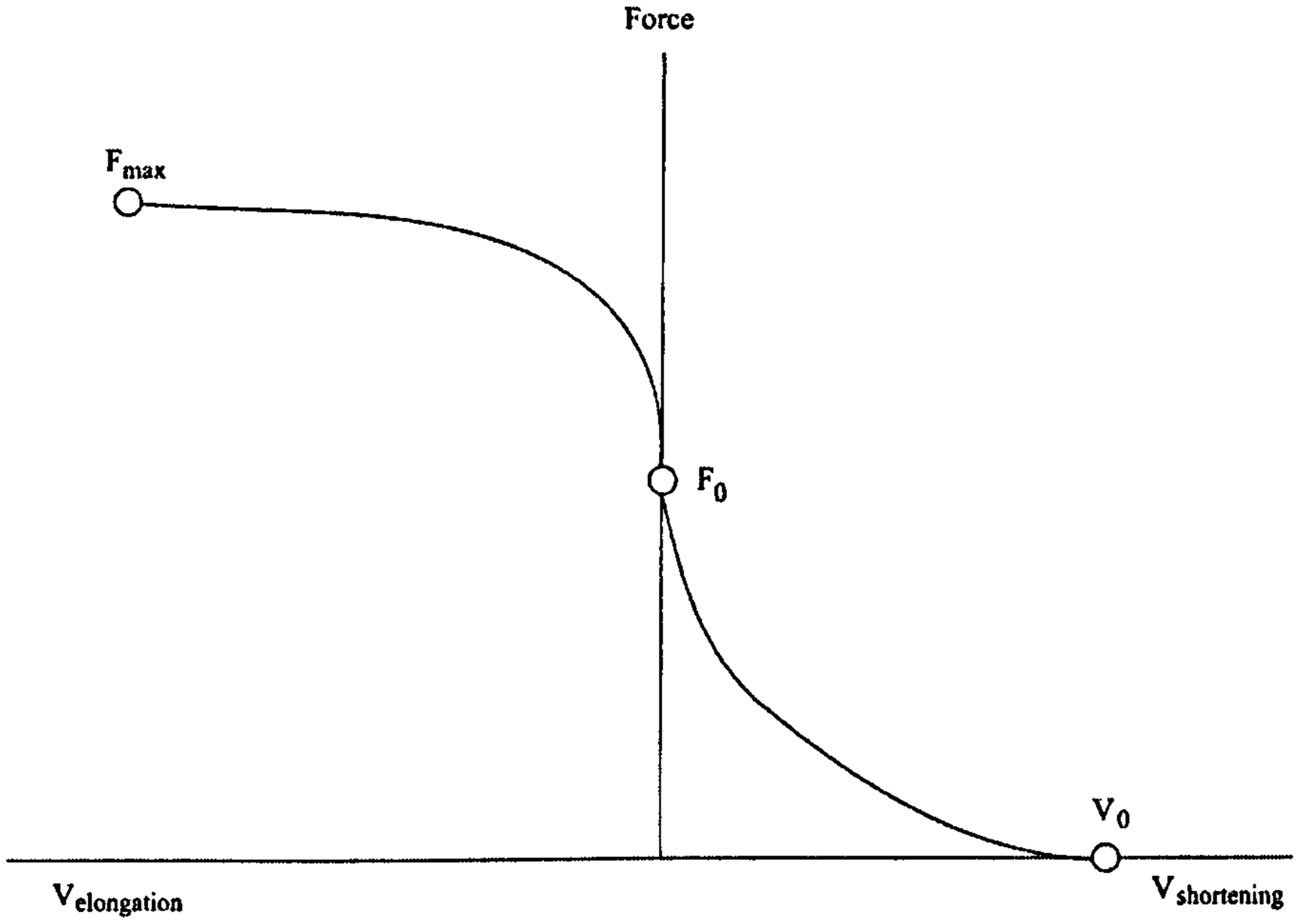

Figure 2.2. The force-velocity relationship for muscle fibres (adapted from Herzog, 2000 p.24).

Edman (1976) demonstrated that the force-velocity relationship has a more complex shape than that which had been previously observed in whole muscle. Edman (1976) found that the force-velocity relationship of single muscle fibres contains two distinct curves each with an upward concavity. The two curves are located either side of a 'breakpoint' which is close to 78% of maximum isometric torque.

Experiments have confirmed (Edman, 1988) that below this 'breakpoint' of approximately 78% of maximum isometric torque there exists a hyperbolic nature of the force-velocity relationship as previously observed (Hill, 1938). The force-velocity relationship, however, undergoes a clear change as the load is raised above this 'breakpoint'.

Force-length relationship

'A muscle's capacity to produce force depends on the length at which the muscle is held, maximum force being delivered near the length that the muscle normally takes up in the body' (Edman, 1992).

When a muscle is stimulated at a variety of lengths, the resulting tension is small at extremes of length and maximal in between these extremes (Chapman, 1985). A characteristic bell shaped curve exists between tension and length. The change in force attained has been explained as being due to the varying number of cross-bridges which can become united between the actin and myosin filaments at different lengths of the sarcomere.

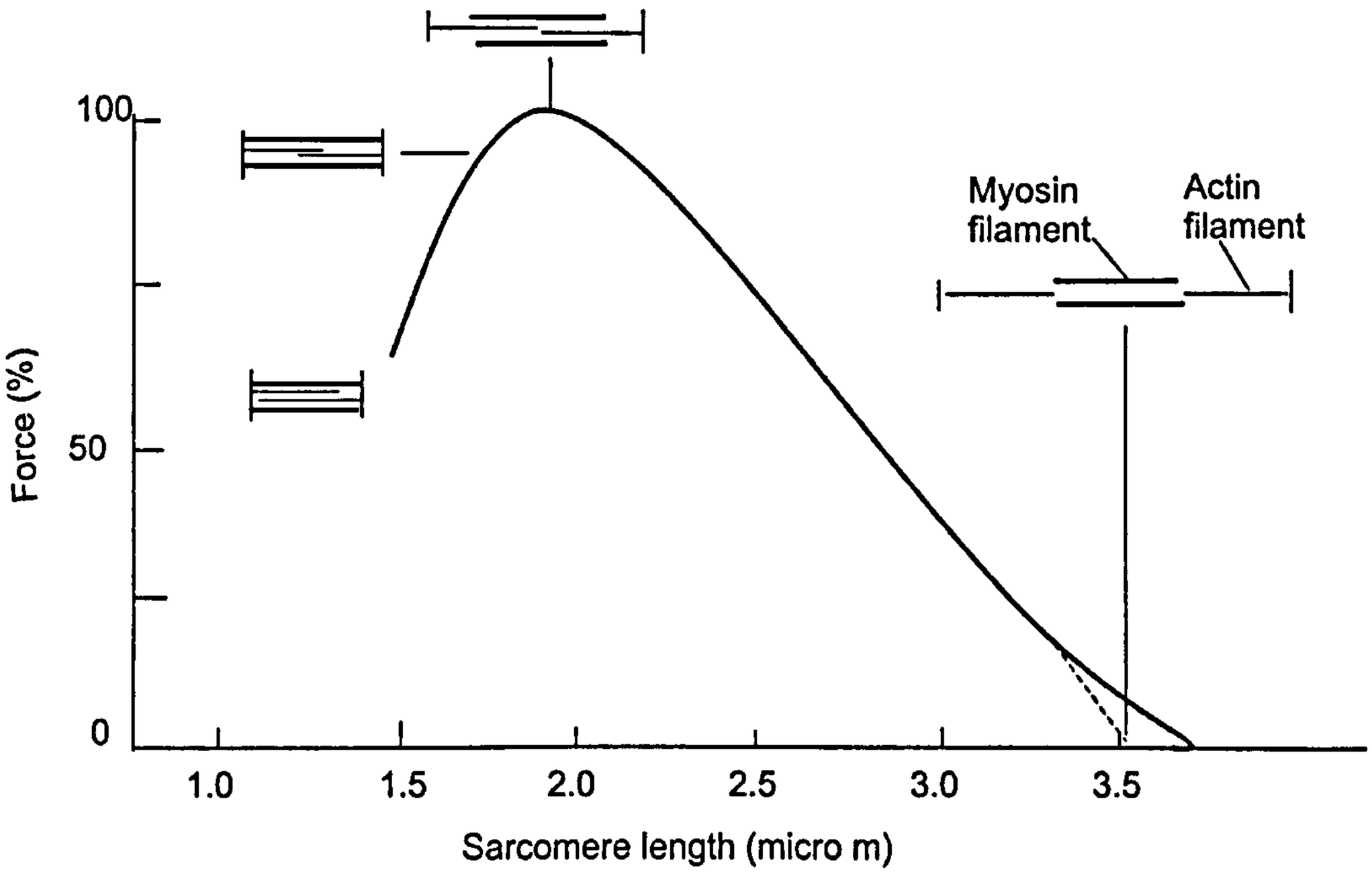

Figure 2.3. The force/length relationship for muscle fibres (adapted from Edman, 1992, p.103).

Lieber (1992) described three parts to the length-tension (or force) curve for isometric contraction; The descending limb, the plateau region and the ascending limb. The descending limb is concerned with sarcomere lengths greater than the optimum. Investigations showed that at a length of 3.65 μm, the muscle developed no active force. This is because there is no overlap of the myosin and actin filaments. Increasing force with decreasing sarcomere length occurred until the muscle reached a sarcomere length of 2.2 μm, at which point the plateau

region was reached. Between 2.0 and 2.2 μm, the muscle force remained constant.

It is clear both the force-velocity and force-length relationships discussed here have a great bearing on the overall performance and strength of muscles in the human body. These two relationships, or the angular equivalent, will be used in this study to determine a function defining the torque produced at a joint.

King and Yeadon (2002) describe a method for determining the maximum torque that can be produced at a joint from isovelocity torque measurements on an individual. An 18-parameter exponential function was fitted to the experimental isovelocity joint torque / angle / angular velocity data. This resulted in a surface that was well behaved over the complete range of angular velocities and within the specified range of joint angles. The torque / angular velocity relationship of the contractile component was modelled using a six parameter exponential function:

$$T = \frac{a + be^{p\omega}}{(1 + ce^{p\omega})(1 + de^{q\omega})}$$

where:

a, b, c, d, p and q are positive constants, $a > b/c$, ω = angular velocity, T = torque.

Each parameter was then expressed as a quadratic function of the joint angle to give angle dependence. This resulted in 18 parameters defining the function. The parameters were calculated by minimising the sum of the squares of differences between the measured torque values and the exponential function using the Simulated Annealing Algorithm (Corana et al., 1987). The exponential function had previously been tested by fitting it to the force-velocity data obtained for a single fibre (Edman, 1988).

An advantage of using an exponential is that it can be fitted to the whole torque / angular velocity relationship as opposed to using two separate functions. A disadvantage, however, is that it does not allow for a discontinuity in slope at zero angular velocity.

Individual muscles

As already discussed the task of modelling muscle is complex. To attempt to model the detailed architecture of individual muscles may appear very daunting. The extreme complexity of simulation models which include individual muscles makes it almost impossible for the muscle parameters to be determined experimentally. In order to obtain these muscle parameter values, individual muscles need to be isolated and this is not possible with living subjects. A method which does not rely on muscle parameter values from the literature is required so that the model can be customised to the individual.

Torque generators

Although modelling all the muscles around a joint as a single torque generator is a great simplification, it has the major advantage that it is possible to experimentally determine the net force capability of the muscles around a joint and hence be able to evaluate the model quantitatively by comparing the performance of the model with the individual's own performance (Yeadon and King, 2002).

Isokinetic dynamometry

To determine muscle properties such as force-velocity and length-tension relationships, researchers have used isokinetic dynamometers where the forces exerted by muscles at a joint can be determined using resultant joint moments (Herzog, 1988). The term isokinetic dynamometer is perhaps slightly misleading and isovelocity may be a more appropriate term which will therefore be used throughout this section. Isovelocity dynamometers have the advantage of recording the joint moment of force at the same time as the contracting muscles cause the joint to rotate at a pre-determined angular rate (Winter, Wells and Orr, 1981). Froese and Houston (1985) used a Cybex dynamometer to measure maximal torque values at controlled angular velocities during extension of the right knee from full flexion to full extension. Maximum isometric torque was measured at a knee angle of 65°, and dynamic torque was measured at angular velocities of 45, 90, 135, 225, and 270°s^{-1}. King (1998) determined contractile element parameters for ankle plantar flexion, knee extension, shoulder flexion and

shoulder extension. The first part of the process of the parameter determination involved the collection of maximal torque data from a Kin-com isovelocity dynamometer. The trials consisted of two repetitions of concentric-eccentric exercise at pre-set angular velocities. The range of angular velocities used varied from $20°.s^{-1}$ to $250°.s^{-1}$, with the sequence being 20, 20, 50, 100, 150, 200, 250, 250, 250, 20, $20°.s^{-1}$. Performing two repetitions at each angular velocity allowed the data to be edited in order to retain the central eccentric-concentric section only in an attempt to ensure that the subject had reached maximum voluntary activation.

Interpreting the results from an isovelocity dynamometer can present numerous difficulties. It has been recognised (Sapega, Nicholas, Sokolow and Saranti, 1982; Winter et al., 1981) that the moments obtained using isokinetic dynamometers are not the same as the joint moments. There are three main areas of concern which have been identified as being responsible for these differences. These are:

- Gravitational effects
- Errors due to the control of the lever arm angular velocity (inertial effects)
- Non-rigidity of the limb/lever system

Gravitational effects

Uncorrected joint moments due to gravitational force acting on the leg whilst using an isovelocity dynamometer can (i) introduce errors into calculations of mechanical work and (ii) substantially alter the value of the knee moment recorded during flexion or extension. King (1998) corrected for gravity using the equation:

$$Tc = Tc \pm Mgd_j\cos\theta$$

Where:

Tc = crank torque

M = mass of the limb

d_j = perpendicular distance from mass centre location to joint centre

θ = crank angle relative to the horizontal

The mass and mass centre locations for each limb were calculated from anthropometric measurements taken on the subject using the mathematical model

of Yeadon (1990b). Many systems now contain an automatic correction for gravity, but it is unclear how accurate they are.

Errors due to the control of the lever arm angular velocity (inertial effects)

A further limitation of the isokinetic dynamometer's control of the lever arm angular velocity has resulted in the production of artefacts within the torque time histories, and these are most prominent when testing proximal joint motions in which a larger moving limb mass and longer levers are involved (Sapega et al., 1982). Torque overshoot is most likely to cause misinterpretation of an isokinetic record if 'peak torque' is used as a measure of strength. Inertial moments affect the peak moment development during the initial acceleration period at high velocities of isokinetic testing and therefore these effects should be considered in order to obtain valid results in isokinetic dynamometry (Iossifidou and Baltzopoulos, 1998).

Non-rigidity of the limb/lever system

In addition to the gravitational effects and the error in the control of the lever arm angular velocity there are other sources accountable for the differences in the moments calculated (Herzog, 1988). One of these results from the assumption that the crank arm and the limb lie parallel to each other. Kinematic data obtained from devices such as the Biodex and Cybex dynamometers pertain to the lever arm being moved by the subject and not necessarily to the limb in motion or to the activated muscles (Taylor, Sanders, Howick and Stanley, 1991). To avoid this problem, King (1998) used a goniometer to obtain the time histories of the joint angle and angular velocity. An optimisation procedure was then used in each trial to synchronise the crank angle (from the dynamometer) and the joint angle time histories.

Sub-maximal force production during eccentric contractions

Another possible problem associated with isovelocity dynamometers identified by James, Sacco, Hurley and Jon (1994) is the uncertainty as to whether the subject is performing maximal contractions. That is, is the subject able to achieve full muscle activation by voluntary effort over the whole range of

movement? No evidence for sub-maximal force production was found, during isometric contractions and slow dynamic contractions the voluntary forces were often greater than those obtained by electrical stimulation (James et al., 1994).

In disagreement with these results Westing, Seger, Karlson and Ekblom, (1988) found eccentric torque-velocity results deviated from those predicted values based on in-vitro experiments. The main difference was the lack of an appreciable increase in torque output over the isometric level and a lack of increasing torque with increasing speed of lengthening. One reason suggested as to why large increases in torque didn't occur with increasing velocity is that a neural mechanism might become active during maximal contractions, thus restricting the maximal tension in a muscle by an inhibitory feedback loop (Westing et al., 1988). It is believed (Westing et al., 1988) that such a tension-restricting mechanism is present to maintain safe tension during isometric and low velocity concentric contractions, above which tension is not normally allowed to rise. In agreement with this, Westing, Seger and Thorstensson (1990) examined the effect of electrical stimulation on torque output during knee extension and found that a torque higher than voluntary could be achieved by applying electrical stimulation on a relaxed quadriceps muscle. They also found that the same procedures did not cause any increase in torque under concentric or isometric conditions. It was concluded that maximal voluntary knee extension does not appear to represent a truly maximal utilization of the torque producing capacity (Westing et al., 1990). In addition, Westing et al. (1988) reported that most subjects felt it was more difficult to perform the eccentric tests, and that the difficulty of movement execution increased with increasing eccentric velocity.

Muscle activation time histories

The majority of muscle models assume the control of the muscle is bang-bang, but as already stated the ability to vary the activation time history instead of having a fixed ramp time is a major advantage. The determination of muscle activation time histories is difficult to achieve experimentally. Some information can be obtained through the use of EMG, but in order to obtain actual activation timings another method has to be employed. Yeadon and King (2002) determined 12 muscle activation parameter values for the 4 torque generators in their model

through optimisation using an evaluation procedure. The evaluation procedure minimised the difference between actual and simulated performances using the Simulated Annealing Algorithm (Corana et al., 1987). The three parameter values at each joint defined the minimum activation level, the time the activation began to ramp up and the time taken to reach full activation.

Freund and Budingen (1978) examined the speed of the fastest possible voluntary contractions for several hand and forearm muscles under isometric and isotonic conditions. The duration of the contractions (ramp time) was measured from onset to peak torque. They determined a theoretical regression line for the contraction time of 100 ms. Experiments by Freund and Budingen (1978) were also performed on the calf of one subject. The contraction duration times were in the 80-90 ms range. Bobbert and van Zandwijk (1999) calculated the rise (or ramp) time defined as the time taken for the signal to increase from 10% to 90% of its peak value the to be 90-112 ms for joint moments.

The maximum activation a muscle can have prior to ground contact is a contentious issue. Kovacs, Tihanyi, Devita, Racz, Barrier and Hortobagyi (1999) found this pre-ground contact level of activity could be up to 80% of maximum activation. This value is probably a bit high and a value of around 50% may be a more sensible maximum initial value.

Inverse dynamics

In addition to using isovelocity dynamometers to determine joint moments/strength parameters, many researchers have used kinetic and kinematic data and performed inverse dynamics analyses in order to determine joint moments (Bobbert and van Ingen Schenau, 1988; Ridderikhoff, Batelaan and Bobbert, 1999; Johnson and Buckley, 2001). In inverse dynamics, the moment at each joint is determined by combining the segmental and joint kinematics, anthropometric measures and external forces. Muscle power can then be calculated as the product of the joint moment and the joint angular velocity. Inverse dynamics is considered to be one of the most important techniques in biomechanics to determine the mechanical work produced by a subject during a movement (Nagano, Gerritsen and Fukashiro, 2000).

Johnson and Buckley (2001) used inverse dynamics analyses to investigate muscle power patterns in the mid-acceleration phase in sprinting. They modelled the thigh, shank and foot segments as rigid bodies and estimated the mass, centre of mass location and moment of inertia of each segment using the regression equations reported by Drillis et al. (1964). Nagano et al. (2000) compared two methods of inverse dynamics in terms of their sensitivity to errors introduced by the locating of anatomical landmarks. The first, which calculates the work produced by muscles at a specific joint is known as the rotational method and the second, known as the translational method, calculates the amount of work produced between adjacent segments rather than the work produced at a joint. It was concluded that the translational method was less sensitive to errors in the location of joint centres and in the location of the centres of mass of the body segments. The rotational method was found to be particularly sensitive to errors in joint centre locations.

Summary of parameter determination

Techniques for the determination of both inertia and muscle parameters have been discussed. The use of the model of Yeadon (1990b) to calculate segmental inertia parameters from measurements taken on the subject would appear to be the most appropriate for this study The use of an isovelocity dynamometer in the determination of strength parameters is an extremely useful method, but one in which care must be taken to ensure accurate values are recorded. Isovelocity dynamometry and torques determined using the angle-driven models (Chapter 6) will be used in the present study in order to obtain the most accurate values possible for joint torques.

Summary

The literature reviewed in Chapter 2 has covered five main sections. The first section has described jumping activities. The second section has focussed on the techniques of investigation which may be used in this study. The remaining sections have addressed all aspects involved in the development and utilisation of a computer simulation model of dynamic jumping in order to answer the questions

posed in Chapter 1. These sections are data collection and analysis techniques, simulation modelling and parameter determination.

The next chapter focuses on the development of simple one and two-segment models of jumping.

CHAPTER 3

SIMPLE SIMULATION MODELS

Introduction

The purpose of this chapter is to:

(a) Investigate the extent to which simple models can be used to assess elite jumping performance.
(b) To gain general understanding of the mechanics of dynamic jumps.

The ability to jump high or long is dependent on a number of factors. As already discussed in the previous chapter, these factors include: the approach parameters, the strength characteristics of the athlete and the athlete's anthropometric parameters. Although simple models dramatically simplify the human body and its motion, such models are used by researchers to replicate the general movement during a dynamic jump (Alexander, 1990). This section will answer the question: "Is a simple one or two-segment model sophisticated enough to be able to assess elite performance of a jumper in terms of predicting realistic approach parameters and heights reached from realistic model parameters?"

One-segment model

Introduction

The one-segment model is the simplest model that can be used in simulating dynamic jumping movements. Such a model was developed in order to simulate the takeoff phase in high jumping. The model comprises a single rigid rod representing the leg, with the whole body mass concentrated at one end of the segment, and a spring attached to the end in contact with the ground. The peak height that the centre of mass was able to reach in the flight phase was calculated. The plant angle ϕ is the angle between the horizontal and the line joining the mass centre to the fixed point of contact O (Figure 3.1). The approach speed is the horizontal velocity of the mass centre immediately before contact of the foot with the ground.

Table 3.1. Input and output variables of the one segment model.

INPUT VARIABLE	Symbol	OUTPUT VARIABLE	Symbol
plant angle	ϕ	time of contact	t
horizontal velocity	$\dot{x}_0$	horizontal velocity at takeoff	$\dot{x}$
vertical velocity	$\dot{z}_0$	vertical velocity at takeoff	$\dot{z}$
spring depression	x_s, z_s	vertical height of mass centre at takeoff	z

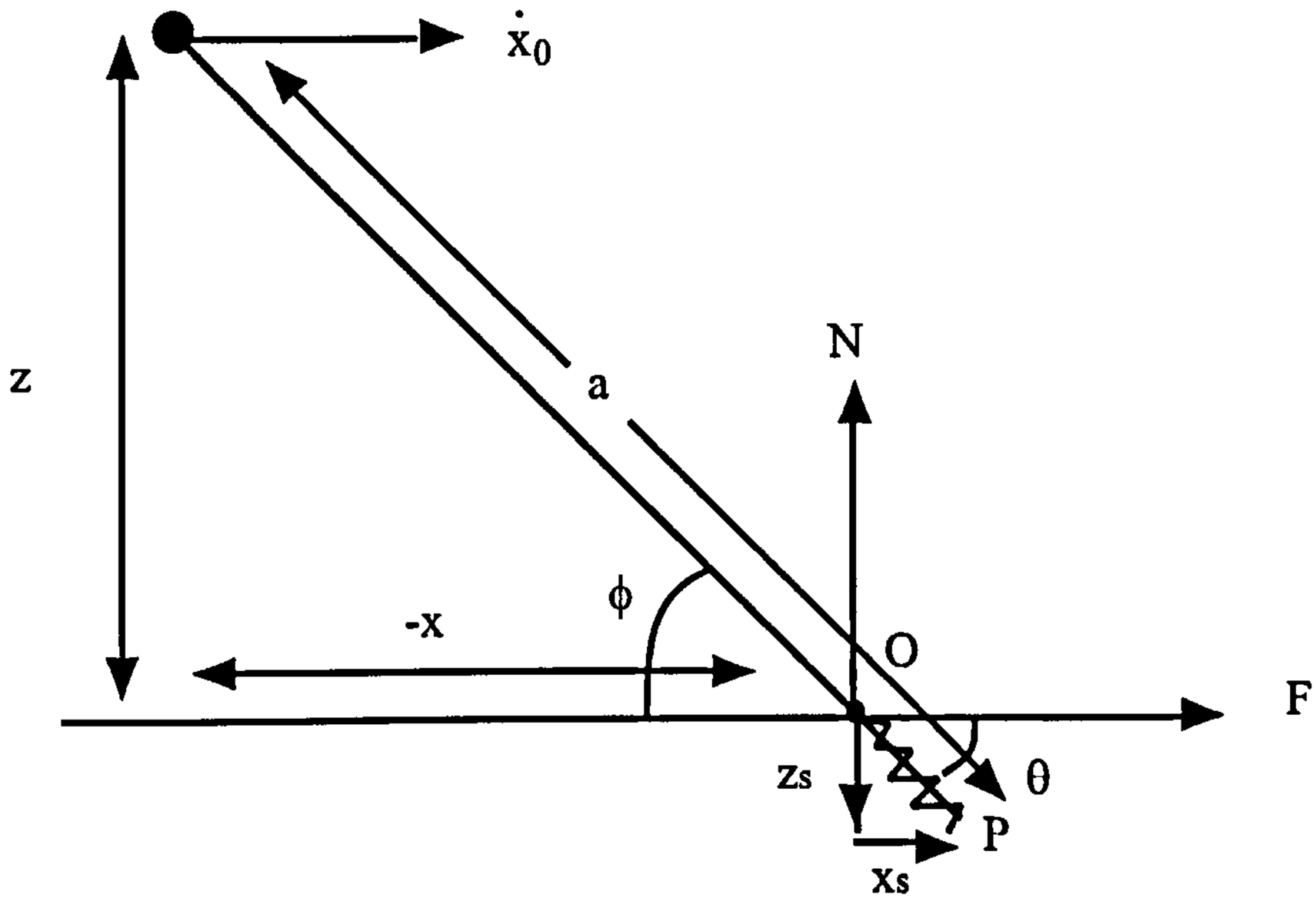

Figure 3.1. A graphical representation of the one segment model.

Methods

In order to simulate the model's contact with the floor a Fortran program was written which enabled the user to calculate the kinematics of the mass centre at the instant of takeoff. These data were subsequently used with equations of constant acceleration to calculate the height or distance that could be reached by the centre of mass in the following flight phase.

Using basic trigonometry, the position of the mass centre in the horizontal and vertical direction from fixed point O was calculated:

$$x = x_s - a\cos\phi$$

$$z = z_s + a\sin\phi$$

Differentiating to find $\dot{x}$ and $\dot{z}$:

$$\dot{x} = \dot{x}_s + a\sin\phi.\dot{\phi}$$

$$\dot{z} = \dot{z}_s + a\cos\phi.\dot{\phi}$$

Differentiating again to find $\ddot{x}$ and $\ddot{z}$:

$$\ddot{x} = \ddot{x}_s + a\sin\phi.\ddot{\phi}. + a\cos\phi.\dot{\phi}^2$$

$$\ddot{z} = \ddot{z}_s + a\cos\phi.\dot{\phi} - a\sin\phi.\dot{\phi}$$

T = tension in spring

$$T = kr_s \qquad \text{where } r_s = \text{extension in spring}$$

$$F = -k_x x_s$$

$$N = -k_z z_s$$

From Newton's Second Law:

$$F = ma$$

$$F = m\ddot{x}$$

$$N - mg = m\ddot{z}$$

$$N = m\ddot{z} + mg$$

Calculating angular momentum H about the end of the rod P

$$H = H_G + m\dot{x}z - m\dot{z}x$$

$$H = I_G\omega + m\dot{x}z - m\dot{z}x$$

$$\text{torque} = \dot{H} = \text{rate of change of angular momentum}$$

$$\dot{H} = I_G\dot{\omega} + m\ddot{x}z + m\dot{x}\dot{z} - m\dot{z}\dot{x} - m\ddot{z}x$$

$$= I_G\ddot{\phi} + m\ddot{x}z + m\ddot{z}x$$

Taking moments of force about O:

$$\text{Torque} = -mg(a\cos\phi - x_s) - Nx_s + Fz_s$$

$$\text{Torque} = -mg(a\cos\phi - x_s) - mgx_s - m\ddot{z}x_s + m\ddot{x}z_s$$

$$\text{Torque} = -mg(a\cos\phi) - m\ddot{z}x_s + m\ddot{x}z_s$$

Equating the two expressions for torque:

$$-mg(a\cos\phi) - m\ddot{z}x_s + m\ddot{x}z_s = I_G\ddot{\phi} + m\ddot{x}z - m\ddot{z}x$$

$$I_G\ddot{\phi} = -mg(a\cos\phi) - m\ddot{z}x_s + m\ddot{x}z_s - m\ddot{x}z - m\ddot{z}x$$

$$I_G\ddot{\phi} = mg(x - x_s) + m\ddot{z}(x - x_s) - m\ddot{x}(z - z_s)$$

$$\ddot{\phi} = \frac{mg(x - x_s) - m\ddot{x}(z - z_s) + m\ddot{z}(x - x_s)}{I_G}$$

$\ddot{\phi}$, $\ddot{x}_s$ and $\ddot{z}_s$ are the three acceleration values required to integrate in order to calculate the movement of mass centre.

In the following differentiation, as dt, the time step, is very small the acceleration over dt is assumed to be constant. The equations of constant acceleration, $s = ut + \frac{1}{2} at^2$ and $v = u + at$, an iterative method and a time step of 0.00001 are used.

$$x_s = x_s + \dot{x}_s dt + 0.5\ddot{x}_s dt^2$$

$$\dot{x}_s = \dot{x}_s + \ddot{x}_s dt$$

$$z_s = z_s + \dot{z}_s dt + 0.5\ddot{z}_s dt^2$$

$$\dot{z}_s = \dot{z}_s + \ddot{z}_s dt$$

$$\phi = \phi + \dot{\phi} dt + 0.5\ddot{\phi} dt^2$$

$$\dot{\phi} = \dot{\phi} + \ddot{\phi} dt$$

The above equations were used to calculate the angle of the rod at takeoff, the angular velocity at takeoff and the vertical and horizontal velocities at takeoff.

Using equations of constant acceleration, the vertical and horizontal distances travelled in flight were calculated:

Vertically: $\dot{z}_t^{\,2} = \dot{z}^2 - 2gz$

Therefore: $z_t = \frac{\dot{z}^2}{2g}$

Height of mass centre above the ground = $z_t + z$

z = vertical location of mass centre at instant of takeoff

$\dot{z}$ = initial vertical velocity of mass centre

$\dot{z}_t$ = final vertical velocity of mass centre

z_t = vertical distance travelled by mass centre in flight

g = acceleration due to gravity

t = time

Horizontally: $x_t = \dot{x}t$

Horizontal distance of mass centre from point of contact = $x_t + x$

x = horizontal location of mass centre at instant of takeoff

$\dot{x}$ = initial horizontal velocity of mass centre

x_t = horizontal distance travelled by mass centre during flight

t = time

The model parameters values were decided upon and these remained the same for all simulations performed. The segment length a, was considered to be 1.0 m. The values for the horizontal and vertical spring constants were optimised to maximise jump height. The resulting values were 25000 Nm^{-1} and 50300 Nm^{-1} respectively. A horizontal approach velocity of 6.7 ms^{-1}, as measured by Dapena (1988), and an initial vertical velocity of 0 ms^{-1} were used for all simulations. Leg plant angle values of 40° and 45° were used, and finally this angle was optimised.

Results

With a plant angle of 40°, the peak height reached by the mass centre was 2.7 m, and with a plant angle of 45°, the maximum height reached was slightly less at 2.61 m. Optimisation programs were subsequently developed and for the same approach speed of 6.7 ms^{-1} an optimised plant angle of 41° resulted in a peak jump height of 2.76 m. Due to the simplicity of the one-segment model, if the approach speed was varied in order to maximise jump height it resulted in the fastest speed possible being the optimum. From observed performances of elite athletes it is obvious that this is not the case.

Conclusion

Using such a simple one-segment model it is not possible to predict an optimum approach speed or even identify that there is one. The model can however predict realistic values for the optimum plant angle.

The single segment model is far too simplistic to accurately represent dynamic jumps. Numerous limitations exist in the model, with perhaps the most obvious being the lack of a knee joint. Models with a knee joint also have an associated joint torque value which prevents the knee from collapsing. The

strength of this knee joint torque limits the speed with which the athlete can approach. If the athlete approaches with a speed above this limit the knee will collapse. With the single segment model there is no knee joint and therefore there is no limit to the speed at which the model can approach.

It can be concluded that single segment models, although useful in predicting optimum approach angles with reasonable accuracy, fail to predict either realistic optimum approach speeds or peak jump heights.

Two-segment model

Introduction

In order to try and gain a better understanding of the approach parameters used in dynamic jumps, a computer simulation model was developed to replicate that of Alexander (1990). The model comprises a leg formed by two rigid massless segments representing the thigh and the shank, with the whole body mass concentrated at the hip (end of the thigh segment). A torque generator, consisting of an angular contractile component representing the muscle is situated at the knee. It is assumed that the ground reaction force R is aligned at the hip H. The line from the point of contact O to the centre of mass makes an angle θ with the horizontal, defined as the leg plant angle. The knee angle ϕ is defined as the angle between the point of contact O, the knee joint k, and the hip joint h (Figure 3.2).

The model was used to simulate the contact phase of the jump and simulations terminated when the vertical ground reaction force, N, became equal to zero. Values for the segment lengths a, initial knee angle ϕ, maximum knee extensor torque T_{max}, and maximum velocity of shortening $\dot{\phi}$max, were taken to be those used by Alexander (1990) (Table 3.4).

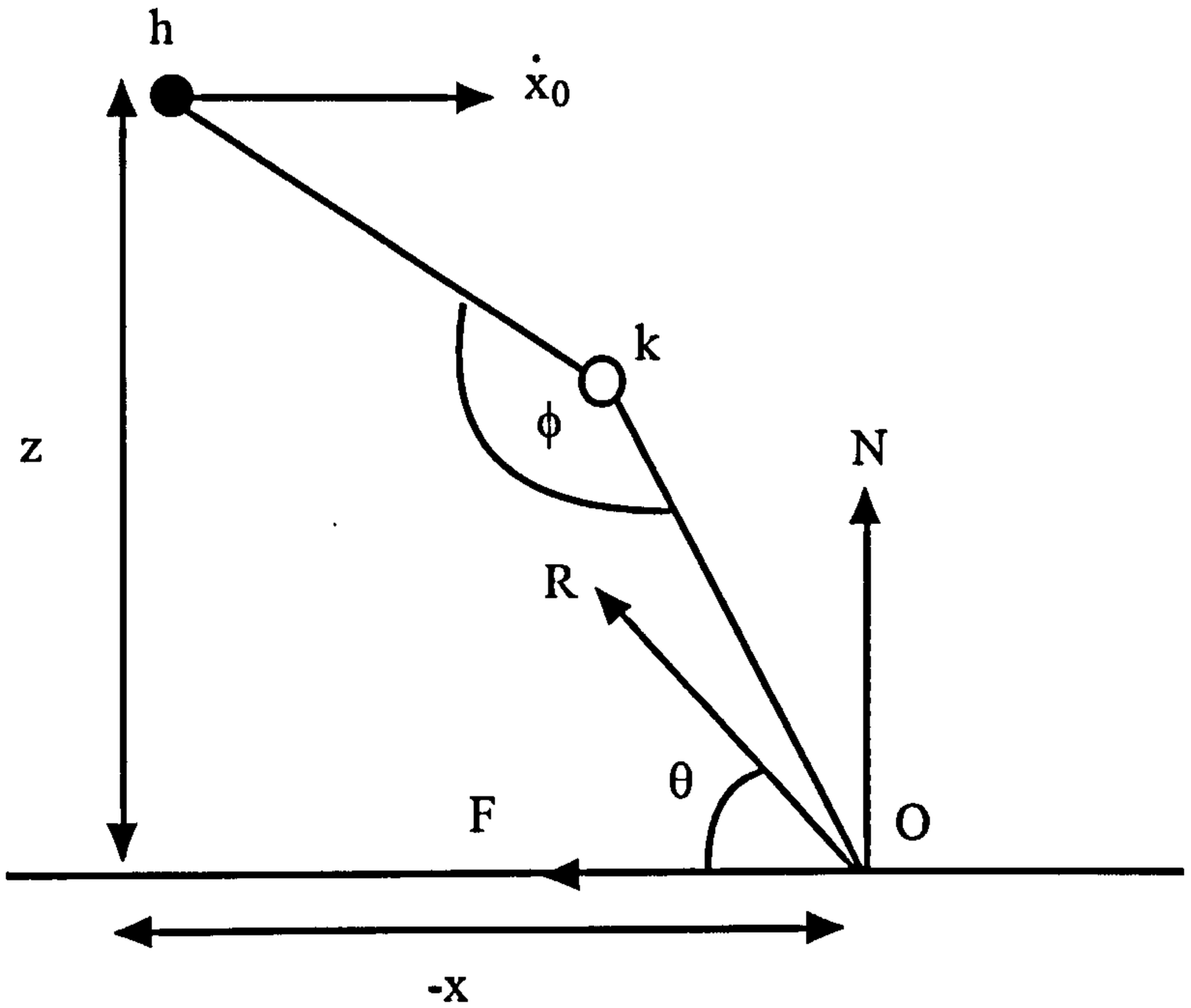

Figure 3.2. A graphical representation of a two segment model with no tendon.

Table 3.2. Input and output variables of the two segment simulation model with no tendon.

INPUT VARIABLE	Symbol	OUTPUT VARIABLE	Symbol
maximum knee extensor torque	T_{max}	vertical velocity at takeoff	$\dot{z}$
maximum velocity of shortening	$\dot{\phi}_{max}$	horizontal velocity at takeoff	$\dot{x}$
plant angle	θ	vertical height of mass centre at takeoff	z
knee angle	ϕ	height reached by mass centre during flight	z_f
knee angular velocity	$\dot{\phi}$	distance reached by mass centre	x_f
horizontal velocity	$\dot{x}_0$	time of contact	t

Again, Newton's Second Law was used to determine the equations of motion during the contact phase in order to calculate the kinematics of the mass centre at the instant of takeoff. These data were subsequently used with equations

of constant acceleration to calculate the height or distance that could be reached by the centre of mass in the following flight phase.

Model with no tendon

This model simulates the contact phase of a jump. Initially the mass centre locations were calculated.

$$x_0 = -2a\sin(\phi/2)\cos\theta$$

$$z_0 = -x_0\tan\theta$$

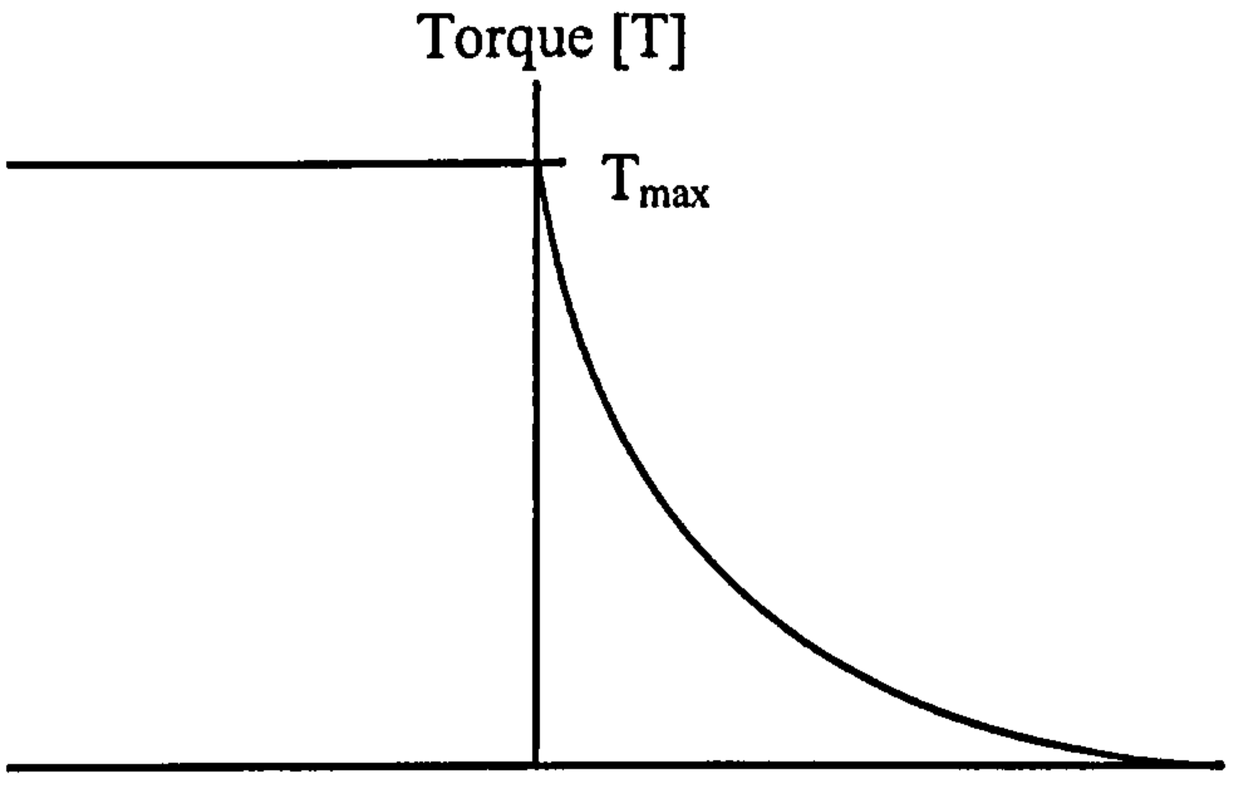

Figure 3.3. A graph showing the relationship between torque and angular velocity of the contractile component.

In order to calculate the value of torque T throughout the contact phase, the relationship between torque and angular velocity $\dot{\phi}_m$, shown in Figure 3.3, was used. This is the relationship used by Alexander (1990) in which the torque in the concentric phase is represented by a typical Hill curve (the curvature of which is defined by G, Hill's curvature constant) and the torque in the eccentric phase is constant.

When $\dot{\phi}$ is less than 0:

$$T = T_{max}$$

Otherwise,

$$T = \frac{\dot{\phi}_{max} - \dot{\phi}T_{max}}{\dot{\phi}_{max} - G\dot{\phi}}$$

It is assumed that the ground reaction force R passes through the centre of mass, which is at the hip location. Calculating the ground reaction force:

$$R = T / a\cos(\phi/2)$$

And the horizontal and vertical components:

$$F = R\cos\theta$$

$$N = R\sin\theta$$

From Newton's Second Law of Motion:

$$F = ma$$

Therefore, the horizontal and vertical accelerations of the mass centre:

$$\ddot{x}_0 = F/m \qquad \ddot{z}_0 = ((N/m) - g)$$

Integrating to give the mass centre velocities

$$\dot{x} = \dot{x}_0 + \ddot{x}_0 dt \qquad \dot{z} = \dot{z}_0 + \ddot{z}_0 dt$$

To give the mass centre position,

$$x = x_0 + \dot{x}_0 dt + (0.5\ddot{x}_0 dt^2)$$

$$z = z_0 + \dot{z}_0 dt + (0.5\ddot{z}_0 dt^2)$$

Calculating the new plant angle:

$$\theta = \tan^{-1}(-z/x)$$

Calculating the new knee angle ϕ, and knee angular velocity $\dot{\phi}$:

$$(x^2 + z^2)^{1/2} = 2a\sin(\phi/2)$$

therefore,

$$\phi = \frac{2\sin^{-1}(x^2 + z^2)^{1/2}}{2a}$$

Differentiating with respect to time:

$$\dot{\phi} = \frac{x\dot{x} + z\dot{z}}{a^2\sin\phi}$$

A tendon was introduced as a rotational elastic component in series with the contractile component within the torque generator, and two further models were developed. The two models were:

1. two-segment model with compliant tendon
2. two-segment model with stiff tendon

The input and output variables of both models are shown in Table 3.3.

Table 3.3. Input and output variables of the two segment simulation model with tendon.

INPUT VARIABLE	Symbol	OUTPUT VARIABLE	Symbol
maximum knee extensor torque	T_{max}	vertical velocity at takeoff	$\dot{z}$
maximum velocity of shortening	$\dot{\phi}_{max}$	horizontal velocity at takeoff	$\dot{x}$
plant angle	θ	vertical height of mass centre at takeoff	z
knee angle	ϕ	height reached by mass centre	z_f
knee angular velocity	$\dot{\phi}$	distance reached by mass centre	x_f
muscle angular velocity	$\dot{\phi}_m$	time of contact	t
tendon angular velocity	$\dot{\phi}_e$		
horizontal velocity	$\dot{x}_0$		
compliance	c		

Model with compliant tendon

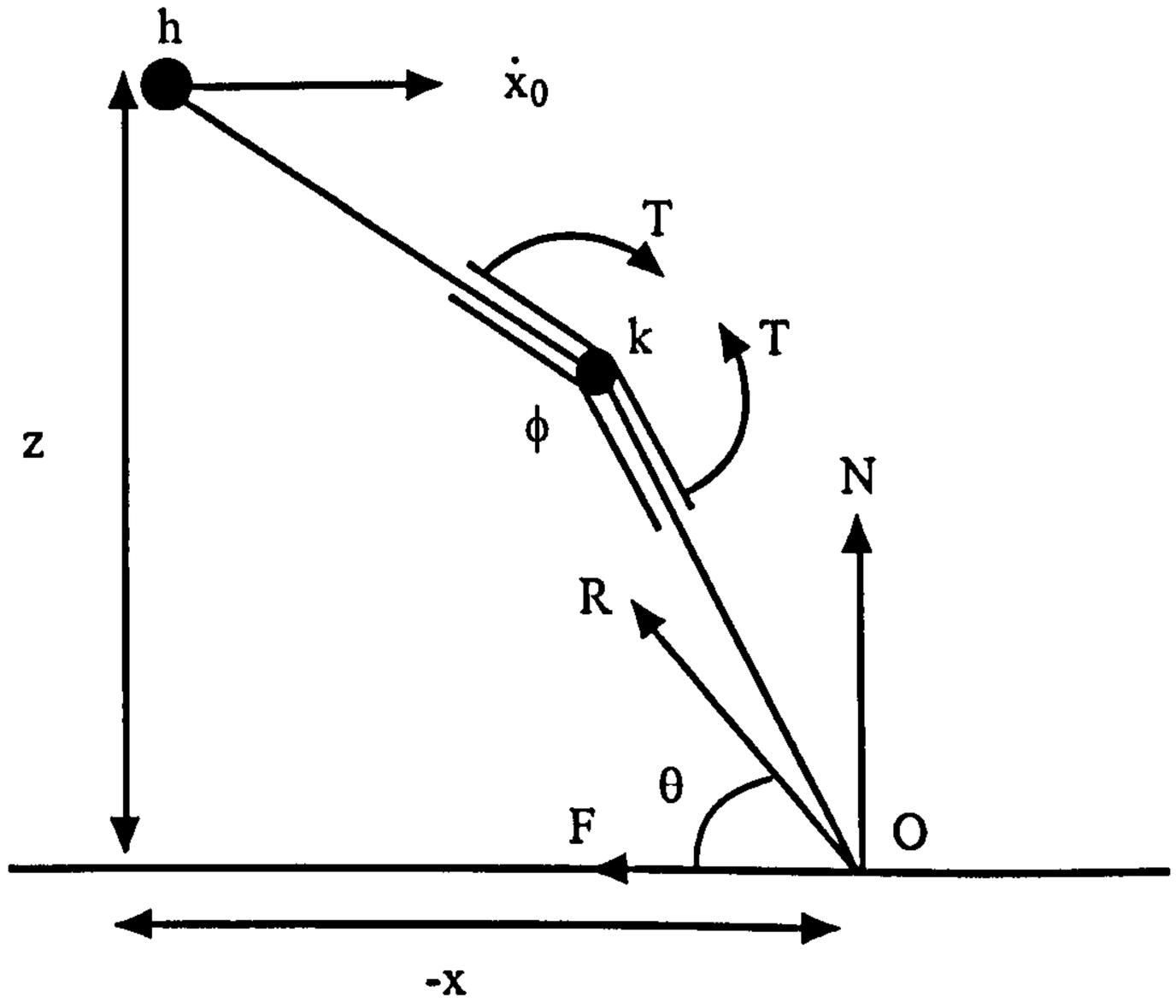

Figure 3.4. A graphical representation of a two segment model with a tendon.

This model is used to simulate the contact phase of a jump. Initially the mass centre locations were calculated:

$$x_0 = -2a\sin(\phi/2)\cos\theta$$

$$z_0 = -x_0\tan\theta$$

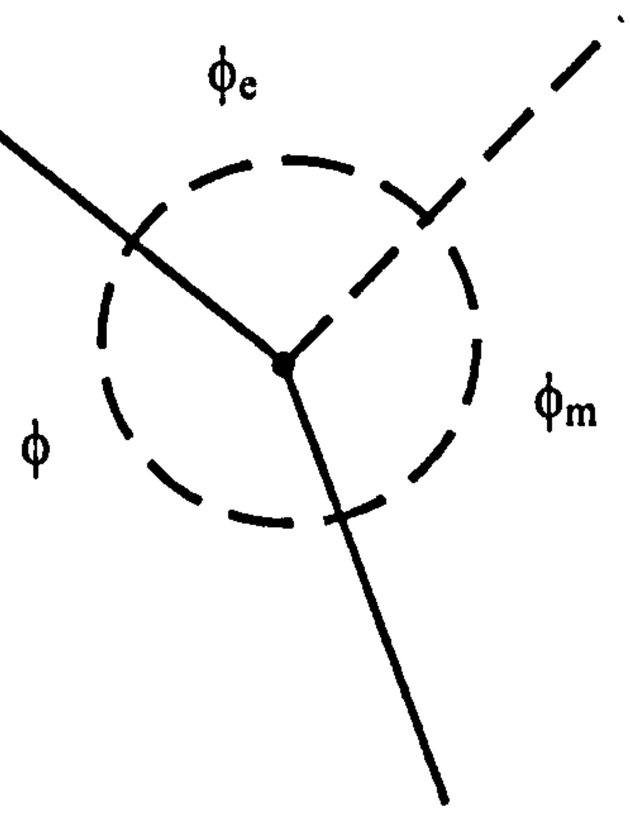

Figure 3.5. A graphical representation of the knee angle, the contractile component angle and series elastic component angle.

$$\phi + \phi_m + \phi_e = 360°$$

The initial torque is dependent on the initial state of the series elastic component. If the muscles are inactive until foot down, the series elastic component would not be strained and T_m would be zero. It is more likely, however, that the muscles develop tension before the foot is set down. Alexander (1990), assumed this torque to be equal to $0.6\,T_{max}$.

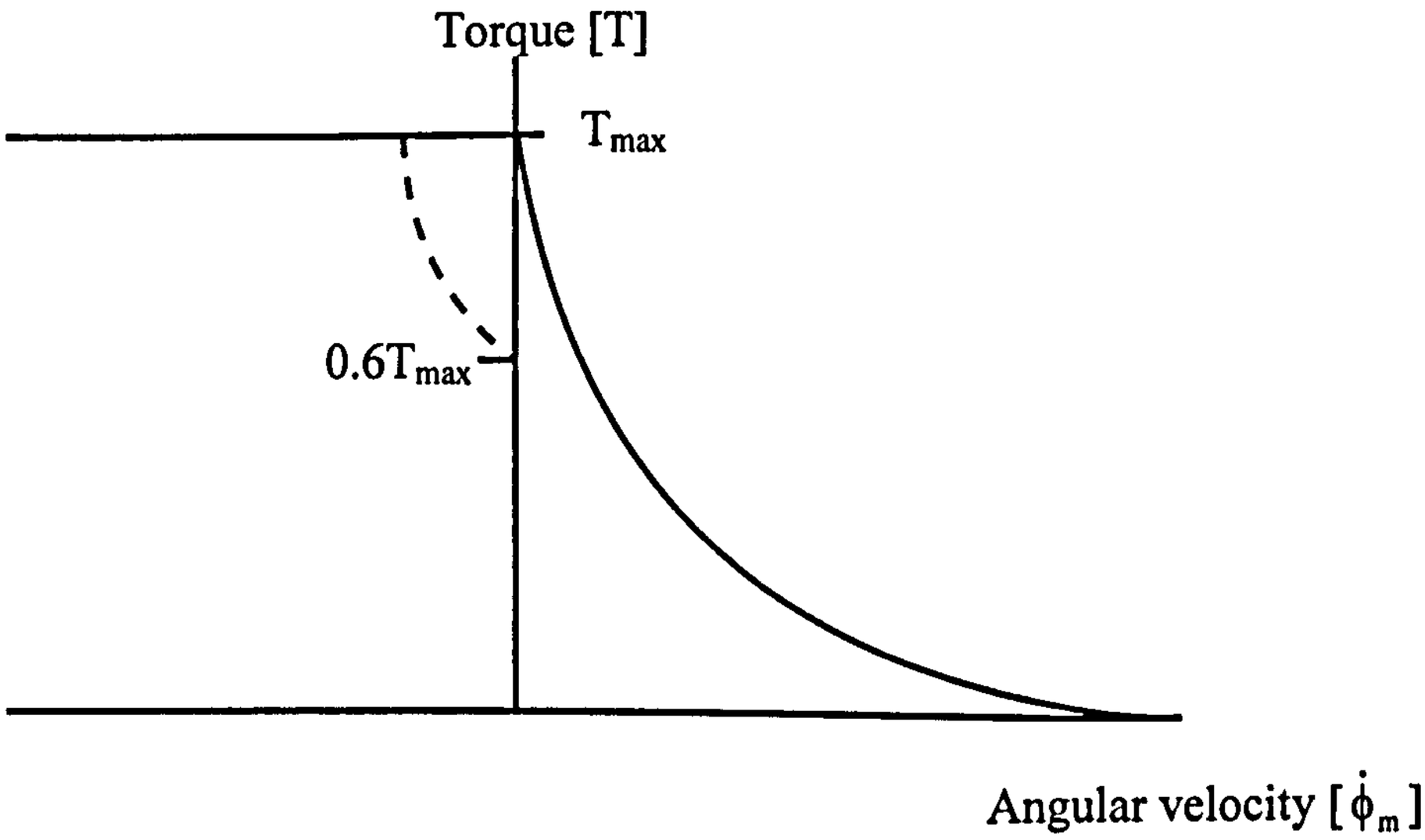

Figure 3.6. A graph showing the relationship between torque of the contractile component and the angular velocity of the contractile component.

The continuous line represents the torque–angular velocity relationship for a stiff tendon model. The broken line represents how the torque initially changes with angular velocity for an elastic tendon model, it is an extension of the right hand side of the graph multiplied by 0.6. It shows how the torque rises from a value of 0.6 T_{max} (Alexander's value of torque at touchdown) to T_{max}. It is then assumed that the torque value follows the continuous line for the rest of the simulation.

The muscle and tendon torque must be equal to each other:

$$T_m = T_e$$

$$T_e = c\phi_e$$

As already stated,

$$\phi + \phi_m + \phi_e = 360°$$

differentiating,

$$\dot{\phi}_e = -\dot{\phi}_m - \dot{\phi}$$

Therefore, the angular velocity of the series elastic component $\dot{\phi}_e$ can be calculated from the initial conditions of the angular velocity of the contractile component $\dot{\phi}_m$ and the angular velocity of the knee joint $\dot{\phi}$.

Calculating torque T_m throughout the contact phase, using the relationship between torque and the angular velocity of the contractile component shown in Figure 3.6. Initially:

$$T_m = \frac{0.6T_{max}(\dot{\phi}_{max} + \dot{\phi}_m)}{\dot{\phi}_{max} - G\dot{\phi}_m}$$

$$\dot{\phi}_e = -\dot{\phi}_m - \dot{\phi}$$

When $\dot{\phi}_m$ is less than or equal to 0:

$$T_m = \frac{T_{max}(\dot{\phi}_{max} + \dot{\phi}_m)}{\dot{\phi}_{max} - G\dot{\phi}_m}$$

$$\dot{\phi}_e = -\dot{\phi}_m - \dot{\phi}$$

Once T_m has reached a value of T_{max} and whilst $\dot{\phi}_m$ is greater than 0:

$$T_m = T_{max}$$

$$\dot{\phi}_e = 0.0$$

Again, there is no change in the muscle torque and therefore no change in tendon torque. Hence, no change in tendon angle and so the tendon velocity must be zero.

Calculating the new plant angle θ:

$$\theta = \tan^{-1}(-z/x)$$

Calculating the new knee angle ϕ, and knee angular velocity $\dot{\phi}$:

$$x^2 + z^2 = 2a\sin(\phi/2)$$

therefore,

$$\phi = 2\sin^{-1}\frac{(x^2+z^2)^{1/2}}{2a}$$

Differentiating with respect to time:

$$\dot{\phi} = \frac{x\dot{x} + z\dot{z}}{a^2\sin\phi}$$

Differentiating T_m, in the equation represented by dotted line:

$$\dot{T}_m = \frac{\ddot{\phi}_m((0.6T_{max}) + GT_m)}{\dot{\phi}_{max} - G\dot{\phi}_m}$$

Therefore,

$$\ddot{\phi}_m = \frac{\dot{T}_m(\dot{\phi}_{max} - G\dot{\phi}_m)}{0.6T_{max} + GT_m}$$

$$\dot{T}_m = \dot{T}_e = c\dot{\phi}_e$$

$$\ddot{\phi}_m = \frac{c\dot{\phi}_e(\dot{\phi}_{max} - G.\dot{\phi}_m)}{(0.6T_{max}) + GT_m}$$

Integrating $\ddot{\phi}_m$ gives the new value of $\dot{\phi}_m$:

$$\dot{\phi}_m = \dot{\phi}_m + \ddot{\phi}_m dt$$

When $\dot{\phi}_m$ is less than or equal to zero, differentiating T_m:

$$\dot{T}_m = \frac{\ddot{\phi}_m(T_{max} + GT_m)}{\dot{\phi}_{max} - G\dot{\phi}_m}$$

Therefore,

$$\ddot{\phi}_m = \frac{\dot{T}_m(\dot{\phi}_{max} - G\dot{\phi}_m)}{T_{max} + GT_m}$$

$$\dot{T}_m = \dot{T}_e = c\dot{\phi}_e$$

$$\ddot{\phi}_m = \frac{c\dot{\phi}_e(\dot{\phi}_{max} - G\dot{\phi}_m)}{T_{max} + GT_m}$$

Again, integrating $\ddot{\phi}_m$ gives the new value of $\dot{\phi}_m$:

$$\dot{\phi}_m = \dot{\phi}_m + \ddot{\phi}_m dt$$

When T_m is equal to T_{max}:

$$\dot{\phi}_e = 0.0$$

Therefore,

$$\dot{\phi}_m = -\dot{\phi}$$

Calculating the ground reaction force:

$$R = T / a\cos(\phi/2)$$

And the horizontal and vertical components,

$$F = R\cos\theta$$

$$N = R\sin\theta$$

From Newton's Second Law of Motion:

$$F = ma$$

Therefore,

$$\ddot{x}_0 = F/m \qquad \ddot{z}_0 = ((N/m) - g$$

Integrating,

$$\dot{x} = \dot{x}_0 + \ddot{x}_0 dt \qquad \dot{z} = \dot{z}_0 + \ddot{z}_0 dt$$

and again,

$$x_0 = x_0 + \dot{x}_0 dt + (0.5\ddot{x}_0 dt^2)$$

$$z_0 = z_0 + \dot{z}_0 dt + (0.5\ddot{z}_0 dt^2)$$

Table 3.4. Model parameter values for the one and two segment models.

MODEL PARAMETER	Symbol	Value
maximum knee extensor torque	T_{max}	860 Nm
maximum velocity of shortening	$\dot{\phi}_{max}$	35.43 rad.s^{-1}
knee angle	ϕ	170°
compliance	c	1716.75 Nm^{-1}
segment length	a	0.5 m
body mass	m	70 kg
curvature constant	G	3

For all three models, the kinematic data at the end of the contact phase were used with equations of constant acceleration, as used with the one-segment model, to calculate the height or distance travelled by the mass centre during the flight phase.

The initial values of the model parameters were those used by Alexander (1990) (Table 3.4). All these values were considered realistic except the value of the maximum knee extensor torque which was put at an unrealistically high value to compensate for the lack of a foot so that realistic ground reaction forces were produced.

Model with stiff tendon

The stiff tendon model was developed in the same way as the compliant tendon model, the only difference between the models being the value of c, the compliance of the series elastic component and the initial activation of the muscle. With the compliant series elastic component the activation started at 60% of the maximum knee extensor torque value and then rose to a maximum as the velocity of shortening of the contractile component increased. The stiff tendon model starts with 100% activation and hence ignores the fact that the muscles may not have been totally activated when the simulation begins.

Results

Using an approach speed of 6.64 ms^{-1} and a plant angle of 45°, as used by Alexander (1990), the peak height reached by the mass centre using the model with no tendon was calculated to be 1.58 m. This was the same for the model with a stiff tendon. With the same approach characteristics the compliant tendon model produced a peak jump height of 1.88 m. Optimisation programs were subsequently developed and using the same approach speed the optimum plant angles were determined for each model. For the stiff / no tendon model, the optimum angle was found to be 40.0°, and for the elastic tendon model it was found to be 49.6°. In separate programs in which both the plant angle and the approach speed were optimised, the optimised plant angles remained the same. For the stiff tendon model the optimum approach speed was 6.87 ms^{-1} resulting in a peak jump height of 1.59 m. For the elastic tendon model, the optimum approach speed was 6.69 ms^{-1}, resulting in a peak jump height of 1.89 m.

Linthorne (1998) tuned Alexander's (1990) model by increasing the value of the maximum torque of the knee extensor, so that an optimum jump height of 2.35 m was achieved. This was done in order that the model produced performances similar to those achieved by elite male competitors. Using the compliant tendon model developed it was decided to try to achieve a performance more similar to those achieved by elite male competitors. The value of the maximum knee extensor torque T_{max}, was increased from a value of 860 Nm used by Alexander to a value of 1120 Nm. The resulting optimum jump height was 2.35 m, from an approach speed of 7.6 ms^{-1} and a plant angle of 47.9°. For the same optimum jump height, Linthorne and Kemble (1998) obtained approach speed of 7.4 ms^{-1}, and a plant angle of 48.0°. In the stiff tendon model, the maximum knee extensor torque had to be increased to a value of 1830 Nm in order to produce an optimised jump height of 2.35 m. The corresponding approach characteristics were an approach speed of 10.20 ms^{-1} and a plant angle of 32.7°. Alexander (1990) commented that in order to compensate for the lack of a compliant tendon, the maximum velocity of shortening could be increased. In the stiff tendon model when the maximum velocity of shortening was increased to a value of 2.5 times the original value, and the maximum knee extensor torque again adjusted accordingly, the optimum approach characteristics became more

realistic, with the optimum approach speed at 8.0 ms^{-1} and the plant angle at 30.2°. The two-segment model with a compliant tendon was used to investigate the effect of knee angle on jump height. Simulations were run in which the knee angle only was varied from 160° to 180° in 2° intervals. Figure 3.7 shows a graph of knee angle against jump height. The jump height linearly increases as knee angle increases up until 180°. After this point the jump height begins to decrease. In conclusion, the straighter the knee at touchdown the better the performance can be.

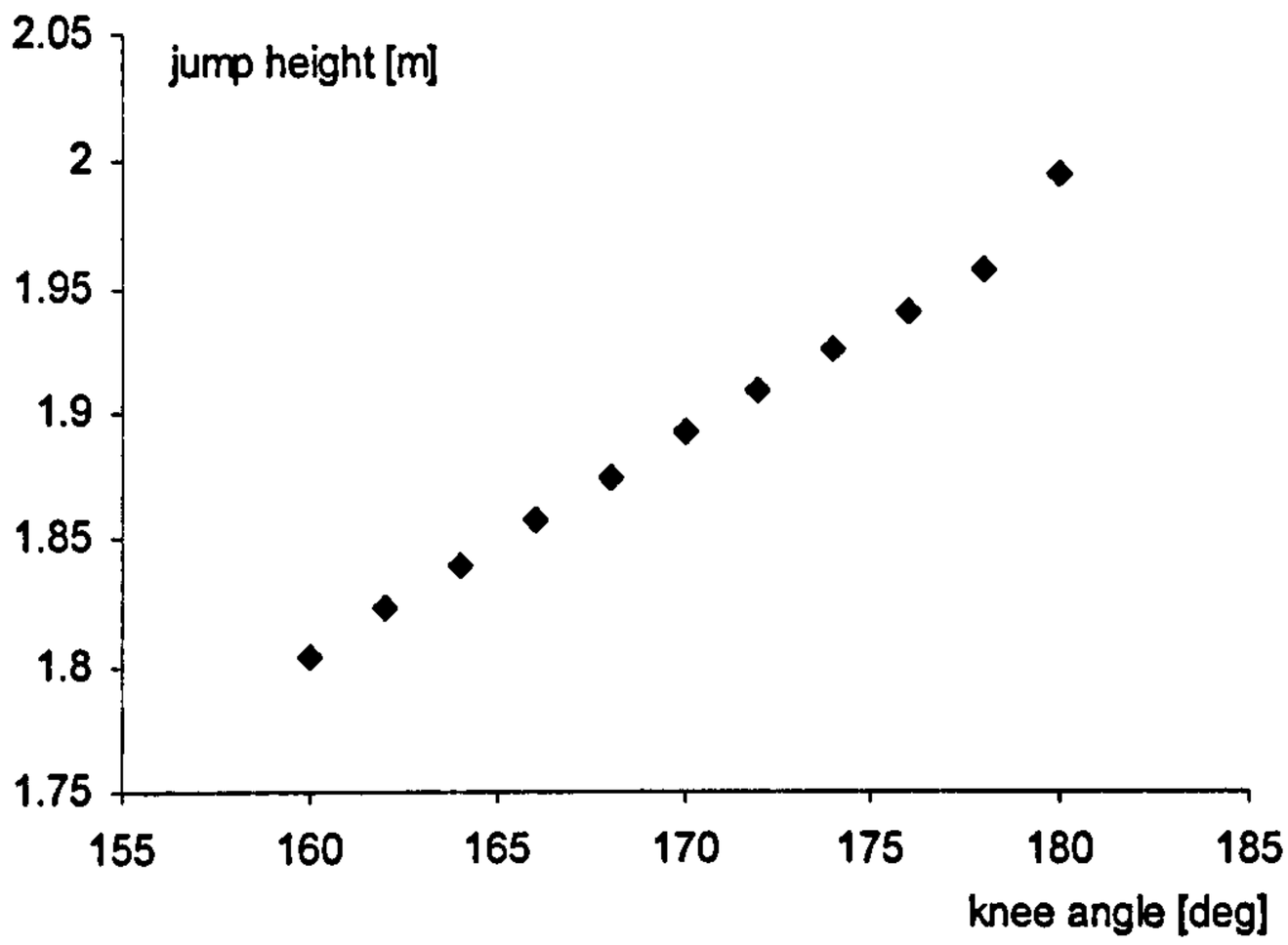

Figure 3.7. The influence of knee angle on jump height.

In any two-segment simulation model with no tendon, the angular velocity of the contractile component in the concentric phase is too high. This is due to the lack of a series elastic component, resulting in the concentric strength being too low. By including a compliant series elastic component in the model, the angular velocity at the knee joint becomes a sum of the angular velocity of the contractile component and the angular velocity of the series elastic component. This results in the angular velocity of the contractile component being lower and hence a greater torque being able to be produced. Increasing the maximum velocity of shortening decreases the concavity of the curve representing the relationship between torque and the velocity of the contractile component. This results in more torque being exerted for a given knee angular velocity.

Like the one-segment model, there are a number of limitations with the two-segment model. One such limitation is that the model has no free limbs. In

reality the athlete would use both arms and the free leg. This 'swinging' of the free limbs increases the height of the mass centre at takeoff and also causes a decrease in the acceleration of the knee angular velocity which allows a greater torque to be exerted in the concentric phase. The model does not include a foot. Consequently, the force at impact rises unrealistically and this probably results in the short contact times. A further limitation is the lack of an elastic foot-ground interface.

Simulation model using Autolev

Introduction

Autolev is an advanced symbol manipulation program which was created to facilitate analyses based on Kane's method for formulating the equations of motion for mechanical systems. Autolev reduces the time and routine nature of producing simulation programs. It also reduces the number of errors which are incurred in simulation modelling. As well as producing the equations of motion for a defined system, Autolev is also able to produce a simulation model of the system in the form of ready to compile Fortran code.

The following section looks at Kane's method of obtaining the equations of motion for a specific system

Kane's method

There exist reference frames N such that, if S is a system possessing p degrees of freedom in N, and F_r and F_r^* (r = 1,...., p) are, respectively, the generalised active forces and the generalised inertia forces for S in N, then the equations,

$$F_r + F_r^* = 0 \quad (r = 1, \ldots, p)$$

Where:

r	the number of degrees of freedom in reference frame N
F_r^*	the generalised inertia forces
F_r	the generalised active forces,

govern all motions of S in any reference frame. The reference frames N are called Newtonian or inertial reference frames.

Generalised active forces are forces which occur due to contact between two bodies in the system. Kane defines these forces as:

$$F_r = \sum_{i=1}^{\nu} {}^{N}v_r^{Pi} \cdot F^{Pi} \qquad (r = 1, \ldots, p)$$

where:

ν	number of paricles that form system S
P_i	the i^{th} particle of the system S
${}^{N}v_r^{Pi}$	the r^{th} partial velocity of P_i in N
F^{Pi}	the inertia force for P_i in N

Generalised inertia forces are those forces which are dependent on the motion and mass distribution of the bodies of the system S. Kane describes these forces as:

$$F_r^* = \sum_{i=1}^{\nu} v_r^{Pi} . R_r^* \qquad \text{where } R_r^* = -m_i a^{Pi}$$

Where:

ν	= number of paricles in the system s
Pi	= the i^{th} particle of the system S
m_i	= the mass of the i^{th} particle of the system S
v_r^{Pi}	= the r^{th} partial velocity of P_i in N
a^{Pi}	= the acceleration of P_i in N

Requirements for Autolev

In order for Autolev to produce these equations of motion, and thus a simulation model of any mechanical system, the user must supply Autolev with the commands which describe the structure and motion of the system together with any external forces and torques acting on the system. Specific information required is (Schaecter et al., 1991):

- An expression for the inertial angular velocity of each rigid body in the system.

- An expression for the inertial velocity of each particle, each rigid body mass centre, and each point at which a force that contributes to generalised active forces is applied
- An expression for the inertial angular acceleration of each body in the system.
- An expression for the inertial acceleration of each particle and each rigid body mass centre.
- Expressions for forces and / or torques that contribute to generalised active forces.

This information results in Autolev being able to perform operations that would be time consuming and tedious if carried out by hand. Although there appears to be a lot of information which needs to be input into Autolev, the process is very simple.

One-segment jumping model

Initially Autolev^{TM}3 Professional was used in the development of a one-segment elastic model. The model comprises a single rigid segment with two springs, horizontal and vertical, at the end of the segment contacting the ground. The mass is concentrated at the centre of the segment. The initial conditions were the same as those used for the single segment model developed manually. The plant angle was initially set at 40°, then 45° and then the plant angle was optimised. The approach speed used for each simulation was 6.7 ms^{-1}. The simulations were performed for the three different values of the plant angle and the peak jump height was calculated. The results are shown in Table 3.5.

Table 3.5. Results of the one segment Autolev model.

Approach speed (ms^{-1})	Plant angle (°)	Peak height (m)
6.7	40	2.669
6.7	45	2.613
6.7	41	2.775

These results are in agreement with the results of the previous one-segment model.

Two-segment jumping model

The equations of motion for a two-segment jumping model were formulated using Autolev^{TM}3 Professional (**Appendix 1**). The planar two-segment model consisting of a shank and thigh, has the majority of the body mass concentrated at the end of the thigh segment. The model contains a spring at the end of the shank segment with horizontal and vertical components, which represents an elastic ground contact. The Fortran code generated by Autolev was customised to simulate jumping. This was done by initially converting the main segment of the code into a subroutine.

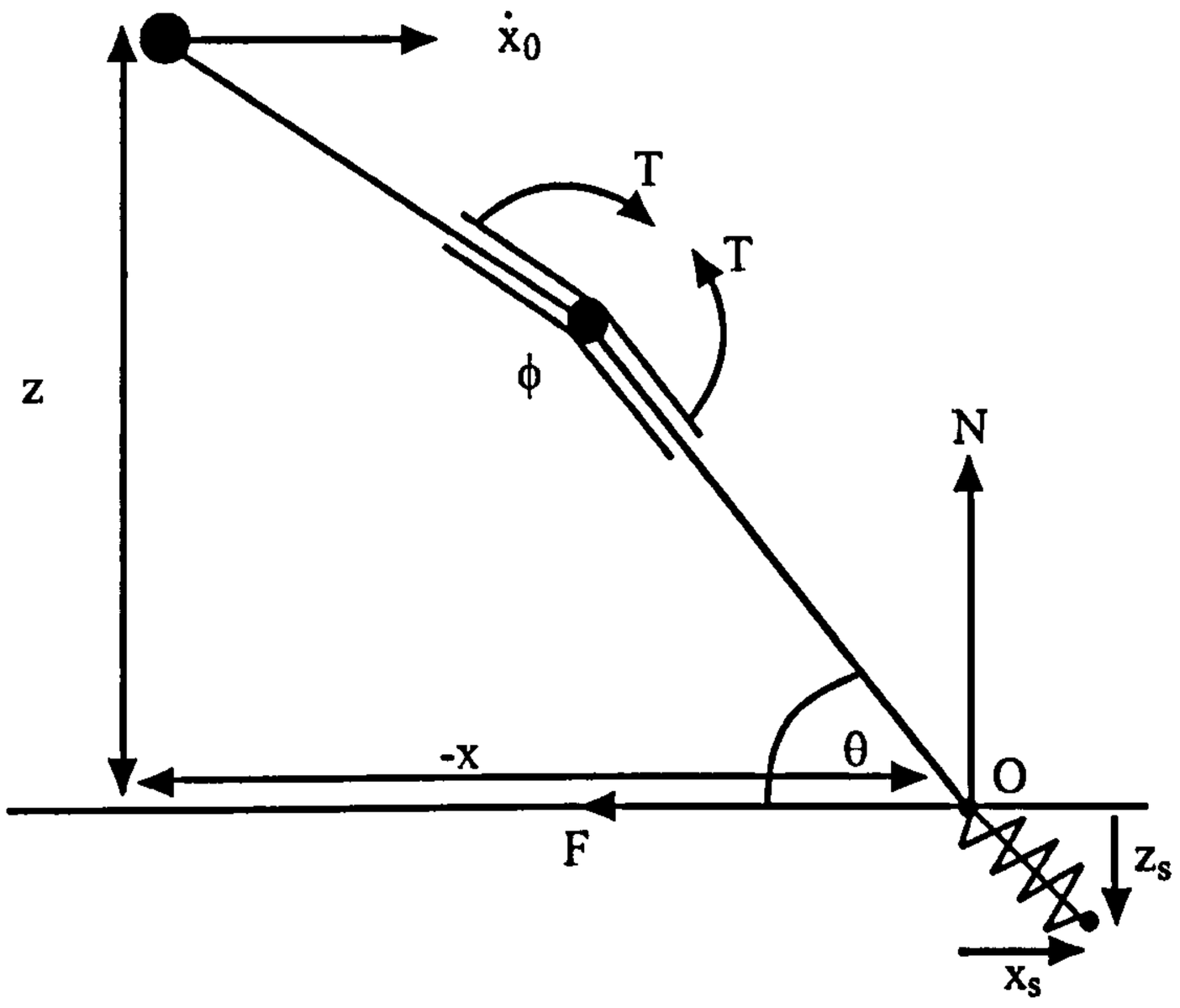

Figure 3.8. A graphical representation of a two segment model produced by Autolev.

T = torque generator at the knee

x_s = horizontal depression of ground

z_s = vertical depression of ground

F = horizontal ground reaction force

N = vertical ground reaction force

Simulations of jumps using the two-segment model with no elastic ground contact begin when the foot is stationary, and thus the model contains no impact. In reality an impact occurs, at the end of which the foot becomes stationary. The two-segment model described above allows an impact phase resulting in a more realistic representation of dynamic jumping. The effect an impact has on velocity of the mass centre was investigated.

Results

Using various stiffness and damping parameter values for the spring at the end of the shank segment the minimum decrease in horizontal velocity from touchdown to the end of the impact phase was found to be 2.6 ms^{-1}. This highlights the fact that the initial speeds used in the previous models, are not the same as the approach speeds. The optimum approach speed calculated using the compliant tendon model with no elastic ground contact was found to be 6.69 ms^{-1}, which would actually correspond to an approach speed of at least 9.29 ms^{-1} if an impact was taken into account.

Wobbling masses

Introduction

A further development in the process, in an attempt to make the simulation models more realistic, was the inclusion of wobbling masses. The following two models contain wobbling masses which are modelled as very basic point masses. A more complex representation of the wobbling masses will be discussed in Chapter 4.

One-segment model with wobbling mass

A one-segment model with wobbling masses within the segment was created using Autolev. The model was produced from the one-segment rigid body model described above. The segment includes a rigid part described as the 'bone' and a non-rigid part, the wobbling mass. The wobbling mass is represented as a point mass and is connected to the bone via a visco-elastic spring.

Values for the masses of the rigid and non-rigid parts of the segment and values for the spring stiffness and damping constants of the visco-elastic spring were taken from Pain (1999).

Table 3.6. Input variables for the one-segment models.

INPUT VARIABLE	SYMBOL	VALUE
initial vertical Velocity	$\dot{z}_0$	3.13 ms^{-1}
initial horizontal velocity	$\dot{x}_0$	0 ms^{-1}
initial angular velocity	$\dot{\theta}_0$	0 $rads^{-1}$
plant angle	θ	90°

Simulations were performed with both the wobbling mass model described above and the rigid body model. The input to the models is shown in Table 3.6. The initial vertical velocity of the segment corresponds to a velocity after a drop from a height of 0.5 m. Except for the masses of the actual segments all other parameter values were identical in the two models. The mass of the segment in the rigid body model was equal to the sum of the mass of the bone and the soft tissue in the wobbling mass model. Initially the visco-elastic springs were made very stiff, and comparisons of the results with the results of the rigid body model were made. The spring constants taken from Pain (1999) were then input into the wobbling mass model and the vertical ground reaction forces were calculated throughout the whole simulation.

Two-segment model with wobbling masses

A two-segment wobbling mass model, which includes wobbling masses within both segments was also developed in Autolev. As with the one-segment model the wobbling masses are represented as point masses which are connected to the bone via visco-elastic springs.

Values used for the masses of the rigid and non-rigid parts of the thigh and shank segments and values for the spring stiffness and damping constants of the

visco-elastic springs were taken from Pain (1999). The body mass not in the thighs and the shanks is concentrated at the hip

Similar simulations to those performed with the one-segment model were repeated with the two-segment model. The initial input variables remained the same and the knee angle ϕ was given an initial value of 170°, in order make the simulations similar to the contact phase of a drop jumping movement. The other parameters between the wobbling mass model and the rigid body were kept the same (with the exception of the masses of the actual segments).

Results

When the visco-elastic springs were stiff the results of the simulations of the rigid body models and the wobbling mass models were identical. This was as expected because with stiff springs the wobbling masses cannot move and in effect become part of the rigid segment.

With the one-segment model, as expected, the ground reaction forces produced using the rigid body model were higher than those produced by the wobbling mass model for most of the simulation when the springs were made more compliant. The peak vertical ground reaction force produced by the rigid body model was 6591 N, and the corresponding peak vertical ground reaction force produced by the wobbling mass model was 6077 N.

In simulations performed using the two-segment model the vertical ground reaction forces for the rigid body model were higher than for the wobbling mass model throughout the whole of the simulation. The peak vertical ground reaction force produced using the rigid body model was 19655 N, and the corresponding peak vertical ground reaction force produced by the wobbling mass model was 16191 N. These values are different to those recorded by Pain (1999) who obtained peak vertical ground reaction forces of 14000 N and 33800 N for the wobbling mass and rigid body models respectively. This may be due to the fact the model used by Pain contains more segments. The models used and the simulations produced here do, however, show this expected difference in the vertical ground reaction forces at impact.

Conclusion

Although the two-segment model developed in Autolev includes an impact phase, it still lacks a number of elements which are considered very important in the takeoff phase of dynamic jumps. Already mentioned are the lack of a foot and the lack of free limbs. The exclusion of both of these contribute to the fact that the simple models discussed here cannot predict realistic optimum approach characteristics and heights reached by the mass centres from realistic model parameters.

Summary

All the models discussed within this chapter are simplifications of the human body. They lack vital characteristics that are needed to accurately describe the mechanics of human movement. In order to simulate an actual performance of an elite jumper successfully, and then investigate or optimise technique, a more complex model is required.

In the following chapter, the development of an eight-segment model, which is considered complex enough to accurately simulate human movement, is discussed.

CHAPTER 4

DEVELOPMENT OF A SIMULATION MODEL

Eight-segment model of jumping

Introduction

When modelling any sporting activity a compromise must be made between the realism and simplicity of the model. Where possible the model should simplify the activity under scrutiny whilst still modelling its main features (Yeadon and Morlock, 1989). This chapter describes the development of three relatively complex eight-segment models which will be used to simulate the takeoff phase of jumping performances. The models developed in Chapter 3, although sufficient to highlight some basic principles of jumping are not sophisticated enough to answer specific questions regarding technique. The models developed in this chapter, once evaluated, will be able to answer questions including "what contributes to optimal technique?" and "how sensitive is the model to changes in model parameter values?".

In order to provide a model with the information needed to simulate a performance different techniques can be used, including: (i) driving the model using the kinematics from an actual performance, angle-driven models, and (ii) driving the model using torques determined from isovelocity dynamometer data (Chapter 6), torque-driven models. The models to be developed in this study are two angle-driven forwards dynamics models and a torque-driven forwards dynamics model.

Using an angle-driven model means the joint angles are predetermined and therefore the technique is very close to that actually used. This makes it easier to match the simulations to the actual performance as fewer variables need to be considered. With a torque-driven model the technique (the joint angle time histories) used by the model is determined from the kinetics. Both types of model are required in this study. The angle-driven models will be used to modify how certain aspects of the performance are modelled and determine subject-specific model parameter values. The torque-driven model will use these parameter values

and after being evaluated will be used to investigate high jumping and long jumping performances.

This chapter consists of a general description of the model along with any assumptions and simplifications. The formulation of equations in Autolev is explained along with how the 'raw' simulation model produced by Autolev was customised for this particular study. Finally, the questions to be addressed by the utilisation of the model will be discussed.

General description of the eight segment models

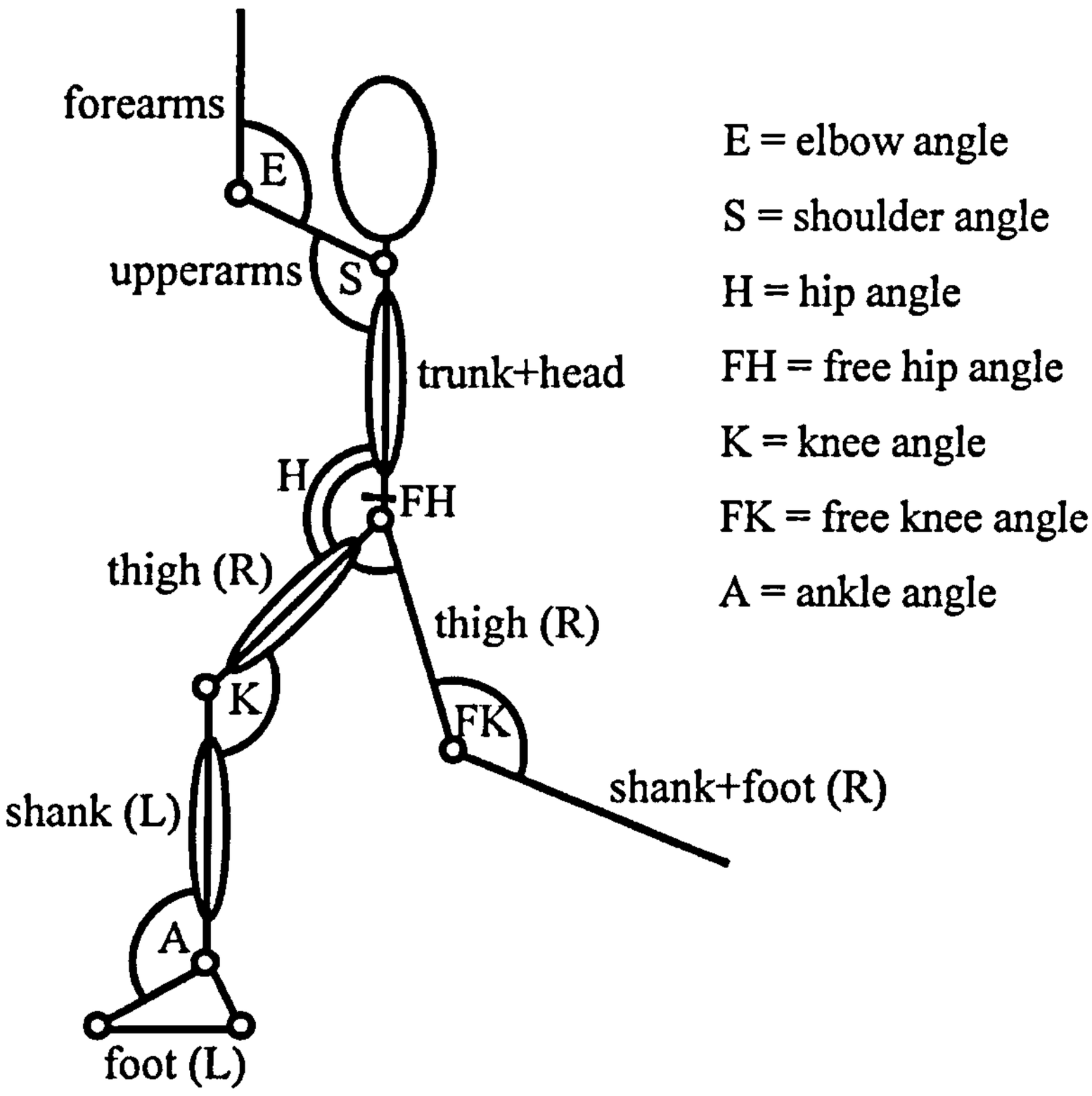

Figure 4.1. Basic structure of the eight-segment model.

The action of high jumping or long jumping requires a relatively complex series of movements of several joints of the body. There are the obvious important angle changes at the knee and hip, but there are also important movement of the free limbs (arms and free leg) which have been identified (Dapena, 1999). In order to be able to simulate these joint changes in the model eight segments were needed (foot, shank and thigh segments on the takeoff leg, shank (& foot) and thigh segments of the free leg, and a trunk and an upper and lower arm) (Figure 4.1). By using eight segments to represent the jumper the

majority of body configuration changes can be simulated. The model has only one upper and lower arm to represent the action of both the left and right arms. This simplification was included after observations of the recorded actual performances (Chapter 5) showed the arms moved relatively symmetrically. A further development of the model was the inclusion of wobbling masses within the shank and thigh segments of the takeoff leg and the trunk segment. The foot segment, unlike the other segments is not modelled as a simple rod, but as a triangular solid. This is to allow points of force application to be situated at both the toe and the heel (Figure 4.2). The force acting at the toe has a horizontal (FT_x) and a vertical (FT_z) component. Similarly the force at the heel has a horizontal (FH_x) and a vertical (FH_z) component. These forces are applied only when the point of force application (heel or toe) is in contact with the ground.

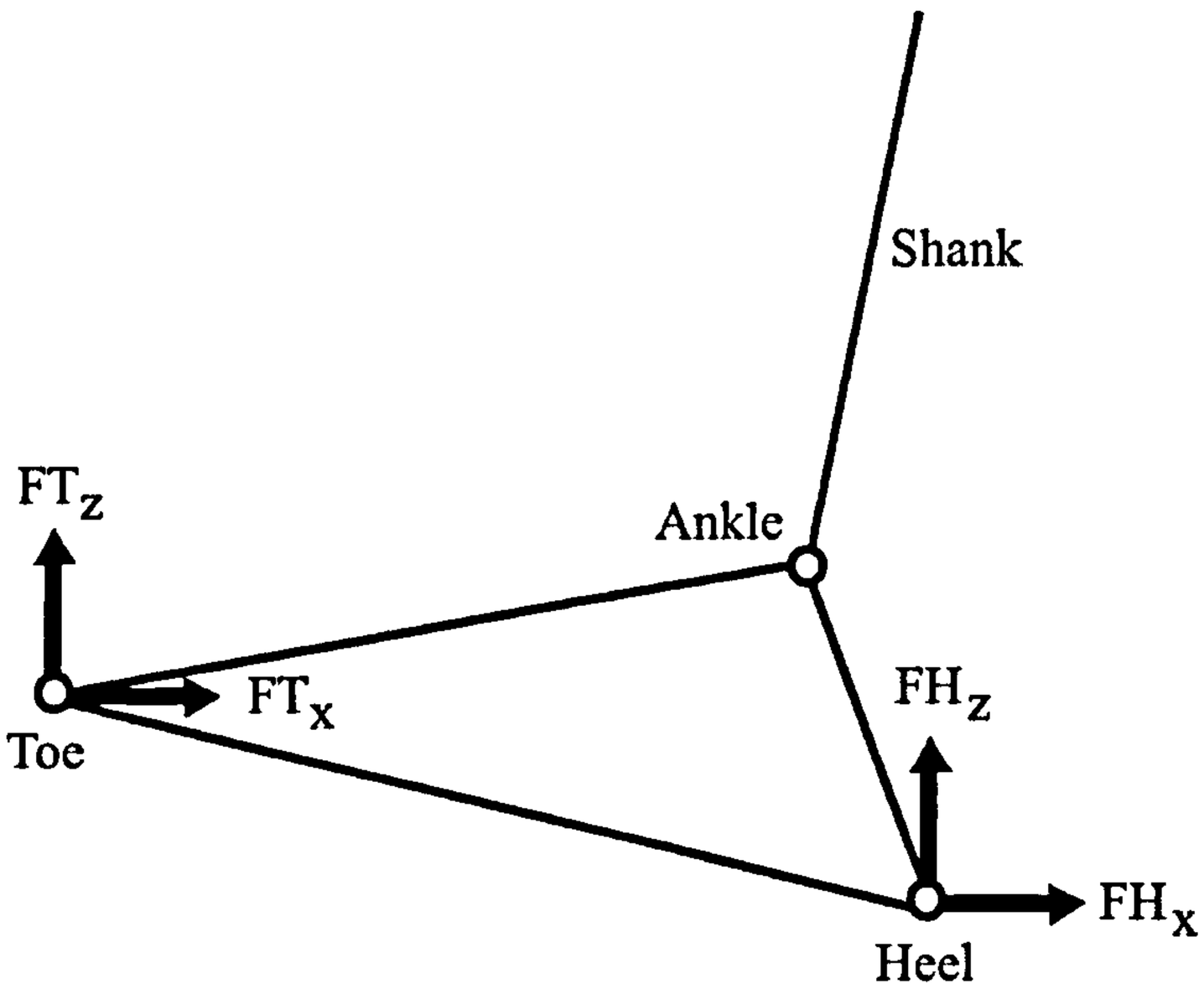

Figure 4.2. Foot segment with acting forces.

Angle-driven models – Models 1 and 2

Description / uses

The first angle-driven model, model 1, requires the time histories of the configuration angles at each joint and the ground reaction forces, obtained from the actual performances, as input. The model has 12 degrees of freedom, 9 of which define the position and orientation of the wobbling masses. Model 1 will

be used to show the chosen structure of the models is sufficient to simulate running jumps. It will also be used to determine wobbling mass parameters, which result in the best match between actual and simulated performances, to be used as initial estimates in model 2.

Model 2 has an identical structure to model 1. The difference between the two models is that instead of inputting actual forces, model 2 has non-linear springs attached at the toe and heel points which represent the foot-ground interface. These springs have horizontal and vertical components with non-linear damping (Figure 4.2). Model 2 will be used to determine spring parameter values for the wobbling masses and foot-ground interface, and the initial trunk angle and angular velocity which result in the best match between actual performances and simulations (Chapter 6). These parameter values will then be fixed and used as inputs into model 3. Model 2 will also be used to determine how the wobbling masses and foot-ground interface can be modelled most realistically.

Models 1 and 2 may also both be used to calculate torque values which along with the Cybex torque data (Chapter 6) can be used in model 3

Model inputs / outputs

Using the force and joint angle time history data the models can be used to simulate the actual performances. The inputs to models 1 and 2 are:

- Initial mass centre velocity
- Initial whole body orientation
- Initial trunk angular velocity
- Joint angle configuration time histories
- Ground reaction force time histories (Model 1 only)

The outputs of the model include the torque time histories required for the given configuration of the body to be maintained, the mass centre location of the body throughout the simulation and the angular momentum of the body at touchdown and takeoff.

From the video analysis of the trials performed in the laboratory, joint angle time histories and their first two derivatives of the ankle, knee, hip, shoulder, elbow, hip of the free leg and knee of the free leg were obtained by fitting the original joint angle data with quintic splines (Wood and Jennings, 1979)

(see Chapter 5 for details). The vertical and horizontal ground reaction force data were each split into two parts to represent the force acting at the toe and at the heel of the model (described in Chapter 5) and used as inputs to model 1. Splines similar to those used for the angle data were fitted to the two sets of horizontal and vertical ground reaction forces.

Modification of joint angle time histories

Fitting a spline to the complete joint angle time histories of each joint, obtained from the video analysis (Chapter 5), may have resulted in the angles and angular velocity estimates around the time of contact being over smoothed due to the rapid joint angle changes during the impact. Although these values might have been sufficiently accurate it was felt there was a need for the inclusion of a function which enabled the angles to vary slightly from these initial estimates. A sine function was used as it kept the initial joint angles fixed whilst allowing the initial joint angular velocities to vary by an amount determined by equation (4.2). A sine function (equation (4.1)) and its first and second derivatives (equations (4.2) and (4.3)) were therefore included in model 1 and 2 for the ankle, knee and hip joint angles, angular velocities and angular accelerations.

$$\phi(t) = \phi_s(t) + \varepsilon(t) \tag{4.1}$$

$$\dot{\phi}(t) = \dot{\phi}_s(t) + \dot{\varepsilon}(t) \tag{4.2}$$

$$\ddot{\phi}(t) = \ddot{\phi}_s(t) + \ddot{\varepsilon}(t) \tag{4.3}$$

Where:

$$\varepsilon(t) = a_1 \sin 2\pi t + a_2 \sin 4\pi t + a_3 \sin 6\pi t + a_4 \sin 8\pi t + a_5 \sin 10\pi t$$

$\phi(t)$ = joint angle

$\phi_s(t)$ = splined joint angle

The values for the constants, a_1 to a_{15}, were varied between tight limits ($-0.02 < a_n < 0.02$, n=1,15) in order to match the simulated and actual performances as closely as possible (Chapter 6).

Torque-driven model – Model 3

Introduction

Model 3 has the same basic structure as models 1 and 2. The major difference is that Model 3 is kinetically and not kinematically driven. The model contains torque generators at the ankle, knee and hip joints of the takeoff leg, the hip joint of the free leg and at the shoulder joint (TA, TK, TH, THF and TS respectively). A diagram of the model is shown in Figure 4.3. The knee joint of the free leg and the elbow joint are driven by joint angle time histories as these joints were not considered particularly important to overall performance. All other joints are driven by torque generators.

Model inputs / outputs

Inputs to the model correspond to the initial conditions of the model at the start of the contact phase / takeoff phase and the time each torque generator was activated. These inputs to the model can be defined as:

- Initial mass centre velocity
- Initial orientation of each segment
- Initial angular velocity of each segment
- Torque profiles for each joint
- Activation time histories
- Joint angle time histories for the elbow and free knee joints

The outputs from the model are given at takeoff, i.e when ground contact is lost. The outputs from the model are:

- Mass centre velocity time histories
- Orientation time histories of each segment
- Angular velocity time histories of each segment
- Whole body angular momentum time histories

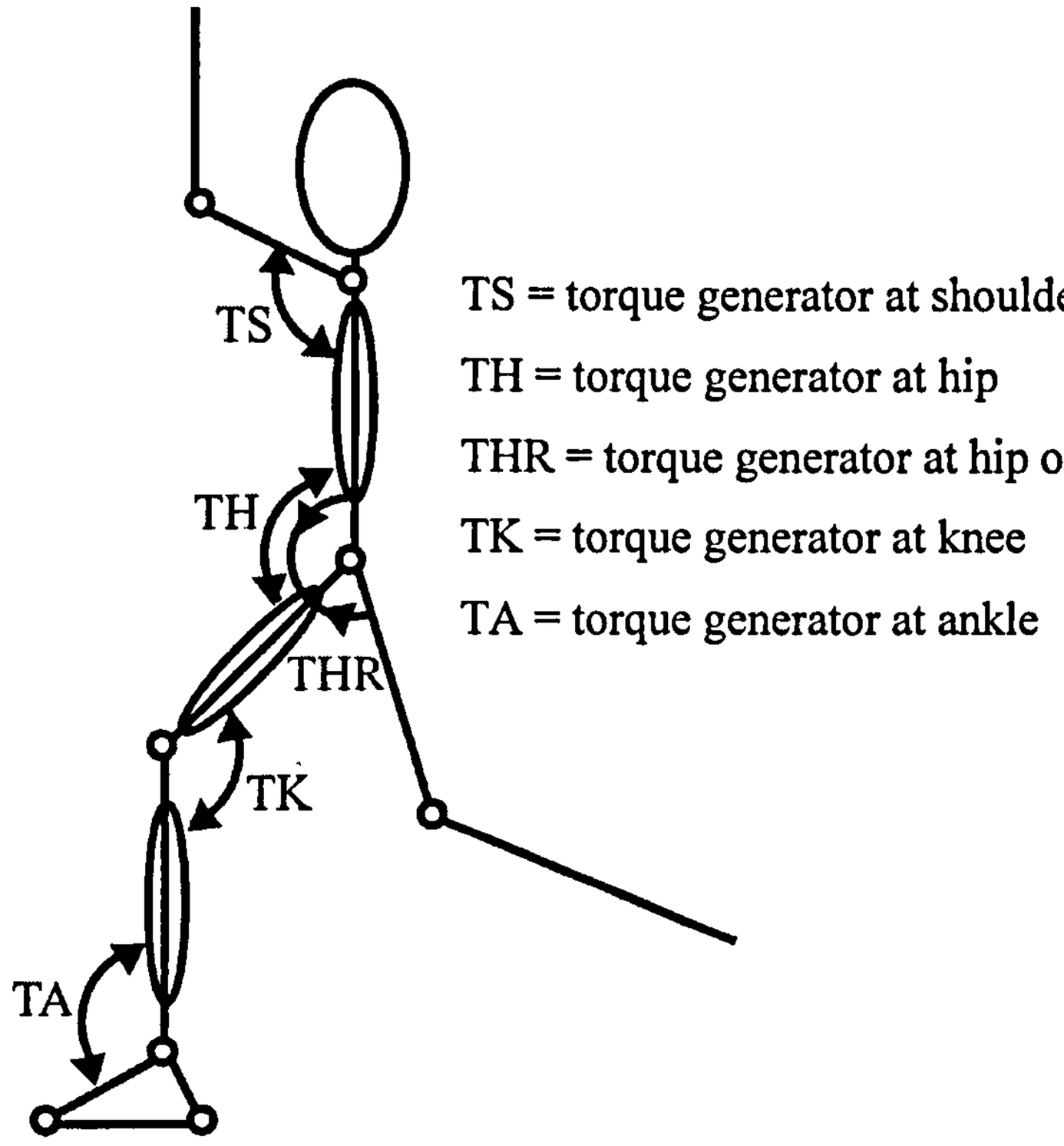

Figure 4.3. Eight-segment torque driven model.

Torque generators

The active torques at each of the ankle, knee, hip, shoulder and free hip joints are represented by two torque generators, one producing flexion and one producing extension. Each group of extensors / flexors are represented as an elastic and contractile element in series. The torque produced by the contractile element was modelled using a nine parameter surface fit (equation (4.4)). The torque produced by the series elastic component was modelled as a linear function of the angle θ_{sec} (equation (4.5)).

For knee extension, hip extension, shoulder flexion and ankle plantar flexion, the torque generator was such that the internal angle of the joint θ was equal to 2π minus the sum of the contractile component angle θ_{cc} and the angle of the series elastic component θ_{sec} as shown in Figure 4.4.

For knee flexion, hip flexion and ankle dorsi flexion the torque generator was such that the internal angle of the joint θ was equal to the sum of the contractile component angle θ_{cc} and the angle of the series elastic component θ_{sec} as shown in Figure 4.5.

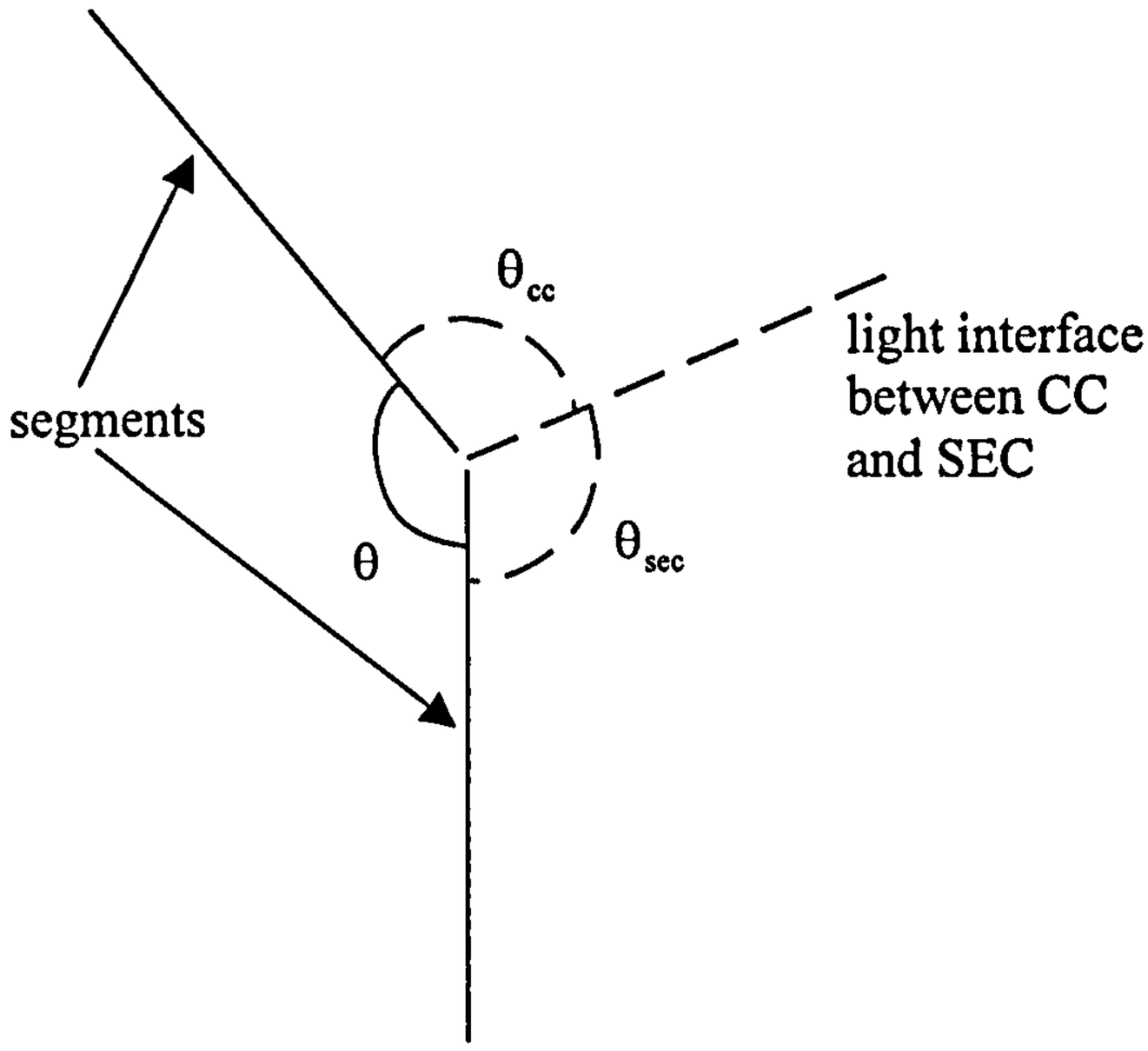

Figure 4.4. Representation of an extensor torque generator.

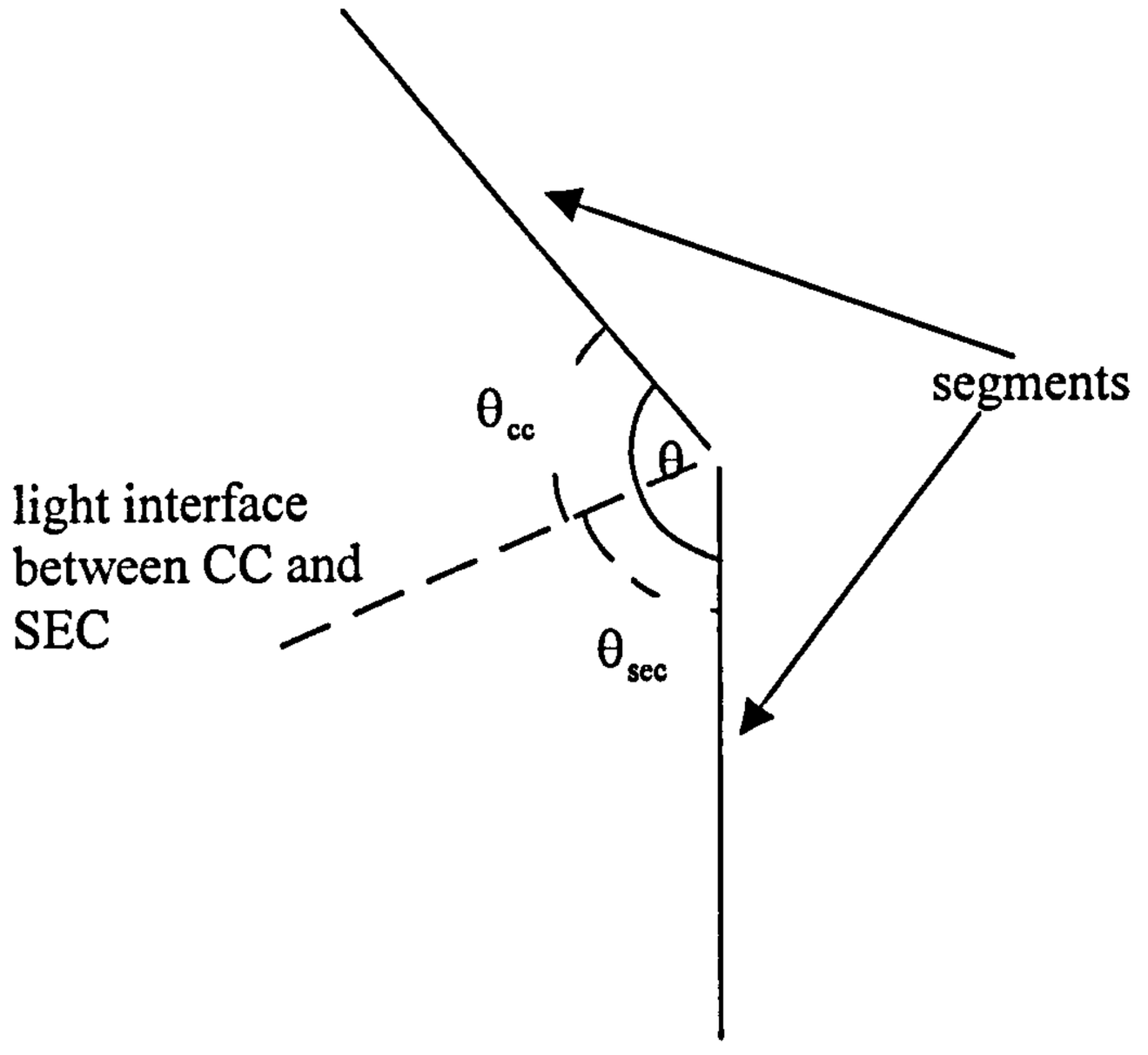

Figure 4.5. Representation of a flexor torque generator.

The muscle parameters for the contractile component and the series elastic component were determined from experimental data on the subject and from data in the literature (Chapter 6).

$$T_{ce} = A(t)F(\theta_{cc}, \dot{\theta}_{cc}) \qquad (4.4)$$

Where:

T_{cc} = torque produced by contractile component at time t

θ_{cc} = angle of the contractile component

A(t) = muscle activation function

F = 9 parameter function (Chapter 6)

$$T_{sec} = K_e \theta_{sec} \quad (4.5)$$

Where:

T_{sec} = torque produced by the elastic component at time t

K_e = series elastic stiffness parameter

θ_{sec} = angle of the series elastic component

Methods

Model development in Autolev

The three eight-segment models were developed in Autolev^{TM}3, the theory behind which is described in Chapter 3. The procedure used to produce a simulation model using Autolev is summarised in Figure 4.6.

Formulation of equations

The equations of motion for the eight-segment models were formulated using Kane's method within Autolev. The Autolev command files, *8segmod.al* and *invdyn.al* describe the structure of the models **(Appendix 1)**. Expressions relating to constrained generalised inertia forces F_r^* and constrained generalised active forces F_r were determined resulting in the equations of motion being formulated. The 'raw' simulation model produced by Autolev utilises a Kutta-Merson numerical integration algorithm, which uses a Runge-Kutta integration method to advance the solution of the equations of motion step by step.

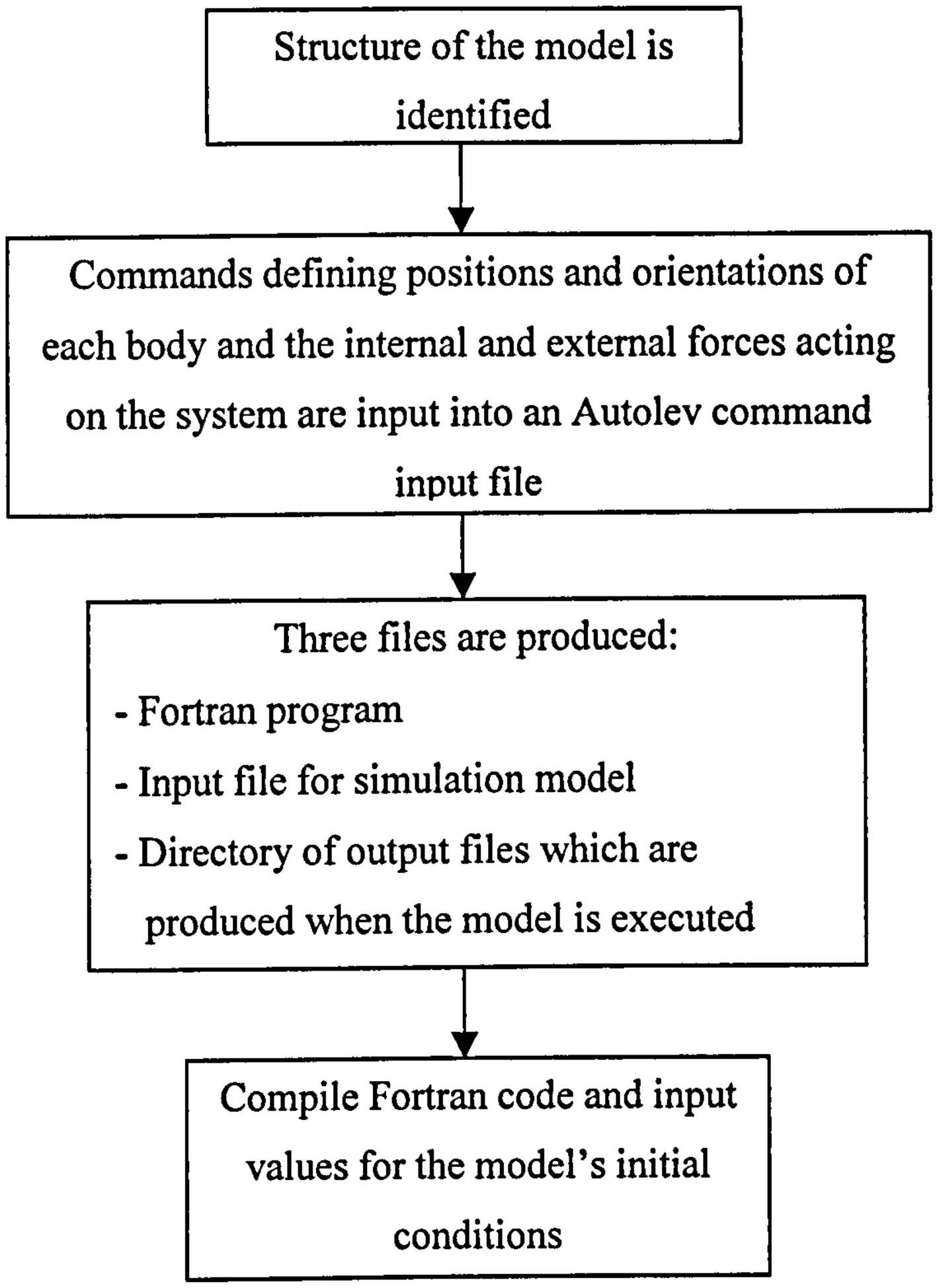

Figure 4.6. A flow chart showing the procedure used by Autolev to create a simulation model.

Customisation

Customisation of the Fortran code produced by Autolev was required. Modifications were made to the model to meet specific needs of the study. None of the modifications affected the equations of motion of the system.

The requirements of the simulation model were:

(i) allow single simulations to be run

(ii) allow evaluation of the models by comparison with actual performances by minimising differences in kinematic and kinetic variables

(iii) optimisation of performance

The customisation of the Fortran code included general alterations and more specific alterations to the raw simulation model related to the input of initial conditions and other parameter values and the defining of the muscle mechanics. These alterations were:

(i) The main segment of the code was converted into a subroutine in order that the whole program could be called from another program such as an optimisation program.

(ii) The Fortran code produced by Autolev requires an input of the horizontal and vertical velocity of the toe. A more accurate value of the centre of mass velocity could be obtained from the video data. The centre of mass velocity is therefore a more accurate input parameter and one which will be used in the evaluation and optimisation of performance (Chapter 7). In order to be able to input the centre of mass velocity as an initial condition a subroutine has to be called from the main program which calculates the toe velocity from the centre of mass velocity before any calculations involving velocities are carried out.

(iii) In models 1 and 2, the joint angle time histories of each of the joints of the body and the ground reaction forces were obtained by calling subroutines which use quintic splines to evaluate the original data.

(iv) In model 3, subroutines defining the torque profiles at each joint were required.

Wobbling masses

During impacts such as landing, non-rigid tissue in the human body moves away from the rigid segment it is attached to. In order to accurately simulate movements involving impacts this movement of 'wobbling masses' needs to be modelled. In the eight-segment models developed in this study wobbling masses are included within the shank, thigh and trunk segments. Each wobbling mass is attached to the corresponding rigid segment via two massless springs. Each spring attaches one end of the wobbling mass to one end of the rigid segment. Each spring has a vertical and horizontal component and the force in the springs is

proportional to the stretch and velocity of them. Equation (4.6) is used to represent these springs.

$$F = -kx^2 - b\dot{x}x \tag{4.6}$$

Where:

F = force in spring

k= stiffness coefficient

b = damping coefficient

x = depression

A representation of the wobbling masses in the model is shown in Figure 4.7. The wobbling masses in this model differ from those included in the one and two-segment models in Chapter 3, where they are simply modelled as point masses rather than segments. The modelling of wobbling masses as point masses was considered too simplistic to represent the movement of the non-rigid tissue in the human body. The positions of each of the wobbling masses in the model are defined using three degrees of freedom. The initial x,y coordinates of one end of the wobbling mass and the orientation of it with respect to the rigid segment to which it is attached are given as initial conditions. The parameters of the wobbling masses needed for the model are the masses, the moments of inertia, and the spring parameters which will be determined in Chapter 6.

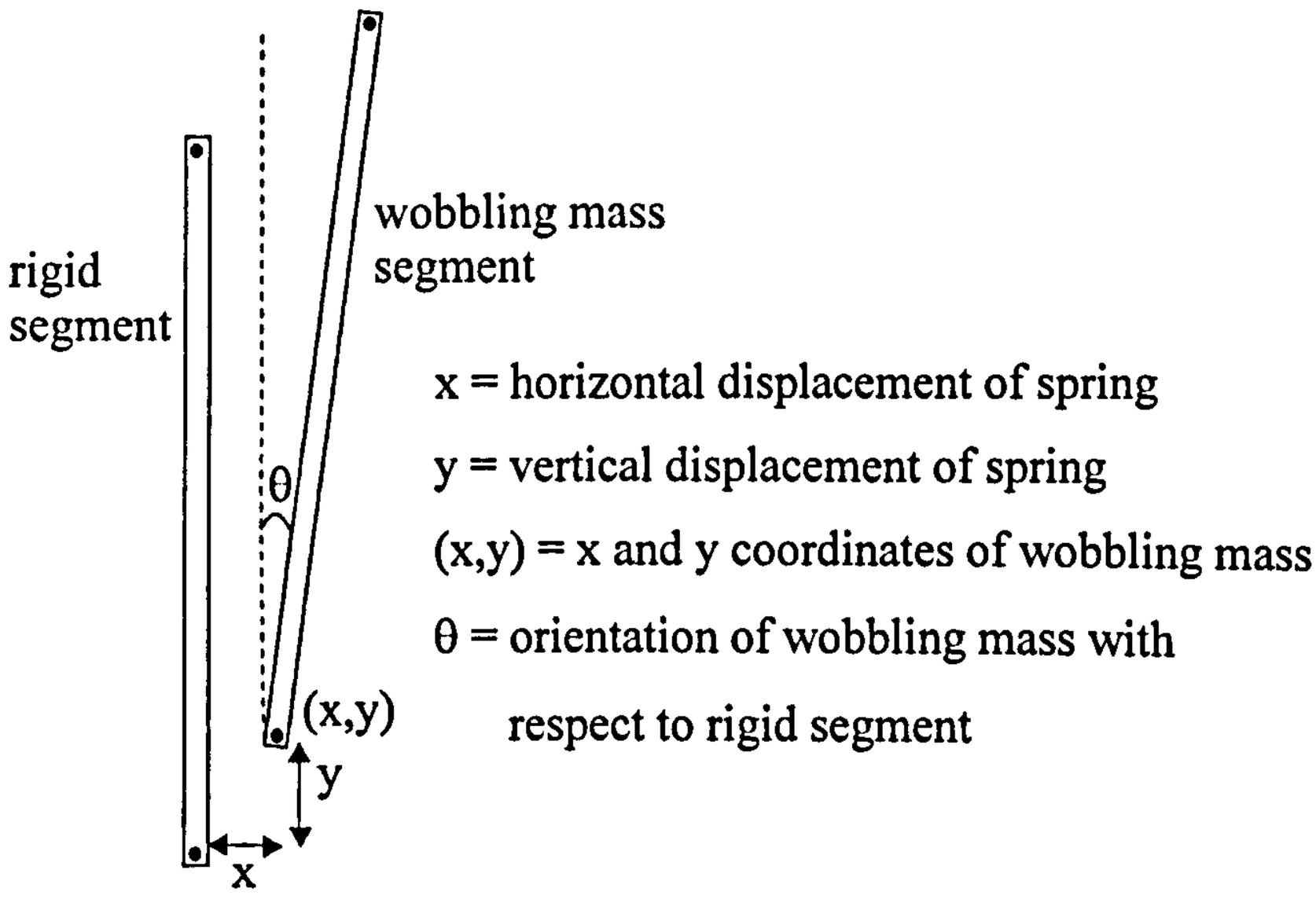

Figure 4.7. Schematic representation of wobbling masses.

The stiffness and damping constants of the springs of the wobbling masses are determined through optimisation using the angle-driven models (models 1 and 2) (Chapter 6).

Modelling the contact phase

The contact between the model and the ground is modelled using horizontal and vertical non-linear massless springs. The force in the springs is dependent on the depression and velocity of the springs, as with the springs used to attach the wobbling masses to the segments. The forces in the springs are defined by:

$$F = -kx^2 - b\dot{x}x \qquad (4.7)$$

Where:

F = force in spring

k= stiffness coefficient

b = damping coefficient

x = depression

Horizontal and vertical springs are situated at the toe and the heel (Figure 4.2). The spring parameters are determined through optimisation using model 2 (Chapter 6).

As the foot has been modelled as a single segment and the points of force application have been located at the heel and end of the toes it is difficult to assign the centre of pressure correctly. This is not so much of a problem when the heel is still in contact with the ground, however, once the heel has lost contact with the ground no forces will be acting at this point therefore all the force and the point of the force application will be at the toe. In reality this is not the case. In a dynamic jumping movement such as the long jump or high jump, once the heel has left the ground the centre of pressure should move from the ball of the foot to the end of the toes smoothly until the time of takeoff. In order for this to be modelled, using the models developed in this study in which there is this simplification of the foot, the vertical force produced at the toe will be divided between the force actually acting at the toe and the force acting at the heel. Whilst the heel is still in contact with the ground, in order to get the centre of pressure in approximately the correct position, which was estimated at being 0.08 m behind the end of the toes, 25% of

the vertical force predicted at the toe was added to the vertical force predicted at the heel leaving 75% to act at the toes. Once the heel had lost contact with the ground the extra force acting at the heel went from 25% of the toe force to 0% of the toe force. This percentage moved smoothly from 25% when the heel was on the ground to 0% when the heel was 0.20 m above the ground level, where it approximately is at takeoff.

It was decided, after initial testing of the model, equation (4.7) used to represent the foot-ground interface was not sufficient to model the ground contact effectively. During the second part of the simulation, the damping that was required initially was too big. It was therefore decided to change the damping characteristics of the springs at the toe and heel once the velocity of the toe and heel respectively had fallen to zero. The new damping values were optimised along with the original stiffness and damping constants and given the same limits as the damping constant used prior to the velocity reaching zero. This was carried out for both the vertical and horizontal forces. A further modification at the foot-ground interface was a change in the equations representing the horizontal force at both the toe and heel. Instead of simply using the displacement in the damping part of the equation, a function involving the displacement was used (equation (4.8)).

$$x' = x/(1 + facdamp.x) \tag{4.8}$$

Where:

x' = function used in spring equation

x = displacement of heel / toe

facdamp = optimised constant

In addition, it was decided that the vertical displacement at the toe and heel affects the horizontal force acting at these points and therefore the horizontal force should be multiplied by a function containing the vertical displacement, namely a constant k multiplied by z^2. Where k is an optimised constant and z is the vertical displacement.

A third modification to the model was in the wobbling masses. After a certain period of time, when the initial movement of the wobbling masses has occurred, more damping is required in the wobbling masses. This is because initially the muscles are not fully activated but after a period of time when they

are fully activated the wobbling masses do not move as much. In order to represent this, the damping parameters of the spring-damper systems at each of the three segments containing wobbling masses were increased over a period of 50 ms by an optimised amount.

A final modification accounted for the movement of the foot in the shoe and digitising errors. Because the foot slips in the shoe as first contact is made the horizontal springs at the toe and heel were given an initial natural length instead of the initial spring length being zero. In addition, it was decided that since errors may have occurred in the digitising of the toe, instead of the toe being down when it reached the initial height of the heel, it was allowed to make contact up to 20 mm above this height.

Model parameters

Model parameters for the customised eight segment models can be divided into four areas: segmental inertia parameters, spring parameters, joint angle time history parameters (for the angle driven model) and torque parameters (for the torque driven model).

Segmental inertia parameters include the mass, moment of inertia and distance to the mass centre of each segment including the wobbling mass segments. Values for these were estimated from direct measurements of the subject and the mathematical inertia model of Yeadon (1990b) (see Chapter 6)

Spring parameters consist of the stiffness and damping coefficients for each spring in the model, including the springs at the toe and the heel which represent the foot-ground interface, and the springs attaching each of the wobbling masses to the corresponding segments. These were determined through optimisation using model 2 (Chapter 6).

Joint angle time histories were obtained from the kinematic data from the actual performances (Chapter 5) and the torque parameters were determined from the isovelocity dynamometer data (Chapter 6).

Initial input conditions

The initial input conditions for the models include the mass centre velocity, whole body orientaion and angular velocity, joint angle configuration

time histories (model 1 and 2 only) and ground reaction forces (model 1 only) for the angle-driven models, and mass centre velocity, orientation and angular velocity of each segment and muscle activation timings for the torque driven model (model 3).

Summary

This chapter has described the development and customisation of three eight-segment models; two angle-driven models and a torque-driven model. Determination of parameters for the torque-driven model is discussed in Chapter 6.

The next chapter describes the collection and analysis of kinematic and kinetic data from dynamic jumping performances. These data are used to obtain initial conditions for the simulations, determine parameter values for the torque-driven model (Chapter 6) and evaluate it (Chapter 7).

CHAPTER 5

KINETIC AND KINEMATIC ANALYSIS

Introduction

This chapter describes the methods used to obtain kinetic, kinematic and electromyography (EMG) data from vertical jumps, drop jumps and running jumps for both distance and height. The kinematic data from the image analysis and the kinetic data from the force plate are needed to determine values for the initial input into the simulation models developed in Chapter 4. The angle-driven models developed in Chapter 4 along with the kinematic data will be used to determine joint torques produced during the jumping performances (Chapter 6). In addition, kinematic and kinetic data on actual performances by the subject are also required so that the simulation models can be evaluated by comparing the output of the models with actual performances.

Laboratory based data collection

Image analysis

Introduction

In this section the procedures used to record and analyse the static and dynamic jumps are described. The video data (along with force and EMG data) were recorded on the first day of a two day data collection. Strength measurements were taken from the subject on the second day.

Data collection protocol

One senior male high jumper of international standard gave consent to perform both static and dynamic jumps whilst data were collected using a force plate, video cameras, a motion analysis system and EMG equipment. The subject performed vertical jumps, drop jumps from various heights using both one and two legged landings, and running jumps for both height and distance from three different approaches. The subject was instructed to use his arms in all trials. Two trials of each type of jump were performed. The vertical jumps performed were

two counter-movement and two squat jumps. The drop jumps were performed from heights of 15, 30, 45, 60 and 75 cm off custom made wooden boxes. Two legged jumps were performed from all heights, one legged jumps were performed only at the lowest two heights. The subject was asked to perform maximally on the counter-movement jumps. For the running jumps, the subject was asked to jump maximally for either height or distance for two trials at each approach of two, four and six strides.

Camera set-up

All trials were recorded using two Sony digital Handycam VX1000E video cameras operating at 50 Hz and a NAC high speed HSV-400 video camera operating at 200 Hz (Figure 5.1). The two 50 Hz cameras used shutter speeds of 1/600 s and the high-speed camera a shutter speed of 1/2500 s. The cameras were set up with fields of view which could be used for recording all the trials and calibration markers. The high-speed camera was used only for recording the takeoff phase of the trials and so required a smaller field of view than the other cameras. One of the 50 Hz cameras was placed in front and to the left of the force plate, at an angle of approximately 30° from the line of direction of travel (Camera 1). The other 50 Hz camera (Camera 3) was positioned almost directly behind the force plate, but slightly to the right so as not to interfere with the subject's approach. The high-speed camera (Camera 2) was positioned perpendicular to the direction of the movement and directly opposite the force plate. The 50 Hz cameras recorded onto digital tapes whilst the high-speed camera recorded onto a SVHS tape in NTSC format. After filming, the digital recordings were copied onto SVHS tapes and time-coded. Similarly the tapes from the high-speed camera were copied onto SVHS tapes in PAL format and time-coded.

Two sets of timing lights were placed near the force plate in order that one set was visible to each of the three cameras. One of the sets of timing lights consisted of 20 light emitting diodes (LEDs) in a straight line whilst the other set in a similar set-up consisted of 10 LEDs. Both sets were used to synchronise the cameras and force plate.

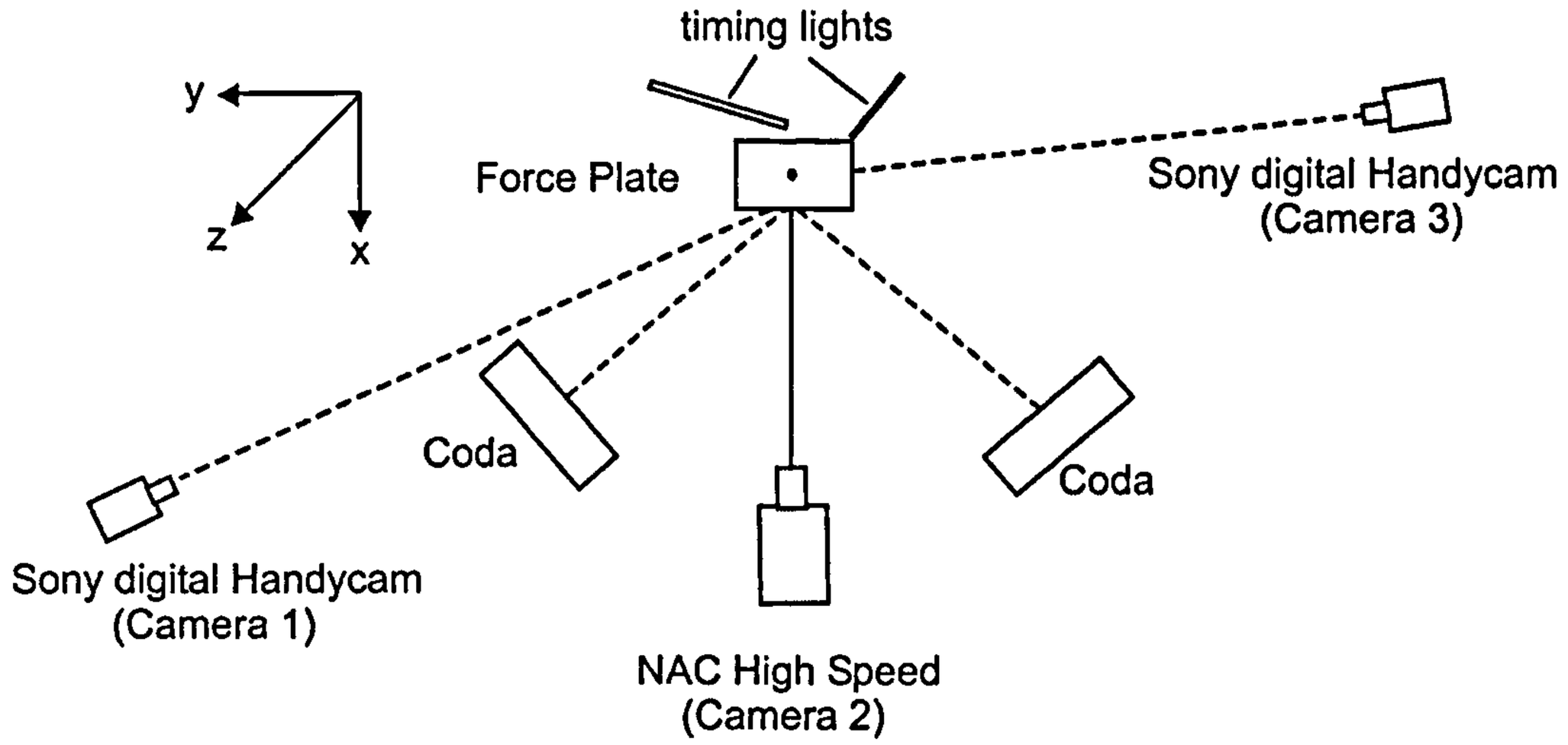

Figure 5.1. Arrangement of cameras and coda units.

Coda

The re-active marker automatic motion analysis system used in this study was the CODA (Cartesian optoelectronic dynamic anthropometer) mpx30 system. The system consists of scanner units containing three special cameras which detect infra-red pulses of light emitted by Coda markers (Figure 5.2). The system can operate up to 800 Hz, when a maximum of 6 markers are used. This was the frequency chosen in the present study. The markers were placed on the subject's left side: on the toe, ankle, knee, hip, shoulder and wrist joints. The LED markers flashed sequentially from the lowest number marker to the highest number marker. The markers used in this study are shown in Figure 5.3. Two scanner units were used to collect data on all the trials videoed.

The Coda mpx30 system is a pre-calibrated system which measures the position of markers within a three-dimensional co-ordinate system which is fixed in relation to the scanner units. The nominal origin is relocated by the user and the orientation of the co-ordinate frame can be reset by alignment transformation in the software. The origin point must be in the field of view of all active Coda scanners and should be approximately equidistant from each Coda. The origin marker in this study was placed in the centre of the force plate. A second marker was placed approximately 1m from the origin marker and in the direction of movement described as the x-axis. The third marker was located so that a line from it to the origin was approximately perpendicular to the x-axis. The distance between the two markers was again approximately 1m. The two scanner units

were placed at the left side of the force plate at approximately 45° to the origin with 90° between them. The two units were placed approximately equidistantly from the force plate (Figure 5.1). The data collection time for Coda was set at 5s for all trials.

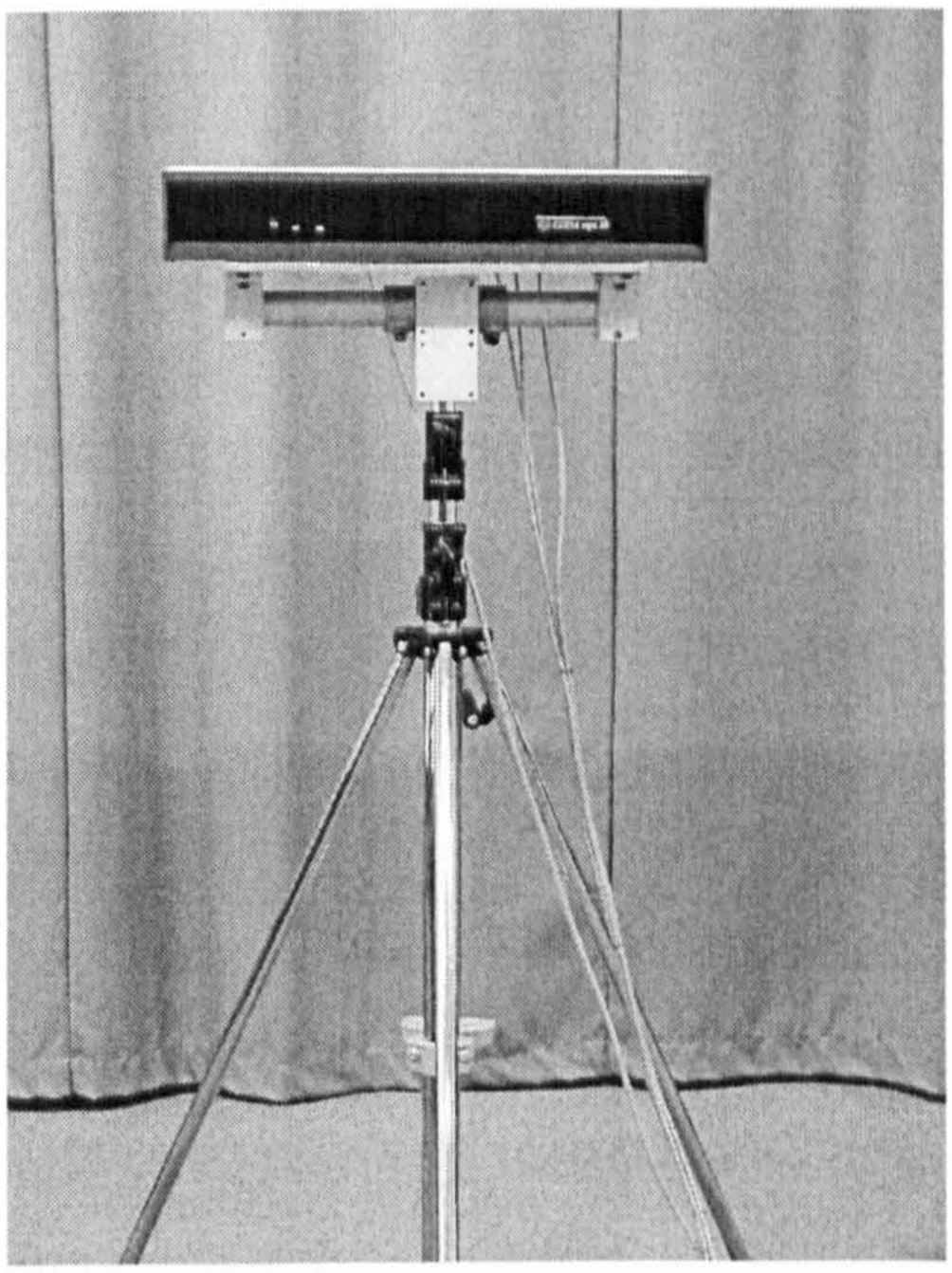

Figure 5.2. A Coda mpx30 scanner unit.

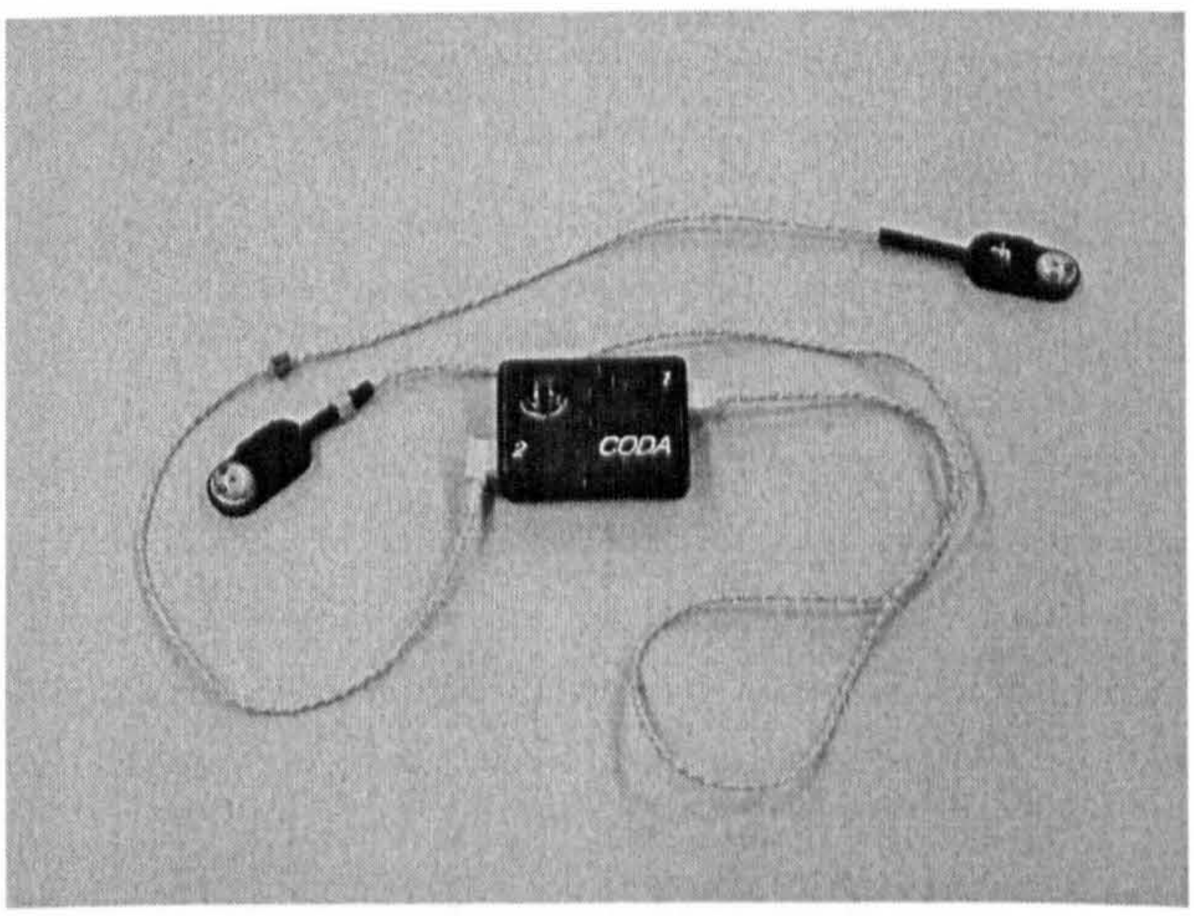

Figure 5.3. Two LED markers with battery.

Calibration set-up

A calibration pole with three markers at known locations was placed on 16 positions within the movement space, which were at known locations relative to

the centre of the force plate, resulting in 48 control/calibration points being identified.

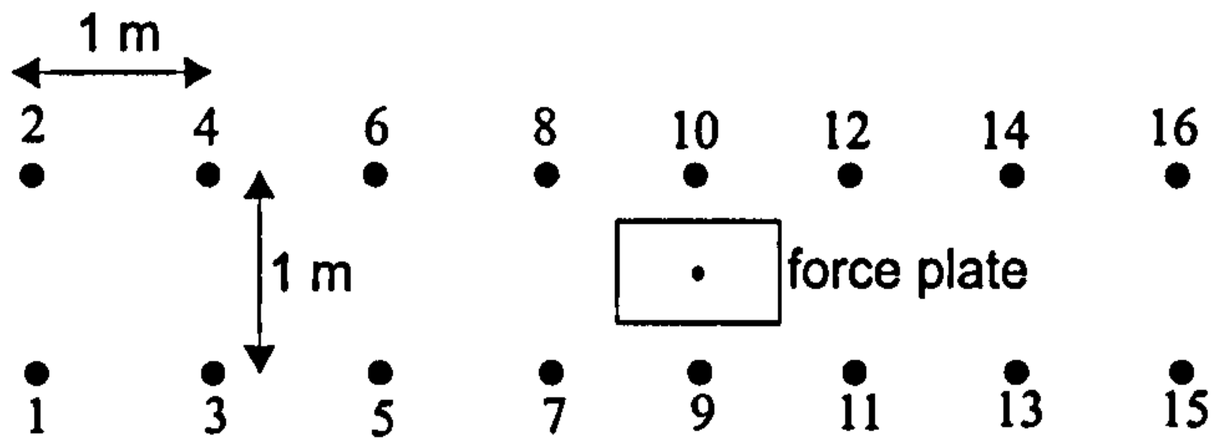

Figure 5.4. Arrangement of calibration poles.

The two dimensional (2-D) locations of the pole relative to the centre of the force plate (0,0) (Figure 5.4) and the locations of the markers relative to the bottom of the pole (Figure 5.5) were measured using steel tapes (Table 5.1). The markers on the pole were constructed from polystyrene balls which had been drilled through their centres. The locations of all calibration points were chosen such that all movements were performed within this space, so that extrapolation outside the calibration volume was minimised. All locations of the pole were visible by the two 50 Hz cameras except that only two of the three balls could be seen at position 15 from Camera 1. The central six positions of the pole could be seen by the high-speed camera.

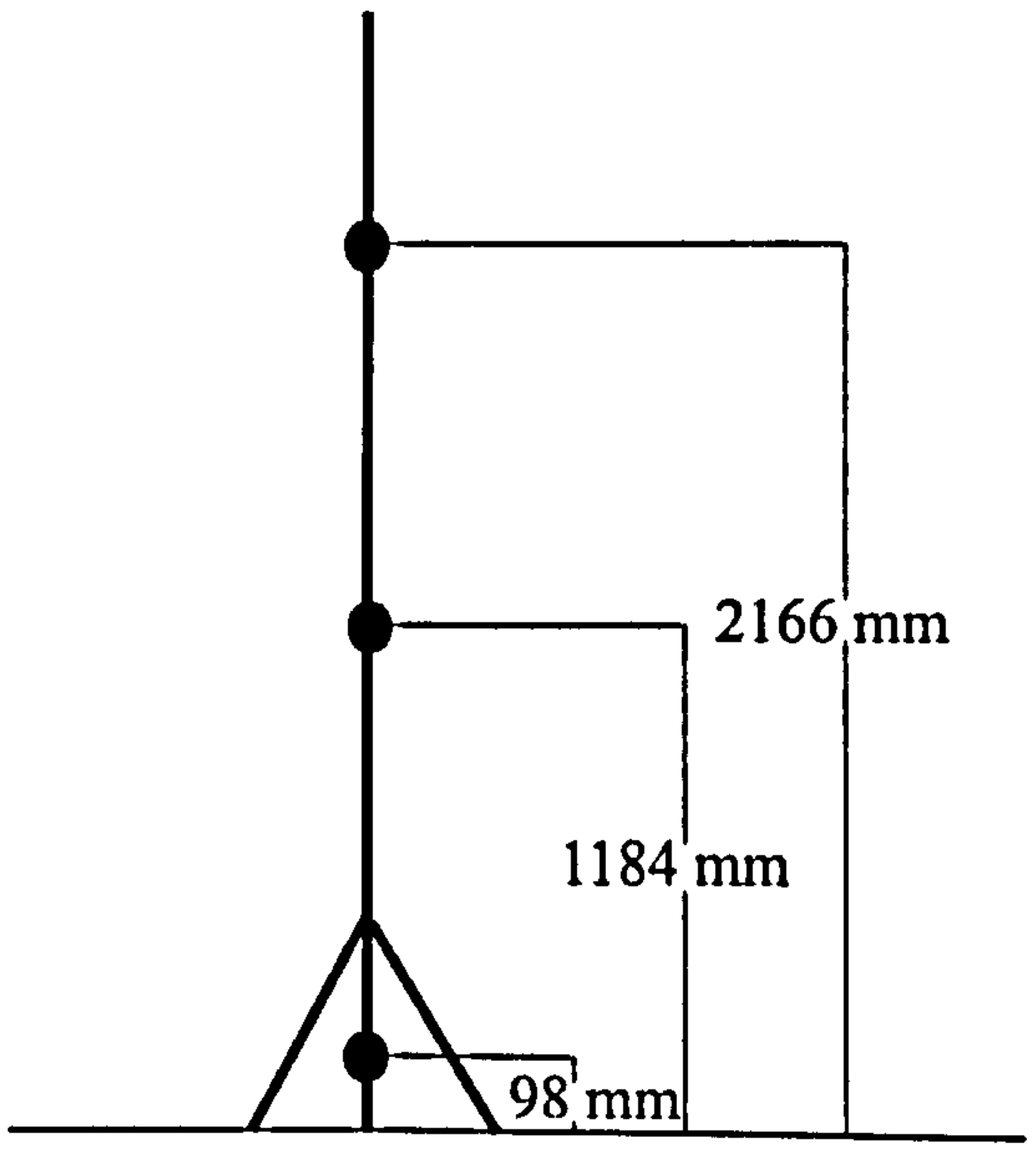

Figure 5.5. Heights of calibration points used in the calibration.

Table 5.1. 3D locations of calibration poles.

Calibration pole; b – bottom, m – middle, t – top	x	y	z
1 (t,m,b)	0.5	-4.0	2.166, 1.184, 0.098
2 (t,m,b)	-0.5	-4.0	2.166, 1.184, 0.098
3 (t,m,b)	0.5	-3.0	2.166, 1.184, 0.098
4 (t,m,b)	-0.5	-3.0	2.166, 1.184, 0.098
5 (t,m,b)	0.5	-2.0	2.166, 1.184, 0.098
6 (t,m,b)	-0.5	-2.0	2.166, 1.184, 0.098
7 (t,m,b)	0.5	-1.0	2.166, 1.184, 0.098
8 (t,m,b)	-0.5	-1.0	2.166, 1.184, 0.098
9 (t,m,b)	0.5	0.0	2.166, 1.184, 0.098
10 (t,m,b)	-0.5	0.0	2.166, 1.184, 0.098
11 (t,m,b)	0.5	1.0	2.166, 1.184, 0.098
12 (t,m,b)	-0.5	1.0	2.166, 1.184, 0.098
13 (t,m,b)	0.5	2.0	2.166, 1.184, 0.098
14 (t,m,b)	-0.5	2.0	2.166, 1.184, 0.098
15(t,m,b)	0.5	3.0	2.166, 1.184, 0.098
16 (t,m,b)	-0.5	3.0	2.166, 1.184, 0.098

Kinetic analysis

A Kistler force plate was used for the collection of kinetic data from all the trials recorded using video. Eight force channels from the force plate were put through the same analogue to digital converter as the Coda cameras, after the force plate and Coda had been triggered simultaneously, and therefore the force and Coda data were synchronised. As the force plate was put into the same analogue to digital system as Coda, the frequency with which the force data were sampled was also 800 Hz. The xy gain range was set at 10,000 Pc/10 V and the z

gain range was set at 50,000 Pc/10 V. As with Coda, the collection time for force data was 5s.

For all trials the subject was instructed to land on the middle of the force plate. If the subject landed off the plate at all a further trial was completed and recorded. Only trials where the subject landed fairly centrally on the force plate were used.

Electromyography

A Biovision EMG system was used for the analysis of muscle activity in all static trials. It was decided that due to the impracticality of moving a non-portable system, collecting EMG data for the dynamic trials would not be viable. Surface electrodes were used and these were placed on eight muscles. EMG data were collected for the tibialis anterior, gastrocnemius, soleus, vastus medialis, quadriceps, medial hamstring, lateral hamstring and gluteus maximus muscles. Two electrodes, positioned next to each other crossing the line of action of the muscle fibres, were placed on each of these muscles. Using the Biovision system, the data were sampled at 1600 Hz using an electrical gain of ± 5V. The collection time for the data in each trial was 6s.

Synchronisation

It was necessary to be able to synchronise the data from all the equipment used. In order to do this a synchronisation unit was used. The synchronisation lights used for the synchronisation of the video cameras were triggered using a remote control. Attached to the back of the remote control was an electrode. When the remote control was pressed, this electrode produced a square pulse in both the trace of the EMG data and in the trace on one of the Coda channels (a second force channel). This synchronisation device was therefore able to synchronise data from video, Coda, force plate and EMG. This was possible as the video images when the synchronisation lights were first seen occurred at the same time as when the square pulse in the traces from the EMG, Coda and force plate data were produced. Channels 0 - 7 of the unit were used for the EMG signals and channel 8 was used as the synchronisation channel used to trigger the second force signal.

Field based data collection

Image analysis

Introduction

A second data collection took place approximately two months after the laboratory-based data collection. The same senior male high jumper performed actual high jump trials outside at a track. The procedures used to record and analyse the jumps are described below.

Data collection protocol

The subject was asked to perform high jump trials from a suitable approach at heights varying from 76-87% of his best height achieved. The subject was instructed simply to clear the bar. In total 24 jumps were completed.

Camera set-up

Four cameras in total were used for the collection of kinematic data from the jumping trials, these included three Sony digital Handycam VX1000E video cameras which recorded at 50 Hz and an NAC high speed camera (as used in the laboratory based data collection) which recorded at 200 Hz (Figure 5.6). One of the Sony cameras was placed along side the bar to get an image of the subject during the flight phase (Camera 1). This camera was used for qualitative purposes only. The other two Sony cameras were placed perpendicular to the final approach stride (Camera 2), and directly behind the subject during the final stride (Camera 4). The high speed camera (Camera 3) was placed directly next to Camera 2. The three Sony cameras all operated with a shutter speed of 1/600 s, and the high speed camera operated with a shutter speed of 1/2500 s. All cameras were placed at a distance from the takeoff area which allowed the whole takeoff phase to be viewed.

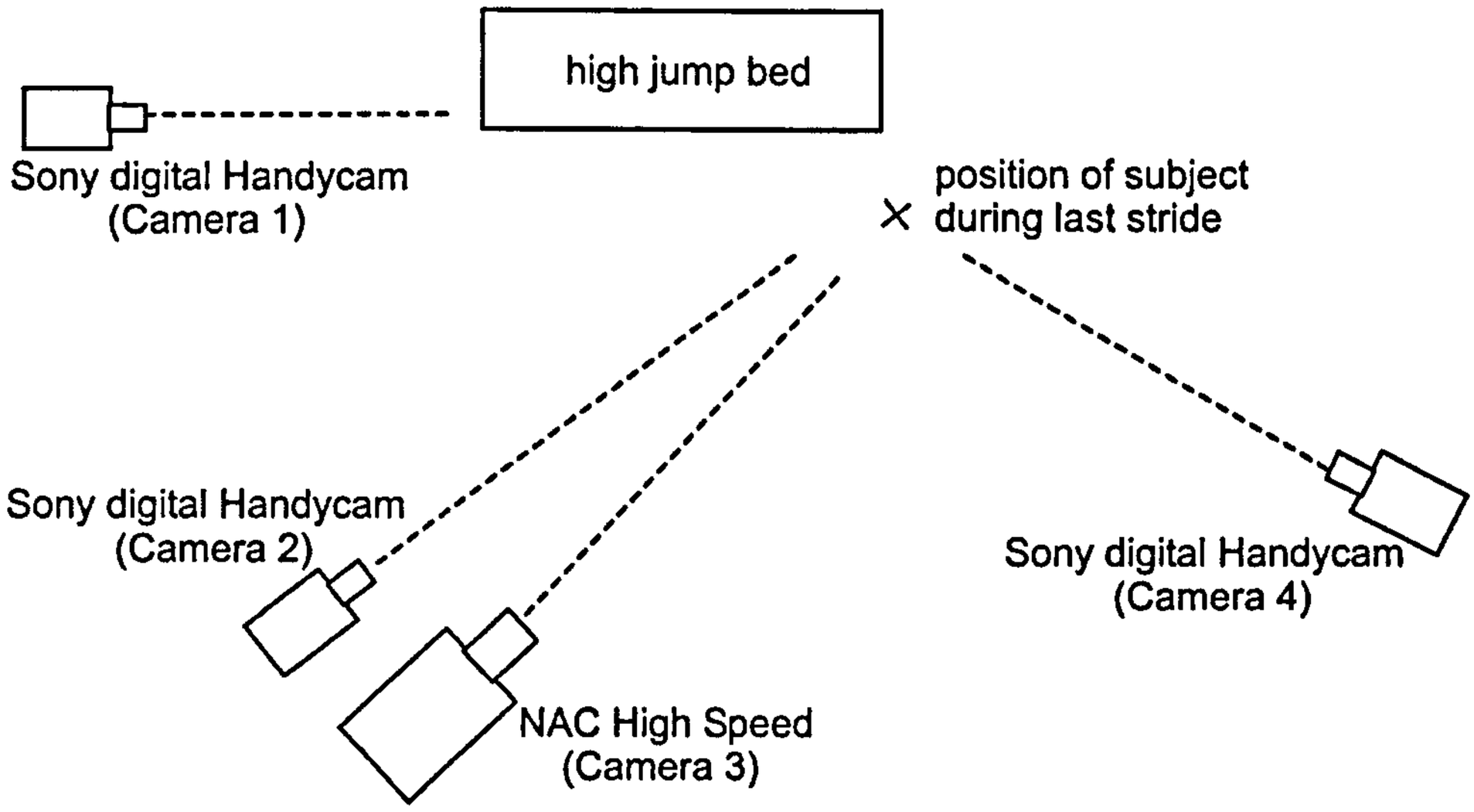

Figure 5.6. Arrangement of cameras for the field study.

Calibration set-up

A calibration pole with three markers at known locations (Figure 5.5) was placed on 11 positions within the movement space, which were at known distances from the origin (0,0).

The 2-D locations of the pole relative to the origin and the locations of the markers from the bottom of the pole were measured using steel tapes. Each camera view had a different number of calibration poles visible (Table 5.2). Locations of the poles are shown in Figure 5.7.

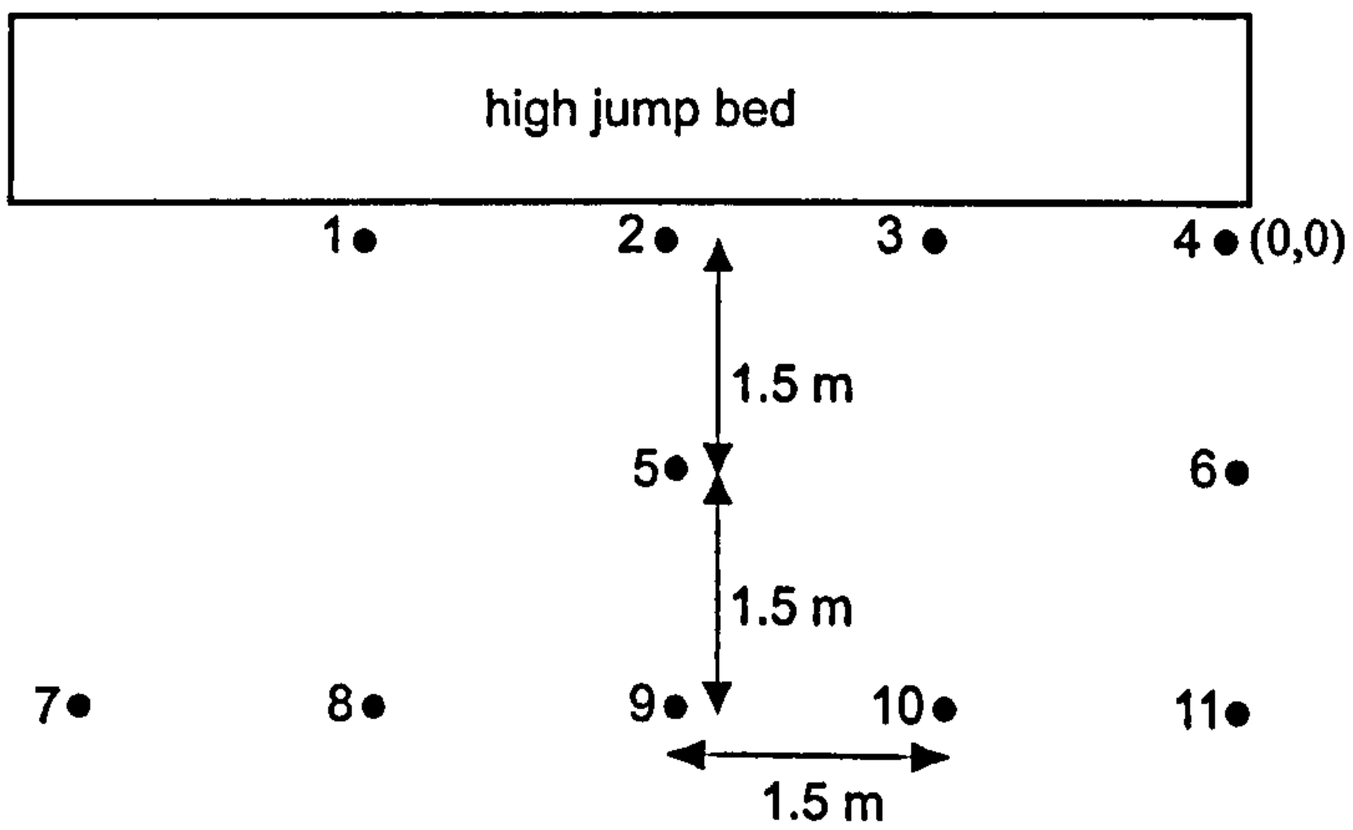

Figure 5.7. Arrangement of calibration poles for the field study.

Table 5.2. Calibration points visible from each camera.

Camera	Calibration poles	Number of calibration points
2 (Sony 50 hz)	1 – 10	30
3 (high speed)	1 – 6, 11	21
4 (Sony 50 Hz)	2 – 5, 8 – 10	21

Data analysis

Laboratory based trials

Force / Coda data

The force data were collected via the Coda system at a frequency of 800 Hz. The Coda system and the force plate were set to record data once the subject indicated he was ready. The remote control for the synchronisation lights was subsequently pressed which resulted in the first light in the series coming on at the same time that the impulse produced by the electrode on the back of the remote control produced a square pulse on the second force channel. The time offset between the force data initially being captured and the time when the synchronisation lights came on was calculated from the time of the pulse on the second force channel and the time of the force data initially being recorded. This allowed manual synchronisation of the force / Coda data and the video data. The time bases of all the movement data were subsequently translated so that the time at which the force plate initially started recording corresponded to time zero for each trial.

Coda

The Coda data were collected in order to analyse many of the running jumps and drop jumps with the intention of determining muscle strength parameters. However, there were significant problems which resulted in the Coda data not being used. These were as a result of the movement of the markers relative to the body landmarks. This was caused by human tissue movement but more detrimentally by the markers having a mass. The video data was therefore required for the analysis of the jumps. Because the video images needed to be

manually digitised, the number of trials which could be analysed was limited due to time constraints. Two trials were chosen. These were **trial 36**, a jump for maximum height, and **trial 46**, a jump for maximum distance. Both trial 36 and 46 were performed using an approach of 6 strides. These trials were chosen as they were considered the best performances. No EMG data were collected for these two trials, therefore, no Coda or EMG data were utilised in this study.

Force

The vertical force were collected through four channels, which corresponded to the force produced at each of the four piezo-electric sensors of the plate. These four force channels were then combined to give two, to represent the force at the front and back of the force plate. The force needed in the angle-driven models (Chapter 4) was a force acting at the toe, and a force acting at the heel. From observation of the video data it was clear that for both the trial for height and the trial for distance the initial contact with the ground was by the heel and the final contact with the ground was by the toe.

When only the heel was in contact with the ground, all the force was considered to act at the heel, similarly, when only the toe was in contact all the force was considered to be acting at the toe. When the whole foot was in contact with the ground the force was split between the heel and toe in a ratio determined by a quintic function which moved the centre of pressure smoothly from the heel to the toe.

The horizontal force data from the original laboratory data collection was incomplete due to the horizontal gain range being set too low. A second laboratory data collection took place. The elite male high jumper performed a series of three running jumps for maximum height and three running jumps for maximum distance and was instructed to perform the jumps in as similar way as possible to the initial trials. The x,y gain range was set at 50,000 Pc/10 V, and it was checked that all the horizontal force data was recorded.

The vertical force data in each of the new trials was compared to the vertical force data in the corresponding initial trial. The trial which matched closest to the original trial in terms of time of contact was chosen to compare forces with. The time of the new trial was scaled so that the contact time was

exactly the same as that of the original trial. Figure 5.8 shows a comparison between the original vertical force trace from trial 46 and the vertical force trace scaled for time from the new chosen trial.

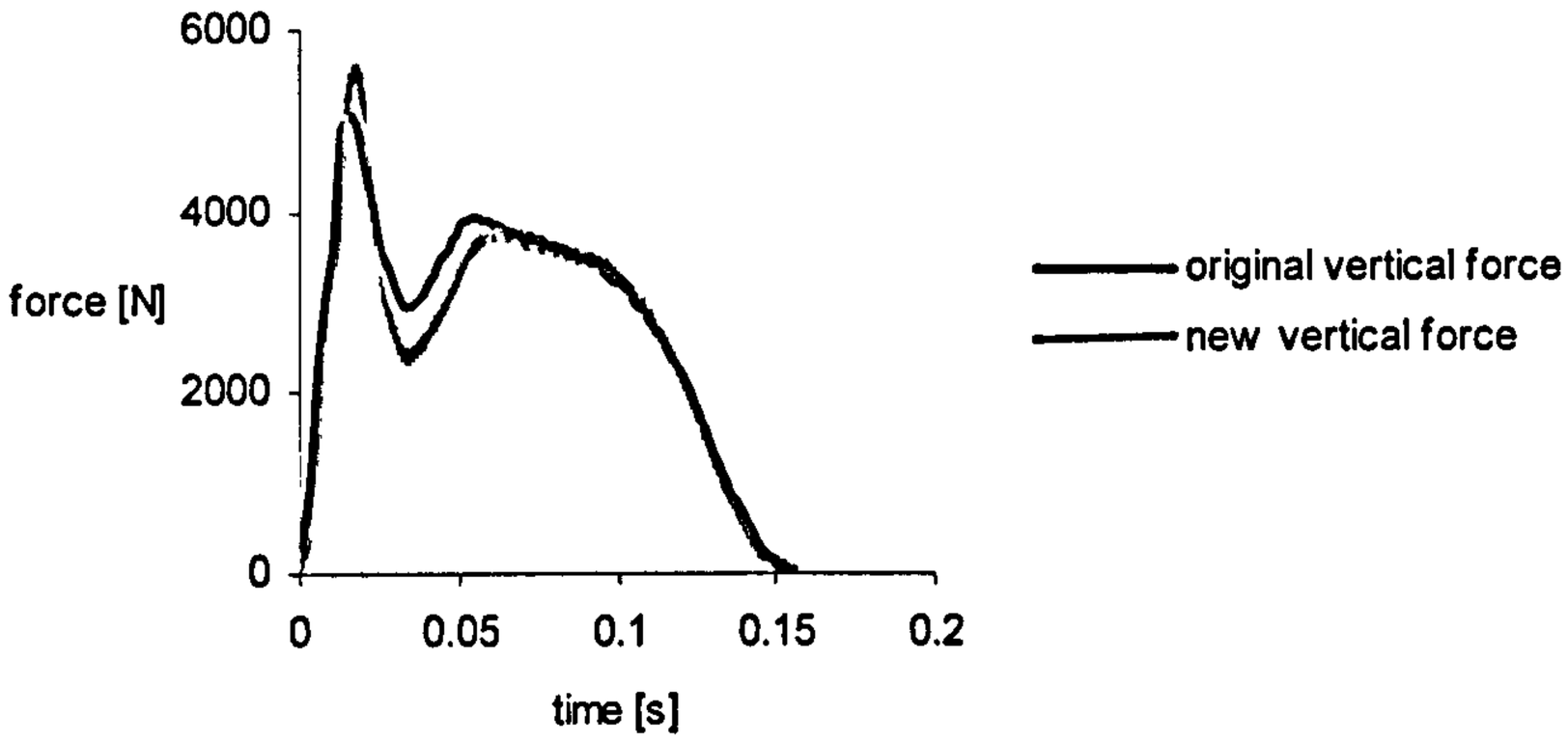

Figure 5.8. New and original vertical force traces for trial 46.

The horizontal force values were initially kept the same, while the time of contact was scaled, and the impulse over the new scaled time was calculated. From the original trials, the horizontal impulse was calculated using the velocity of the mass centre at touchdown and takeoff (equation (5.1)).

$$\text{Impulse} = mv - mu \qquad (5.1)$$

Where: m = mass, v = velocity at takeoff, and u = velocity at touchdown

The horizontal force was subsequently scaled in order to give an impulse equal to that calculated for the original trial. Figure 5.9 shows a comparison of the horizontal force collected during the original and second data collections, to show the beginning and end of the two graphs are similar.

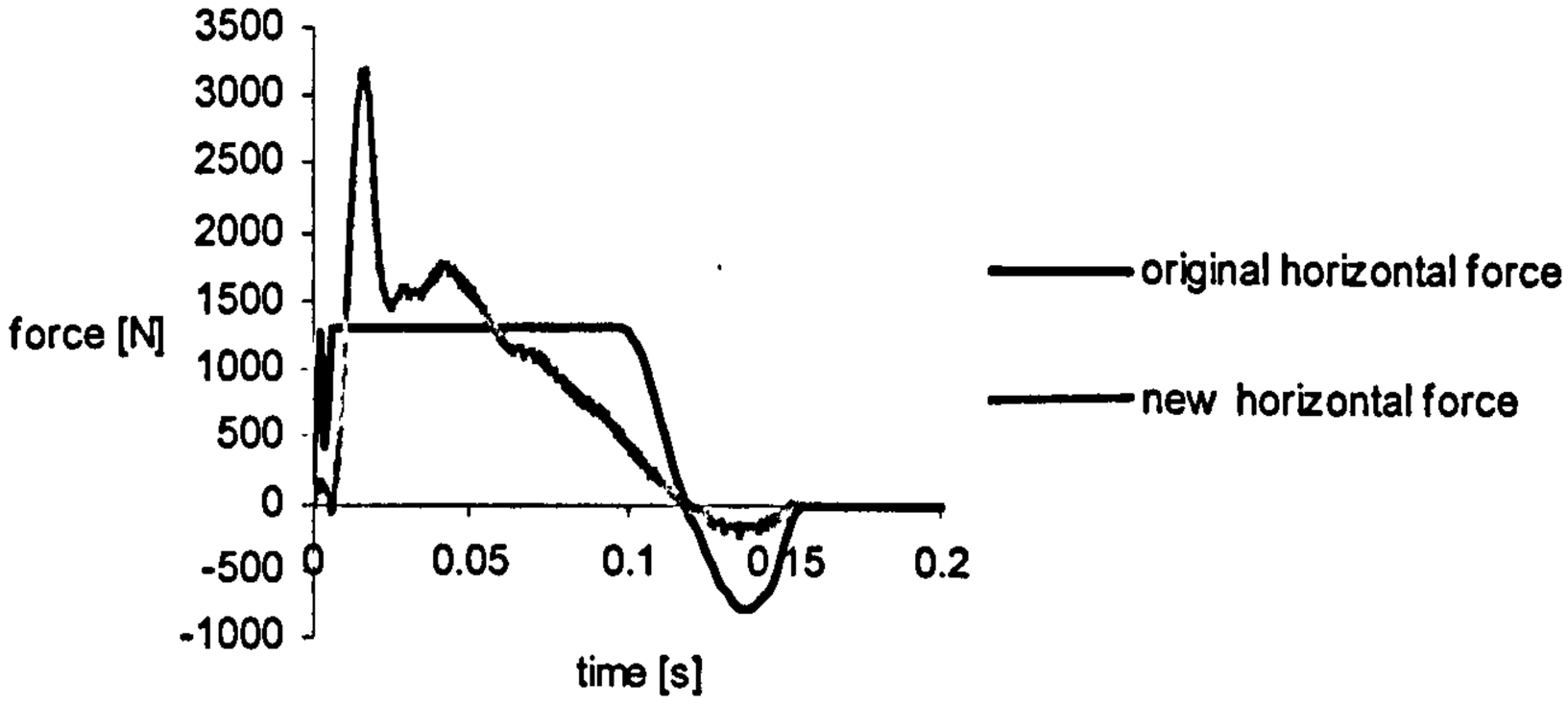

Figure 5.9. New and original horizontal force traces for trial 46.

Finally, the horizontal force was split into the horizontal force at the toe and at the heel using the same technique used for the vertical force.

Video

The video data were digitised using the Target system (Kerwin, 1995). Prior to digitisation of the movement data, the calibration volume was digitised.

Calibration

Five images of the calibration volume were digitised along with two reference frames. The digitised coordinates of the calibration markers were used to calibrate each camera view, obtaining the 12 camera DLT parameters required.

From the measured 3-D locations of the calibration points together with the digitised coordinates each camera view was calibrated separately by solving for the 12 Direct Linear Transform (DLT) parameters in the method of Karara (1980) (equations (5.2 and 5.3)). The 12 parameter DLT reconstruction includes a correction for radial lens distortion (equations (5.3)).

$$u' = \frac{L_1 x + L_2 y + L_3 z + L_4}{L_9 x + L_{10} y + L_{11} z + 1}$$

$$v' = \frac{L_5 x + L_6 y + L_7 z + L_8}{L_9 x + L_{10} y + L_{11} z + 1} \qquad (5.2)$$

where u' and v' are the undistorted digitised co-ordinates and:

$$\begin{aligned} u' &= u + \Delta u \\ &= u + (u - u_0) r^2 L_{12} \\ v' &= v + \Delta v \\ &= v + (v - v_0) r^2 L_{12} \end{aligned} \qquad (5.3)$$

Where:

(u,v)	digitised locations
(x,y,z)	3-D locations of the digitised points
$L_1 - L_{11}$	DLT parameters
u,v	distorted digitiser co-ordinates
u_0, v_0	centre of the image
r	distance between digitised point and centre of the lens

L_{12} radial lens distortion parameter

The DLT parameters were obtained using a linear least squares equation solver (Stewart, 1973). The root mean squared (rms) reconstruction errors for the calibration points in each of the three axes (x,y,z) were calculated.

Camera 3 (50 Hz) was paired with both Camera 1 (50 Hz) and Camera 2 (200 Hz) in order to calculate the DLT parameters for each camera. This resulted in two sets of parameters for Camera 3 which varied slightly from each other as a result of using different combinations of calibration points.

Due to tapes being changed in the video cameras between the trial 36 and trial 46, and hence the chance of camera movement, the calibration volume was re-digitised at the end of the all the trials. DLT parameters for the two pairs of cameras, for trials after the tapes had been changed, were calculated from the second set of digitised calibration points resulting in two sets of DLT parameters for each camera pairing. These two sets of DLT parameters were, however, very similar, showing none or very little camera movement had occurred.

Movement data

The movement data files for trials 36 and 46 consisted of two digitised reference frames followed by the digitised movement sequence. The two reference frames consisted of digitised points of fixed locations in the field of view identical to those digitised in the calibration files. These points were digitised in both the calibration and movement data files in order to check that no movement of the camera had occurred. There was found to be no systematic movement of the digitised points in the reference frames and hence it was assumed no movement of the camera had occurred. In each field of the movement sequence 15 points were digitised. These were the wrist, elbow, shoulder, hip, knee, ankle and toe on both sides of the body and the centre of the head. The views from all three cameras were digitised (in every field where all the body landmarks were visible) for both trials.

Synchronisation

Camera 3 was again paired with Camera 1 and Camera 2 in order to obtain 3-D locations of the digitised points throughout the jumping trials. The two sets of digitised co-ordinates for each trial for both camera pairings were synchronised to within one field by identifying a common event in each camera view, namely, the first foot contact with the force plate. The method of Yeadon and King (1999) was subsequently used to synchronise the data from all camera views to within 1 ms. Quintic splines were tightly fitted to the digitised data. One set was then interpolated to give digitised data at the same time as the second data set.

3-D reconstruction

For each camera pairing, the synchronised digitised co-ordinates, the 12 DLT parameters for each camera and the 11 segment inertia data (Chapter 6) were entered into the video analysis program *hj15.f*. The 3-D locations of each digitised point were reconstructed using the method of Karara (1980). The least squares solution to this resulted in the 3-D location of each digitised point which was closest to the four planes by minimising the sum of squares of the residual distances. The video analysis program determined the RMS distances of the reconstructed points from the four planes. These RMS distances for all points were determined in each of the three axes (x,y,z).

Weightings

For the reconstruction of the digitised data from Camera 2 (200 hz) and Camera 3 (50 Hz), it was necessary to interpolate the quintic spline fitted to the digitised video data from Camera 3 in order to give four times as much information as was digitised. During the contact phase it was suggested that the sampling rate of 50 Hz (Camera 3) was not sufficient and that the interpolation of these data would result in data which was not a true representation of the movement. In order to investigate this the z co-ordinate of the left ankle location of each field during the contact phase was plotted for Camera 3 (50 Hz) and Camera 2 (200 Hz), to consider whether the function for the data from Camera 2 was a lot more complex than that from Camera 3. From the graphs it was concluded that a frequency of 50 Hz was sufficiently high enough for the data

being collected and so the horizontal and vertical data from both cameras were all given equal weightings.

Time base

Once each trial had been synchronised it was possible to use the same time base for all the recordings of each trial. With the pairing of Cameras 1 and 3, the time offset translated the time base of Camera 3 on to the time base of Camera 1. With the pairing of Cameras 2 and 3, the time offset translated the time base of Camera 3 onto the time base of Camera 2 to give data at 200 Hz and not 50 Hz. All the recordings of each trial were then translated onto the time base of Camera 1 as Camera 1 was the only Camera which could clearly see the synchronisation lights. Using the time base of Camera 1 for all views therefore enabled the movement data to be synchronised with the force and Coda data. In addition all time bases were translated so that the initial foot contact with the force plate corresponded to time zero for each trial.

Segment length correction

The thigh and trunk lengths calculated from the re-constructed digitised data and those determined from anthropometric measurements (Chapter 6) differed by over 50 mm. It was hypothesised that this was due to the hip being digitised lower than it should have been, due to the hip location being hard to identify. In order to correct for this, the midpoint of the left and right hip was moved by 8.5% along the mid-hip to mid-shoulder line to reduce the length of the trunk and increase the length of the thigh.

The change in the mid-hip position resulted in the trunk segment length in trial 36 decreasing from 619 mm to 566 mm and in trial 46 decreasing from 600 mm to 549 mm. These changes resulted in the trunk lengths in both trials moving closer to the anthropometric measurement of trunk length of 534 mm. The change in mid hip position, in turn, resulted in the thigh length in trial 36 increasing from 414 mm to 460 mm and in trial 46 increasing from 397 mm to 433 mm, again moving closer to the anthropometric measurement of thigh length of 429 mm. The 8.5% change in trunk length was decided upon as it resulted in the trunk and the thigh length differing from the anthropometric measurements by almost the

same amount. After these alterations, the trunk was still too long compared to the anthropometric measurement but this could be accounted for by the fact the shoulders are raised when the arms are lifted above the head, hence stretching the length of the trunk.

Field based trials

A similar procedure was used for the analysis / processing of the data collected outside as for the data collected in the laboratory. The main difference between the two being that only video data and no force data were collected outside. These data were collected in order to compare the jumping trials performed in the laboratory with an actual high jump performance in terms of approach characteristics and height reached by the mass centre.

Video

Calibration

Camera 4 was paired with Camera 2 and Camera 3 in order to calculate the DLT parameters for each camera. Again this resulted in two sets of DLT parameters for the common camera (Camera 4) which varied slightly.

Movement data

As with the data collected in the laboratory, in each field of the movement sequence 15 points were digitised. The views from all three cameras were digitised for every field where all the body landmarks could be seen for trial 11. This trial used was an attempt at 2.00 m which the subject failed but was very close to clearing. This was considered the best performance by the subject.

3-D reconstruction

The common event used to manually synchronise the two views within each camera pairing to within one field was taken to be takeoff. The 3-D locations of each digitised point were calculated in exactly the same way as with the data collected in the laboratory. The time-offsets between Camera 2 and Camera 4, and Camera 3 and Camera 4 were subsequently determined using the method of Yeadon and King (1999).

Time base

With the pairing of Cameras 2 and 4, the time offset translated the time base of Camera 2 on to the time base of Camera 4. With the pairing of Cameras 3 and 4, the time offset translated the time base of Camera 4 onto the time base of Camera 3 to give data at 200 Hz and not 50 Hz. All the recordings of each trial were then translated onto the time base of Camera 4.

Data required

The following section will describe the procedures used to calculate the required kinematic data for the jumping performances in the laboratory from the reconstructed 3D locations of the digitised body landmarks.

Contact and takeoff times

Six times of contact and takeoff were identified for each jumping trial as follows:

(i) penultimate takeoff
(ii) touchdown
(iii) toe-down
(iv) heel-off
(v) takeoff
(vi) landing

To identify these times, the displacements of the toe and ankle, and the force data were used. The times for the penultimate takeoff, identified as the first field after the non-takeoff foot had lost contact for the last time, and the landing, identified as the last field prior to landing, were identified to the nearest field from the video recordings of the 50 Hz camera only. The touchdown, toe-down, heel-off and takeoff were all identified from the force data to the nearest 0.00125 of a second. These four times were also identified to the corresponding field from the 50 Hz camera. Touchdown was identified as the first field the heel was in contact with the force plate, toe-down as the first field the toe was in contact with the force plate, heel-off as the first field after the heel had lost contact, and takeoff as the first field after the toe had lost contact.

Location and velocity of the mass centre

The location and velocity of the mass centre at touch down and takeoff were calculated using the times of contact and takeoff along with the 3D locations of the digitised landmarks and force data and equations of constant acceleration.

The velocity of the mass centre at takeoff was calculated using the 50 Hz video data. The position of the mass centre in the field immediately after takeoff and the field immediately prior to landing were obtained. Using this positional data and equation (5.5), the velocity of the mass centre in the field immediately after takeoff was calculated. The time difference between this field and takeoff was known and therefore the velocity of the mass centre at takeoff could be calculated using equation (5.4).

$$v = u + at \tag{5.4}$$

The vertical velocity of the centre of mass at touchdown was calculated using the vertical velocity at takeoff and the vertical takeoff impulse calculated from the force data.

As the horizontal force data were initially missing, the horizontal velocity at touchdown was calculated using the 200 Hz video data. The 50 Hz video data were of no use as there were not two fields during the last airborne phase. The same method as used with the 50 Hz data to calculate the takeoff velocities was employed to calculate the touchdown velocities.

Using the 200 Hz video data and the mass centre velocities obtained above, the positions of the mass centre in the field just prior to touchdown and just after takeoff were obtained. Using the time of touchdown and the time of takeoff and equation (5.5), the positions of the mass centre at touchdown and takeoff were calculated.

$$s = ut + \frac{1}{2}at^2 \tag{5.5}$$

Where:

s = displacement

u = initial velocity

t = time

a = acceleration

Orientation and configuration angles / angular velocities

The time histories of the angles and angular velocities of the ankle, knee, hip, shoulder, elbow, free hip and free knee joints, and trunk with respect to the horizontal were calculated for the whole of the contact phase from the 3-D locations at 200 Hz obtained from Camera 2 and Camera 3. All angles were determined from the 2-D coordinates of the joint centres ignoring the effect of movement of the joint centres away from a vertical plane running parallel to the direction of travel. The angles were calculated from the sine and cosine of each angle using the method described in Yeadon (1990a) which ensured that the angle time histories were continuous.

To smooth the time histories of the calculated angles and to calculate the angular velocities quintic splines (Wood and Jennings, 1979) were fitted to the time histories of each angle. The closeness of fit at each point was based on the difference between the data and a pseudo data set which was generated by averaging the two angles from the two adjacent times.

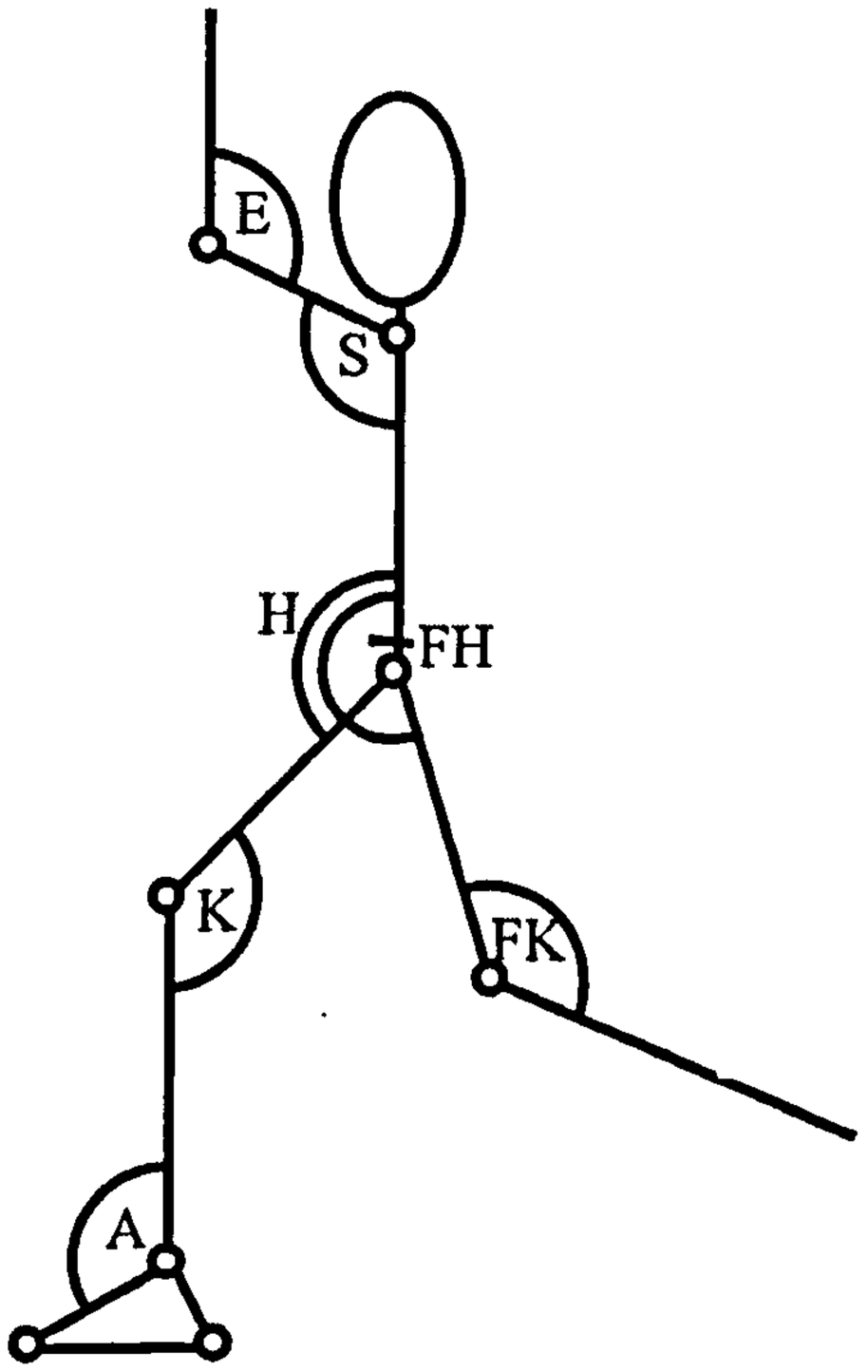

E = elbow angle

S = shoulder angle

H = hip angle

K = knee angle

A = ankle angle

FH = free hip angle

FK = free knee angle

Figure 5.10. Angle definitions.

Angular momentum

The model of Yeadon (1990c) was used to determine the angular momentum at takeoff from quintic spline coefficients fitted to the orientation and configuration angles throughout each performance. The angular momentum estimates for each digitised frame of post flight were averaged to give a better estimate of angular momentum at takeoff.

Ground reaction forces

The ground reaction forces produced during the jumps were obtained from the force plate via the Coda system and were divided into forces at the heel and toe.

Results and discussion

The following results were obtained from the analysis of the video and force data collected during the jumping trials performed in the laboratory and the high jumping trial performed at an athletics track. The results include the reconstruction errors and the accuracy of the calibration. The data required for the simulation models is also discussed.

Reconstruction errors and accuracy

Laboratory based data collection

The locations of the digitised calibration markers were reconstructed in order to estimate their accuarcy. The DLT parameters for each pairing are shown in Table 5.3. The (x,y,z) coordinate errors of the reconstructed locations of the calibration points are shown in Table 5.4. These DLT parameters values are those used for trial 36, however, as already stated these were very similar to those used for trial 46.

Table 5.3. DLT parameters for each camera pairing (laboratory).

Camera 1 and Camera 3 pairing		Camera 2 and Camera 3 pairing	
Camera 1	Camera 3	Camera 2	Camera 3
434.277	-1630.070	-1264.236	-1630.071
1755.758	-877.706	3483.026	-877.706
1366.991	-57.353	-6.140	-57.353
8042.801	6190.194	6209.315	6190.194
-1078.208	46.244	-1164.846	46.244
363.212	-691.540	-88.301	-691.540
1332.541	1640.230	3301.729	1640.230
2323.109	2691.796	746.987	2691.796
-0.081	-0.008	-0.198	-0.008
0.065	-0.117	-0.012	-0.117
0.043	0.004	-0.016	0.004
0.000	0.000	0.000	0.000

Table 5.4. Average reconstruction errors of the calibration points (laboratory).

Camera pairing	number of markers	X error [m]	Y error [m]	Z error [m]	mean error [m]
Camera 1 & Camera 3	47	0.013	0.016	0.006	0.012
Camera 2 & Camera 3	18	0.011	0.005	0.003	0.006

Field based data collection

The accuracy of the reconstruction of the 3-D locations of the calibration points was calculated and the (x,y,z) co-ordinate errors of the reconstructed locations of the calibration points are shown in Table 5.6, and the DLT parameters for each camera pairing are shown in Table 5.5.

Table 5.5. DLT parameters for each camera pairing (field).

Camera 2 and Camera 4 pairing		Camera 3 and Camera 4 pairing	
Camera 2	Camera 4	Camera 3	Camera 4
-1725.639	-1104.005	2491.157	-1104.005
707.823	-2216.681	1314.658	-2216.681
40.615	29.176	41.296	29.176
9476.804	7182.792	9603.741	7182.792
-44.854	144.430	-101.119	144.430
-144.837	-43.592	-207.072	-43.592
1850.795	2439.531	2680.898	2439.531
1506.980	2484.446	1957.088	2484.446
-0.020	0.022	-0.022	0.022
-0.032	-0.013	-0.032	-0.013
0.002	0.006	-0.001	0.006
0.000	0.000	0.000	0.000

Table 5.6. Average reconstruction errors of the calibration points (field).

Camera pairing	number of markers	X error [m]	Y error [m]	Z error [m]	mean error [m]
Camera 2 & Camera 4	18	0.008	0.006	0.005	0.006
Camera 3 & Camera 4	12	0.010	0.007	0.008	0.009

Accuracy of video frequency

The frequency of the high speed NAC camera was checked using a Quartz timing light system. This was performed in order to check that the frequency of the camera was 200 Hz. The camera was found to have an error of less than 1 part in 24,000, putting the frame rate at 200 ± 0.0083 Hz. It was therefore considered reasonable to use a value of exactly 200 Hz.

Description of the jumping performances

Figures 5.11 and 5.12 show the computer graphics sequences of the actual performances of the jumps for height and distance respectively. The two sequences of graphics show the approach, touchdown, takeoff, flight phase and landing.

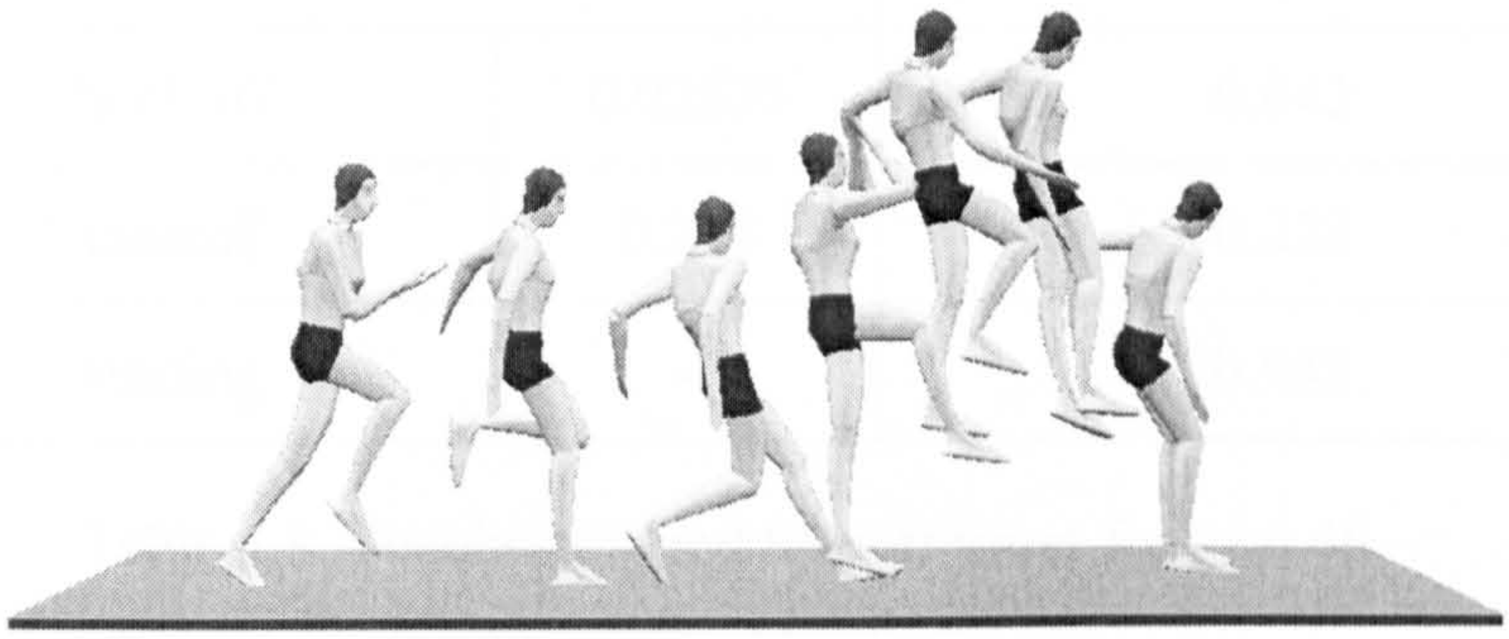

Figure 5.11. Computer graphics sequence of the jump for height.

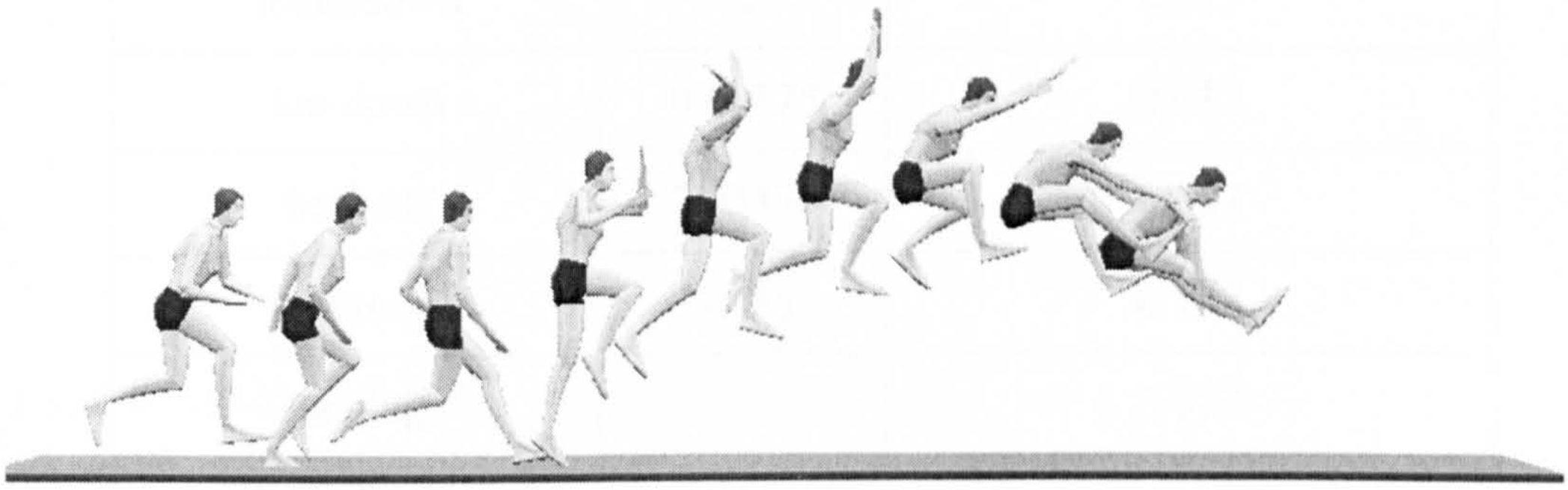

Figure 5.12. Computer graphics sequence of the jump for distance.

Times of contact and takeoff

The total time of contact for the jump for height (trial 36) was 205 ms and for the jump for distance (trial 46) it was 155 ms. Tables 5.7 and 5.8 show the identified contact and takeoff times for trial 36 and trial 46 respectively along with the corresponding 50 Hz video field time.

Table 5.7. Touchdown and takeoff times for trial 36.

	Time (s)	Corresponding 50 Hz field (s)
penultimate takeoff	-	-0.018
touchdown	0	0.002
toe-down	0.00625	0.022
heel-off	0.02375	0.042
takeoff	0.205	0.222
landing	-	0.942

Table 5.8. Touchdown and takeoff times for trial 46.

	Time (s)	Corresponding 50 Hz field (s)
penultimate takeoff	-	-0.043
touchdown	0	0.017
toe-down	0.00375	0.017
heel-off	0.03375	0.037
takeoff	0.155	0.157
landing	-	0.977

Location and velocity of mass centre

During the trial for maximum height (trial 36) the mass centre reached a maximum height of 1.83 m and travelled a distance of 1.98 m between takeoff and landing. During contact the mass centre moved vertically 0.35 m and horizontally 0.58 m. During the jump for maximum distance (trial 46) the mass centre reached a height of 1.91 m and travelled a distance of 4.49 m between takeoff and landing. During contact the mass moved 0.23 m vertically and 0.90 m horizontally.

The mass centre horizontal velocity during the contact phase of trial 36 decreased from 4.40 ms^{-1} to 1.89 ms^{-1}, whilst the vertical velocity increased from –0.86 ms^{-1} to 3.31 ms^{-1}. In trial 46 the horizontal velocity of the mass centre during the contact phase decreased from 6.97 ms^{-1} to 5.31 ms^{-1}, whilst the vertical increased from –0.43 ms^{-1} to 3.47 ms^{-1}.

In the actual high jumping trial the horizontal velocity during the contact phase decreased from 6.55 ms^{-1} to 4.36 ms^{-1}, whilst the vertical velocity increased from –0.36 ms^{-1} to 4.02 ms^{-1}. The height reached by the mass centre was 2.01 m.

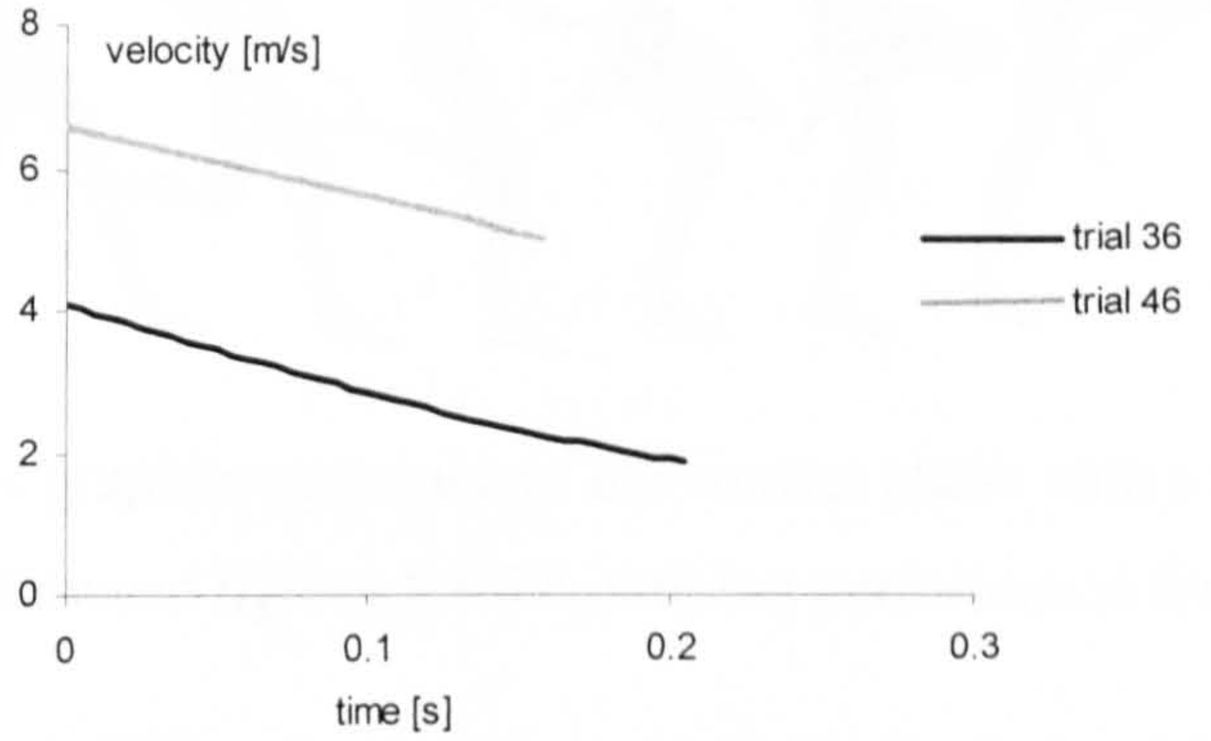

Figure 5.13. Horizontal velocity of the mass centre during the contact phase.

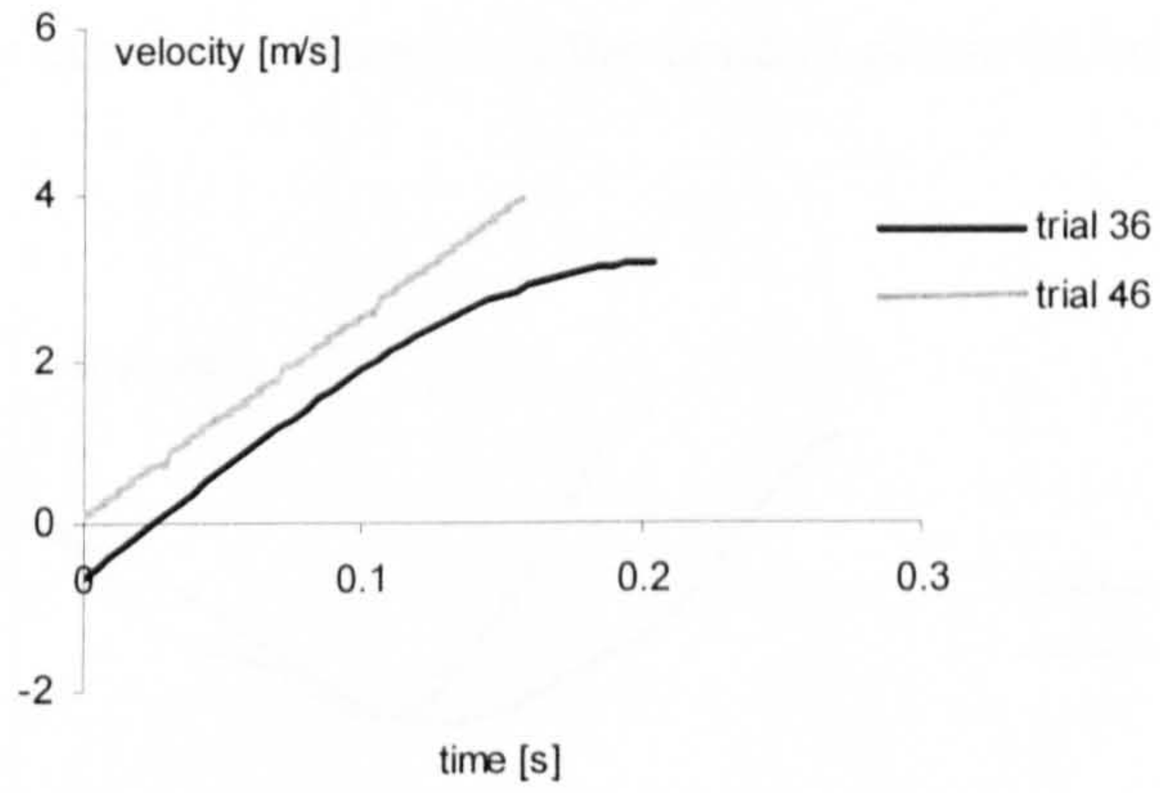

Figure 5.14. Vertical velocity of the mass centre during the contact phase.

Orientation/configuration

Figures 5.15 and 5.16 show computer graphics sequences of the configuration of the body during the contact phase for the jumping performances for height and distance respectively.

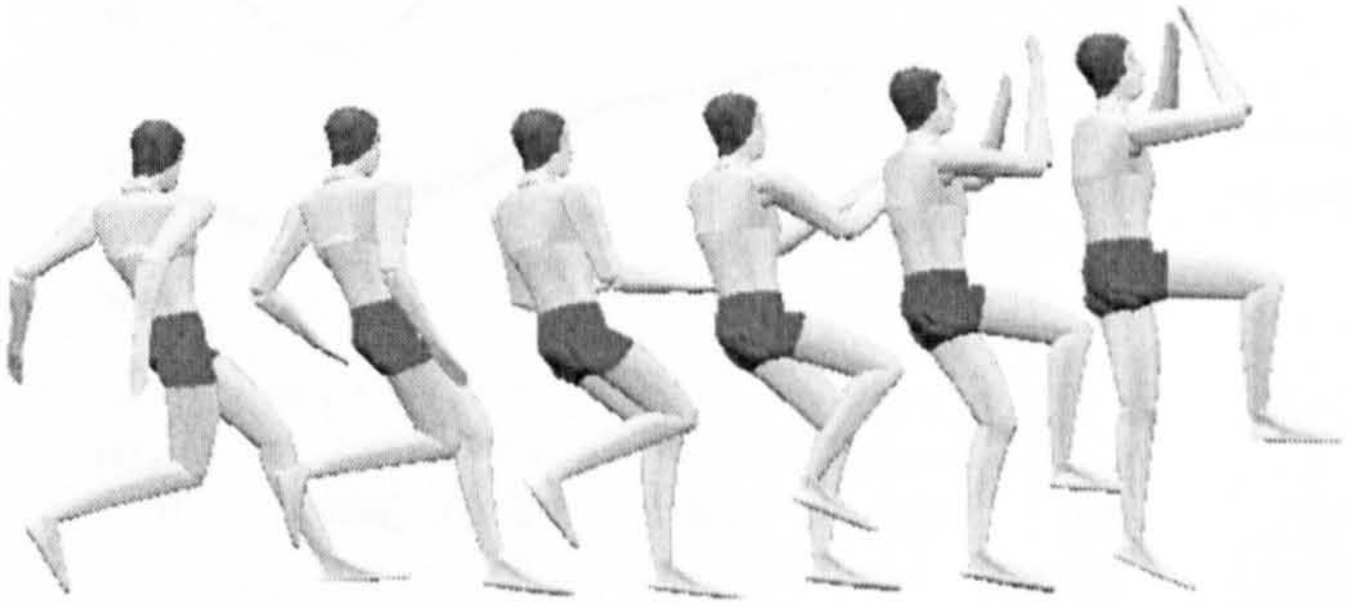

Figure 5.15. Computer graphics sequence of the contact phase with a 0.5 m spacing between figures for the jumping performance for height.

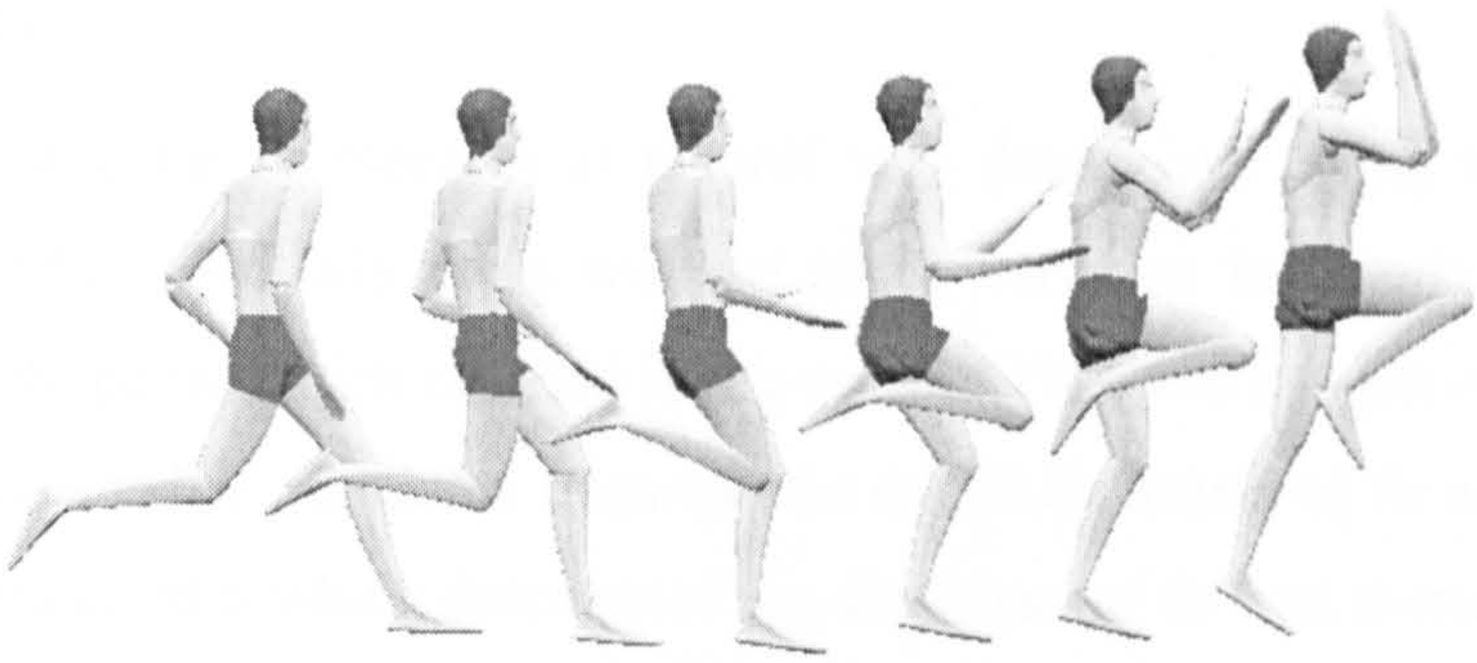

Figure 5.16. Computer graphics sequence of the contact phase with a 0.5 m spacing between figures for the jumping performance for distance.

In both jumping performances the knee angle decreased and then increased until the leg was almost straight at the point of take off (Figure 5.17). The trunk angle remained fairly constant throughout the contact phase in both performances (Figure 5.18).

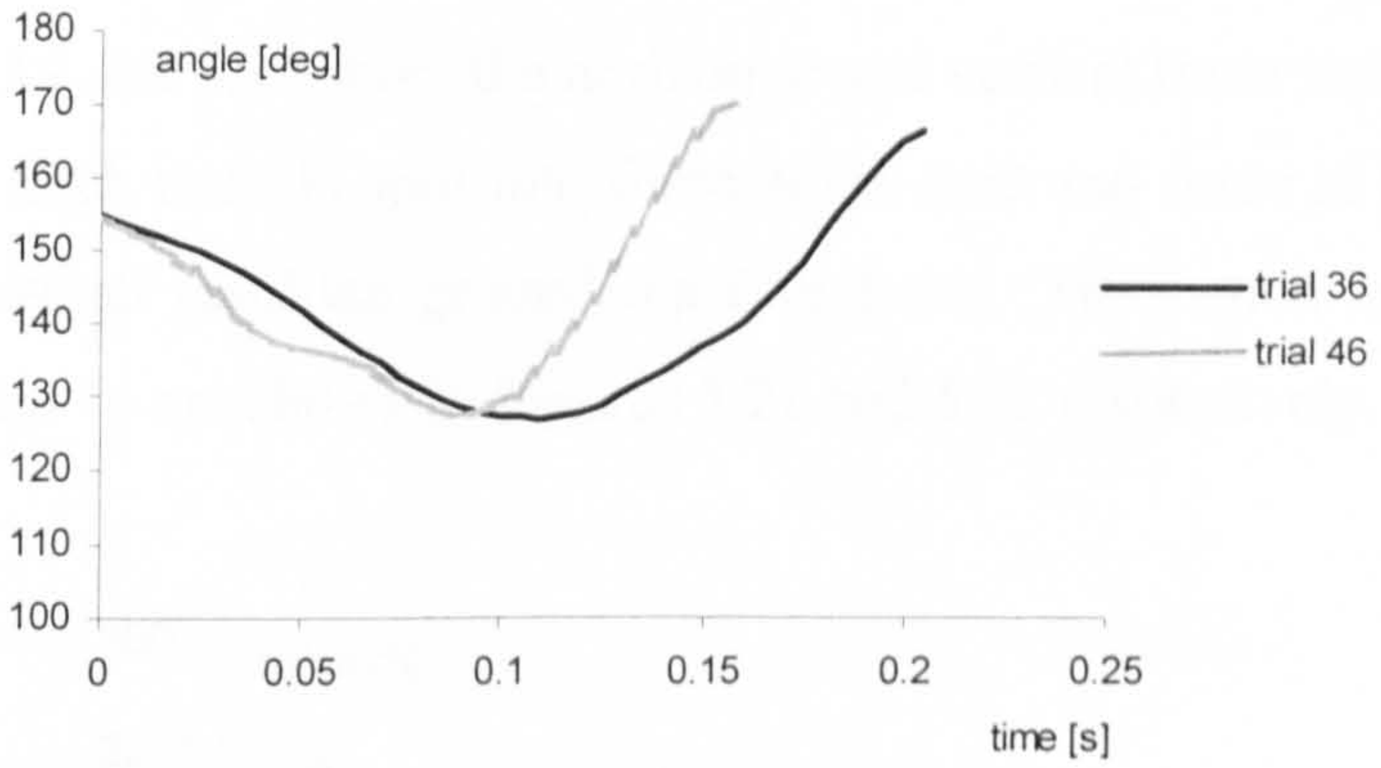

Figure 5.17. Knee angle during contact.

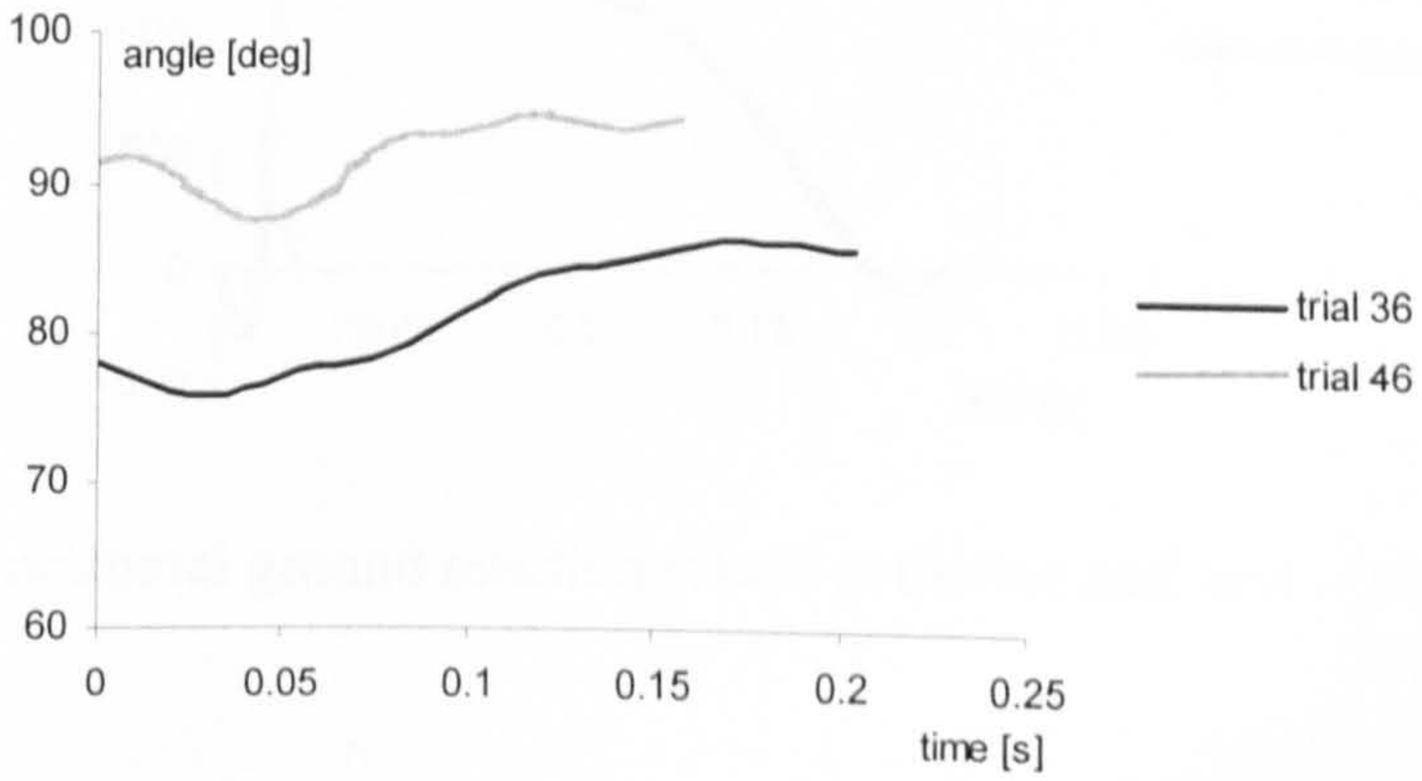

Figure 5.18. Trunk angle during contact.

Angular momentum

The angular momentum at takeoff was determined using the model of Yeadon (1990c). Initially there was too much variation in angular momentum over the flight phase which resulted in big errors. This was a result of the angular velocity values being calculated from splines with a closeness of fit which was too tight. The value of S which determines the closeness of fit was therefore changed from 1.0 to 0.5. If S is very small the splines fit every data point so the error is high. If S is larger more smoothing occurs but this may result in good data being lost.

In trial 36 the angular momentum at takeoff was calculated as 4.9 ± 3.0 $kgm^2.s^{-1}$. An angular momentum of 5.0 ± 3.0 $kgm^2.s^{-1}$ at takeoff was calculated for trial 46.

Ground reaction forces

Figures 5.19 and 5.20 show the horizontal and vertical force traces for trial 36 respectively. Each trace is split into force at the heel and force at the toe but also shows the overall resultant ground reaction force. Horizontal and vertical force traces for trial 46 are shown in Figures 5.21 and 5.22 respectively.

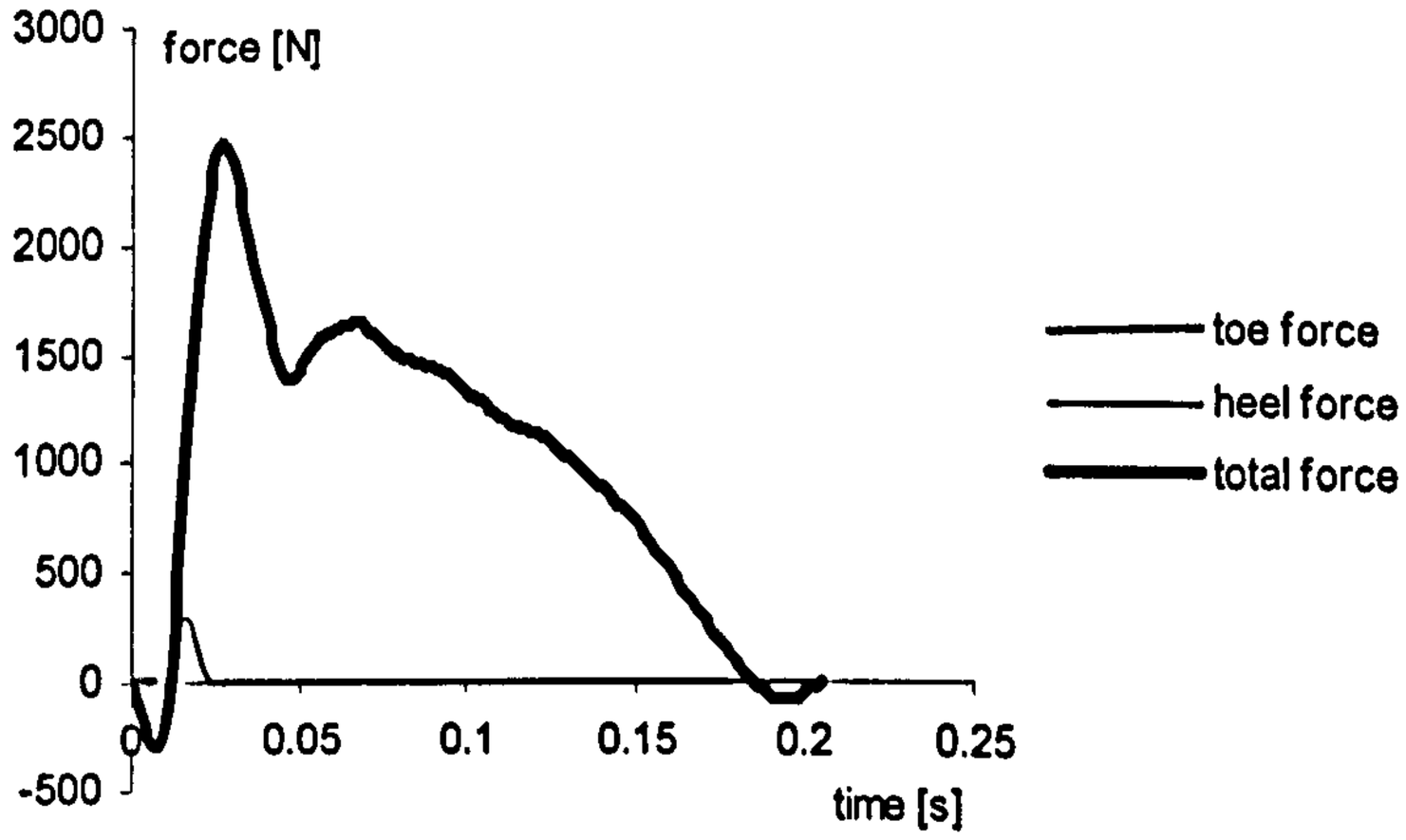

Figure 5.19. Horizontal ground reaction forces at the toe and heel – trial 36.

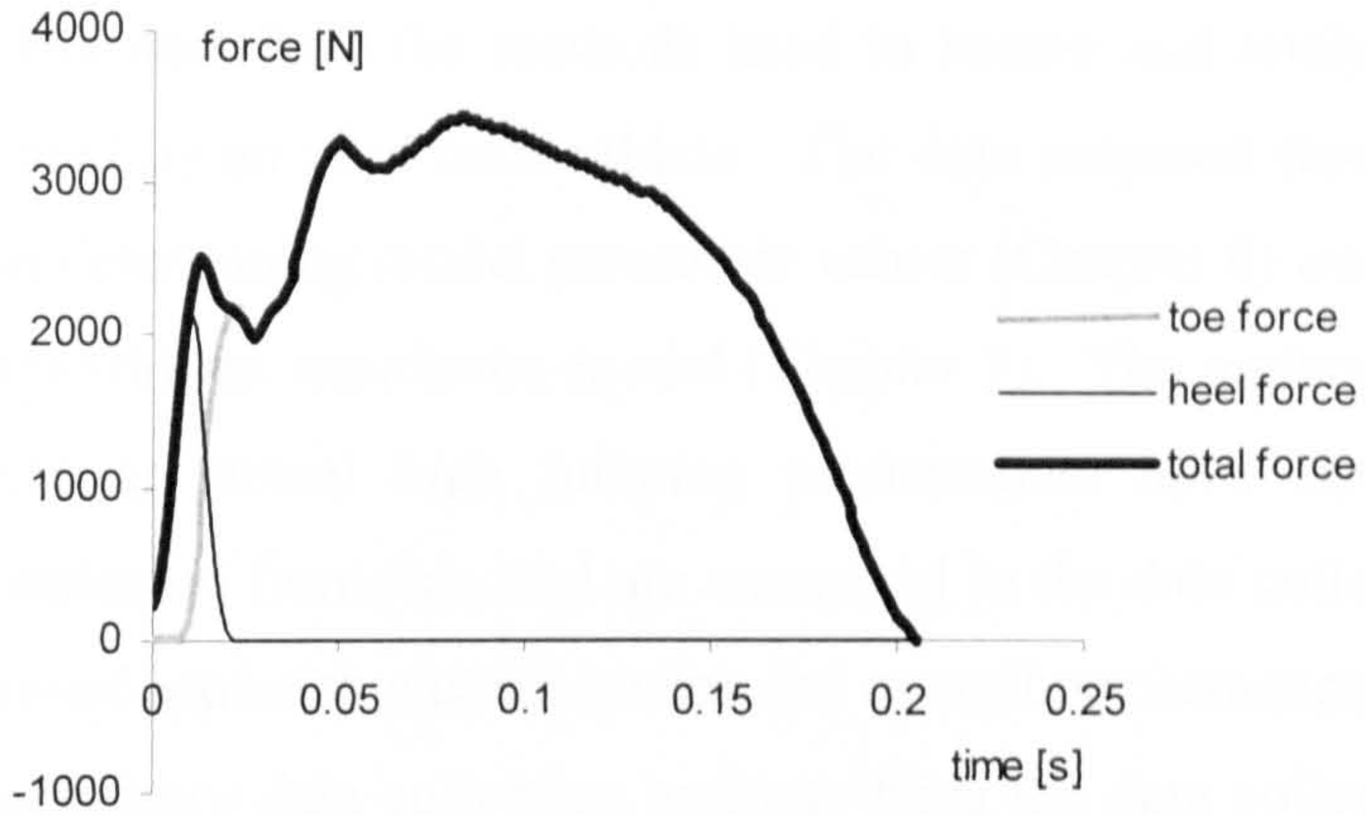

Figure 5.20. Vertical ground reaction forces at the toe and heel– trial 36.

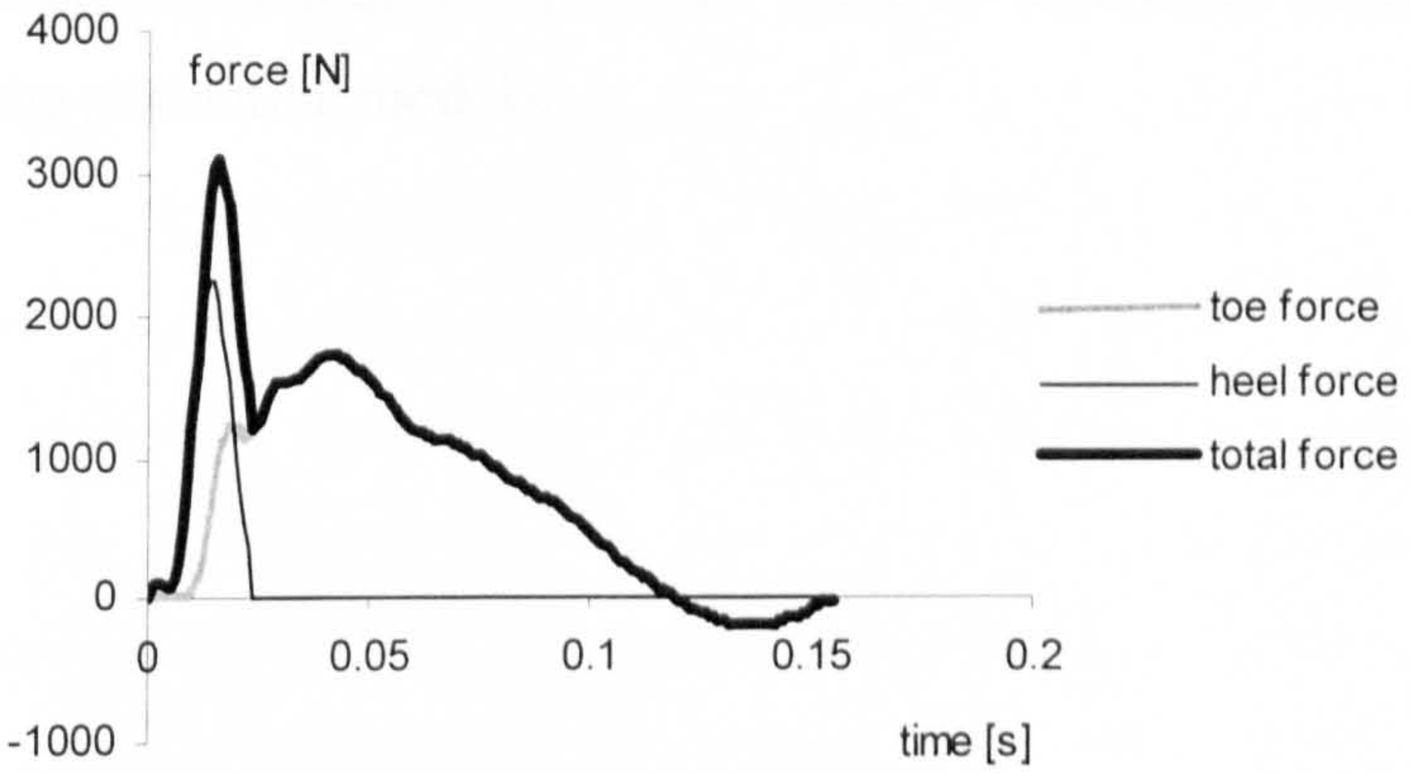

Figure 5.21. Horizontal ground reaction forces at the toe and heel – trial 46.

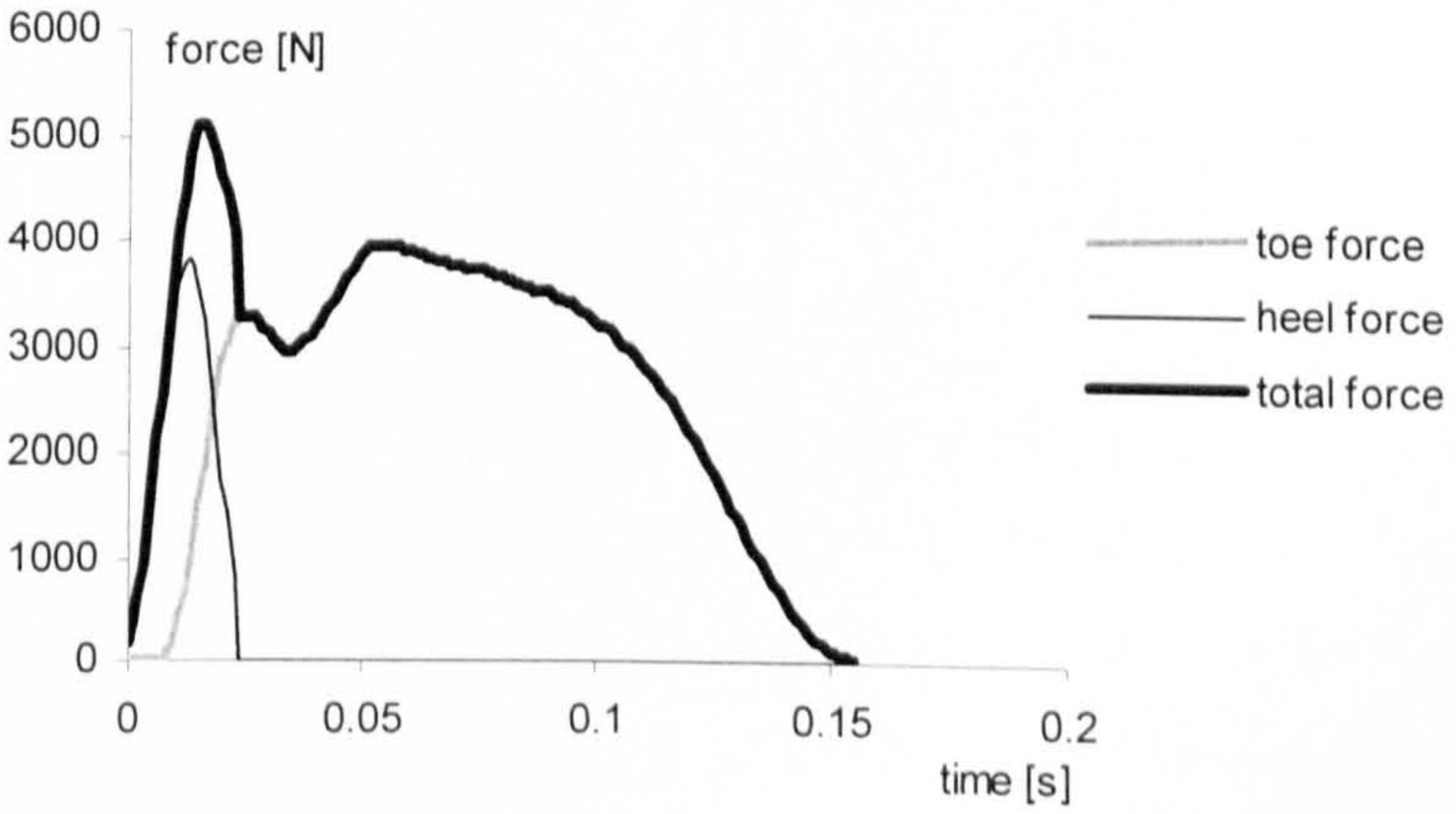

Figure 5.22. Vertical ground reaction forces at the toe and heel– trial 46.

Summary

This chapter has described the methods used to record and analyse two jumping trials performed by an elite male athlete. The data obtained from these recordings are used in determining model parameter values (Chapter 6) and in the evaluation of the torque-driven simulation model (Chapter 7). The methods used to record and analyse an actual high jumping performance have also been described. The data obtained from this trial are compared to the data collected in the laboratory in terms of approach characteristics and overall performance. Only two trials from the laboratory data collection and one from the data collection at the track were chosen to be analysed. This was due to time constraints but was considered sufficient to be able to evaluate the model successfully.

The next Chapter describes the methods used to determine parameter values to be used in the simulation models.

CHAPTER 6

PARAMETER DETERMINATION

Introduction

Chapter 4 discusses the development of three eight-segment models used to simulate the takeoff phases in the long jump and the high jump. The parameters which need to be determined and entered into the models in order for them to be successfully evaluated are also discussed. These parameters include inertia and strength parameters. These parameters are determined from measurements taken on the subject performing the jumping trials. The inertia parameters are calculated from anthropometric measurements and the strength parameters are obtained from data collected using a Cybex isovelocity dynamometer and based on the method of King (1998). The strength parameters define the relationship between maximum torque, joint angle and joint angular velocity for a given joint. In addition, the joint torques determined using the angle-driven simulation models (models 1 and 2) are compared with the maximum torques obtained from the Cybex isovelocity dynamometer.

This chapter describes the methods used and the results obtained from the determination of these inertia and strength parameters along with a comparison of the actual performances and simulations of the angle-driven models.

Inertia

Introduction

Inertia data, comprising the lengths, mass, mass centre locations and moments of inertia of each segment of the body, are required for both the video analysis, in order to calculate the whole body mass centre location, and for the simulation models developed in Chapter 4. The 3-D video analysis requires data for 11 body segments, whilst the 2-D simulation models require the inertia data for eight segments.

There are a number of methods available for calculating the inertia parameter values as discussed in Chapter 2. The most practical of these was to

use a geometric model and anthropometric measurements taken directly from the subject.

Methods

95 anthropometric measurements were taken from the subject and used as input to the inertia model of Yeadon (1990b). The inertia model used the segmental density values of Chandler (1975) as initial estimates. These values were subsequently adjusted until there was an exact match between estimated whole body mass and actual whole body mass as measured using Seca Alpha digital scales. The model splits the body into 11 segments calculating the inertia parameters for each of the segments. When a segment in the simulation model represented both the left and right limb (arms), the masses and moments of inertias of the two limbs were summed to give the segmental parameters of the segment. The shank and foot of the free leg were combined as a single segment in the model using the Parallel Axis Theorem. The inertia parameters for the segments with wobbling masses were assumed to be the values for the combined rigid and wobbling mass segments. Assumptions about the inertia parameters of the rigid body parts (of the segments containing wobbling masses) were made, and using the Parallel Axis Theorem the inertia parameters of the wobbling masses were calculated. Ratios of rigid body mass to wobbling mass were based upon data from Clarys and Marfell-Jones (1986) and calculated using an adapted method of Pain (1999) (details in **Appendix 2**).

Wobbling masses

Values for the individual limb masses and their percentage composition of fat and bone were taken from Clarys and Marfell-Jones (1986), who determined these values using six embalmed cadavers (3 male and 3 female). Values for the percentage composition of bone and fat and total mass of the whole body were taken from Clarys et al. (1984). These values were determined using 25 cadavers from which the six in the 1986 study were taken.

Mass and percentage compositions of bone and fat were not given for the trunk so these values were calculated from whole body and individual limb masses and their percentage compositions.

For each of the shank, thigh and trunk segments (the segments with wobbling masses in the simulation model), the mass which was neither bone nor fat was assumed to be muscle. The amount of fat in each of the three segments was expressed as a percentage of the total body fat. These values were subsequently used to calculate the percentage fat in the trunk, thigh and shank of the subject, along with the total percentage body fat of the subject determined from skin-fold measurements.

The amount of fat in the segments from the cadaver data was more than the amount of fat in the segments of the subject in this study. This excess fat was re-distributed resulting in the segment containing the correct amount of fat. This re-distribution was achieved in two ways:

(1) converting all excess fat to muscle

(2) keeping the muscle to bone ratio constant

The two methods resulted in two values for the percentage of bone in each of the three segments. These two values were considered to be the two extremes, and the initial guess for the ratio of bone to wobbling mass (fat + muscle) was taken as the average of these two values.

Details of the methods used to calculate the ratio of wobbling mass to rigid (bone) in the shank thigh and trunk segment are given in **Appendix 2.**

Results

The segmental inertia parameters used as input into the simulation models are presented in Table 6.1, and the values for the rigid and wobbling mass segments are presented in Table 6.2. The values for the mass centre location are taken from the proximal end of the segment.

Table 6.1. Segmental inertia parameters for the simulation model.

segment	mass [kg]	CM location [m]	length of segment [m]	moment of inertia [kg.m^2]
head + trunk	38.948	0.370	0.898	2.170
upper arms	5.322	0.137	0.317	0.050
lower arms	3.804	0.166	0.481	0.055
left thigh	10.869	0.181	0.429	0.172
left calf	4.777	0.191	0.459	0.075
left foot	1.478	0.090	0.243	0.006
right thigh	10.588	0.184	0.435	0.176
right calf + foot	6.115	0.247	0.450	0.161

Table 6.2. Segmental inertia values for the rigid and wobbling mass segments.

link	segment	mass [kg]	CM location [m]	moment of inertia [kg.m^2]
trunk + head	rigid	4.052	0.449	0.275
	wobbling mass	34.896	0.361	1.694
thigh	rigid	2.638	0.215	0.043
	wobbling mass	8.232	0.170	0.125
shank	rigid	1.554	0.230	0.028
	wobbling mass	3.223	0.172	0.044

Foot anthropometric values

The simulation models described in Chapter 4 require more foot anthropometric parameter values than were initially measured. A total of five values were required to describe the foot, these were the horizontal distance L2 between the toe and the heel, the horizontal distance L1 between the toe and the ankle, the vertical distance L3 between the toe and the ankle, and the horizontal and vertical distances L4 and L5 respectively from the toe to the centre of mass (Figure 6.2).

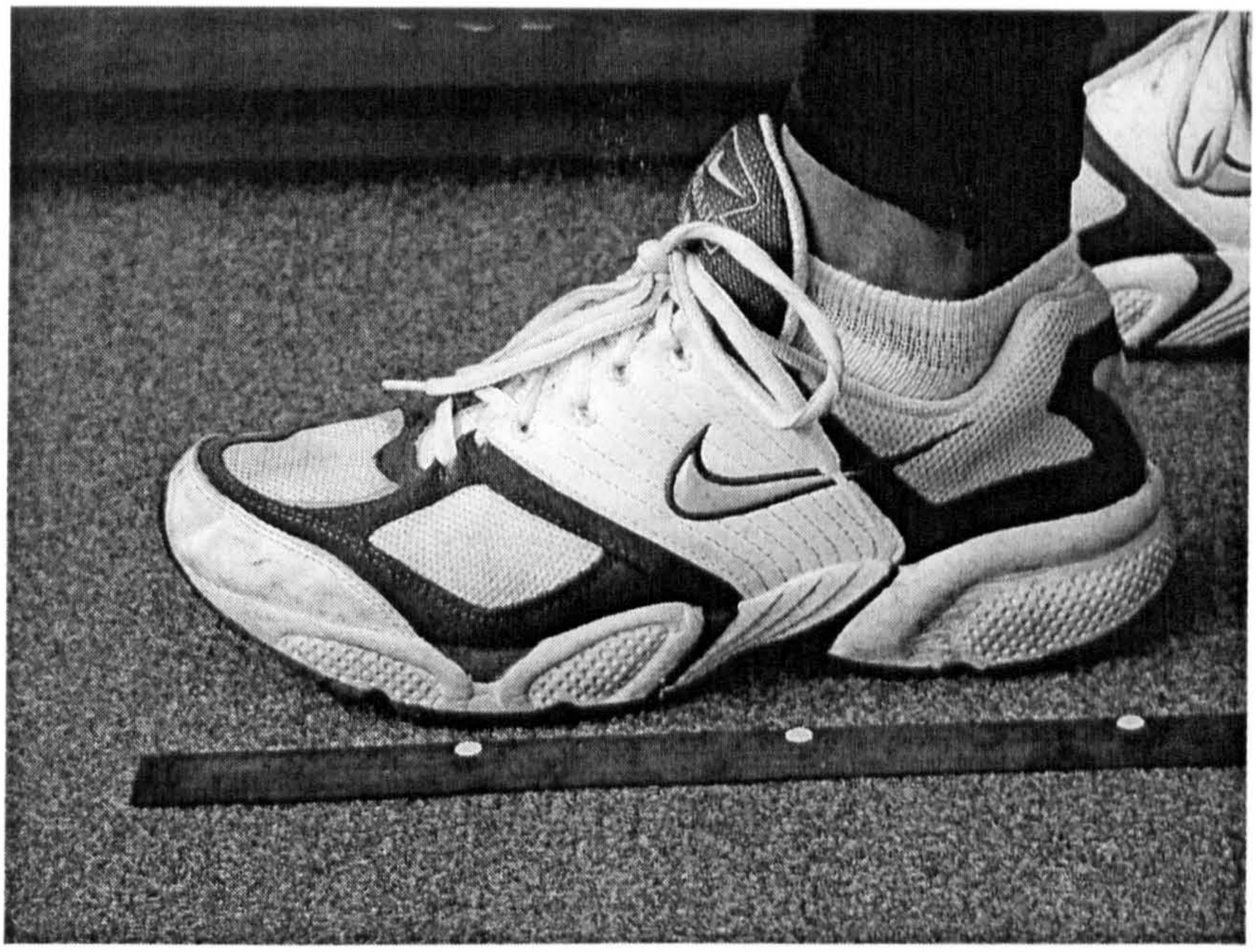

Figure 6.1. Photograph of the subject's foot being measured.

In addition to the 95 anthropometric measurements already taken, measurements were taken of the length of the foot, the horizontal distance from the toe (end of foot) to the ankle, the horizontal distance from the heel to the ankle and the vertical distance of the ankle from the ground. Measurements were taken with both the shoe on and the shoe off. The distance L2 between the model's toe and heel was measured with the subject's shoe on. L1 was calculated by subtracting the measured horizontal distance between the ankle and heel from L2. L3 was the measured vertical distance between the ground and the ankle. The centre of mass of the foot was taken from the data of Chandler (1975) and scaled to the subject's foot. The inertia parameters for the foot are shown in Table 6.3.

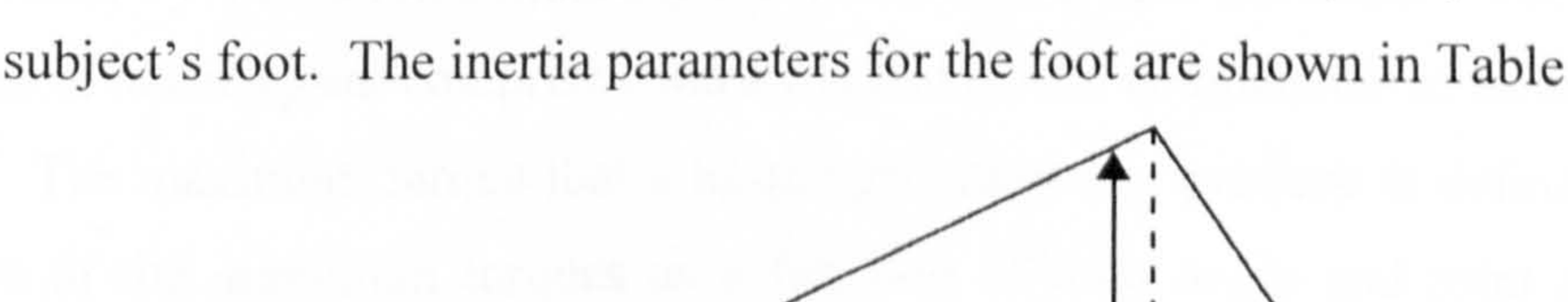

Figure 6.2. Anthropometric measurements of the foot.

Table 6.3. Inertia values for the left foot.

total mass	0.4780 kg
moment of inertia	0.0060 kg.m^2
L1	0.1615 m
L2	0.2365 m
L3	0.1080 m
L4	0.1124 m
L5	0.0336 m

Summary of inertia parameters

If the segmental inertia parameters estimated using the inertia model of Yeadon (1990b) result in the simulation models giving accurate results the inertia parameters may be thought to be accurate.

Strength parameters

Introduction

The torque-driven simulation model requires the net torque produced at each of the torque driven joints, by the two torque generators, to be known. These are the torques which produce ankle plantar and dorsi flexion, knee extension and flexion, hip extension and flexion and shoulder flexion. The torques produced are represented by a function simulating the action of a torque generator. The torque generators at each joint comprise contractile and elastic components in series.

The maximum torque that a torque generator can produce is defined by a surface of the maximum torques as a function of joint angle and joint angular velocity. The surface is produced from experimental data collected on an isovelocity dynamometer, to determine the contractile component strength parameter values, and data in the literature to determine series elastic component parameters values.

Methods

Series elastic component parameters

The series elastic component for each joint was modelled as a linear spring with a resting length of zero. One parameter was needed to define the torque in the series elastic component at each joint, as the torque produced by the series elastic component was dependent on the angle of the series elastic component extension around the joint. Figure 6.3 shows the extension of the series elastic component for the knee extensor.

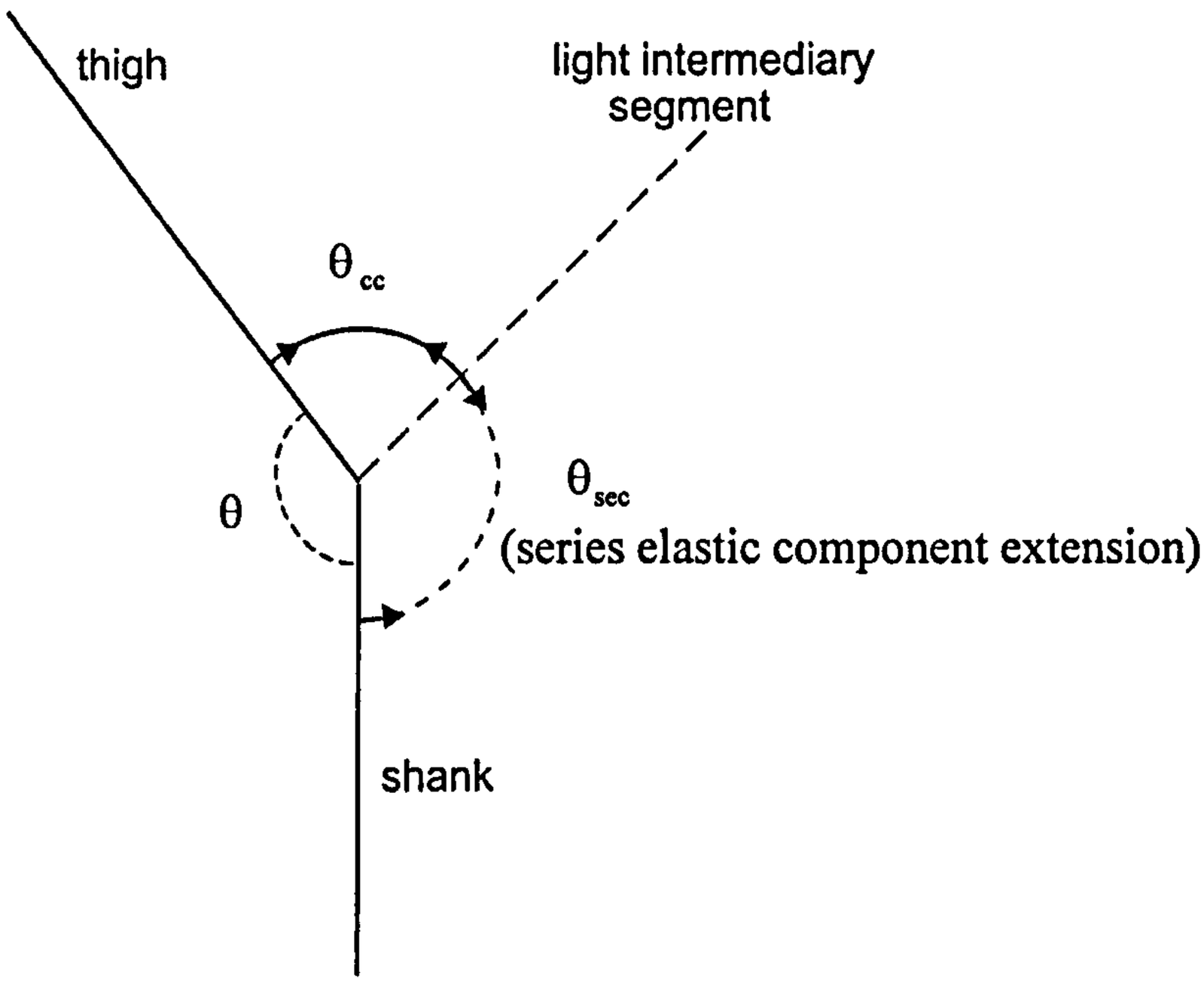

Figure 6.3. Series elastic component extension for the knee extensor.

The lengths, moment arms and the cross-sectional areas of each major muscle group at each joint were estimated from the literature (Pierrynowski, 1995; Jacobs, Bobbert and van Ingen Schenau, 1996). Previously the series elastic component has represented the tendon properties only (King, 1998). It has been identified (Maganaris and Paul, 2002), however, that it is not only the tendon which exhibits elastic properties but also parts of the muscle itself. The aponeuroses possess elastic properties and hence need to be included as part of the series elastic component. The length of the series elastic component in each muscle group used to determine the stiffness were calculated from data on the tendon lengths, muscle belly lengths, individual fibre lengths and pennation angles (Pierrynowski, 1992). The distance the aponeuorsis extends along the muscle

belly was calculated using the individual fibre length multiplied by the cosine of the pennation angle. Lengths of the series elastic components and the moment arms were then scaled to the subject's dimensions using a ratio of height / mass and segment lengths from the subject in this study and those in the studies of Pierrynowski (1995) and Jacobs et al. (1996) respectively. The maximum isometric joint torque at each joint was assumed to be equal to the maximum isometric torque collected on the isovelocity dynamometer at each joint. This torque was then divided between the muscle groups acting at the joint using a ratio of cross-sectional area multiplied by moment arm. The muscle / tendon parameter values are shown in Table 6.4.

Table 6.4. Muscle and tendon parameter values scaled to the subject.

	series elastic component length [mm]	muscle X-sectional area [mm^2]	moment arm [mm]	maximum isometric joint torque [Nm]
soleus	326	11868	47	186
gastrocnemius (ankle)	394	6167	47	97
tibialis anterior	247	-	42	56
rectus femoris (knee)	419	3357	43	54
vasti	315	16922	43	273
hamstrings (knee)	285	8831	27	175
gastrocnemius (knee)	394	6167	18	40
gluteus maximus	85	12716	64	257
hamstrings (hip)	285	8831	79	222
rectus femoris (hip)	419	3357	36	288

Calculation of tendon stiffness

The maximum isometric torques at each joint were divided up into the maximum torque at each muscle group of the joint as stated above. For each muscle group the tendon stiffness was determined. Various values for the percentage stretch within the series elastic component during isometric contraction have been reported in the literature. These range from 4.3% (de Zee and Voigt, 2001) to 5.5% (Muramatsu et al., 2001). A value of 5% was decided upon in the calculation of the stiffness of the series elastic component in this study as it was within the limits of all values reported. The change in length of the series elastic component was calculated using this percentage and the calculated length of the series elastic component. The calculated change in length of the series elastic component was then converted into a change in angle of the series elastic component by dividing by the moment arm. Finally the series elastic component stiffness was calculated by dividing the maximum isometric torque by the change in angle of the series elastic component. To obtain a series elastic component stiffness of the joint, the series elastic component stiffnesses of each muscle group at the joint were summed. Table 6.5 contains the calculated series elastic stiffness for each joint. The series elastic component stiffness of the shoulder was taken from the literature (King, 1998) due to lack of data on the shoulder geometry.

Table 6.5. Calculated series elastic component stiffness of each joint.

joint	stiffness [$Nm.rad^{-1}$]
knee extension	857.3
knee flexion	339.9
hip extension	5091.7
hip flexion	495.98
ankle plantar flexion	767.1
ankle dorsi flexion	222.7
shoulder flexion	1500.0

Details of the methods used to calculate the series elastic component parameter values are given in **Appendix 2.**

Contractile component parameters

Isovelocity dynamometers allow the calculation of the maximum joint torques possible over a range of angles and angular velocities. This section describes the method used to calculate joint torques during isometric and repeated concentric-eccentric movements. The repeated concentric-eccentric movement is used in order to replicate the actions during the takeoff in dynamic jumping.

A Cybex NORM isovelocity dynamometer is controlled by an IBM compatible 486 DX2 computer which employs a user-friendly touch screen control interface. The Cybex NORM can record torques up to a value of 500 ft.lbs (678 Nm) in both concentric and eccentric modes which permit angular velocities up to $500°s^{-1}$.

The Cybex isovelocity dynamometer was calibrated according to the manufacturer's recommendation. The crank arm was aligned to a neutral position (90° below the horizontal) using a spirit level. The data were collected via a 7-pin amphenol connector. A rectified torque signal was available on the auxiliary interface panel at pin 6 of the 7-position amphenol connector. The torque from the dynamometer was rectified so that it was always positive (ranging from 0 to +10 volts) whether the torque was applied in a clockwise or anti-clockwise direction. An analogue position signal was available on the auxiliary interface panel at the miniature phone jack's centre conductor positioned directly below the amphenol connector. The output from this connector ranges from 0 to 8.33 volts, and increases as the dynamometer arm moves clockwise. In addition to the isovelocity dynamometer data, two goniometers were used to collect joint angle data. The isovelocity dynamometer data and the goniometer data were recorded simultaneously. The data from the isovelocity dynamometer and the data from the goniometers were passed into a synchronisation unit and then into a laptop where the data were converted from an analogue to a digital signal, by an analogue to digital converter card (16 bit). The angle signal was passed into Channel One, the torque signal into Channel Two and the goniometer data into Channels Three and Four. All the data were recorded at 1000 Hz.

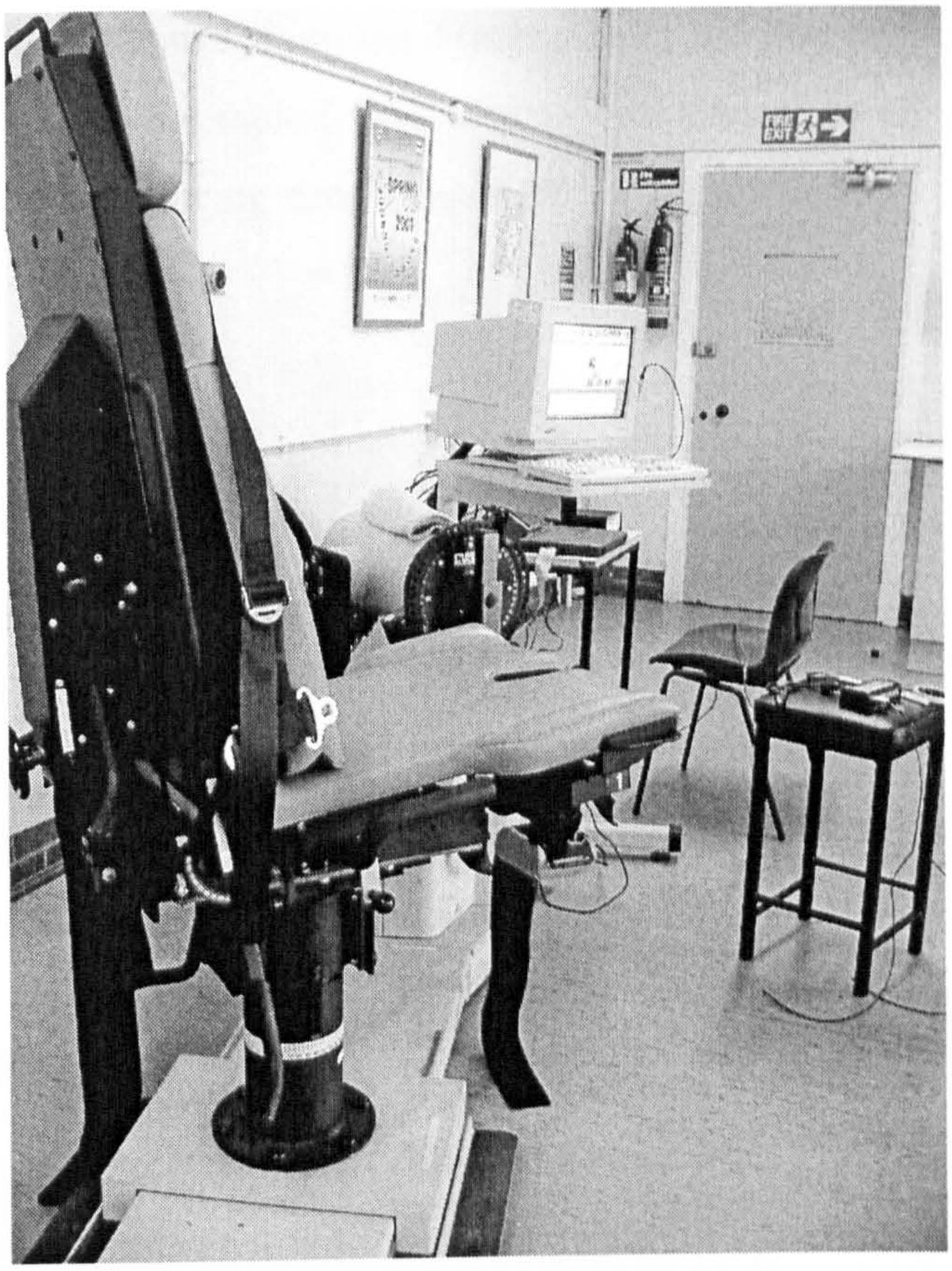

Figure 6.4. The Cybex NORM isovelocity dynamometer.

Written consent

The subject signed a written consent form agreeing to take part in the study. The consent form consisted of a protocol approved by the University Ethical Advisory Committee (**Appendix 3**). The consent form allowed the subject to withdraw from the study at any time.

Calibration of the dynamometer

As well as the initial calibration following the protocol supplied by the user's manual, a further calibration was performed using a static load. The crank arm was raised until it was at 0° horizontal, checked using a spirit level. Loads of 2.1 kg, 11 kg, 20.8 kg, 40.6 kg, and 61.25 kg were applied to the crank arm. These loads were individual free weights and were applied using chains so that the loads hung vertically. With each load, 2 s of data at a frequency of 1000 Hz were recorded. Data were recorded using the dynamometer software so that a comparison between the recorded torque and the applied torque could be made.

The length of the crank arm, from the dynamometer rotation centre to the point of load application, was measured, and the torque created with each load was calculated using the following simple equation:

$$T = F.d \qquad (6.1)$$

Where:

T = torque created

F = load applied

d = length of crank arm

The dynamometer was calibrated further for angles in order to compare the actual crank angle and the recorded crank angle. Passive isometric contractions were performed at every 10° from 0° horizontal to 90° vertical. At each of the 10 positions, 2 s of data were recorded, again at a frequency of 1000Hz.

Calibration of the goniometer

The two goniometers were calibrated before use. The calibration protocol involved data being collected with the goniometer at known angles. The angles ranged from 0° to 135° with recordings taken every 22.5°. The range was chosen as it was considered to span the range of motion of the joints during the trials. The angles were drawn on a flat surface using a protractor. The goniometer was placed at each of the angles in turn and 2 s of data at a frequency of 1000 Hz were recorded

Exercise protocol

The joints were tested in the following order: knee, ankle, hip and shoulder. The subject performed both isometric trials for all joints and repeated concentric–eccentric trials for the knee, hip and shoulder. Trials were performed for both directions of movement (extension and flexion) for the knee, ankle and hip. Only flexion was performed at the shoulder. The subject was asked to perform maximally in all trials. The subject performed isometric contractions at intervals of 10°, throughout the range of motion of the joint. All isovelocity trials of the protocol comprised two repetitions of the concentric–eccentric exercise. This was done in order to get the subject to perform maximally during the middle eccentric–concentric phase to represent the action in a takeoff in the high jump or

long jump. The sequence of velocities of the concentric–eccentric trials was $50°s^{-1}$, $100°s^{-1}$, $150°s^{-1}$, $200°s^{-1}$, $250°s^{-1}$, $300°s^{-1}$, $350°s^{-1}$ and $400°s^{-1}$; for shoulder flexion and hip flexion the fastest speed was not used.

Range of motion

The range of motion used at each joint was programmed into the dynamometer computer (Table 6.6). For each joint / action the subject's limb was positioned at anatomical zero. These ranges of motion of the crank angle are given in terms of this position. These ranges of motion were controlled / determined by the subject who was instructed to choose as large a range as was comfortable.

Table 6.6. Ranges of motion at each joint.

joint/action	crank angle range
knee (extension)	-5° - 74°
knee (flexion)	23° - 111°
hip (extension)	-12° - 84°
hip (flexion)	29° - 114°
shoulder (flexion)	73° - 139°
ankle (flexion and extension)	52° - 100°

Data collection

At each joint tested, the subject was allowed a few trials to become familiar with the machine for that particular joint, before recording began. When the subject indicated he was ready to begin the trial, recording of the data began. This was initiated by setting the software on the laptop to simultaneously start collecting all the data. The Cybex machine allowed collection of crank angle, angular velocity and torque data, and the software on the laptop was set to record this for a specified duration of time. Data were collected for 8 s for the isometric trials and 12 s for the concentric-eccentric isovelocity trials. Between trials the subject was allowed to rest while still secured to the dynamomter and with the goniometers still attached until he was ready for the next trial. Between the

testing of each joint the subject was removed from the dynamometer and allowed to move freely.

Data analysis

Analysis of the data was divided into two sections to obtain a set of joint torques as a function of joint angle and joint angular velocity. The two sections were:

1. Calibration of the dynamometer and goniometer and editing the torque and angle data time histories to the sections of each trial required for analysis
2. Using the torque and angle data collected with the dynamometer and goniometers in order to correct for differences between the joint and crank angle, angular velocity and torque. Also, to correct the torque values for segment and crank weight.

Dynamometer calibration

The torques recorded by the dynamometer software and the corresponding calculated torques are shown in Table 6.7.

Table 6.7. Torque measurements of the dynamometer.

trial	calculated torque [Nm]	measured torque [Nm]
1	13	13
2	45	45
3	80	82
4	150	155
5	224	231

The torque measurements recorded by the dynamometer over a 2 s period were within 7 Nm of the torque calculated from the hung load. This corresponds to a systematic difference in the torques of approximately 3%. Assuming the loads were weighed correctly, this corresponds to a maximum error in the crank length of 12 mm (approximately 3%). This systematic error in the crank length

was likely to occur and therefore there was no reason to believe the torque values given by the dynamometer were not the true values of the torque being produced.

The torques recorded by the dynamometer software were subsequently plotted against the mean value of the digital signal collected from pin 6 of the amphenol connector. The digital signal was linearly regressed against the recorded torque to give:

$$T = 75.079V - 1.5337 \quad (6.2)$$

Where:

T = torque recorded by dynamometer software

V = voltage from pin 6 of the amphenol connector

The correlation coefficient between the torque recorded by the software and the digital signal was 1.000, and the standard error was 0.56 Nm .

Data at 10 different crank angles were recorded and the mean values of the analogue signal collected from the miniature phone jack centre conductor over a period of 2 s at 1000 Hz were then regressed against the known angles as measured by the dynamometer. The regression analysis yielded the following calibration equation.

$$A = 122.52V - 255.89 \quad (6.3)$$

Where:

A = crank angle as measured by the dynamometer

V = voltage from miniature phone jack centre conductor

The correlation coefficient between the actual angle and the recorded angle was 0.9999, and the standard error was calculated to be 0.24°.

Goniometer calibration

The mean values of the digital signals for the two goniometers were regressed against the known angles used in the calibration procedure. The predicted angles were calculated using the following regression equations.

Goniometer one:

$$A = 92.557V - 152.39 \quad (6.4)$$

Goniometer two:

$$A = 94.491V - 169 \quad (6.5)$$

Where:

A = known angle

V = voltage from goniometer

The correlation coefficient, r^2, between the mean value of the recorded digital signal and the actual angle for goniometer 1 was 0.9994, and for 2 0.9999 with standard errors of 1.14° and 0.37° respectively.

Goniometer attachment

The goniometer was attached to the subject in a straight position using double sided sticky tape when the joint was straight and fully open. The connecting cables were further secured using duct tape. It was not possible to measure the ankle angle with the goniometer as the subject's positioning in the dynamometer prevented the goniometer being placed around the joint.

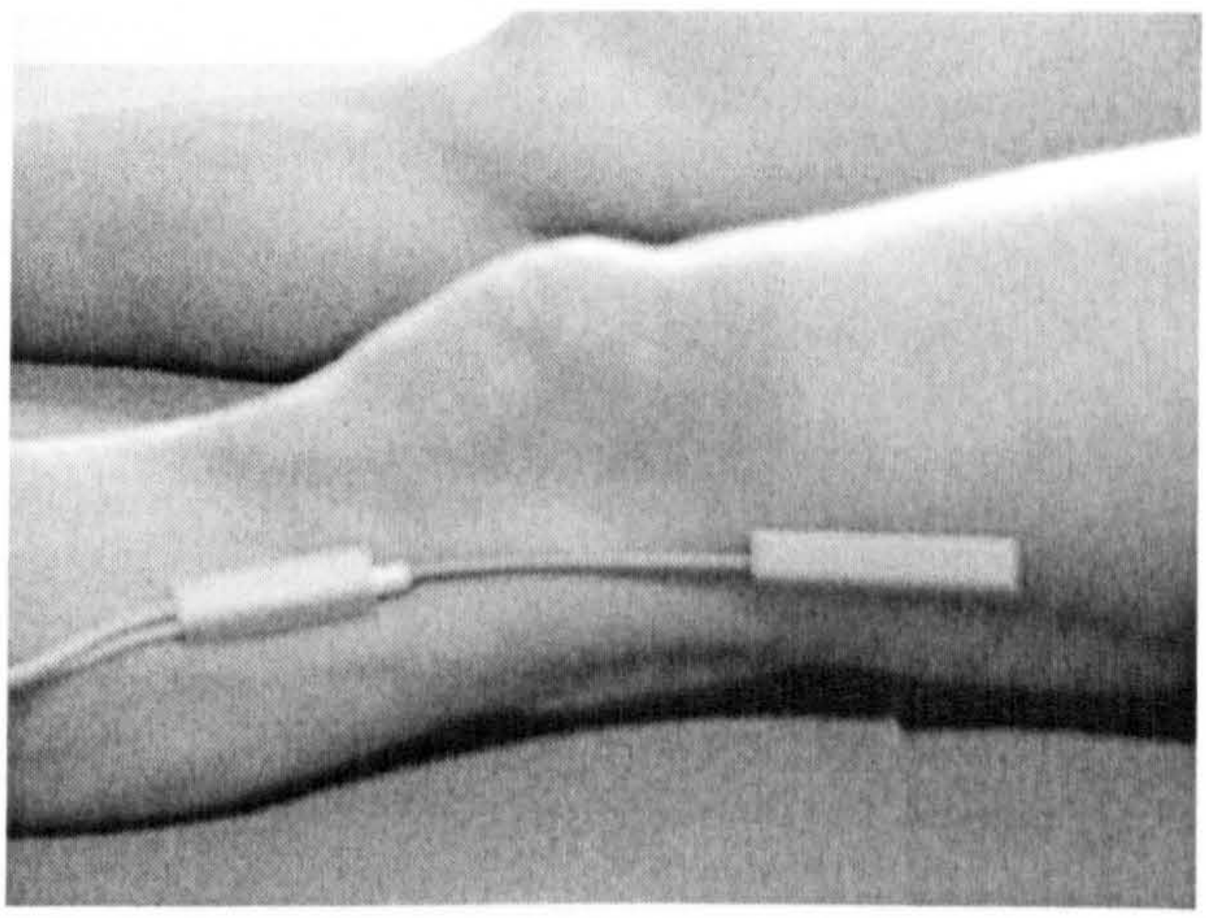

Figure 6.5. Positioning of the goniometer at the knee joint.

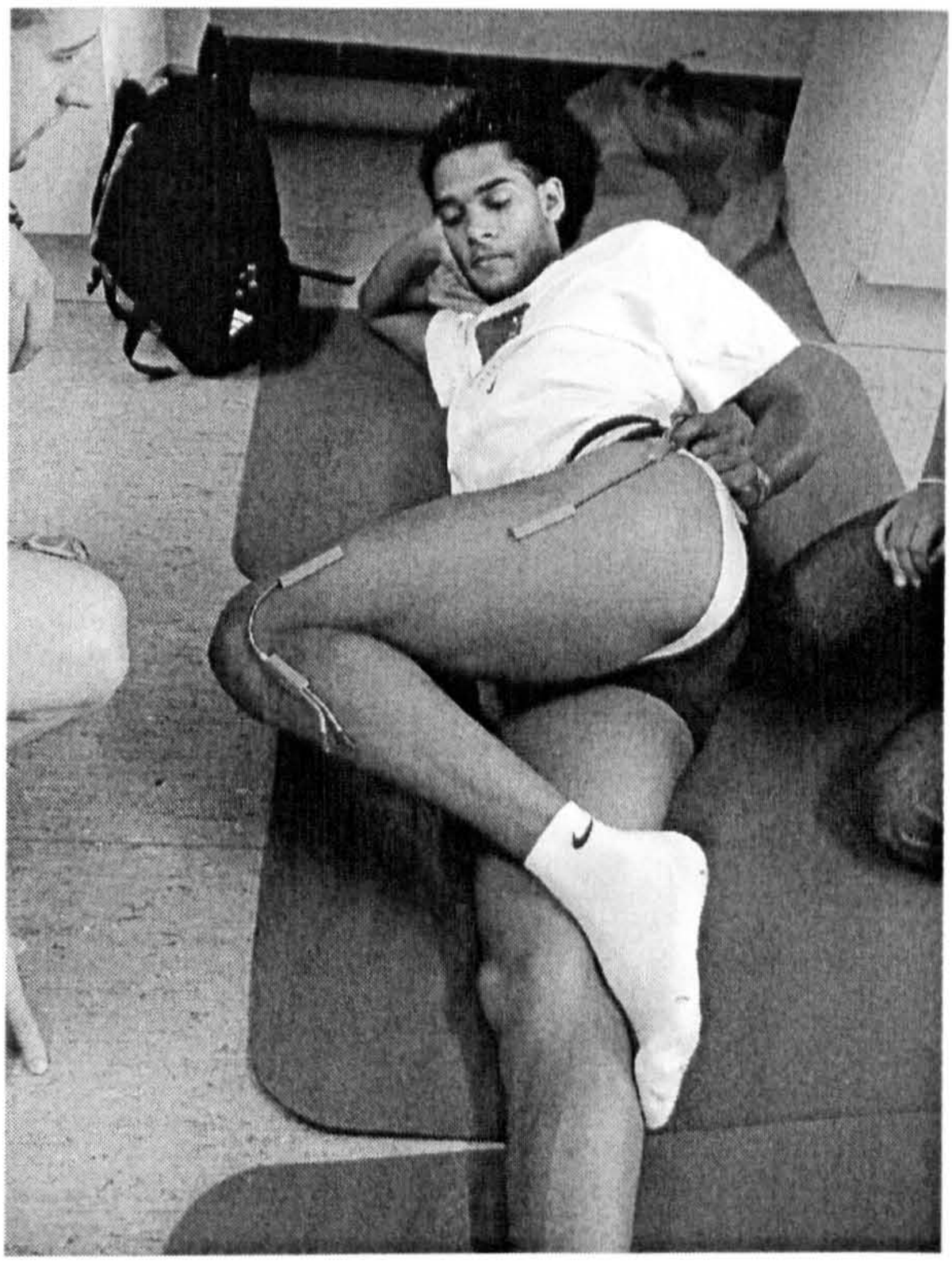

Figure 6.6. Position of the goniometers at the knee and hip joints.

Positioning of the subject

The subject was positioned on the machine so that the crank and joint axes were aligned as close as possible. The subject was secured in each position using Velcro straps to prevent excessive movement.

For the knee joint the subject was positioned in a seated position with the knee not being tested secured with a Velcro strap, a further strap was placed around the waist of the subject.

For the ankle joint the subject laid on the machine in a prone position. The dynamometer used a separate attachment which isolated the ankle joint and allowed plantar flexion.

For the hip joint the subject was placed in a reclined position and for the shoulder joint the subject laid in a supine position. With both joints a Velcro strap was placed around the chest.

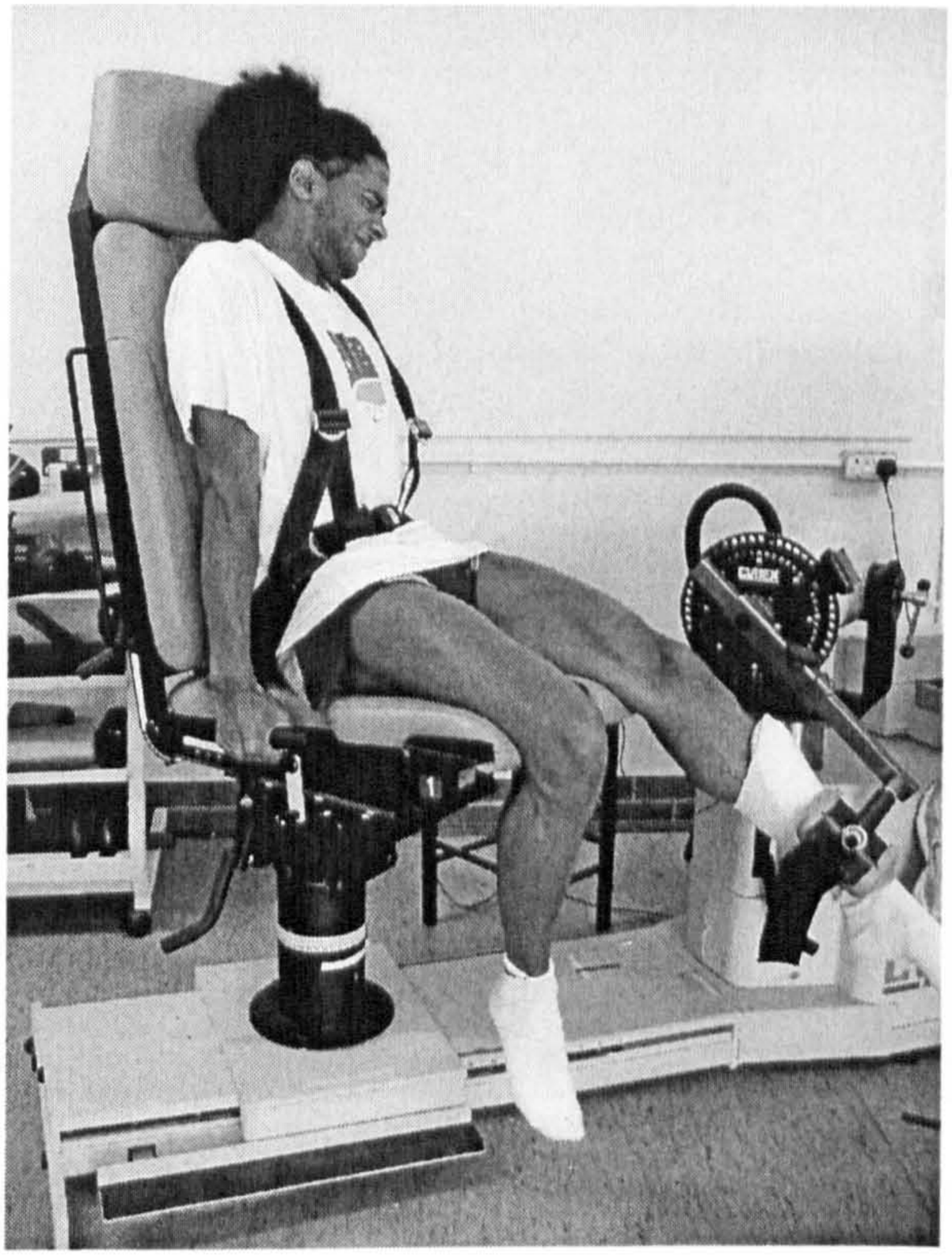

Figure 6.7. Positioning of the subject for knee extension.

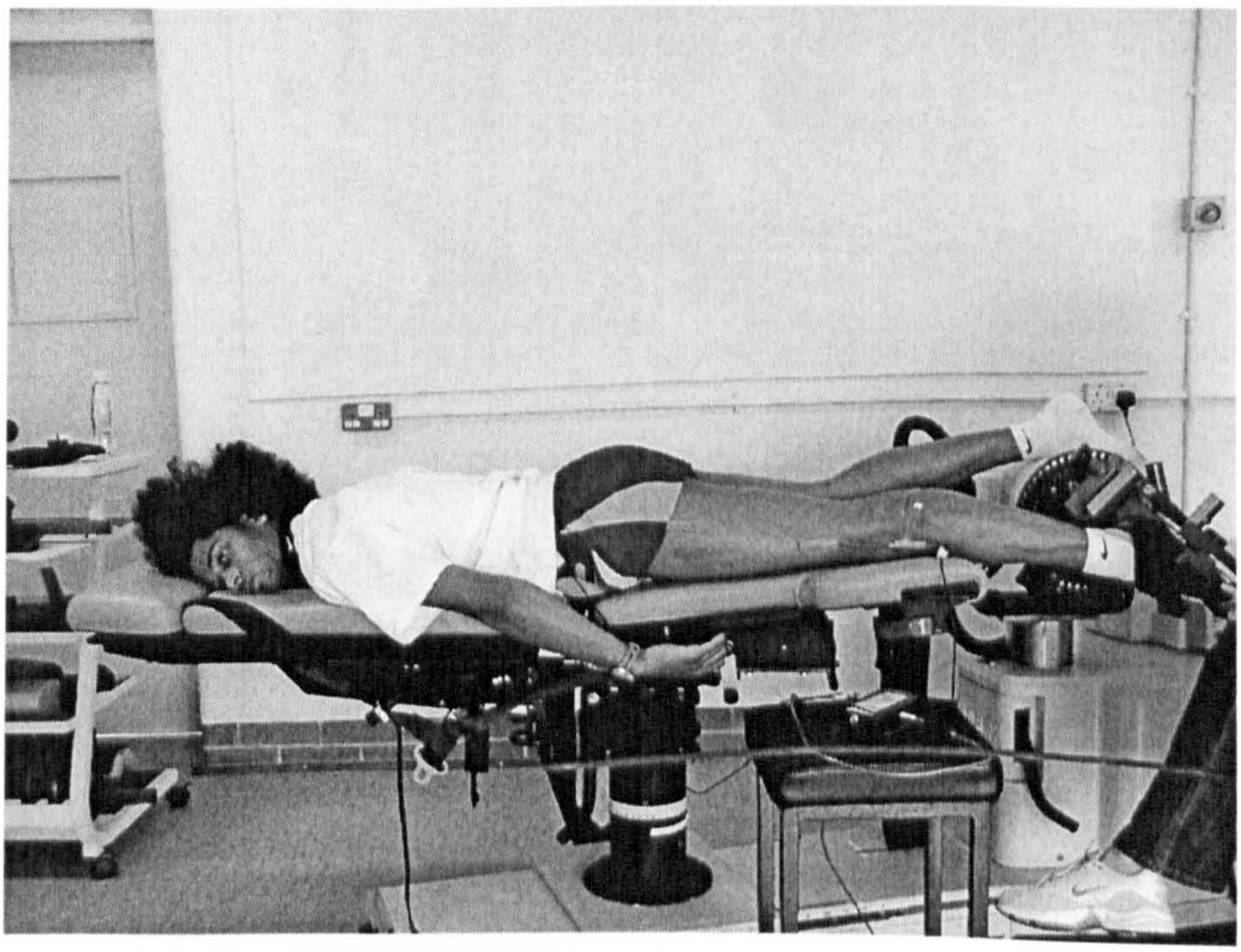

Figure 6.8. Positioning of the subject for ankle plantar / dorsi flexion.

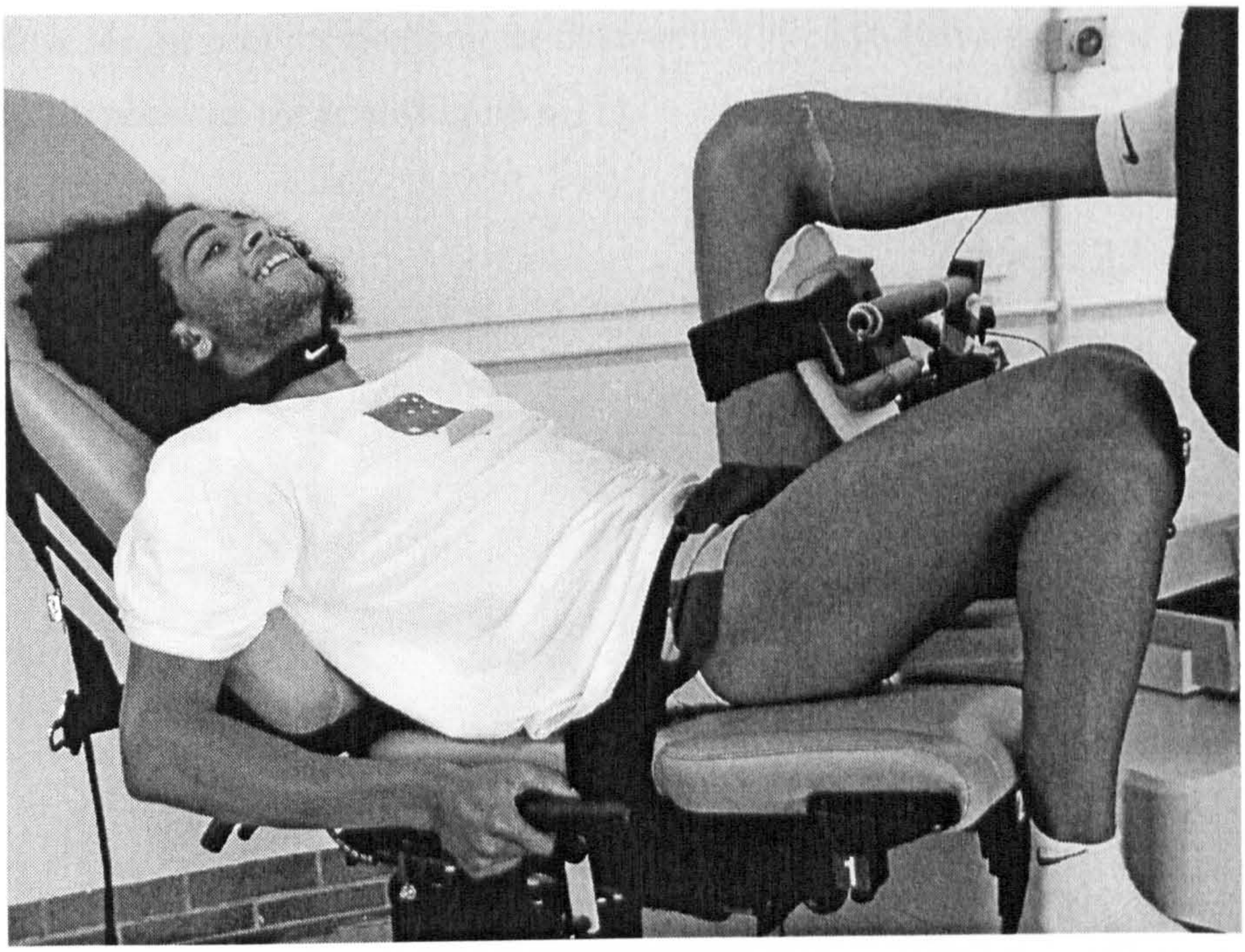

Figure 6.9. Positioning of the subject for hip extension.

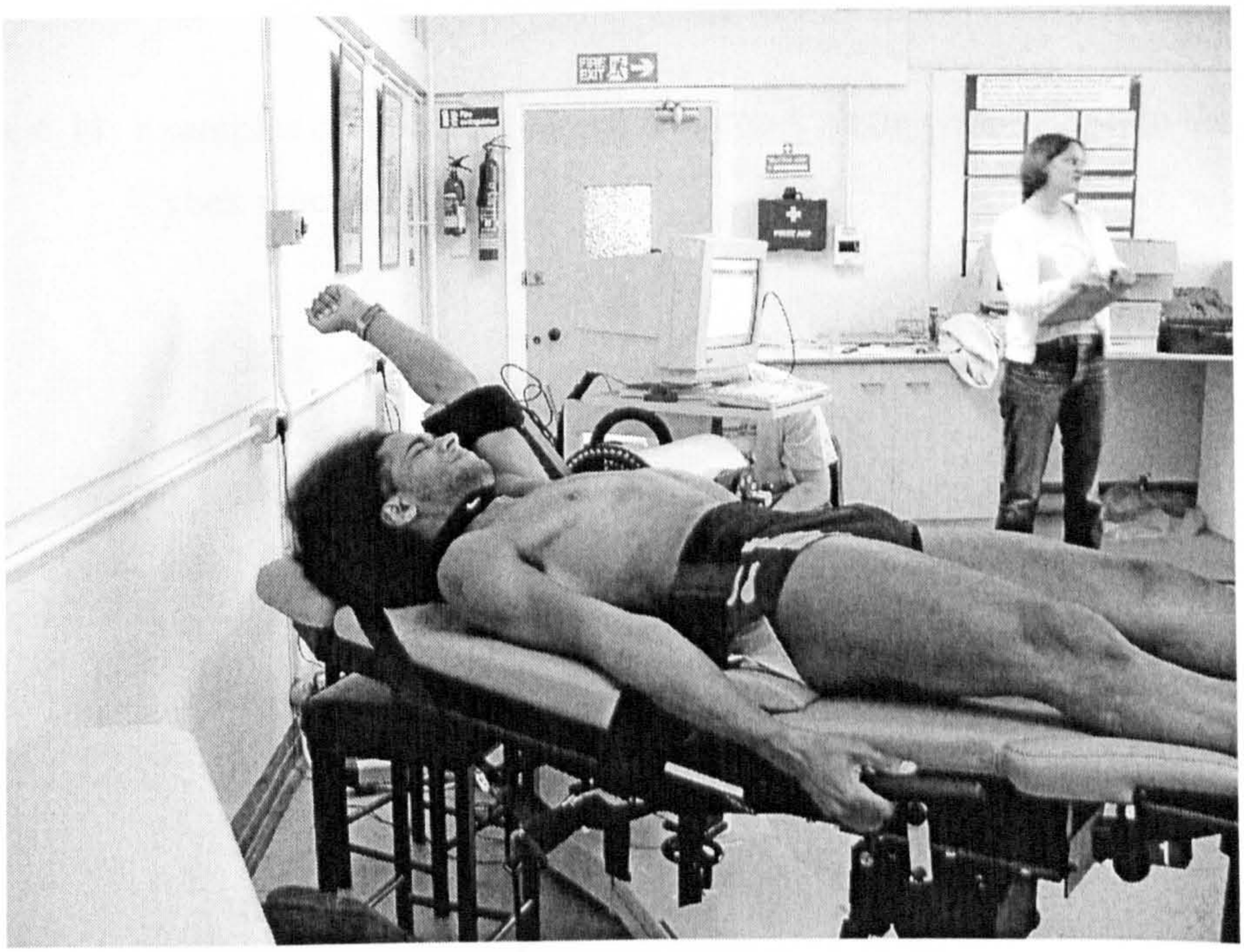

Figure 6.10. Positioning of the subject for shoulder flexion.

Editing data files

Once all the trials had been completed each one was individually edited. All the concentric-eccentric files containing the time histories of the crank angle,

the crank torque and the goniometer data were edited to leave a central eccentric-concentric phase of the trial (Figure 6.11).

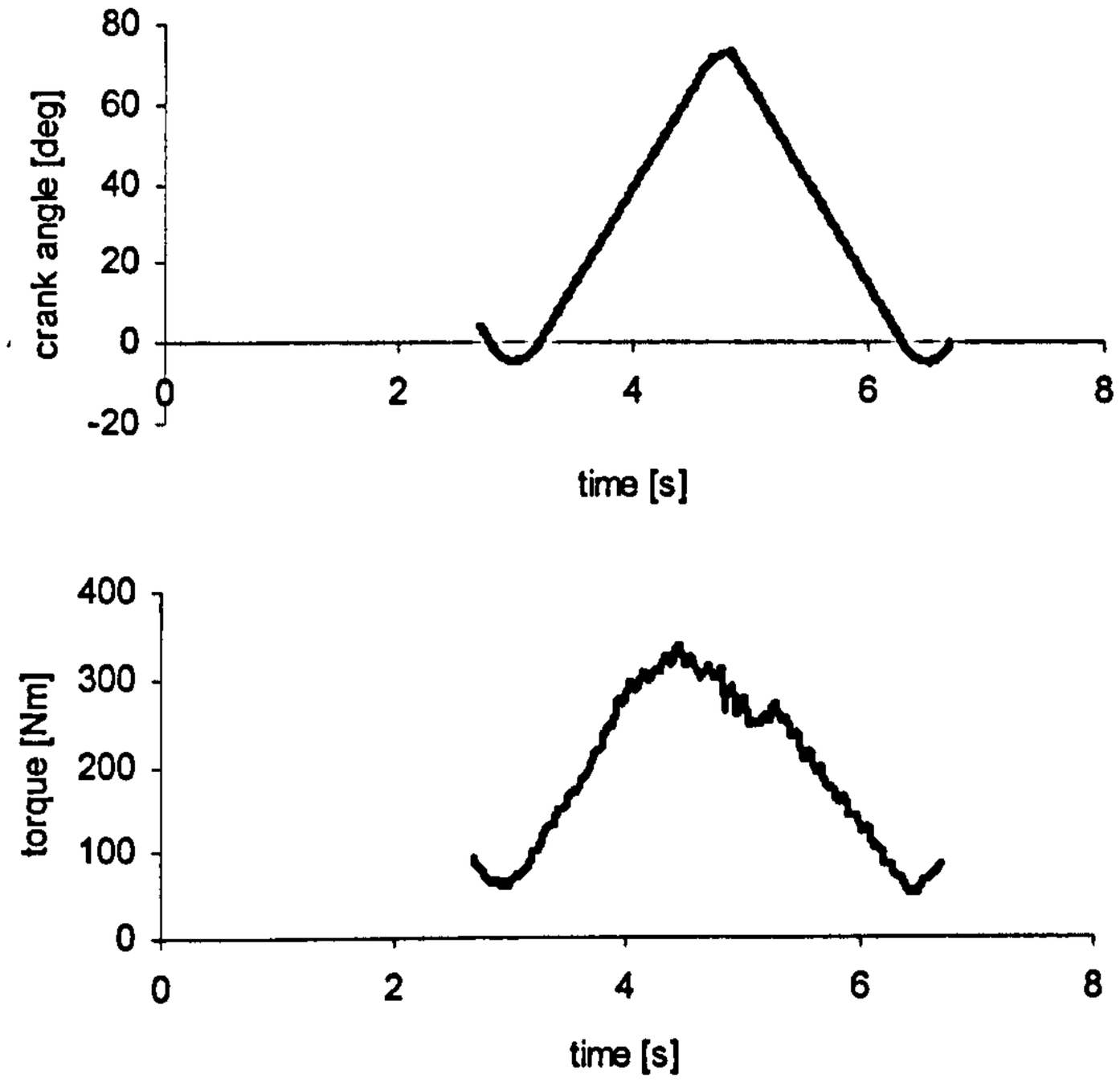

Figure 6.11. Examples of an edited torque and crank angle data files from the Cybex machine.

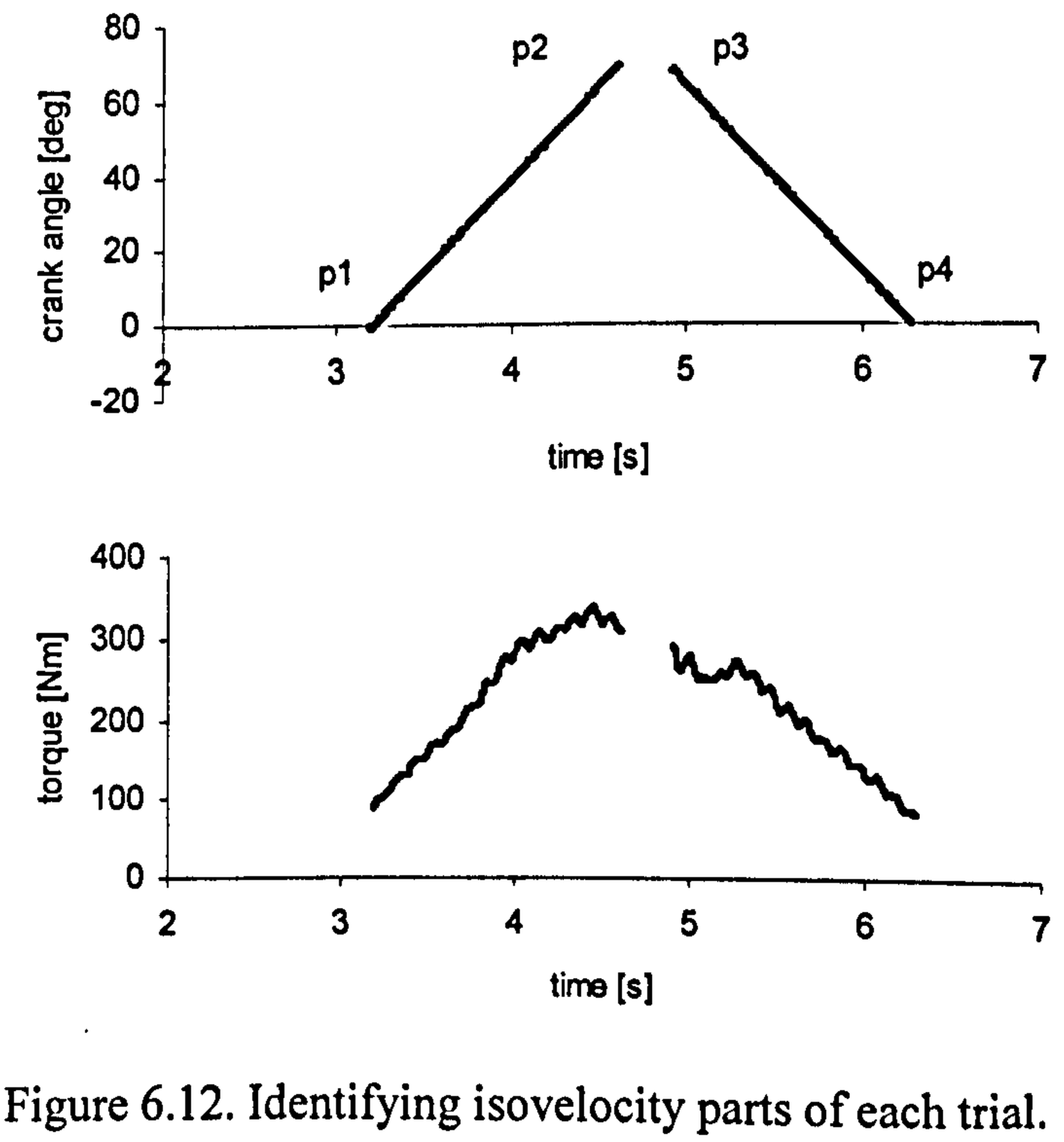

Figure 6.12. Identifying isovelocity parts of each trial.

The isovelocity portions of this central phase were then identified (Figure 6.12). For each of the isometric trials a central isometric section was identified which contained the peak torque value.

Filtering

The goniometer data contained a lot of unwanted noise (Figure 6.13) and so filtering was required. Filtering was carried out on all isovelocity trials and was achieved using a program in Matlab. The data were filtered at 12 Hz, to give a signal containing the useful information (Figure 6.14). A filter cut-off frequency of between 4 and 8 Hz is often used because most human movement is of low frequency (Challis, Bartlett and Yeadon, 1997). As the movements performed in this study were more dynamic than general human movement a frequency of 12 Hz was chosen to be sure all important information was kept.

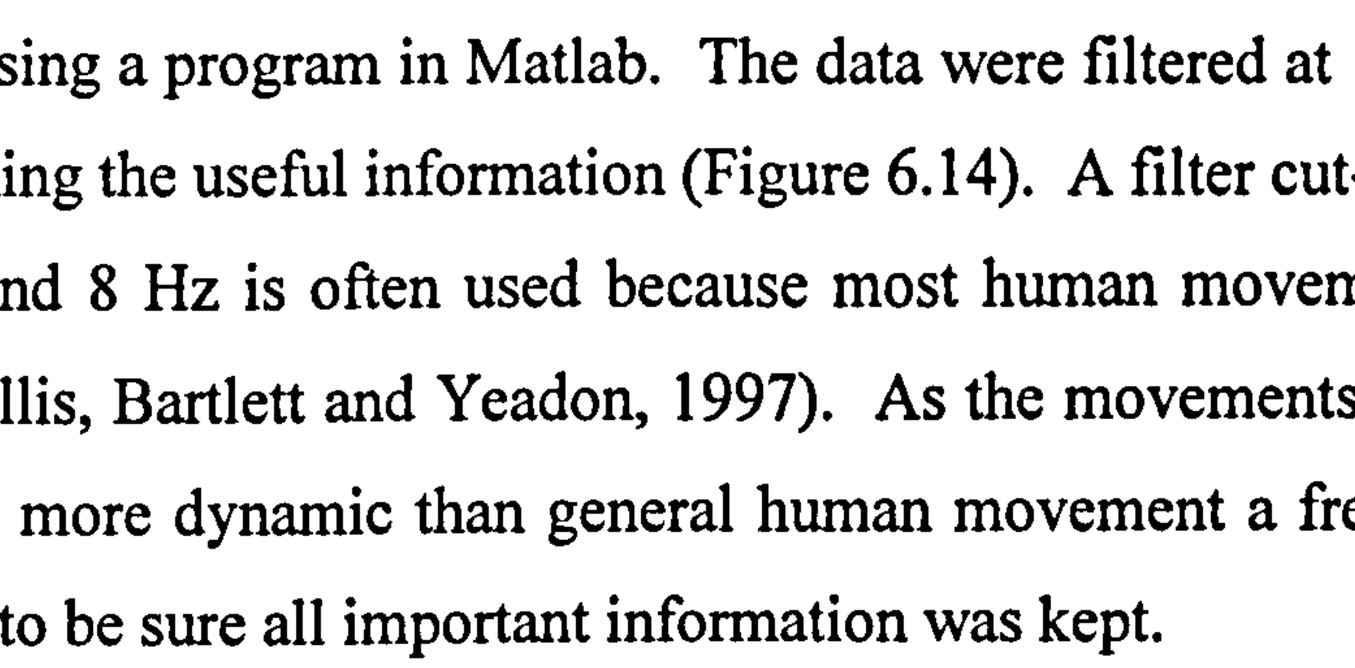

Figure 6.13. A sample of raw goniometer data.

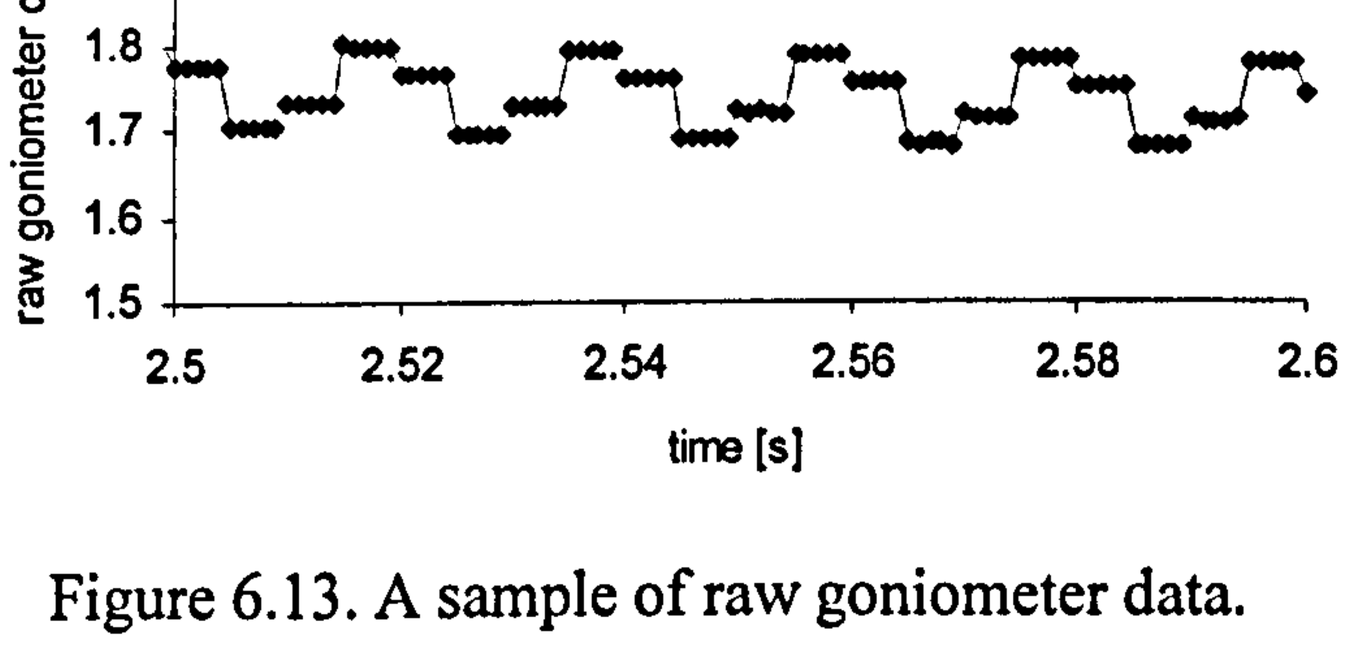

Figure 6.14. A sample of filtered goniometer data.

Crank / joint angle regression

For all the concentric-eccentric trials, crank angle was linearly regressed against time for the isovelocity portions of the concentric-eccentric phases. The relationship between the crank angle and time was expressed in the form of equation (6.6).

$$\theta(t) = x_1 t + x_2 \qquad (6.6)$$

Where:

$\theta(t)$ = crank angle at time t

x_1 = regression coefficient (crank angular velocity)

x_2 = constant

t = time

Equation (6.6) was then used to calculate a set of new crank angle data. Similarly a linear regression was also performed on the joint angle data for the isovelocity portions, and the equation produced was used to calculate a set of new joint angle data. The angular velocity of both the crank arm and the limb was taken as the value of x_1 in this equation.

Calculating limb angle with respect to the horizontal

All trials were filmed using a Sony digital Handycam video camera. Using the video, the angles of the thigh in the case of the knee joint, the trunk in the case of both the hip and shoulder joint and the shank in the case of the ankle joint were estimated with respect to the horizontal. Table 6.8 shows the estimated angles for each joint and action.

Table 6.8. Angles of the thigh / trunk segment w.r.t the horizontal.

Joint / action	angle of thigh / trunk [°]
knee extension	7
knee flexion	5
hip extension	15
hip flexion	15
ankle plantar and dorsi flexion	5

These angles were required in order to calculate the joint angle with respect to the horizontal to be used in the segment weight correction.

Segment weight correction

The dynamometer used in this study measured and recorded the torque produced using a cuff on the crank, which attached the limb to the crank during the trial. It is necessary to correct for the weight of the subject's limb in order to get the torque produced by the subject during each trial (Winter et al., 1981). Depending on the direction of the joint action it was necessary to add or subtract the torque created by the weight of the subject's limb from the crank torque. When the subject is working against gravity the weight correction increases the measured torque, but when the subject is working with gravity the weight correction decreases the measured torque. In order to correct for gravity, the mass and mass centre location of each limb, and the time history of the limb angle relative to the horizontal throughout the trial were required. The mass and mass centre locations of each limb were determined using anthropometric measurements and the inertia model of Yeadon (1990b). The limb relative to the horizontal was calculated from the goniometer data and the estimated angle of the thigh or trunk. In the case of the ankle, the joint angle was assumed to be equal to the crank angle as no goniometer data and therefore no joint angle data were collected at the ankle. The corrected crank torque was calculated using equation (6.7)

$$T_c = T_c \pm (Mgd\cos\phi) \qquad (6.7)$$

Where:

T_c = crank torque

M = mass of limb

d = perpendicular distance from mass centre location to joint centre

ϕ = joint angle relative to horizontal (crank angle in case of ankle)

Crank arm weight correction

As with the correction for the weight of the limb, a correction needs to be done for the weight of the crank arm. For each of the joints tested, a passive

isometric trial was completed without the subject, at 0° from the horizontal. This was achieved once the dynamometer was set-up for use with the subject. The corrected crank torque was calculated using equation (6.8).

$$T_c = T_c \pm T_w \cos\theta \qquad (6.8)$$

Where:

T_c = crank torque

T_w = passive isometric torque of crank arm

θ = crank angle relative to horizontal

This torque, corrected for both crank arm and segment weight, was considered to be the actual torque produced at the crank by the subject.

Conversion of crank torque to joint torque

The recorded torque time histories from the trials on the isovelocity dynamometer were those torques produced at the crank and not the required torques produced at the joint. The relationship between joint torque and crank torque was calculated as follows (King, 1998):

$$T_j = T_c . \frac{d_j}{d_c} \qquad (6.9)$$

Where:

T_c = crank torque

T_j = joint torque

d_c = crank moment arm

d_j = joint moment arm

Using the video of the trials, the endpoints of the appropriate limb (joint centres) and the centre of the dynamometer cuff were digitised at five different angles for each joint. An average ratio of the limb moment arm to the total limb length was calculated and using the actual length of the limb (from the anthropometric data) the limb moment arm length was determined. The crank arm length was measured during the data collection, therefore the ratio of limb moment arm to crank arm length could be determined and hence the joint torque

could be calculated using equation (6.8). For knee flexion only, the crank length was altered during the trials. There were therefore two values of the ratio of crank to joint arm length for knee flexion. All the ratios are shown in Table 6.9.

Table 6.9. Moment arm correction factor used for each trial.

joint	knee	Knee	hip	hip	shoulder
action	extension	flexion	extension	flexion	flexion
d_j / d_c	0.837	0.976 / 0.8765	1.197	0.9372	0.82

Isometric trials

For each isometric trial, the maximum torque was identified and an average crank and joint angle were determined over the isometric section. The ratio of limb to crank arm length determined for the concentric-eccentric trials, along with equation (6.9), was also used to calculate the joint torque for the isometric trials.

Maximum torque values

For each joint / action (excluding the ankle), the torques collected over the isovelocity sections for each angular velocity (concentric and eccentric) were input into a computer program *cybexsplin.f* along with their corresponding joint angles. The torques were splined at each joint angle at which the raw data were collected. The maximum and minimum torque values exerted by the subject at each angular velocity and the mean value of the torques produced over the isovelocity section were determined along with the angle at which they occurred. The maximum torque values were of most interest, however, these values contained considerable noise. A much smoother curve could be fitted to the mean torque values to get maximum torque values with less noise, the average torque values were regressed against the maximum torque values. For each joint this resulted in a set of 14,16 or 18 (depending on the number of trials at each joint) joint angular velocities, maximum torque values and an r^2 value. The r^2 values for joint varied between 0.713 and 0.930.

Muscle model

A muscle model was developed by fitting the experimental joint angle, joint angular velocity and torque data to give a smooth surface of maximum torque as a function of angle and angular velocity.

Introduction

The following section describes the procedures used to fit a surface to the collected isovelocity dynamometer data, so that torques produced at the joints could be predicted in the simulation models.

Method

Many authors have studied the force-velocity relationship in muscle. Hill (1938) found a hyperbolic relationship for the force-velocity relationship in whole muscle (Figure 6.15). Hill's hyperbolic function is, however, only valid for concentric muscle actions.

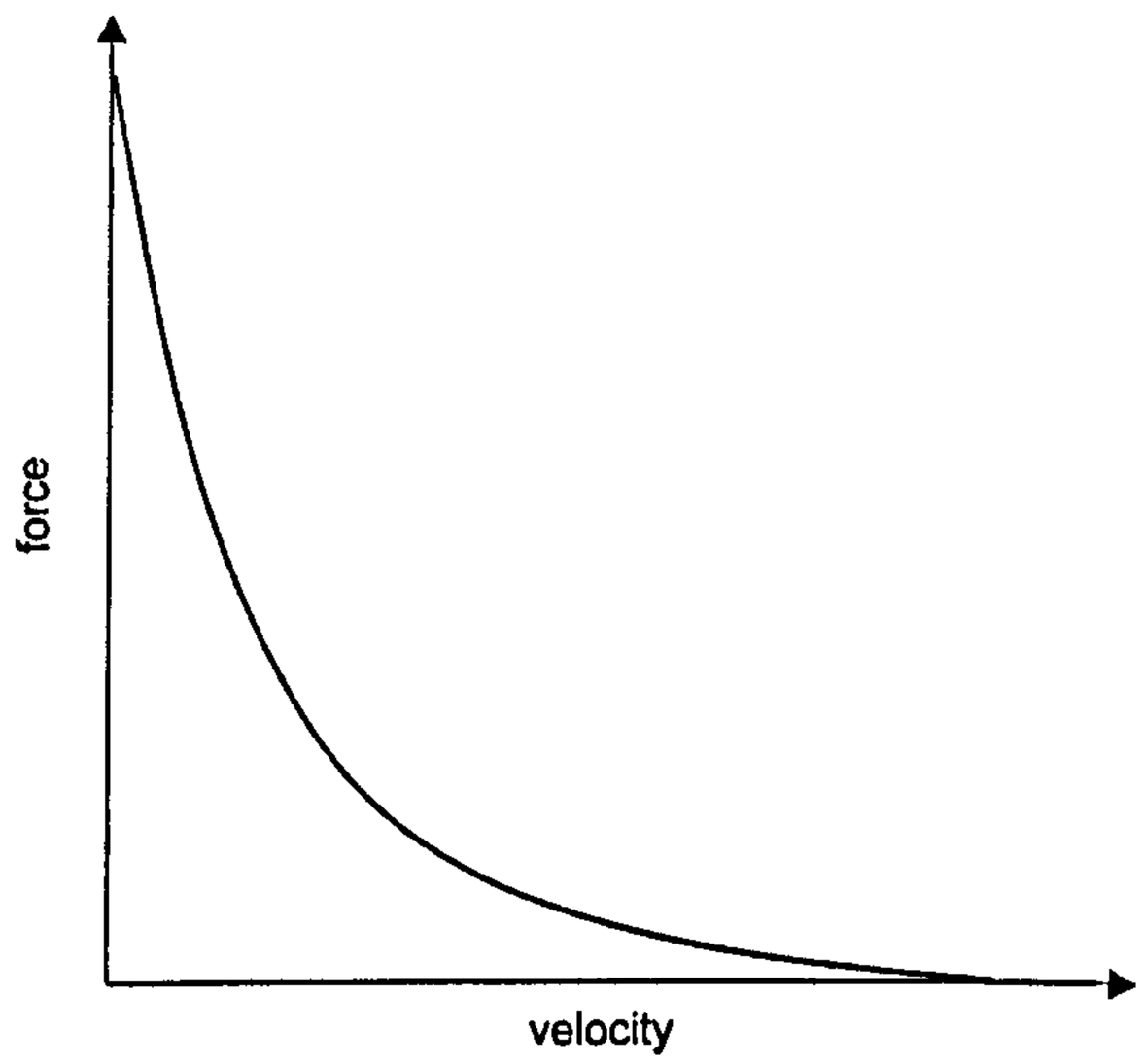

Figure 6.15. Force-velocity relationship of whole muscle (Hill, 1938).

Fitting a function to the data

A function was required which would fit the experimental data collected. Two hyperbolic functions, one representing the concentric phase and one representing the eccentric phase were used. The hyperbolic function representing the concentric phase was a rotational equivalent of the classic Hill hyperbola.

Four parameter function

The maximum torque values were fitted to a rotational equivalent of Hill's hyperbolic function and a second hyperbolic function for the eccentric phase using a four parameter function (Figure 6.16). This was achieved using Simulated Annealing (Corana et al., 1987). The four parameters were, T_{max}, the maximum torque value in the eccentric phase, T_0, the isometric torque value, ω_{max}, the angular velocity value at which the curve reaches zero torque, and ω_c defined as the asymptote which the Hill hyperbola approaches . The 4 parameter function was fitted using the following equations:

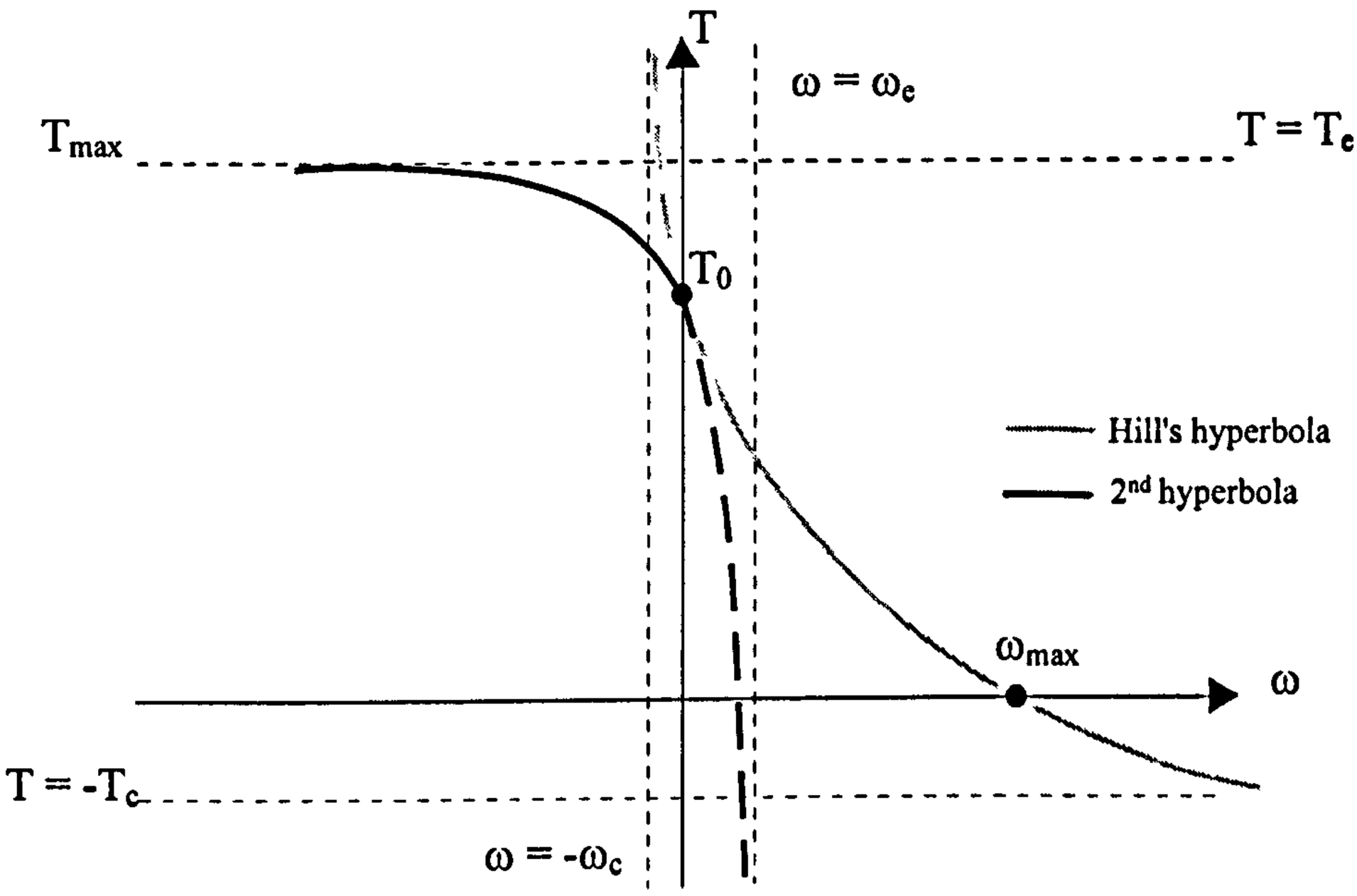

Figure 6.16. Four parameter hyperbolic function.

In the concentric phase the relationship between T and ω is given by the classis Hill hyperbola:

$$(T + T_c)(\omega + \omega_c) = C$$

which has asymptotes at $T = -T_c$ and $\omega = -\omega_c$.

when $\omega = 0, T = T_0$: $\quad (T_0 + T_c).\omega_c = C$

when $\omega = \omega_{max}, T = 0$: $\quad T_c(\omega_{max} + \omega_c) = C$

$$T = \frac{C}{(\omega_c + \omega)} - T_c \qquad (\text{if } \omega \geq 0) \qquad (6.10)$$

Where:

$$T_c = \frac{T_0 \omega_c}{\omega_{max}} \tag{6.11}$$

$$C = T_c(\omega_{max} + \omega_c) \tag{6.12}$$

In the eccentric phase the relationship between T and ω is given by the rectangular hyperbola:

$$(T_e - T)(\omega_e - \omega) = -E$$

which has asymptotes $T = T_e$ and $\omega = \omega_e$.

$$\text{when } \omega = 0, T = T_0: \quad (T_{max} - T_0).\omega_e = -E, \quad \text{where } T_{max} = T_e$$

$$T = \frac{E}{(\omega_e - \omega)} + T_{max} \quad (\text{if } \omega \leq 0) \tag{6.13}$$

where:

$$\omega_e = \frac{(T_{max} - T_0)}{kT_0} . \frac{\omega_{max}.\omega_c}{(\omega_{max} + \omega_c)} \tag{6.14}$$

where:

k = ratio of the slope between concentric and eccentric phases

$$E = -(T_{max} - T_0).\omega_e \tag{6.15}$$

The four parameters were calculated by minimising the cost function which was equal to the root mean square (RMS) difference between the known raw maximum torques and the calculated torques using equation (6.10) and equation (6.13). The value of k was set at 4.3, the theoretical value which Huxley (1957) predicted with his original model. This four parameter function was independent of joint angle.

Although the four parameter function fitted the data well in the eccentric phase it did not fit it well in the concentric phase. The raw data appeared to have a plateau in the concentric phase, highlighting that differential activation may be present due to muscle inhibition during eccentric movements on the isovelocity dynamometer (Figure 6.17). That is, during the eccentric phase the muscle is not

at T_{max} , but at some level below it, i.e not fully activated (Westing et al., 1990). It is only sometime during the concentric action that the muscle goes to full activation. The four parameter function curve therefore represents a tetanus curve and further parameters were needed to produce a function which fit the data better. With the shoulder flexion data there was no evidence that there was any differential activation.

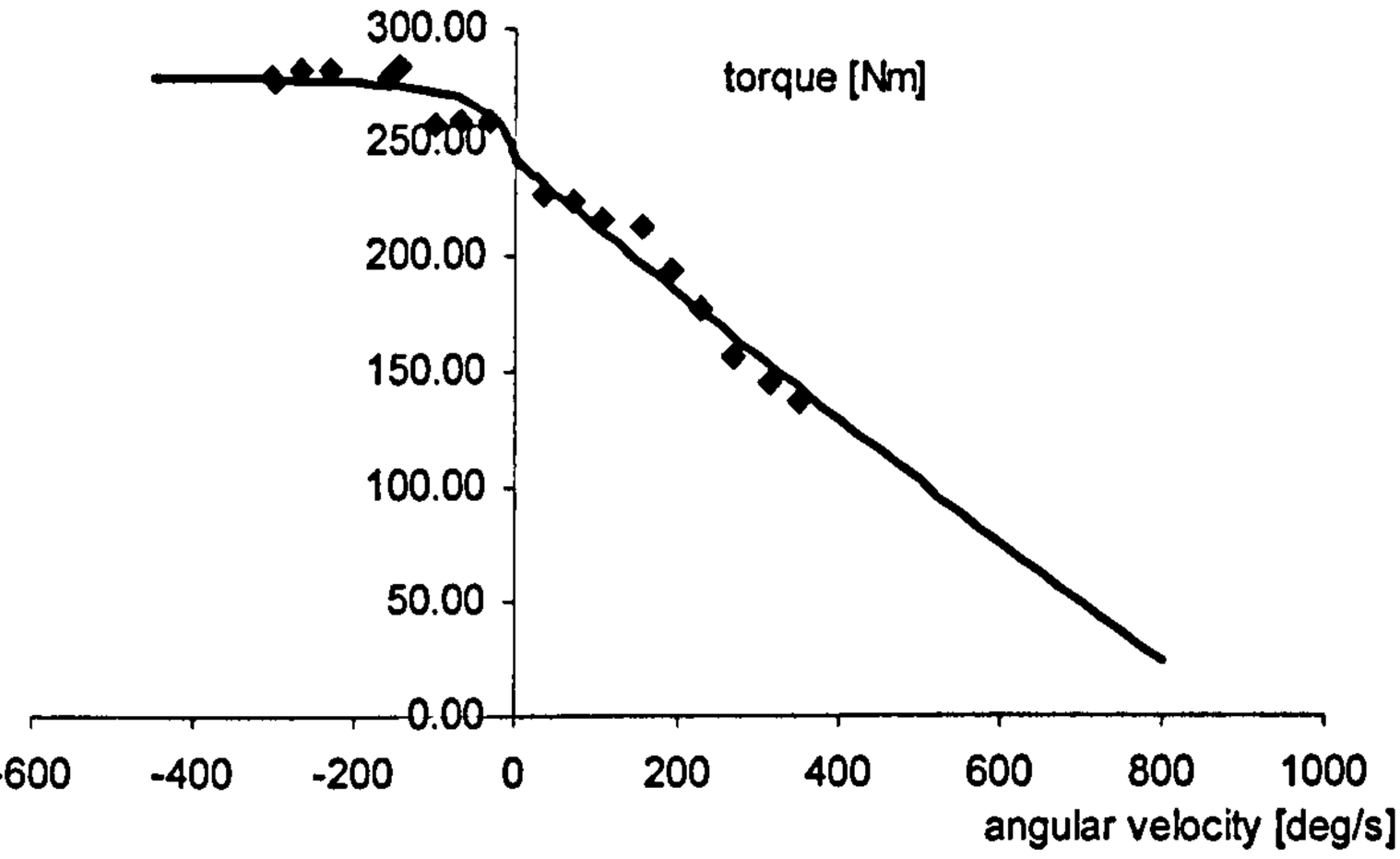

Figure 6.17. Splined averaged torques fitted with a four parameter function for knee extension highlighting a plateau in the concentric phase.

Seven parameter function

A seven parameter function was decided upon and this was fitted to the maximum torque values for the knee and hip joints. The parameters were the four parameters of the tetanus curve plus 3 parameters defining differential activation, these being, a_{min}, the lowest level of activation in the eccentric phase, m, the gradient of the slope that the activation increases at with angular velocity, and ω_1, the angular velocity value at the mid-point of the slope (Figure 6.18). The maximum activation level, a_{max}, was assumed to be equal to 1. The differential activation was governed by equation (6.16).

$$\omega - \omega_1 = \frac{+m(a - 0.5(a_{min} + a_{max}))}{(a_{max} - a)(a - a_{min})} \qquad (6.16)$$

Where:

a = activation level

ω = angular velocity

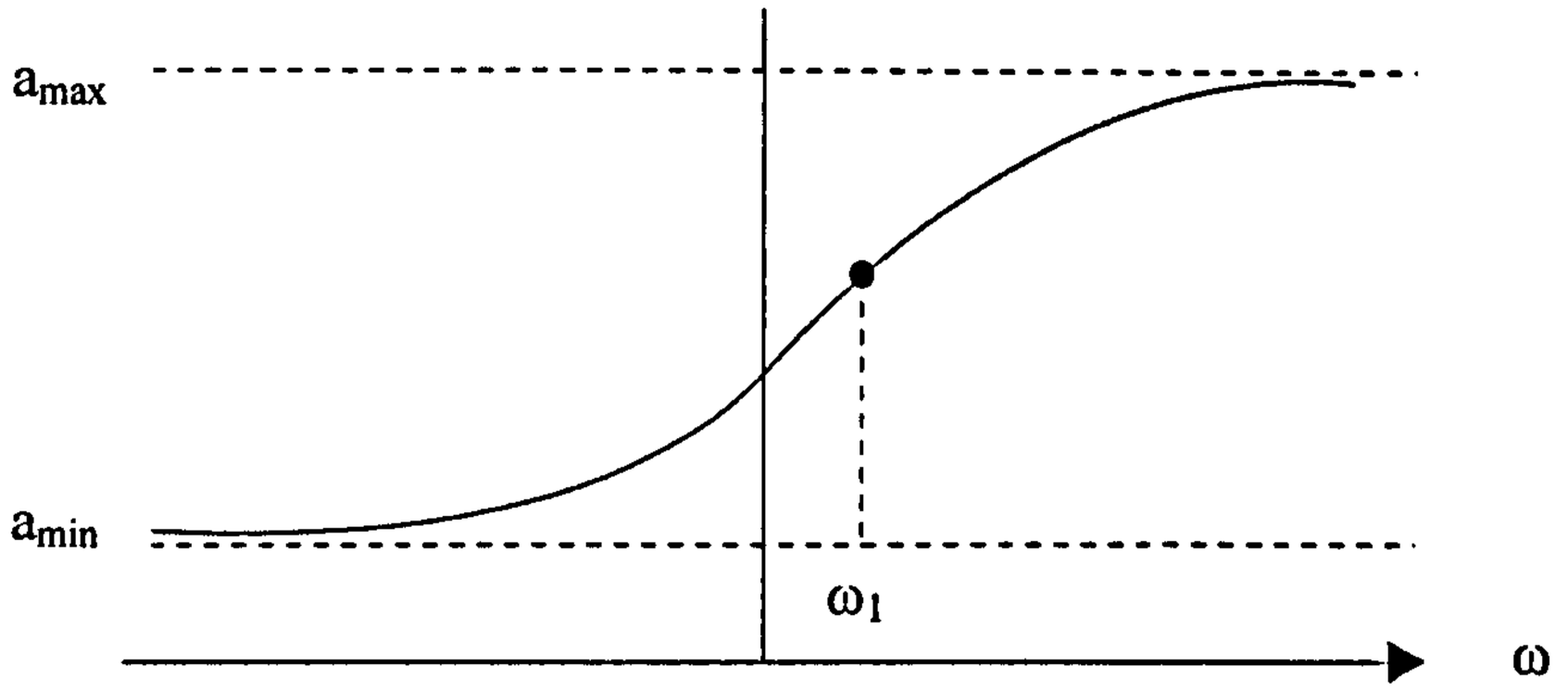

Figure 6.18. Differential activation function.

The torques calculated from equations (6.10) and (6.13) were then multiplied by the activation level a. Figures 6.19 and 6.20 show the seven parameter fit for knee extension and a trace of the activation function over the same period.

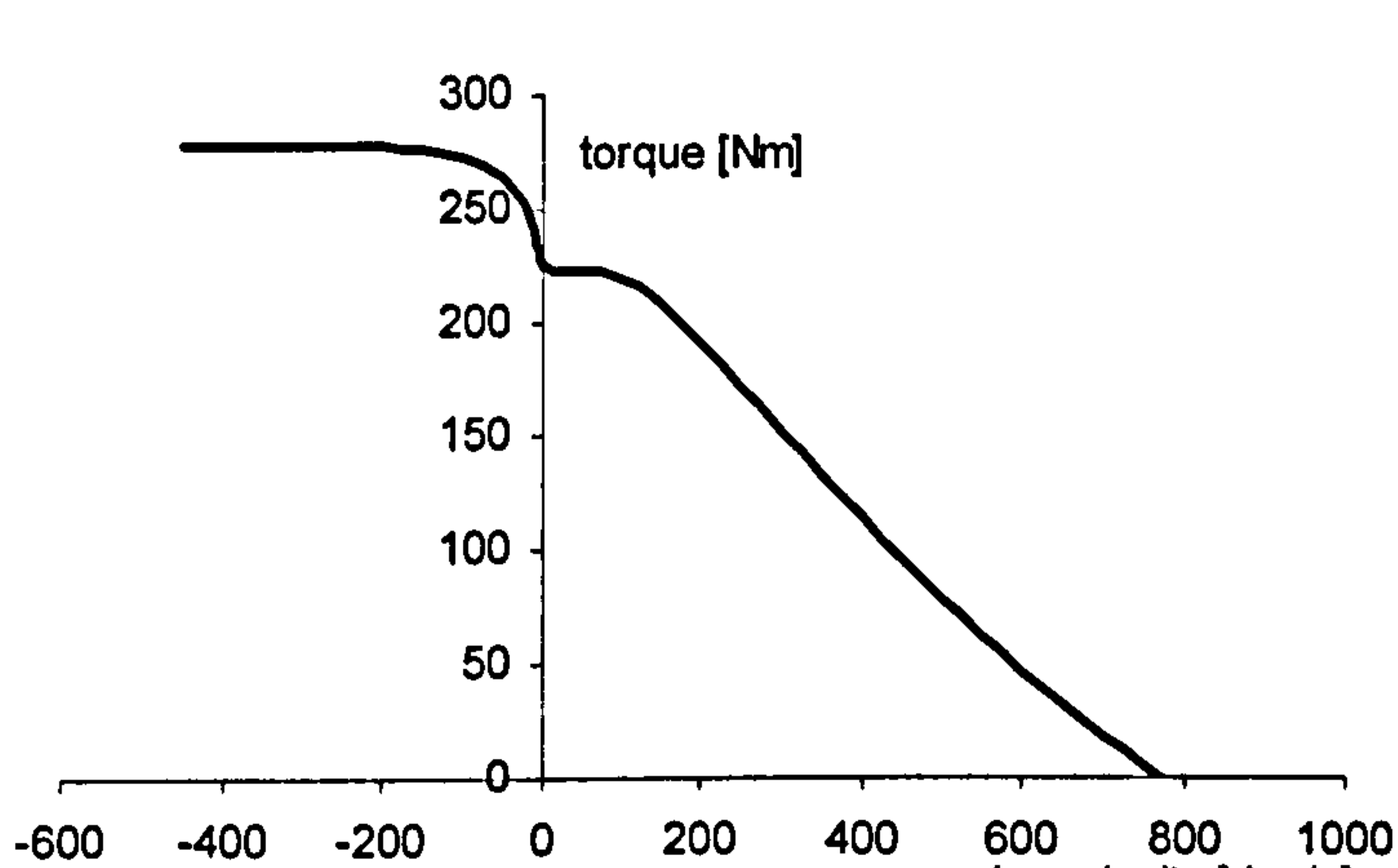

Figure 6.19. Seven parameter fit for knee extension.

Figure 6.20. Differential activation function for knee extension.

The torque parameter values for the seven parameters were obtained using the Simulated Annealing algorithm (Corana et al., 1987). Some constraints on the parameter values were necessary to keep the parameters realistic as different combinations of parameters could result in very similar curves.

Monotonically decreasing function constraint

A further constraint was included in the function which forced the torque to monotonically decrease with increasing angular velocity. This constraint had little effect on the RMS difference between the raw data torques and the calculated torques for knee extension, knee flexion and hip flexion. For the hip extension however, because the constraint resulted in the RMS difference increasing from 4.32 Nm to 22.25 Nm, it was decided therefore to remove the constraint for this particular action. This meant the function did not monotonically decrease in the eccentric phase, however, the increase was only 5% of the maximum torque achieved during the eccentric phase.

Parameter values

Maximum isometric torque values for each joint action were recorded using the isovelocity dynamometer, and these values were considered to be good indicators of the actual isometric torque which could be achieved at full muscle activation. From the literature (Harry et al., 1990) the ratio of eccentric torque, T_{max} to isometric torque, T_0 is essentially constant at a value of 1.5.

As many combinations of T_{max} and a_{min} result in the correct eccentric torque level, it was decided to impose a sensible value on T_{max} which may not occur if allowed to vary. Therefore, T_0 was set at the maximum isometric torque value achieved on the dynamometer and T_{max} at a value 1.5 times greater than this. a_{min} was subsequently set at a value which resulted in the correct eccentric torque level being achieved.

The values used for T_{max} and T_0 for each joint / action are shown in Table 6.10.

Table 6.10. T_{max} and T_0 values.

Joint / action	T_{max} [Nm]	T_0 [Nm]
knee extension	491	328
knee flexion	322	215
hip extension	719	480
hip flexion	433	289
shoulder flexion	143	95

For each of the remaining five parameters required for the function, constraints were needed to keep their values realistic. ω_{max} was constrained using the video data of the dynamic jumps performed in the laboratory. For each joint / action the maximum angular velocity achieved in the concentric phase of the dynamic jump was considered to be the minimum value for ω_{max}. King (1998) fixed ω_{max} at this value, but rather than forcing it to be one specific value, in this study, the upper limit was set to be 20% bigger than the actual value recorded, in order to allow some flexibility. Not much knee flexion occurred during the actual movement and hence not many angular velocity values were recorded, therefore it was decided to use the value for knee extension. Upper and lower limits of ω_{max} are shown in Table 6.11.

Table 6.11. Upper and lower limits of ω_{max}.

Joint / action	lower limit ($rad.s^{-1}$)	upper limit ($rad.s^{-1}$)
knee extension	13.4	16.1
knee flexion	13.4	16.1
hip extension	14.2	17.1
hip flexion	24.9	29.9
shoulder flexion	24.0	28.8

a_{min} did not need to be constrained as the values of T_{max} and T_0 were fixed. The only constraint on m, the gradient of the activation slope was that it was a

positive number, therefore the lower limit was set at zero. ω_1 was limited to lie between 0 rad.s^{-1} and 6 rad.s^{-1}. These limits were chosen as maximum activation of the torque generators was expected to be achieved between these two values. As with m, the only constraint put on ω_c was that it was positive.

Shoulder joint

Although no differential activation occurred during shoulder flexion the isovelocity data was at some reduced level compared to the tetanus curve. T_{max}, T_0 and a_{min} were determined in the same way as for the other joints, however, a_{min} was the activation level which was maintained throughout the whole function, and not just the initial activation level. This was achieved by setting both m and ω_1 equal to zero. The values of ω_c and ω_{max} were optimised which resulted in a seven parameter function.

Data were collected for shoulder flexion only, however, in the simulation model both shoulder flexion and shoulder extension were required. It was therefore assumed that the shoulder extensors were as strong as the flexors.

Nine parameter function

The seven parameter function, although able to fit the maximum torque values well, was not angle dependent. The seven parameter fits at each angle were independent of the seven parameter fits at the other angles, therefore there was the potential for large discrepancies between one fit and the next. Two further parameters were needed to define how the torque changes over an angle range, and therefore these two parameters were needed in order to fit a surface. The two parameters, k_2 and θ_{opt} were determined by a quadratic fitted to the whole of the torque data and not just the maximum values. A quadratic was considered sufficient to fit the torque data as a function of angle. The torque values were obtained by evaluating a spline fitted to the raw data at ten angles for each angular velocity. The angle values taken were the maximum and minimum angles for each joint / action and eight angles in between. The nine parameter function was defined by equation (6.17). The two parameters were determined using Simulated Annealing (Corana et al., 1987) in order to minimise the cost function which was equal to the root mean square (RMS) difference between the known raw torques

and the calculated torques using equation (6.17). The seven parameters values already determined were kept constant. The quadratic equation resulted in a percentage drop off from maximum torque at θ_{opt}.

$$T_{(\theta,\omega)} = T_{\omega}(1 - k_2(\theta - \theta_{opt})^2) \qquad (6.17)$$

Where:

$T_{(\theta,\omega)}$ = angular velocity and angle dependent torque

T_{ω} = angular velocity dependent torque (seven parameter function)

θ_{opt} = optimum angle at which maximum torque occurs

k_2 = rate at which torque drops off from optimum angle

The nine optimised parameters for knee extension and flexion, hip extension and flexion and shoulder flexion are shown in Table 6.12.

Table 6.12. Nine parameter surface fit to the Cybex data.

	knee extension	knee flexion	hip extension	hip flexion	shoulder flexion
T_{max} [Nm]	491	322	719	433	143
T_0 [Nm]	328	215	480	289	95
ω_{max} [rad.s^{-1}]	13.4	15.0	14.2	24.9	28.8
ω_c [rad.s^{-1}]	21.2	16.5	3.2	14.0	4.5
a_{min}	0.56	0.58	0.46	0.69	0.24
m	0.49	0.43	0.29	5.02	0.00
ω_1 [rad.s^{-1}]	1.1	0.53	0.45	6.00	0.00
θ_{opt} [rad]	2.0	3.6	1.6	3.6	0.5
k_2	0.53	0.08	0.27	0.33	0.09

Inverse dynamics data

The eight-segment angle-driven model (model 2) (Chapter 4) was used to calculate joint torque time histories throughout the simulation at the ankle, knee, hip and shoulder joints. Unexpectedly high torques were found to occur at the knee within the first 50 ms of contact. This initial peak in the torque, determined

using the angle-driven simulation model, is not fully understood. It is likely to be a passive torque if it does actually occur. Alternatively it may not really be there but be due to a modelling error, such as the knee being modelled as a simple pin joint. Other possibilities for this peak occurring which were looked at were the angular acceleration at the joint or the wobbling masses being inaccurate. Quasi-statics, however, were used to show these two factors made little difference to the torques produced.

After the initial peak, the torque level reached in the eccentric phase was similar to that reached in the isovelocity dynamometer trials. It was therefore decided to proceed with the isovelocity dynamometer data which King (1998) found to be adequate.

Two curves were plotted for each joint / action showing the peak torque produced at a range of angular velocities. The curve predicting the highest torques was the four parameter tetanus curve. The second curve represented the seven parameter fit to the Cybex data. Figure 6.21 shows a graph of the two curves for knee extension.

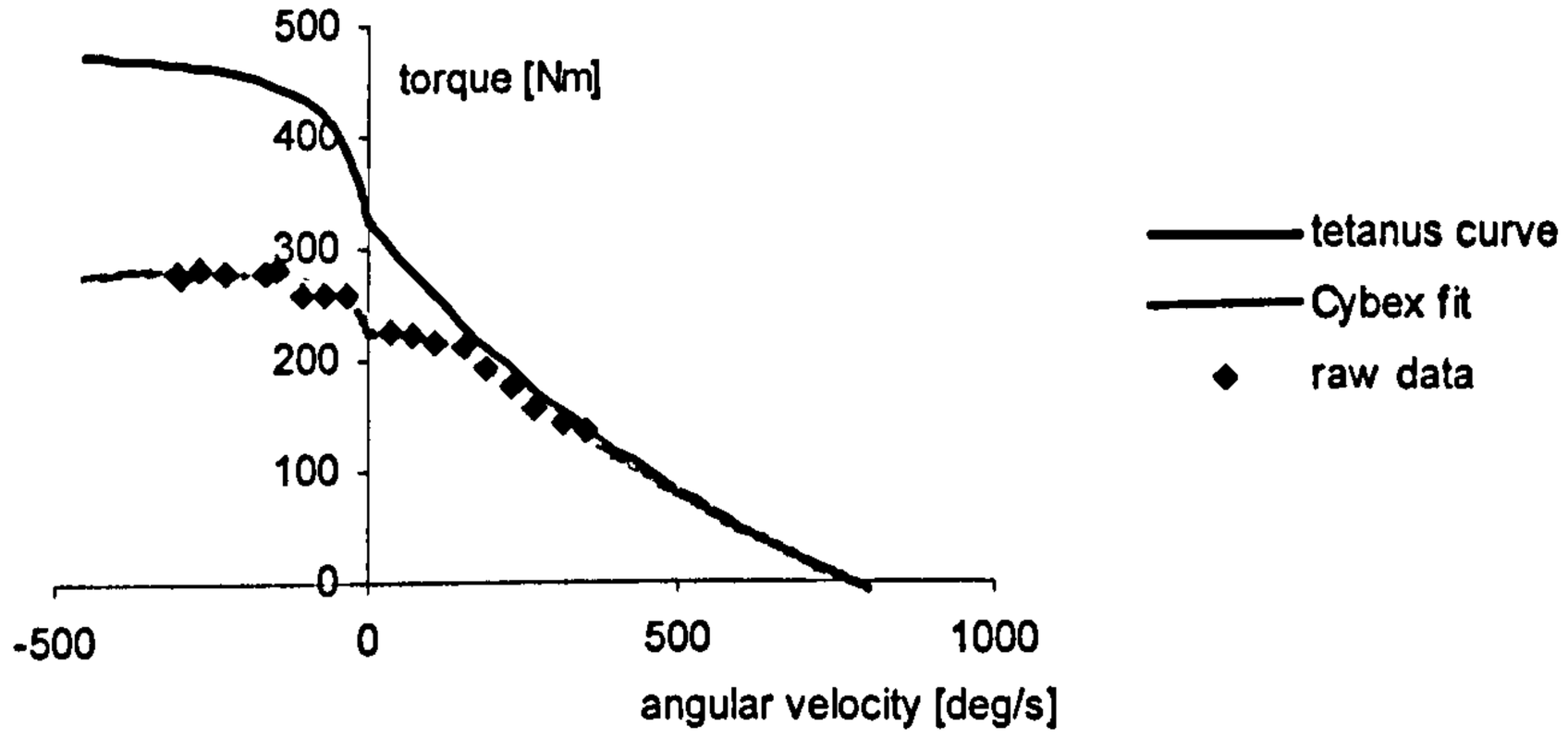

Figure 6.21. Tetanus and Cybex fit curves for knee extension.

Ankle joint

The difficulty in collecting data at the ankle using the Cybex isovelocity dynamometer resulted in insufficient data. The only data collected at the ankle were isometric torques. As with the other joints these torque data were used to determine the values of T_0 and T_{max}. The value of T_{max} was assumed to be 1.5 times the isometric value T_0.

The value of ω_{max} was set to be 10% greater than the maximum ankle angular velocity obtained from the video data, forcing its value to be equal to the average of the two limits used for the other joints. To obtain the remaining four parameters for a seven parameter fit, the average of the values for the other joints was calculated (after the largest and smallest values had been removed).

The parameters needed to define the torque-angular velocity relationship for ankle dorsi flexion were determined in the same way as for ankle plantar flexion.

Obtaining a nine parameter function for the ankle joint had to be done in a different way to the other joints due to the lack of data collected. The only angle dependent data were the isometric torque values which were collected at five different angles. These data were used to determine the optimum angle θ_{opt}, at which the maximum torque could be achieved. The plantar flexion isometric torque values were fitted with a straight line, with the angle at which the maximum isometric torque was achieved being θ_{opt}. It was decided that for the angles greater than θ_{opt} the torque would drop off at a rate determined by the slope of the fitted line. This rate of drop off was then divided by T_{max} for ankle plantar flexion in order to make the drop off a percentage of maximum torque. For angles smaller than θ_{opt} the torque would remain at the value determined by the seven parameter function and would not drop off, as it was assumed that the highest torque from the raw data was the peak value. For dorsi-flexion, a quadratic was fitted to the five isometric torque values and θ_{opt} was determined by differentiating the quadratic equation, putting it equal to zero and solving for the angle x. The rate at which the torque dropped off was determined by the quadratic equation. As with plantar flexion this value was then divided by T_{max} in order to make the drop off a percentage of the maximum torque.

Results

The calculated nine parameters for each joint and action are shown in Table 6.13, along with the raw data and surface fits (Figures 6.22 to 6.26). The parameters define the maximum torque as a function of joint angle and angular velocity.

Table 6.13. Nine parameter function values for a surface fit to the Cybex data.

	knee extension	knee flexion	hip extension	hip flexion	shoulder flexion	ankle plantar	ankle dorsi
T_{max} [Nm]	491	322	719	433	143	424	96
T_0 [Nm]	328	215	480	289	95	283	65
ω_{max} [rad.s^{-1}]	13.4	15.0	14.2	24.9	28.8	15.7	15.7
ω_c [rad.s^{-1}]	21.2	16.5	3.2	14.0	4.5	15.3	15.3
a_{min}	0.56	0.58	0.46	0.69	0.24	0.57	0.57
m	0.49	0.43	0.29	5.02	0.00	0.46	0.46
ω_1 [rad.s^{-1}]	1.1	0.59	0.45	6.00	0.00	0.86	0.86
θ_{opt} [rad]	2.0	3.6	1.6	3.6	0.5	1.5	1.9
k_2	0.53	0.08	0.27	0.33	0.09	0.43	0.55

(a)

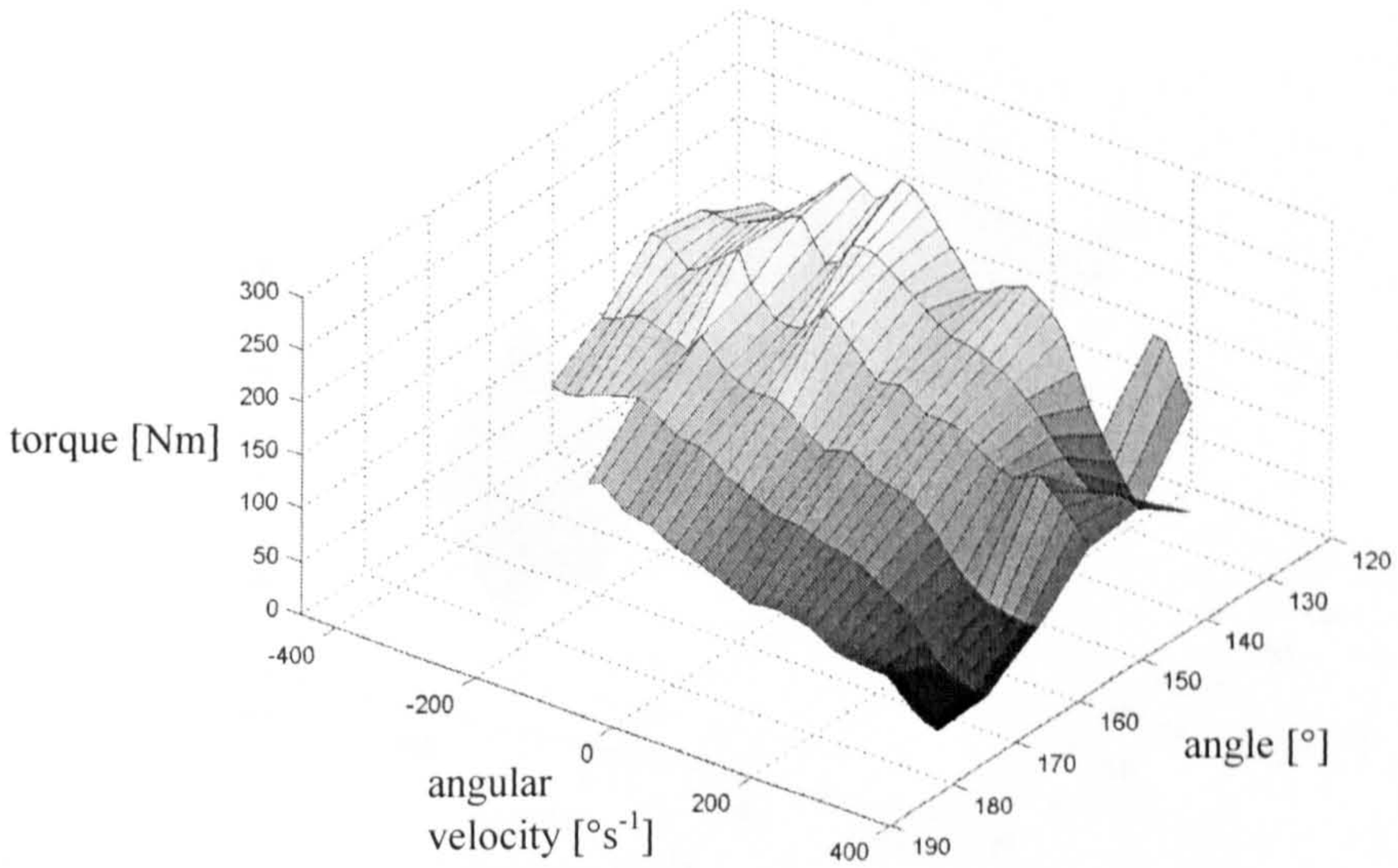

(b)

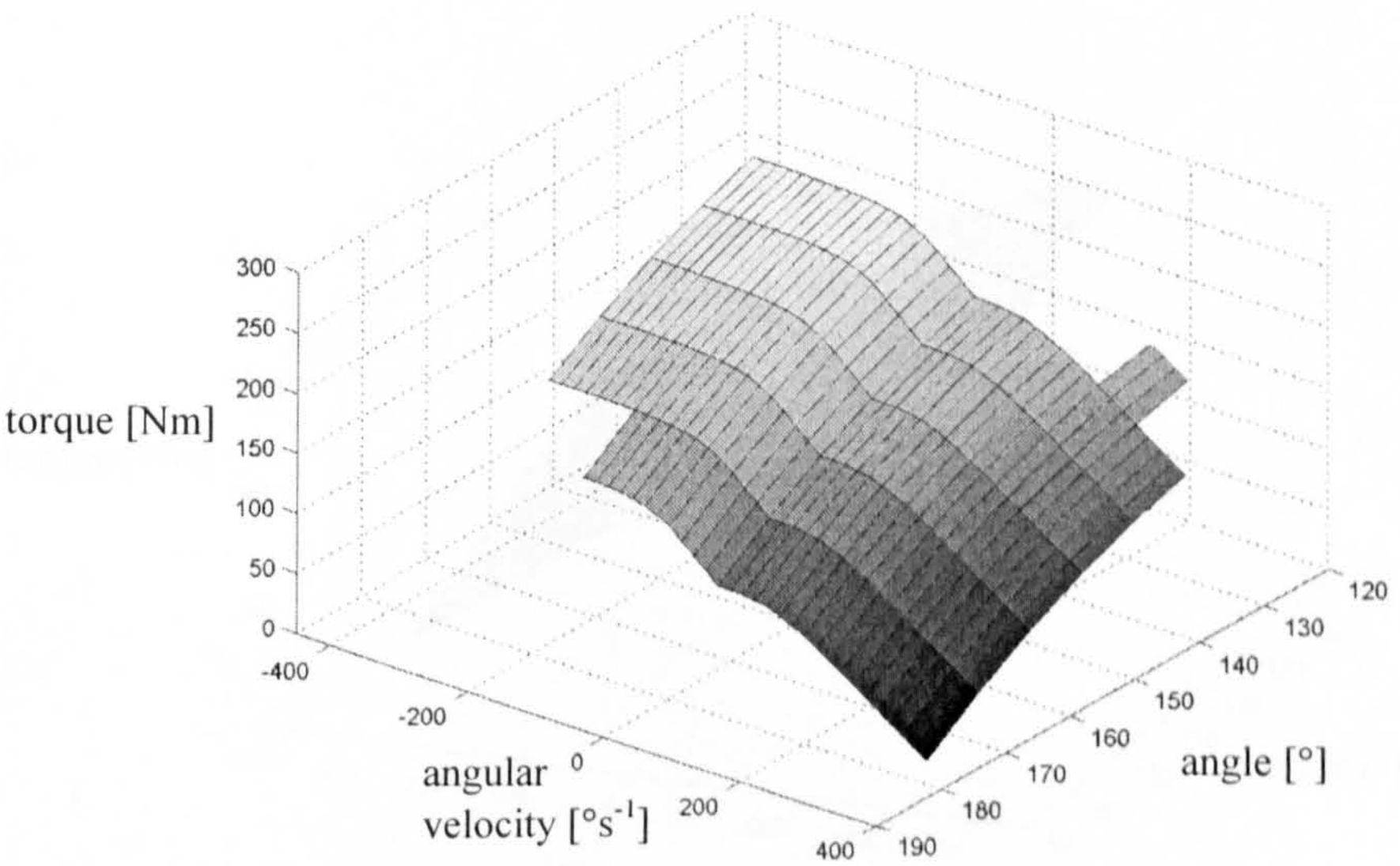

Figure 6.22. 3D surfaces of the torque/ angular velocity/ angle relationship for knee extension for (a) raw Cybex data and (b) 9 parameter function fitted to the Cybex data.

(a)

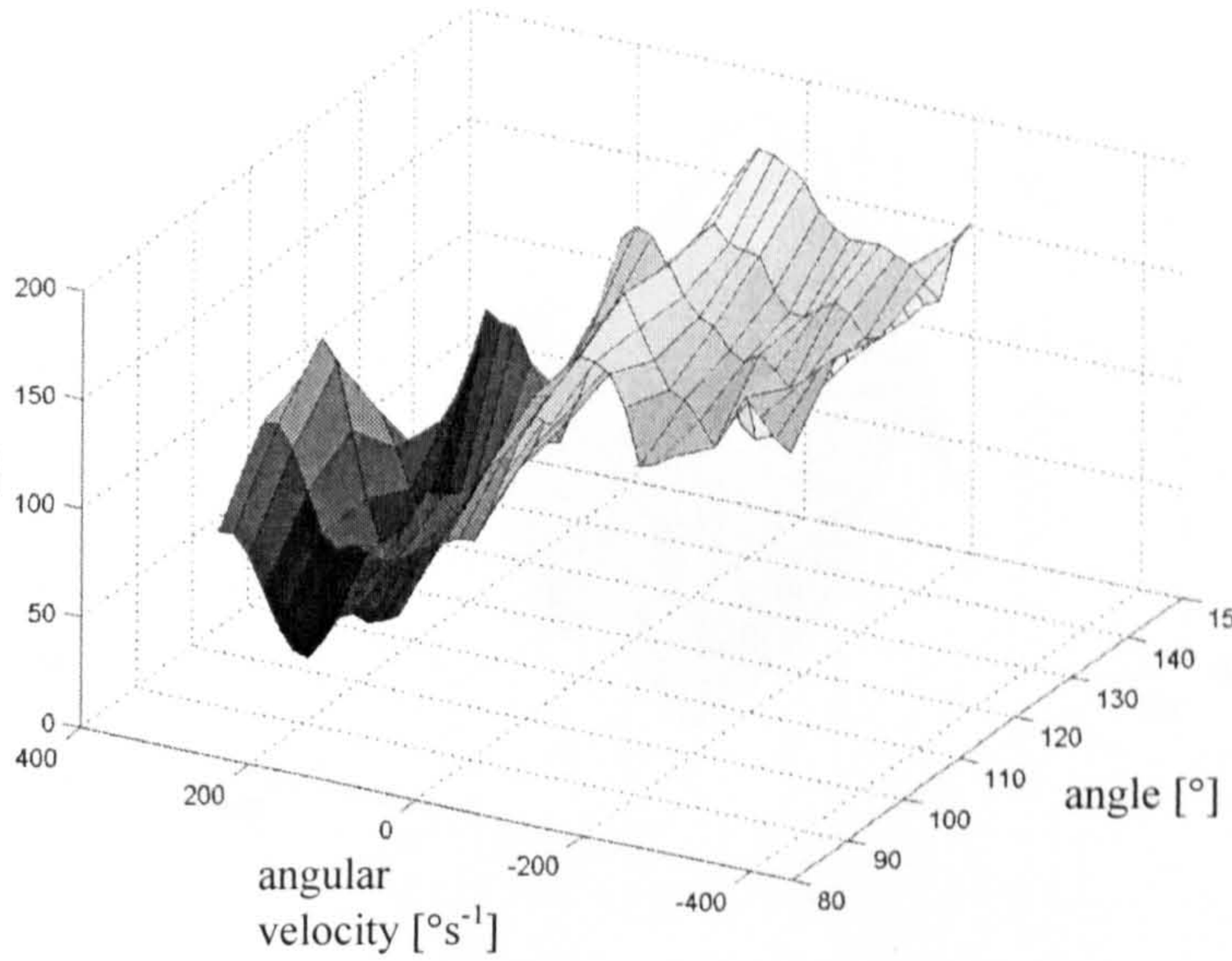

(b)

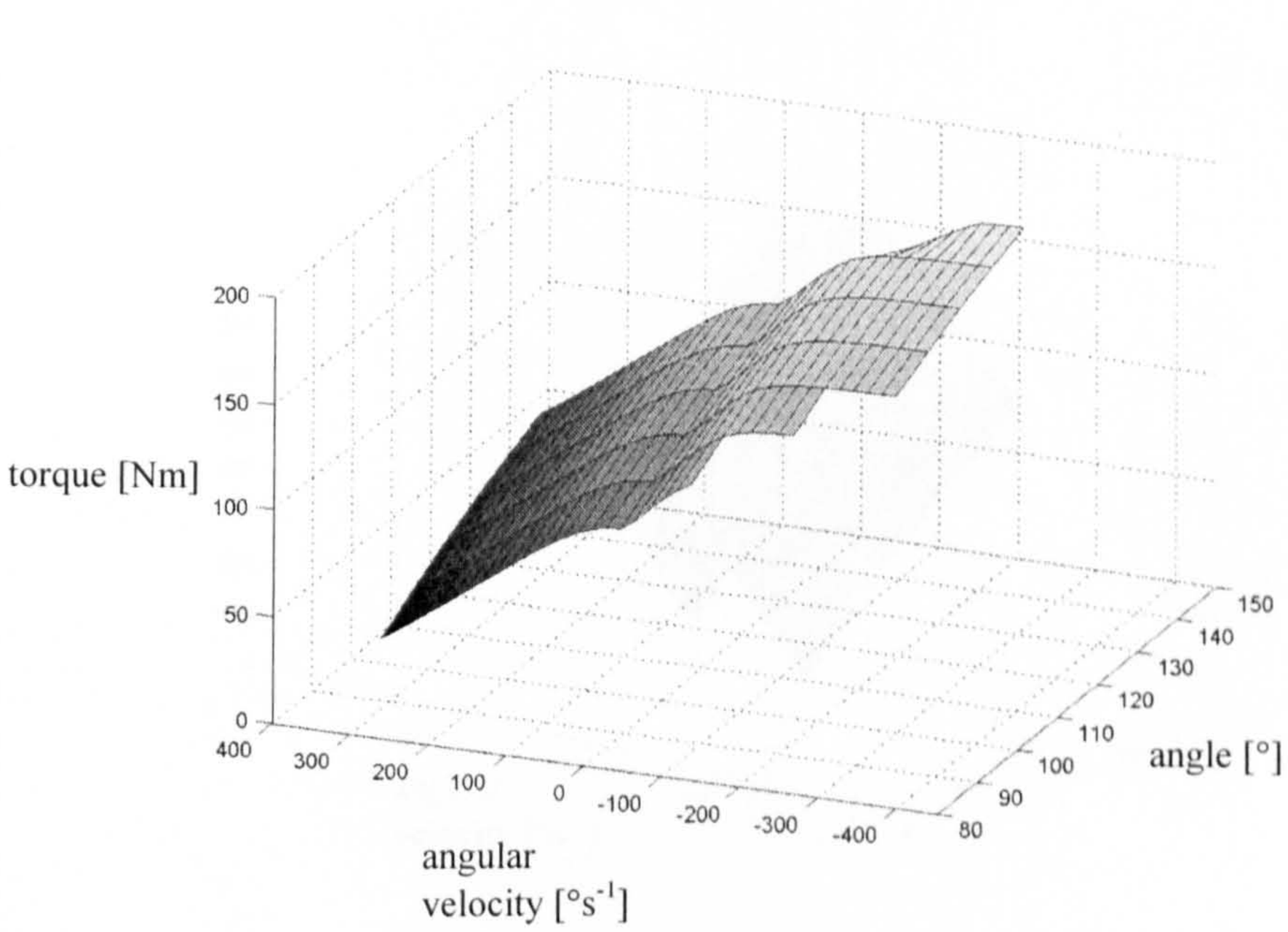

Figure 6.23. 3D surfaces of the torque/ angular velocity/ angle relationship for knee flexion for (a) raw Cybex data and (b) 9 parameter function fitted to the Cybex data.

(a)

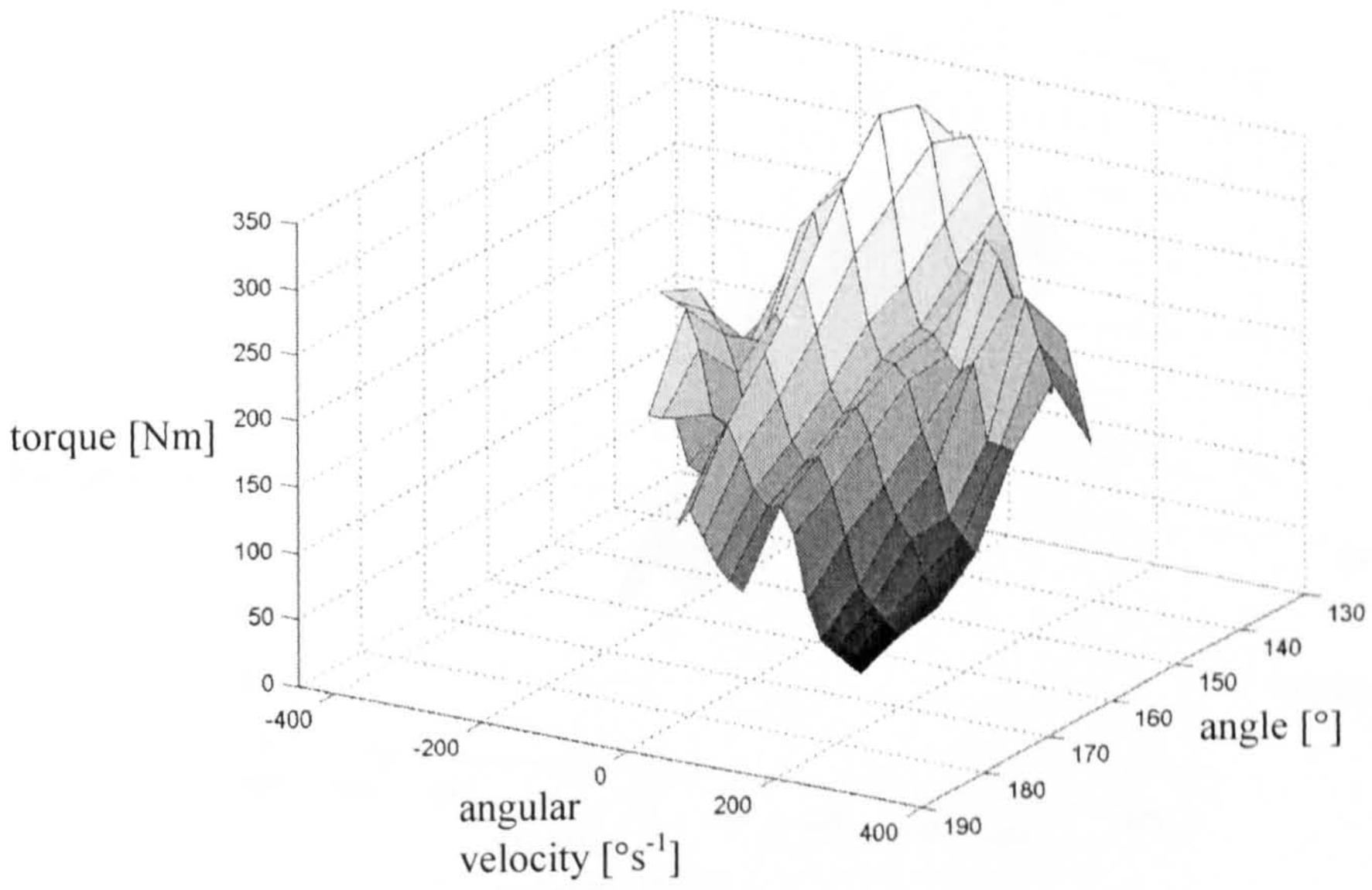

(b)

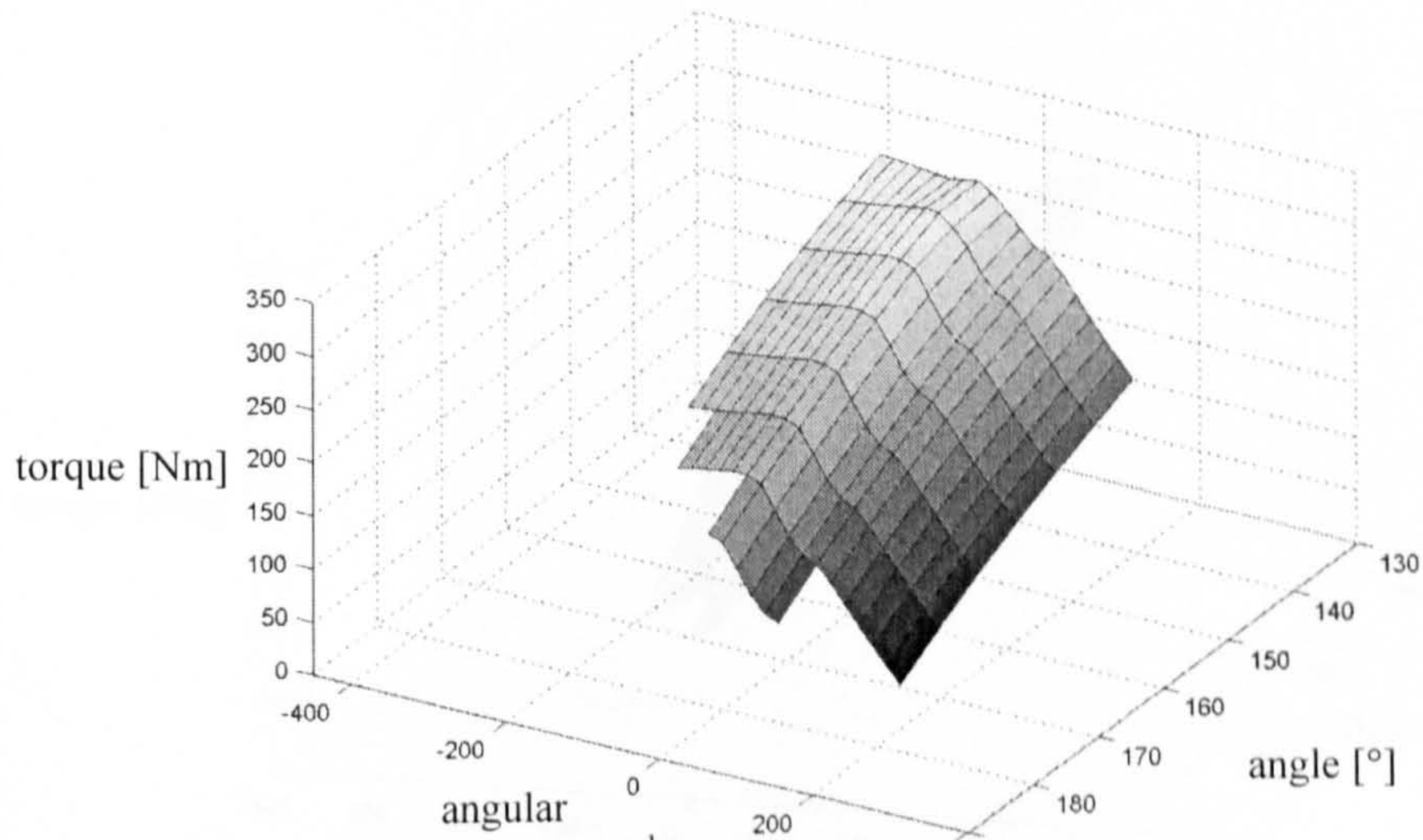

Figure 6.24. 3D surfaces of the torque/ angular velocity/ angle relationship for hip extension for (a) raw Cybex data and (b) 9 parameter function fitted to the Cybex data.

(a)

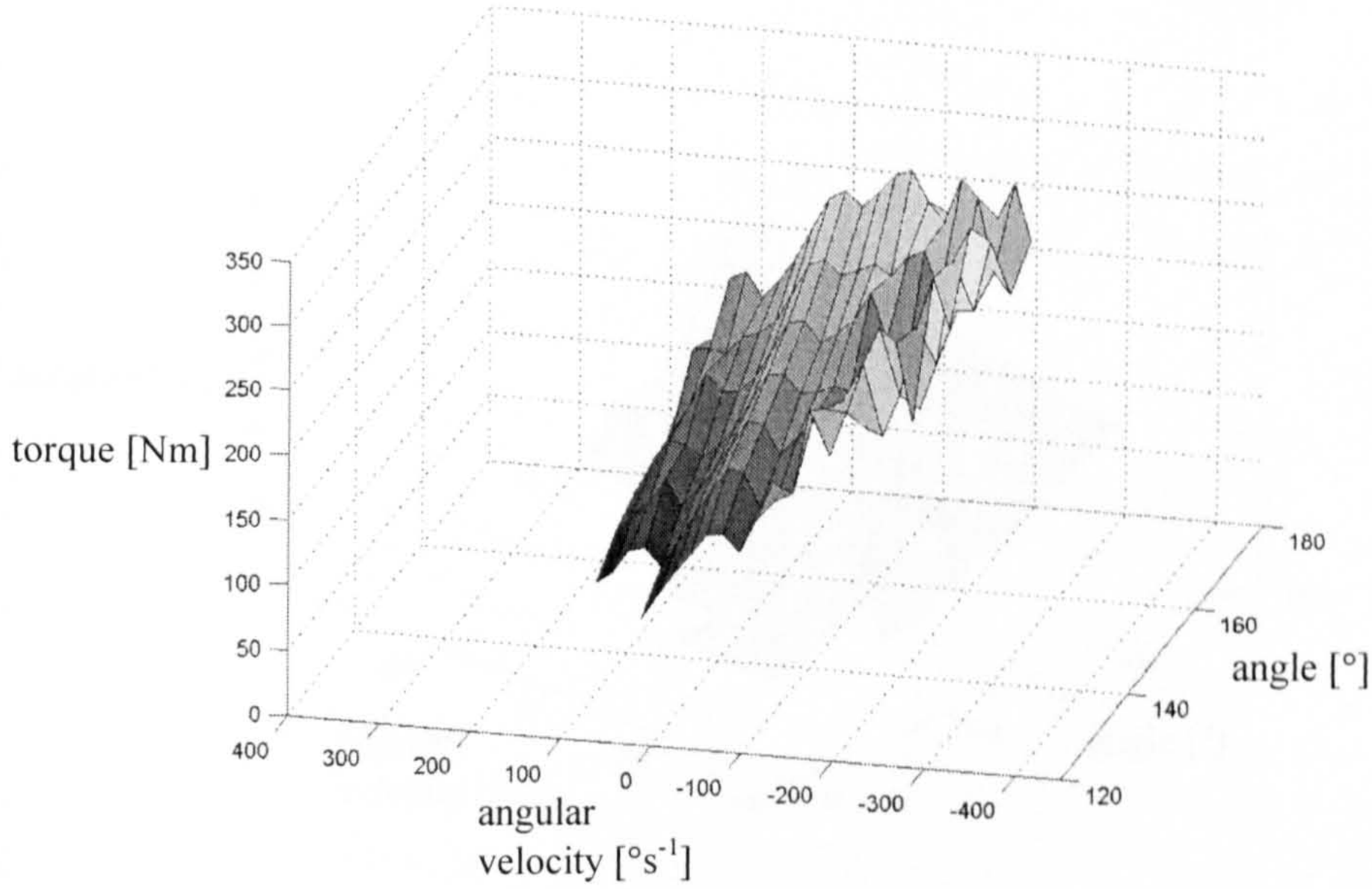

(b)

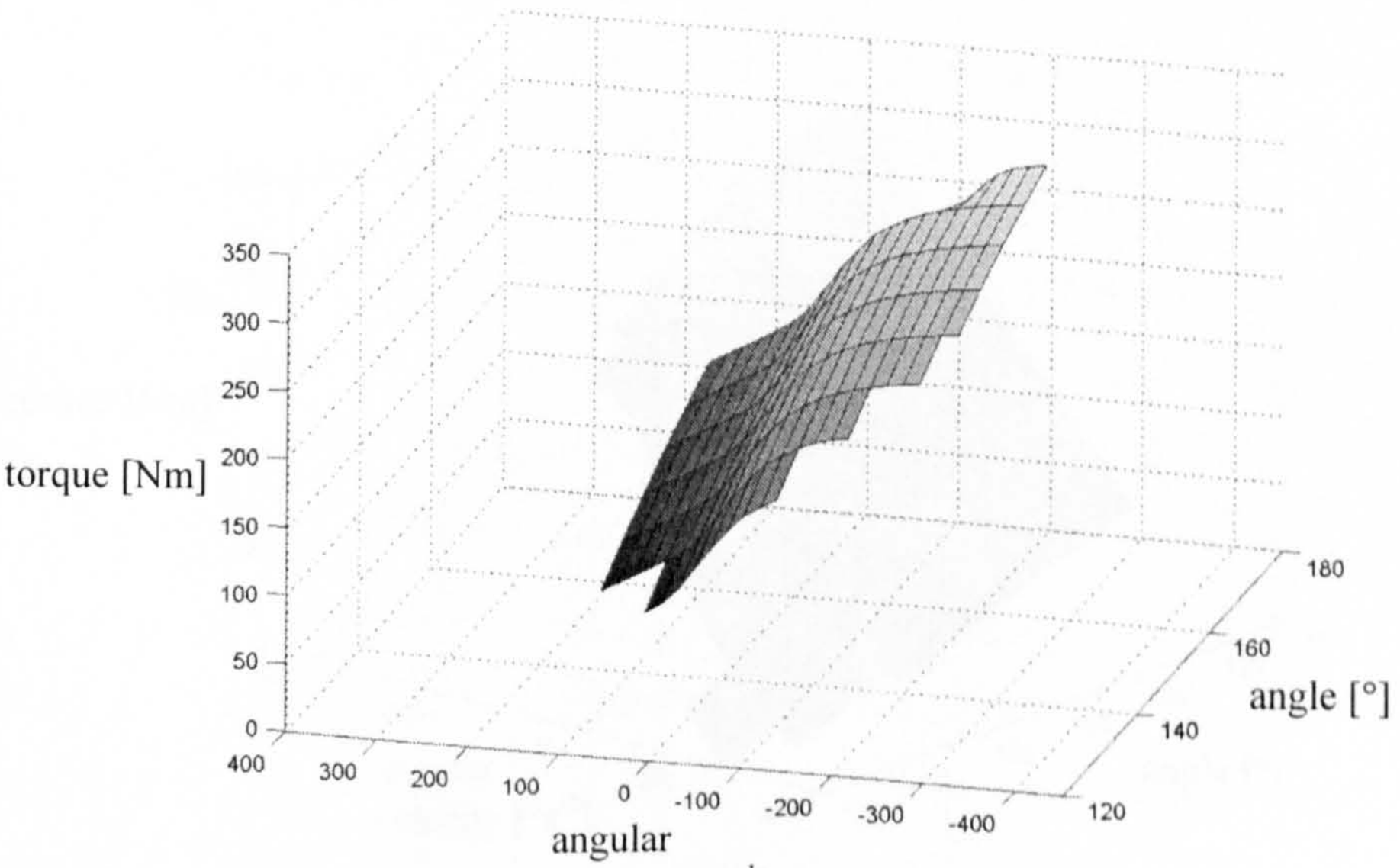

Figure 6.25. 3D surfaces of the torque/ angular velocity/ angle relationship for hip flexion for (a) raw Cybex data and (b) 9 parameter function fitted to the Cybex data.

(a)

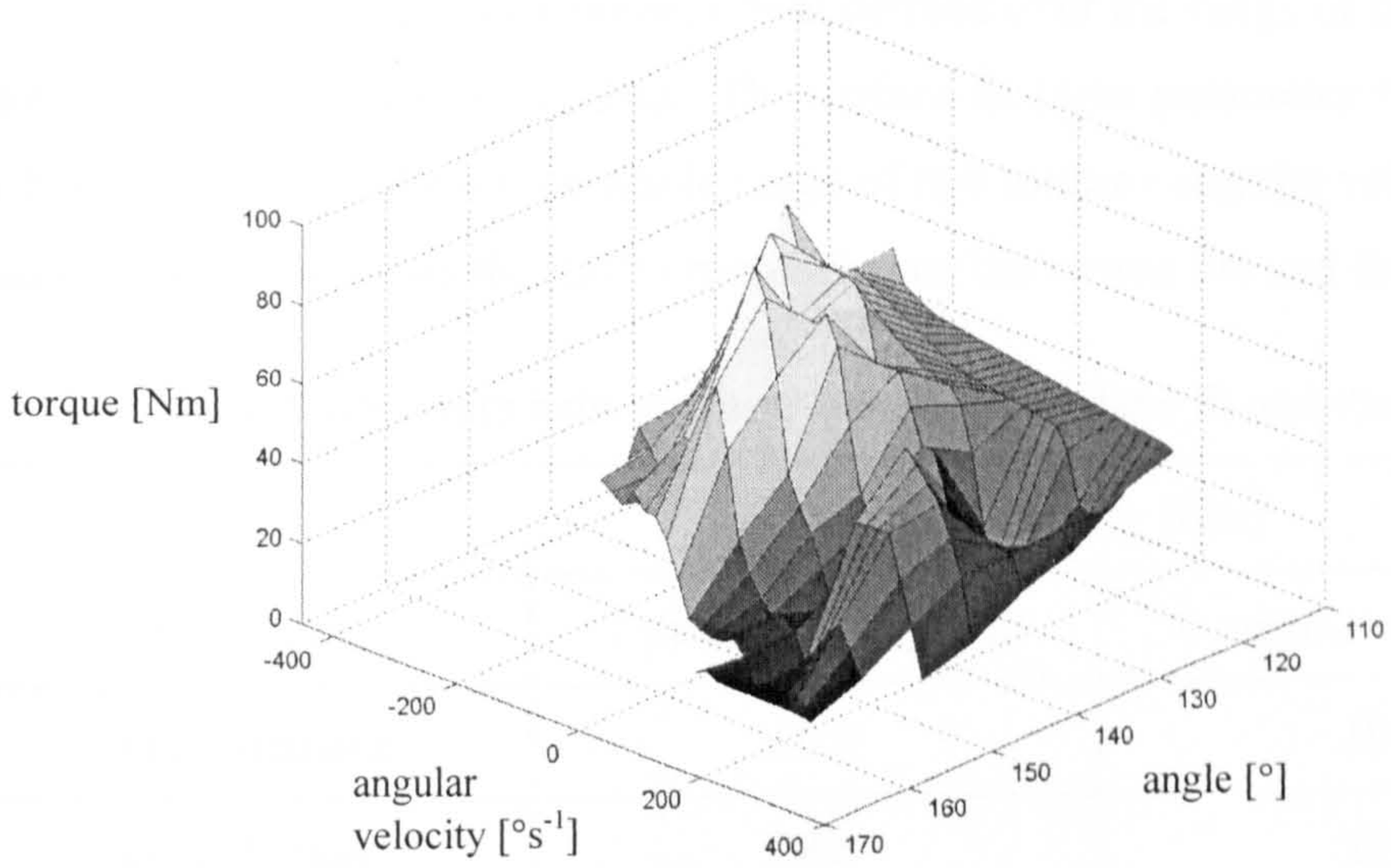

(b)

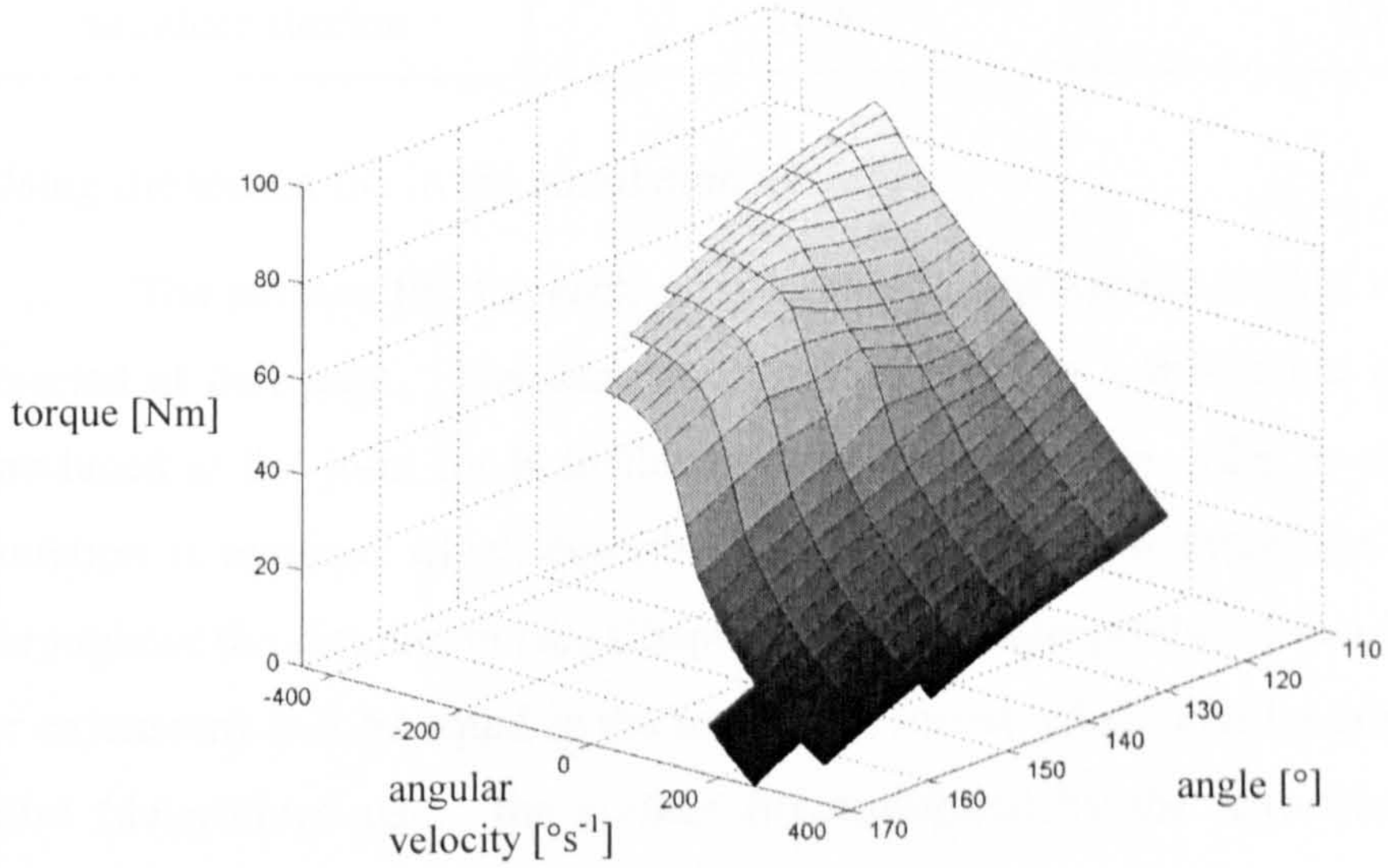

Figure 6.26. 3D surfaces of the torque/ angular velocity/ angle relationship for shoulder flexion for (a) raw Cybex data and (b) 9 parameter function fitted to the Cybex data.

RMS differences between the torque functions and the raw data

The seven parameter function was defined over the range of the maximum raw torque / angular velocity data. The surface fit (nine parameter function) was subsequently defined over the whole range of raw torque / angular velocity / angle data. Table 6.14 shows the RMS errors between the torque fits and the raw data.

Table 6.14. RMS errors between the 9 parameter surface fit and the raw data.

	RMS error [Nm]	
joint/action	7 parameter function	9 parameter function
knee extension	18.9	29.3
knee flexion	18.6	33.8
hip extension	24.9	42.1
hip flexion	34.0	36.7
shoulder flexion	14.5	17.6

Using the torque fits in the simulation models

The surface fits for each joint predict the maximum torque which can be exerted at that joint. The simulation model requires a prediction of the torque produced at the joint for both flexion and extension. In order to achieve this a function is required which describes the torque generator activation time history throughout the simulation (see Chapter 7). The torque produced at a joint (flexion or extension) will be equal to the maximum torque which can be produced at the joint (determined using the surface fit) multiplied by the activation level A(t) (equation (6.18))

$$T(t) = A(t).T_{max}(\theta, \omega) \qquad (6.18)$$

The surfaces are expressed as a function of joint angle and angular velocity. However, this does not allow for a series elastic component.

Muscle-tendon complex

The muscle model for each of the joints consisted of a contractile and an elastic component in series. The set-up of the muscle-tendon complex was

different for extension and flexion at each joint. Figure 6.27 shows the set-up of the muscle tendon complex for knee extension and knee flexion. This set-up was the same for the ankle, hip, shoulder and free hip joints.

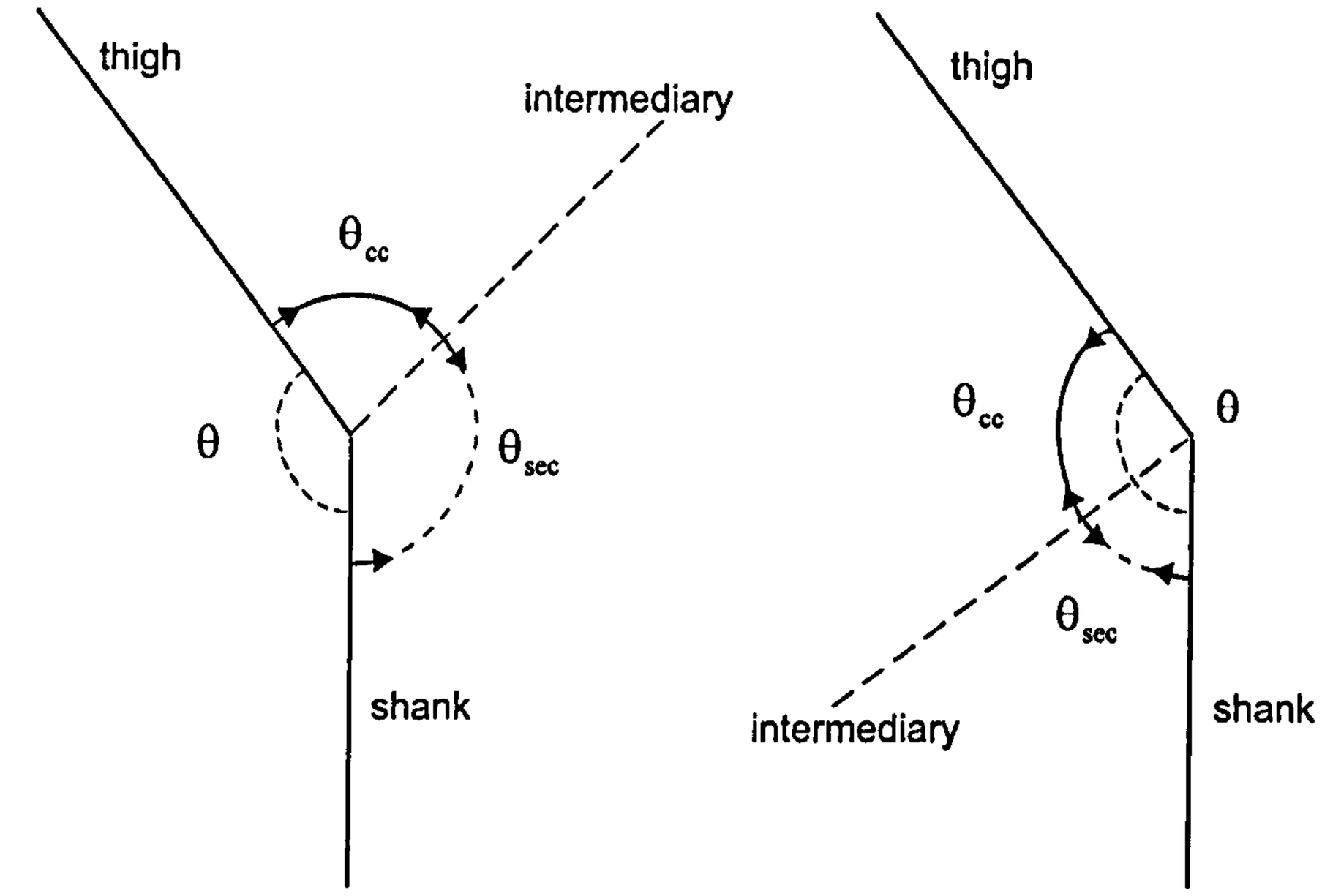

Figure 6.27. Muscle-tendon complex set-up for the knee joint.

In order for the torque generators to predict the torque produced at each of the joints the nine parameter function needed to be in terms of the contractile component angle and angular velocity rather than joint angle and angular velocity.

King (1998) found that the joint angular velocity was approximately equal to (or equal and opposite to) the contractile component angular velocity throughout the isovelocity parts of each of the Cybex trials used to fit the nine parameter function. The joint angle, however, was slightly more difficult to transform to the contractile component angle. Equations (6.19) and (6.20) show how the two angles are related for extension and flexion of a joint respectively.

Extension: $$2\pi = \theta + \theta_{cc} + \theta_{scc} \quad (6.19)$$

Flexion: $$\theta = \theta_{cc} + \theta_{sec} \quad (6.20)$$

$$T_{sec} = k.\theta_{sec} \quad (6.21)$$

Where:

k = stiffness of series elastic component

Using the torque / angle / angular velocity data set and assuming the torque collected on the Cybex machine was produced by the contractile component only, θ_{sec} was calculated by setting the contractile component torque equal to the series elastic component and using equation (6.21). The contractile component angle was then calculated from θ_{sec} and the θ (joint angle) using equations (6.19) or (6.20). k_2 and θ_{opt} were subsequently recalculated using the calculated contractile component angles. In the case of the ankle, the angle data from the isometric trials were transformed in the same way and k_2 and θ_{opt} were recalculated in the same way that they were initially determined. Table 6.15 shows the recalculated values of k_2 and θ_{opt} for each muscle / action.

Table 6.15. Recalculated values of k_2 and θ_{opt}.

	k_2	θ_{opt}
knee extension	0.72	3.9
knee flexion	0.15	3.4
hip extension	0.27	4.7
hip flexion	0.15	3.7
shoulder flexion	0.05	6.6
ankle plantar flexion	0.37	4.5
ankle dorsi flexion	0.45	1.7

Initially (at time zero) the set-up of the muscle tendon complex (i.e. the joint angle, the contractile component angle and the series elastic component angle) needed to be determined. This was achieved by putting the series elastic component torque equal to the contractile component torque. Making the assumption that the angular velocity of the series elastic component was equal to zero and therefore the contractile component angular velocity was equal (or equal and opposite) to the joint angular velocity, the contractile component torque was calculated using the nine parameter function and the elastic component torque was calculated using equation (6.21).

Once the two equations were equated and θ_{sec} was put in terms of θ and θ_{cc} (equations (6.19) and (6.20)), θ_{cc} could be calculated.

θ_{cc} at the end of the first iteration was subsequently determined using the contractile component angular velocity and making the assumption that the angular velocity remained constant over this first iteration.

For each iteration of the simulation models after time zero, the contractile component angle and the joint angle were initially known and the contractile component angular velocity needed to be determined. Maximum series elastic component torque was calculated (equation (6.21)). The contractile component torque was assumed to be equal to this value in order for the contractile angular velocity to be calculated. The contractile component angle needed for the next iteration was then calculated using this contractile component angular velocity just calculated (equation 6.22):

$$\theta_{cc} = \theta_{cci} + \frac{1}{2}(\dot{\theta}_{cc} + \dot{\theta}_{cci})dt \qquad (6.22)$$

Where θ_{cci} and $\dot{\theta}_{cci}$ were the estimates of the contractile component angle and angular velocity at the beginning of the iteration.

Spring parameters

Spring parameter values for both the wobbling masses and the foot-ground interface were determined through optimisation using the eight-segment angle-driven simulation models.

Initial guesses for the wobbling mass stiffness and damping constants were obtained using the first angle-driven model, model 1. Nine parameters values were required, three stiffness and six damping constants. Within a segment the stiffness and damping constants of the springs at each end of the segment were assumed to have the same value. The damping constants for each segment changed over a period of time, after the initial movement of the soft tissue, from the first parameter value to the second and hence six damping parameters were required.

The joint angles were set at fixed values for the whole of the simulation, and the initial mass centre velocities were set so that the model performed the contact phase of a drop jump from a height of 0.5 m. The forces at the toe and the

horizontal force at the heel were set to zero, so that all the force developed was the vertical force at the heel. The body configuration / orientation was such that the model landed on its heel. The stiffness and damping constants for the foot-ground interaction were varied until a sensible depression of the floor horizontally and vertically was achieved (< 0.04 m) and the ground reaction force curve contained a peak vertical force of a sensible magnitude (4000-6000 N). Once this was achieved, the wobbling mass stiffness and damping constants were varied until each of the three wobbling masses moved away from the corresponding rigid segment with magnitude which was considered realistic (Table 6.25).

Initial estimates for the spring parameter values for the floor were taken from Gilchrist and Winter (1996). The data used to develop their model were taken from a three-dimensional gait analysis of a young male walking at a self selected speed across two force platforms. The vertical and horizontal stiffness constants obtained were 40,000 Nm^{-1}, the vertical damping used was 300 Nsm^{-1}, and the horizontal damping used was 400 Nsm^{-1}. These three values were chosen as the initial estimates when a linear representation of the spring-damper systems was used and re-calculated to give equivalent values when a non-linear representation was used. These values were then allowed to vary in order to optimise the match between actual performance and simulations. Again nine parameter values were required, vertical stiffness and damping constants at the toe, vertical stiffness and damping constants at the heel, horizontal stiffness and damping constants (which were the same at both the toe and the heel as the horizontal ground reaction forces at the heel and toe were assumed to be equal), and three second damping constants to replace the initial ones after the velocity of the heel / toe had fallen to zero.

Spring parameter determination though optimisation

Yeadon and Challis (1994) described the need to evaluate theoretical predictions by comparing results with experimental data. This section describes the method used to determine the accuracy of the eight-segment simulation models of both high jumping and long jumping by using a combination of simulations and data obtained from collections in the laboratory.

Information from each of the performances analysed in Chapter 5 was required in order to compare these to the simulations. The kinematic data required from the actual performances were:

- Initial conditions for the start of each simulation
- Takeoff characteristics
- Joint angle / angular velocity time histories (angle-driven models only)
- Movement of the foot

The initial conditions were required so that each simulation could start with the same initial characteristics as the actual performance. The takeoff characteristics, the joint angle and joint angular velocity time histories and the deformation of the foot during contact with the ground were required to compare actual performances and simulations.

Initial conditions

Tables 6.16, 6.17 and 6.18 show the kinematic data obtained from the analysis of dynamic jumps at the time of touchdown of the foot.

Table 6.16. Horizontal and vertical velocities of the mass centre from actual performances at the time the foot made contact with the ground.

	v_{cmx} [ms^{-1}]	v_{cmy} [ms^{-1}]
Trial 36	-4.40	-0.85
Trial 46	-6.87	-0.43

Table 6.17. Body orientation and configuration angles from actual performances at the time the foot made contact with the floor.

	ank_a [°]	kne_a [°]	hip_a [°]	shr_a [°]	elb_a [°]	$rhip_a$ [°]	$rkne_a$ [°]	$trunk_a$ [°]
Trial 36	101	157	149	-55	134	185	108	78
Trial 46	99	151	135	-21	116	198	127	90

Table 6.18. Joint and trunk angular velocities from actual performances at the time the foot made contact with the floor.

	ank_ω [$°s^{-1}$]	kne_ω [$°s^{-1}$]	hip_ω [$°s^{-1}$]	shr_ω [$°s^{-1}$]	elb_ω [$°s^{-1}$]	$rhip_\omega$ [$°s^{-1}$]	$rkne_\omega$ [$°s^{-1}$]	$trunk_\omega$ [$°s^{-1}$]
Trial 36	-14	-399	175	981	-75	-235	-584	-77
Trial 46	-26	-288	3	465	-68	-830	-1371	46

Where:

v_{cmx} = horizontal mass centre velocity

v_{cmy} = vertical mass centre velocity

ank, kne, hip, shr, elb, rhip, rkne represent: ankle, knee, hip, shoulder, elbow, free hip and free knee and subscripts a and ω denote angle and angular velocity respectively

trunk represents: trunk with a and ω representing segment angle and angular velocity respectively

Takeoff characteristics

The takeoff characteristics of the dynamic jumps obtained from the kinematic analysis include the horizontal and vertical mass centre velocities, the trunk orientation and the whole body angular momentum. Values for these characteristics for both trials are shown in Table 6.19.

Table 6.19. Takeoff characteristics from kinematic analysis of dynamic jumps.

	v_{cmx} [ms^{-1}]	v_{cmy} [ms^{-1}]	trunk orientation [°]	angular momentum [$kgm^2.s^{-1}$]
Trial 36	-1.89	3.31	86	4.94
Trial 46	-5.31	3.47	93	4.99

Joint angle / angular velocity time histories

In the evaluation of the torque-driven model the ankle, knee, hip, shoulder, free hip and trunk angles from the actual performances were used. In the angle-driven models the joint angle time histories from the actual performances were

used to drive the model. Therefore, the trunk angle at takeoff only was required in the comparison of actual performances and simulations. In trial 36 the ankle, knee and hip angles all decreased before increasing during contact, while the other joints increased or decreased continuously throughout the contact. In trial 46, only the ankle and knee decreased before increasing. The minimum ankle and knee angles (and minimum hip angle in trial 36) as well as the final angles at takeoff of the ankle, knee, hip, shoulder, free hip and trunk were all used in the evaluation / comparison procedure. Tables 6.20 and 6.21 show the values of the angles used in the evaluation procedure for each of the trials.

Table 6.20. Body orientation / configuration for each performance at takeoff.

	ank_a [°]	kne_a [°]	hip_a [°]	shr_a [°]	$rhip_a$ [°]	$trunk_a$ [°]
Trial 36	106	167	179	105	94	86
Trial 46	101	166	190	87	89	93

Table 6.21. Minimum ankle, knee and hip angles for the two performances.

	ank_{amin} [°]	kne_{amin} [°]	hip_{amin} [°]
Trial 36	78	132	148
Trial 46	68	133	-

Where:

ank_a = ankle angle
$knee_a$ = knee angle
hip_a = hip angle
shr_a = shoulder angle
$rhip_a$ = free hip angle
$trunk_a$ = trunk angle
ank_{amin} = minimum ankle angle
kne_{amin} = minimum knee angle
hip_{amin} = minimum hip angle

Deformation of the foot during contact with the ground

The deformation of the foot was determined from the image analysis so that this aspect of the actual performances and simulations could be compared.

The movement of the foot which was considered important in comparing actual performances and simulations was made up of six displacements:

(i) maximum horizontal displacement of the ankle
(ii) maximum vertical displacement of the ankle
(iii) maximum horizontal displacement of the toe
(iv) maximum vertical displacement of the toe
(v) horizontal displacement of the toe during contact
(vi) vertical displacement of the toe during contact

A summary of the foot movement during contact in the actual performances is shown in Table 6.22.

Table 6.22. Summary of foot movement during contact in actual performances.

	Trial 36	Trial 46
horizontal maximum displacement of the ankle [$f1_{max}$]	-0.01	-0.01
vertical maximum displacement of the ankle [$f2_{max}$]	-0.03	-0.02
horizontal maximum displacement of the toe [$f3_{max}$]	-0.02	-0.04
vertical maximum displacement of the toe [$f4_{max}$]	-0.04	-0.02
horizontal displacement of the toe during contact [f3]	-0.01	-0.02
vertical displacement of the toe during contact [f4]	-0.00	-0.01

In order to determine the spring parameters, the simulations were matched to the performances of both trial 36 and trial 46 as closely as possible. This was achieved by using Simulated Annealing (Corana et al., 1987) and minimising a cost function based on the differences between certain kinematic values in the actual performances and simulations. The actual performances and simulations were matched by varying the following parameters:

(i) trunk angle at touchdown
(ii) trunk angular velocity at touchdown
(iii) wobbling mass stiffness and damping constants
(iv) ratio of wobbling mass to bone in the shank, thigh and trunk
(v) 15 constants in the sine series (Chapter 4)

The trunk angle at touchdown was allowed to vary by ± 1° from the actual trunk angle determined from the video data. The trunk angular velocity was allowed to vary by ± 50°s^{-1} from the actual value. Wobbling mass stiffness and damping constants were initially varied by ± 50% from the initial estimates. The ratios of wobbling mass to bone in the shank, thigh and trunk segments were varied from initial estimates (Table 6.2) between upper and lower limits (details in **Appendix 2**). The 15 constants in the sine series were varied between ± 1°.

Since small errors in the force data may have lead to large errors in the displacement data in the angle-driven model with forces input (model 1), four further parameters, which allowed the inputted horizontal and vertical forces for each trial to have a correction factor of ± 1% for systematic error, were optimised. With the angle-driven model with springs at the toe and heel to represent the ground reaction forces (model 2), the stiffness and damping constants of these spring-damper systems were also varied and subsequently optimised along with the parameters above.

With model 1 the time of contact of the simulation was fixed at the value obtained from the actual performances. This was not the case for model 2.

Criteria for comparing actual and simulated

For simulations produced using model 1, three criteria were used to compare the actual performances and simulations. The criteria were body orientation at takeoff, whole body angular momentum at takeoff and linear momentum at takeoff. Each criterion consisted of one or more variables which characterised each performance (Table 6.23).

Table 6.23. Criteria and corresponding variables for force-driven model.

Criterion	variable
orientation	trunk angle
angular momentum	angular momentum
linear momentum	horizontal linear momentum vertical linear momentum

For the simulations produced using model 2 three further criteria were introduced to compare the actual performances and simulations. These criteria were the time of contact, the ground reaction forces and the configuration angles at takeoff (Table 6.24).

Table 6.24. Additional criteria and corresponding variables for spring-driven model.

criterion	variable
time of contact	time of contact
ground reaction forces	horizontal ground reaction force vertical ground reaction force
configuration	ankle angle knee angle hip angle shoulder angle free hip angle elbow angle free knee angle

Ground reaction forces

The ground reaction forces compared between the actual performances and simulations were made up of six parts. These were, the horizontal and vertical ground reaction forces at the toe, the horizontal and ground reaction forces at the heel, and the total horizontal and vertical ground reaction forces. The total ground reaction forces were given twice the weighting of each of the other four parts.

Objective function and weightings

A score was calculated for each simulation as a measure of how well the simulation matched the actual performance. This was made up of individual scores representing how well each of the individual criteria (Table 6.23) were matched. The scores for angular momentum, linear momentum, time of contact and ground reaction force represented the average percentage difference between the actual performance and simulations (equation (6.18)). The scores for orientation and configuration represented the difference between the actual

performance and simulations in degrees (equation (6.19)). Errors in degrees and errors in percent were considered to give a similar measure of how well the actual performances and simulations matched. The weightings for each variable were set equal to the inverse from the actual performance, with the exception of the angular momentum. The angular momentum at takeoff in the actual performance had a value close to zero, therefore dividing by this value would give a score not representative of how well the two performances were matched. For the angular momentum at takeoff a value for the weighting was decided upon which resulted in a 1% error in the value of angular momentum being equivalent to 1° error in rotation, as degrees and percentage errors had already been considered to be comparable.

$$S = 100.\sqrt{\frac{\sum_{i=1}^{n}\left(\frac{s_i - a_i}{a_i}\right)^2}{n}} \qquad (6.18)$$

$$S = \sqrt{\frac{\sum_{i=1}^{n}(s_i - a_i)^2}{n}} \qquad (6.19)$$

Where:

S = score

s_i = value of variable i from simulated performance

a_i = value of variable i from actual performance (or substitute value)

n = number of variables in objective function part

Each part of the objective function was then squared. The sum of these individual parts of the objective function was divided by the number of parts and finally square rooted (equations (6.18) and (6.19)).

Penalties in objective function

Displacement of the foot during the simulation was considered important, however, this was not included in the objective function as the actual displacements of the foot determined from the video data contained considerable noise. Instead the foot displacements in the simulations were checked to see if they were reasonable. Any of the displacements which disagreed with the actual

foot displacements by more than 30 mm were included in the cost function as a penalty in order to prevent this occurring. For every 1 mm above 30 mm that the simulated foot displacements differed from the actual foot displacements a penalty of 1% was incurred.

A further aspect of the simulated performance which was considered important, was movement of the wobbling masses. This was considered important in matching actual performances and simulations, but was not included in the cost function as actual values could not be determined. Values for wobbling mass excursion in the thigh and the shank obtained from Pain (2001) were 0.018 m and 0.032 m respectively, however, the jumping trials in this study were much more dynamic than the trials in the study by Pain (2001), and included horizontal movement. It was therefore considered likely that more wobbling mass movement would occur. Although the amount of wobbling mass movement was not considered to be as critical as other kinematic aspects of the performance, realistic movement was required. Upper limits were set for the resultant movement of each of the wobbling masses in the shank, thigh and trunk segments (Table 6.25) and it was decided that as long as they did not exceed these limits the movement of the wobbling masses was realistic. If, however, they did move further than this a penalty was included in the cost function. For every 1mm the wobbling masses moved beyond the upper limits a 1% penalty was included. The solution would therefore hopefully be one in which the wobbling mass excursions did not exceed these limits.

Table 6.25. Upper limits for movement of the wobbling masses.

segment	maximum wobbling mass movement
shank	0.050 m
thigh	0.075 m
trunk	0.100 m

Angle-driven model with forces input (model 1)

In the simulations of the jumps for both height and distance the position of the toe from (0,0) (the centre of the force plate) was such that the ankle was in exactly the same position as in the actual performances. Using the initial

conditions (Tables 6.16, 6.17 and 6.18) the positions of the mass centre at touchdown in the actual performances and simulations were compared (Table 6.26).

Table 6.26. Initial mass centre locations from actual performances and simulations.

	simulated		actual	
	x_{cm}	y_{cm}	x_{cm}	y_{cm}
Trial 36	0.60	0.96	0.60	0.92
Trial 46	0.50	0.96	0.50	0.95

These differences in the initial centre of mass position were present because the centre of mass location in the actual performances was calculated using an 11-segment model (Yeadon, 1990b), whereas the centre of mass location in the simulations was determined using the eight-segment model.

Comparisons of the takeoff characteristics and movement of the foot for the actual performances and simulations are shown in Tables 6.27 and 6.28 respectively.

Table 6.27. Comparison of the takeoff characteristics between actual performances and simulations.

		Trial 36	Trial 46
simulated	v_{cmx} [ms^{-1}]	-1.90	-5.31
actual		-1.89	-5.31
simulated	v_{cmy} [ms^{-1}]	3.26	3.35
actual		3.31	3.47
simulated	trunk orientation [°]	85	88
actual		86	93
simulated	angular momentum [$kg.m^2.s^{-1}$]	2.72	4.99
actual		4.94	4.99

Table 6.28. Comparisons of the foot movement between actual performances and simulations.

		Trial 36	Trial 46
simulated	$f1_{max}$ [m]	-0.00	-0.03
actual		-0.00	-0.01
simulated	$f2_{max}$ [m]	-0.06	-0.03
actual		-0.03	-0.02
simulated	$f3_{max}$ [m]	-0.01	-0.05
actual		-0.02	-0.04
simulated	$f4_{max}$ [m]	-0.05	-0.03
actual		-0.04	-0.02
simulated	f3 [m]	0.02	-0.05
actual		-0.01	-0.02
simulated	f4 [m]	0.03	0.02
actual		0.00	-0.01

For the simulations of the jumps for height and distance, objective function scores of 3.0 and 2.5 respectively were obtained. The individual scores for the different parts of the objective function are shown in Table 6.29.

Table 6.29. Individual objective function scores for model 1.

	Score	
	Trial 36	Trial 46
orientation	0.5°	5.06°
angular momentum	7.39%	0.00%
linear momentum	1.08%	2.50%

As stated previously, the eccentric levels of the joint torques determined using this model were not very different from the eccentric level of the torques

obtained using the isovelocity dynamometer. This model was therefore only used to obtain wobbling mass parameter values to be used in model 2.

Angle-driven model with springs (model 2)

Simulations were run to try and match the simulation and actual performances using the three criteria used above along with the time of contact, the joint (configuration) angles at takeoff and the ground reaction forces. Unlike with model 1, in which the end of the simulation was pre-determined, with model 2 the simulation ended when the vertical forces at the heel and toe fell to zero. The time of contact, therefore, became an important criterion which should be matched in the simulations. The configuration angles at takeoff also became important because of this difference in the time of contact. Improving the match of the seven configuration angles between the actual performances and simulations resulted in an improvement in the match between contact times.

Including the ground reaction forces in the objective function required matching the individual parts of the horizontal and vertical forces as well as the total horizontal force and the total vertical force from the actual performances and the simulations at each iteration of the simulation.

As with model 1, the position of the toe from (0,0) (the centre of the force plate) was such that the ankle was in exactly the same position as in the actual performances. Using the initial conditions (Tables 6.14, 6.15 and 6.16) the position of the mass centre at touchdown in the actual performances and simulations were compared (Table 6.30).

Table 6.30. Initial mass centre locations from actual performances and simulations.

	simulated performance		actual performance	
	x_{cm}	y_{cm}	x_{cm}	y_{cm}
Trial 36	0.61	0.95	0.60	0.92
Trial 46	0.50	0.96	0.50	0.95

Table 6.31 shows a comparison of orientation / configurations angles at takeoff and Table 6.32 shows a comparison of the takeoff conditions between the actual performances and simulations.

Table 6.31. Comparison of the configuration orientation angles at takeoff for actual performances and simulations.

		Trial 36	Trial 46
simulated	trunk [°]	83	87
actual		86	93
simulated	ankle [°]	108	103
actual		106	101
simulated	knee [°]	167	163
actual		167	166
simulated	hip [°]	178	192
actual		179	190
simulated	shoulder [°]	105	87
actual		105	87
simulated	free hip [°]	94	89
actual		94	89
simulated	elbow [°]	80	71
actual		80	71
simulated	free knee [°]	92	52
actual		92	52

Table 6.32. Comparison of the takeoff conditions for actual performances and simulations.

		Trial 36	Trial 46
simulated	v_{cmx} [ms^{-1}]	-1.92	-5.48
actual		-1.89	-5.31
simulated	v_{cmy} [ms^{-1}]	3.25	3.26
actual		3.31	3.47
simulated	angular momentum [$kg.m^2.s^{-1}$]	5.05	5.30
actual		4.94	4.99
simulated	time of contact [s]	0.205	0.155
actual		0.205	0.155

The ground reaction forces were compared throughout the whole of the simulation. The actual force data were splined throughout the contact phase and compared to the force data obtained at each iteration in the simulation. This comparison was done in terms of the horizontal and vertical force at the toe, horizontal and vertical force at the heel and total horizontal and vertical force. Figures 6.28 and 6.29 show a comparison between the horizontal forces in the actual performances and simulations in jumps for height and distance respectively. Figures 6.30 and 6.31 similarly show a comparison between the vertical forces for the two performances.

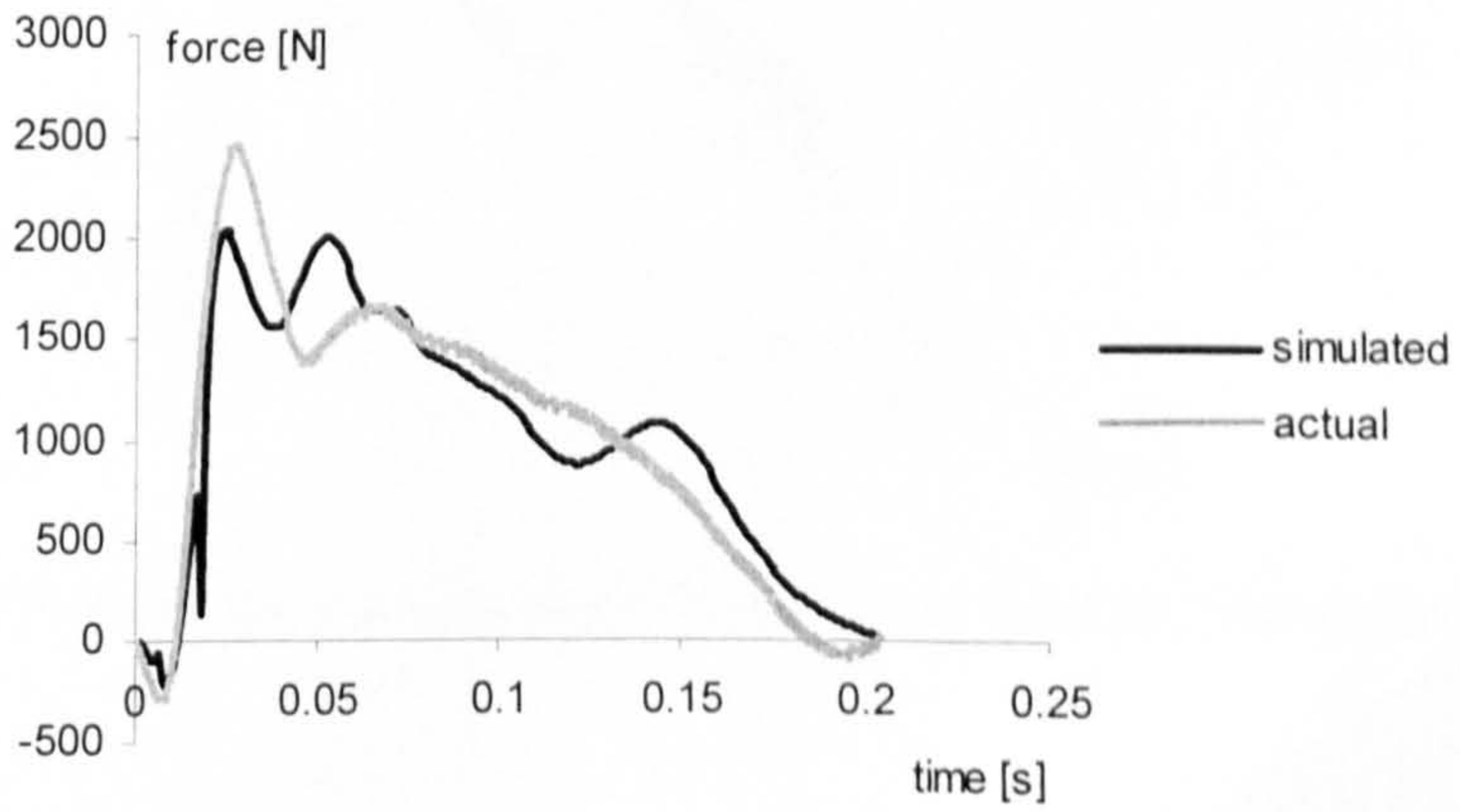

Figure 6.28. Horizontal ground reaction forces for the trial for maximum height.

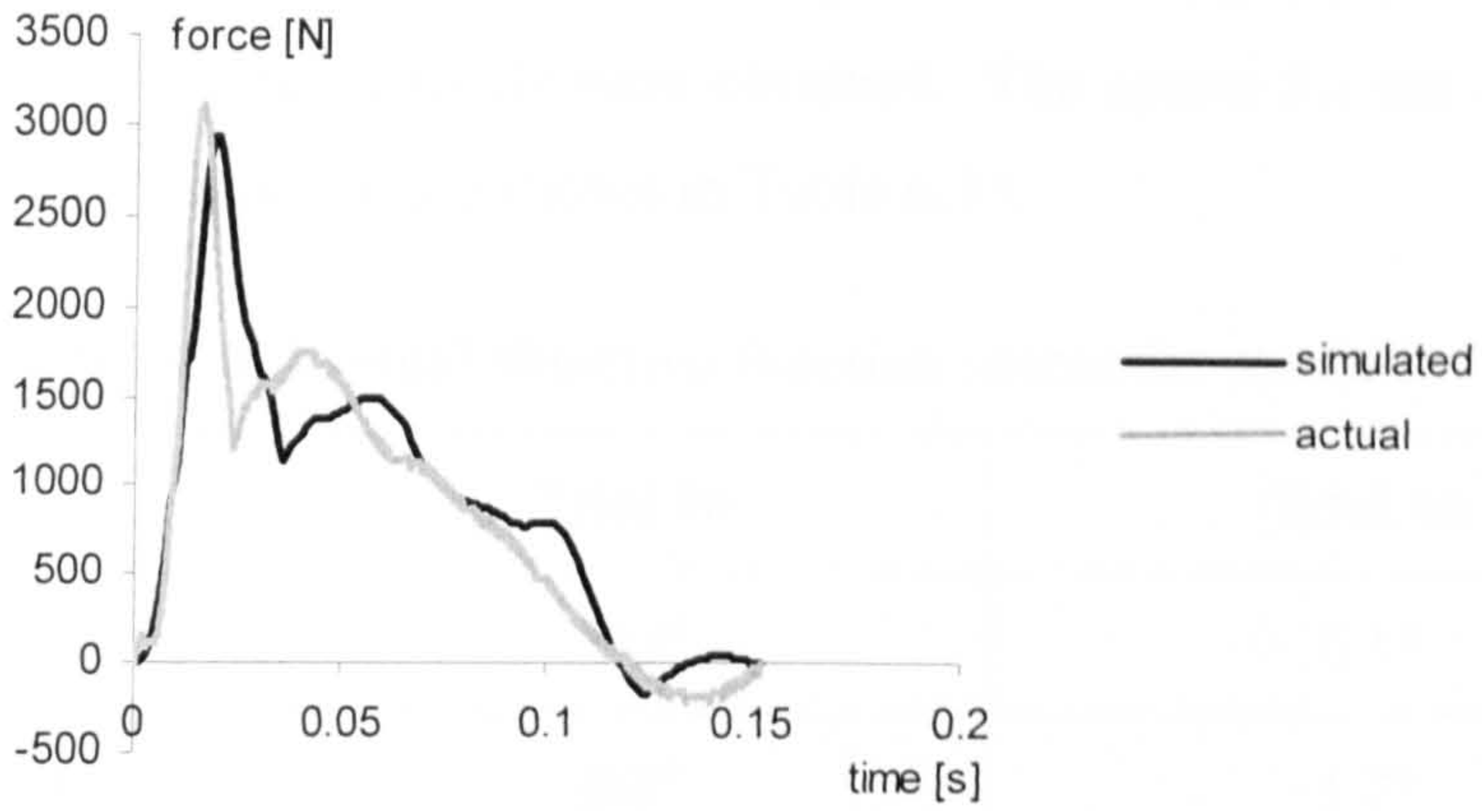

Figure 6.29. Horizontal ground reaction forces for the trial for maximum distance.

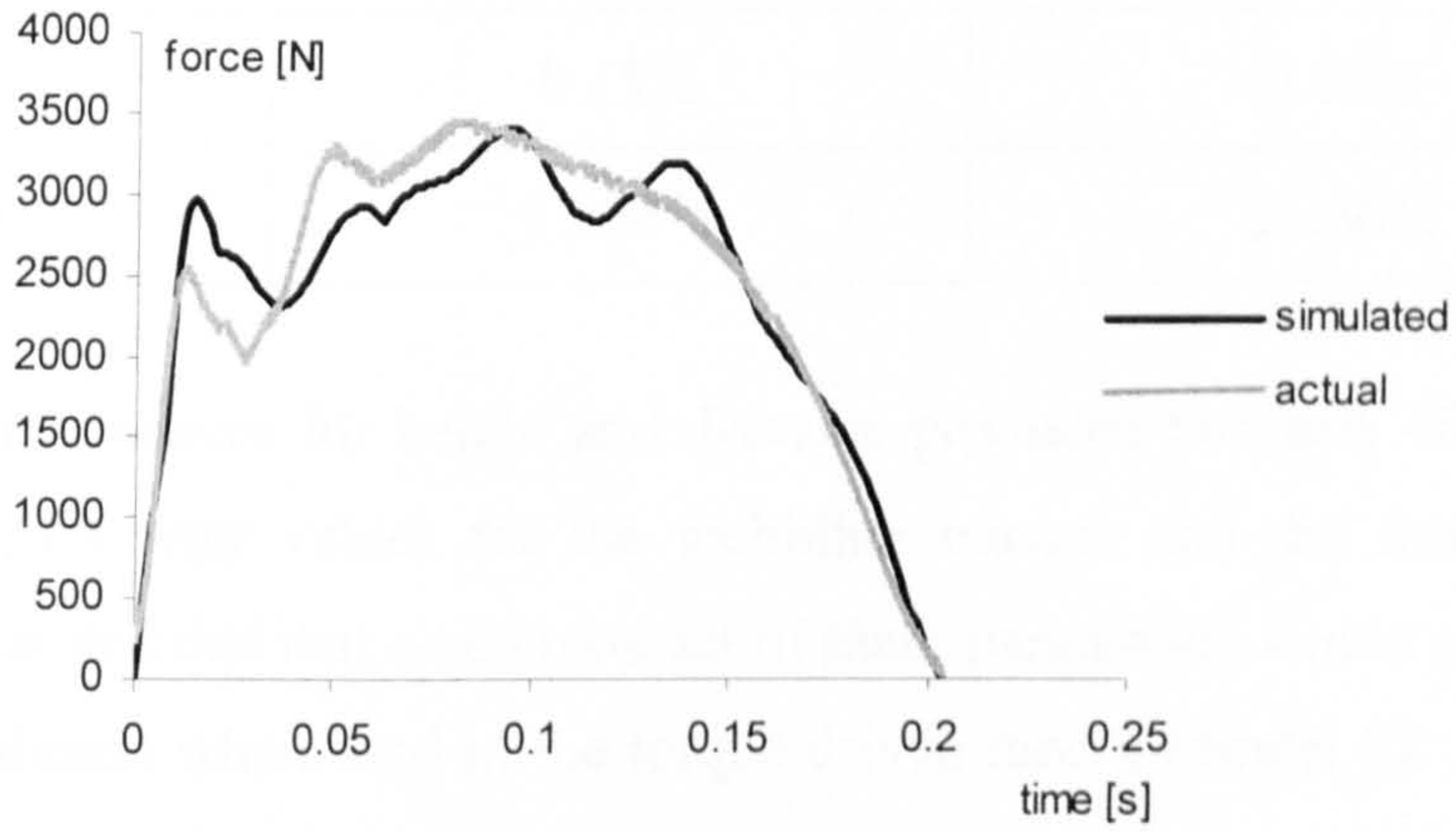

Figure 6.30. Vertical ground reaction forces for the trial for maximum height.

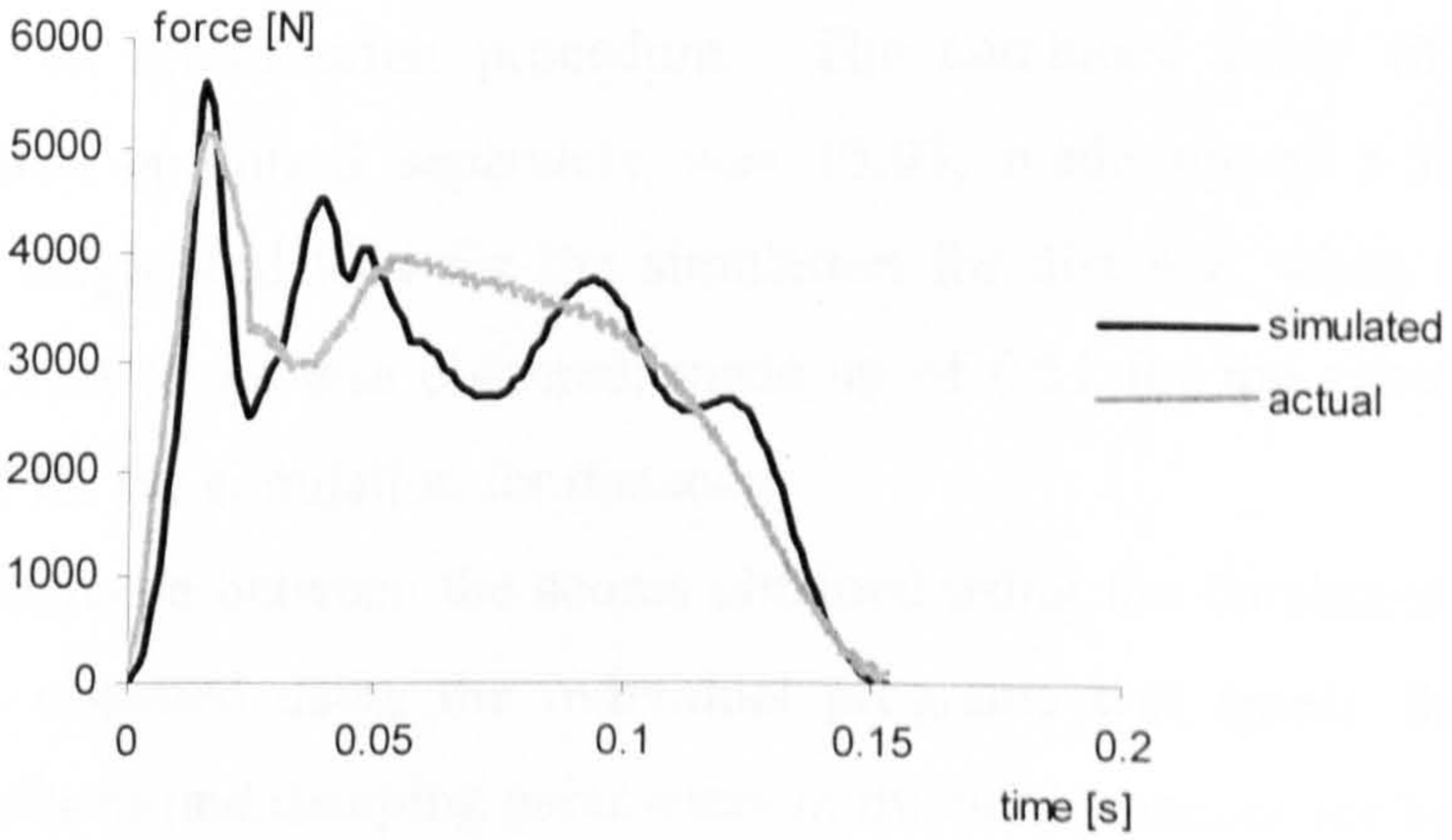

Figure 6.31. Vertical ground reaction forces for the trial for maximum distance.

In the simulations of the jumps for height and distance, objective function scores of 5.84 and 9.09 respectively were obtained. The scores for the individual parts of the objective function are shown in Table 6.33.

Table 6.33. Individual objective function scores for model 2.

	Trial 36	Trial 46
orientation	3.0°	6.1°
configuration	0.8°	1.7°
angular momentum	0.36%	1.05%
linear momentum	1.62%	4.85%
time of contact	0.15%	0.00%
force	13.24%	21.66%

The performances for height and distance produced two sets of stiffness and damping parameter values for the wobbling masses and the foot ground interface. It was decided that a common set of these parameters would result in a more robust solution when used in the torque-driven model (model 3). The two simulation programs were combined, resulting in an overall score made up of a score from each simulation. All the stiffness and damping parameters and the ratios of wobbling mass to rigid mass were input as common parameters to both simulations in an optimisation procedure. The combined score of the two simulations when optimised separately was 15.03, made up of 5.59 for the simulation for height and 9.44 for the simulation for distance, when optimised together a score of 16.42 was obtained, made up of 6.51 for the simulation for height and 9.90 for the simulation for distance.

This difference between the scores obtained using the combined program and the scores obtained using the individual programs was small, therefore a single set of stiffness and damping parameters in the performances for both height and distance could be used in the torque driven model with confidence of a good match between the actual performances and simulations.

Tables 6.34, 6.35, 6.36 and 6.37 contain all optimised stiffness and damping parameters, for the foot-ground interface and the wobbling masses

respectively, which are used in the torque-driven model (Chapter 7). Table 6.35 contains the optimised initial conditions which are specific for the simulations for height and distance respectively.

k1, k3 and k5 are the initial stiffness constants, k1 is the horizontal stiffness constant, k3 is the vertical stiffness constant at the toe and k5 is the vertical stiffness constant at the heel. k2, k4, and k6 are the corresponding damping constants. kk2, kk4 and kk6 are the damping constants after the velocities of the toe and heel have fallen to zero, and facdamp is a constant in the function used to represent displacement in the equations for horizontal force (Chapter 4).

Table 6.34. Optimised stiffness parameters of the foot-ground interface.

Variable	Coefficient [Nm^{-2}]
k1	339847
k3	2070599
k5	160715

Table 6.35. Optimised damping parameters of the foot-ground interface.

variable	Coefficient [Nsm^{-2}]
k2	1462752
k4	51354
k6	134572
kk2	47171
kk4	22583
kk6	3980628
facdamp	571 (no units)

Table 6.36. Optimised stiffness parameters of the wobbling masses.

Variable	Coefficient [Nm^{-2}]
k9	311917
k17	384134
k25	306260

Table 6.37. Optimised damping parameters of the wobbling masses.

Variable	Coefficient [Nsm^{-2}]
k10	936
k18	6184
k26	568
kk10	7560
kk18	1001
kk26	239

k9, k17 and k25 are the stiffness constants of the wobbling masses in the shank, thigh and trunk segments respectively. k10, k18 and k26 are the initial damping constants of the wobbling masses in the shank, thigh and trunk segments respectively, and kk10, kk18 and kk26 are the amounts the corresponding initial damping constants are increased by over a 50 ms period.

Table 6.38. Optimised initial conditions for each simulation.

	Trial 36	Trial 46
$trunk_{\omega}$	$-95°s^{-1}$	$49°s^{-1}$
$trunk_{a}$	78°	90°
slipx	-0.005 m	0.005 m
slipy	0.020 m	0.020 m

$trunk_a$ and $trunk_\omega$ are the initial trunk angle and angular velocity respectively, slipx is the natural length of the horizontal spring at the toe and heel and slipy is the natural length of the vertical spring at the toe.

Summary

This chapter has described the determination of inertia, spring and strength parameters. These parameter values are input into the eight-segment torque-driven model (model 3) which is evaluated before being used for investigating optimal jumping technique (Chapter 7).

CHAPTER 7

MODEL EVALUATION AND OPTIMISATION

Introduction

The eight-segment torque-driven model developed in Chapter 4 needed to be evaluated before it could be used for applications with any confidence. This chapter explains the evaluation of the model along with it's use in the optimisation of performance of jumps for both maximum height and maximum distance.

Evaluation

Description of the torque-driven model

The eight-segment torque-driven model contains torque generators at the ankle, knee, hip, shoulder and free hip joints which produce extension or flexion of the joint. Each group of extensors / flexors is represented as elastic and contractile components in series as described in Chapter 6. The parameters used to define the maximum torque at each joint were determined using Cybex isovelocity dynamometer data (Chapter 6). The model contains wobbling masses represented by spring-damper systems (Chapter 6). The foot-ground interface is also represented by two spring-damper systems, where the stiffness and damping parameters were determined through optimisation using the angle-driven models (Chapter 6).

The following two sections describe changes that were made to the torque-driven model after initial simulations.

Modelling passive torques

There is little support for the inclusion of a parallel elastic component (PEC) in a model of human muscular contraction within the normal working ranges of the joints (Chapman, 1985). However, if movement is outside this range a parallel elastic element defining the passive torque may be necessary. During the jumping trials in this study, the free hip extended beyond 180°, which was considered outside the working range of motion. It was therefore considered

necessary to include a passive torque. This extra passive torque was added to the torque determined by the nine parameter function when the free hip was extended beyond 180° (full extension). The additional torque followed a linear function from 150 Nm at 225° to 0 Nm at 180°. The value of the passive torque at 225° was estimated during trials in which the hip underwent passive stretching beyond the range of active extension using a customised rig attached to the force plate.

Isometric ankle strength

After several attempts of simulating jumps for both height and distance using the torque-driven model it was decided that the isometric torque values used to define the torque – angle - angular velocity relationship at the ankle were not high enough. This was evident as the simulation model produced a vertical velocity at takeoff with a much smaller magnitude than the vertical velocity produced by the subject during the actual performances. The lack of strength at the ankle in the model was attributed to the fact that the method for testing the ankle on the isovelocity dynamometer did not allow the subject to produce torques which are possible during other activities. This was due to the subject positioning and the machine attachment used for this joint. The torques determined by the angle-driven models were therefore used instead of the isometric values determined from the isovelocity dynamometer.

The ankle plantar flexion torques produced in the simulations for both height and distance using the second angle-driven model, model 2, had peak isometric values of about 500 Nm. This value was divided by the differential activation level at ω_0 (when angular velocity equals zero), determined using values of a_{min}, ω_1 and m (averaged from the other joints), to give a value for T_0. The value of T_{max} was assumed to 1.5 times this value as with the other joints. The resulting values for T_{max} and T_0 for plantar and dorsi flexion are shown in Table 7.1. New SEC stiffness values at the ankle were subsequently calculated

Table 7.1. T_{max} and T_0 values for the ankle.

	T_{max} (Nm)	T_0 (Nm)
plantar flexion	1054	702
dorsi flexion	243	162

Torque generator activation profile

Torque time histories required to produce the desired angle changes were output from model 2 for simulations for both maximum height and maximum distance (Chapter 6). These torque time histories were then input into the torque-driven model (model 3) with the hope of reproducing the same optimum simulation produced by model 2. This was done in order to check the code for both the angle-driven and torque-driven models were identical.

During the first 40-50 ms the two models produced almost identical ground reaction forces (Figures 7.1 and 7.2) suggesting that with an appropriate torque generator activation profile the torque-driven model could produce simulations very similar to the optimum simulations produced using the angle-driven models. After this, however, the two simulations became dramatically different. The reason was probably not errors in the program, but small errors in the splined torques and kinematics which became bigger when integrated over time. Figures 7.1 and 7.2 show how the simulation by the torque-driven model ended after 75 ms. Forcing the model to use specified torque time histories resulted in the model producing a very poor simulation.

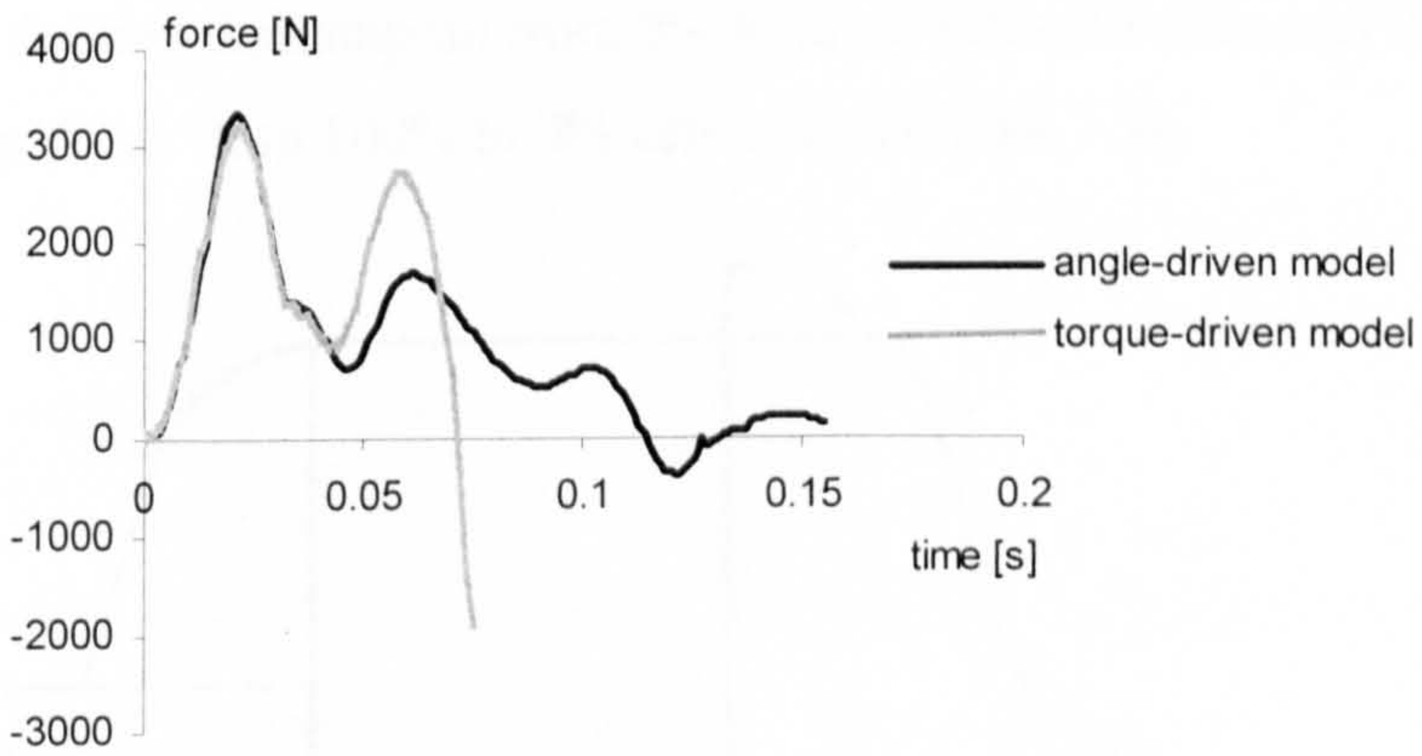

Figure 7.1. Horizontal ground reaction forces produced during simulations by the two models.

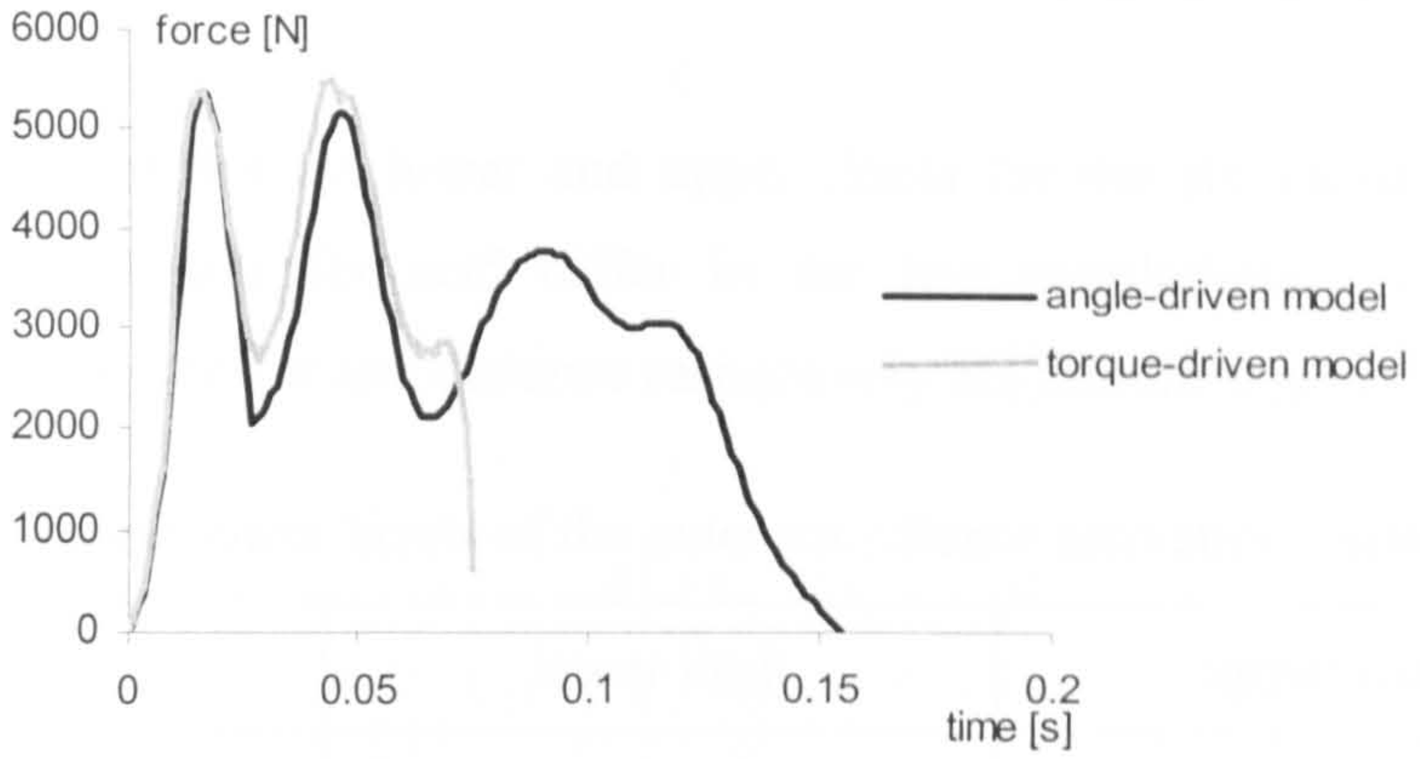

Figure 7.2. Vertical ground reaction forces produced during simulations by the two models.

Using the torque-driven model in which the torques were defined by a torque / angle / angular velocity profile, an attempt was made to match the actual performances and simulations by varying the activation time histories in an optimisation procedure. Six variables were needed to define the activation time histories of the extensor muscles (ankle, knee and hip), and the flexor muscles (shoulder and free hip) (Figure 7.3). The six parameters defined two quintic functions. One defined the ramp up from 0% to up to full activation and the other defined the ramp down from 100% to 0% activation (Figure 7.3).

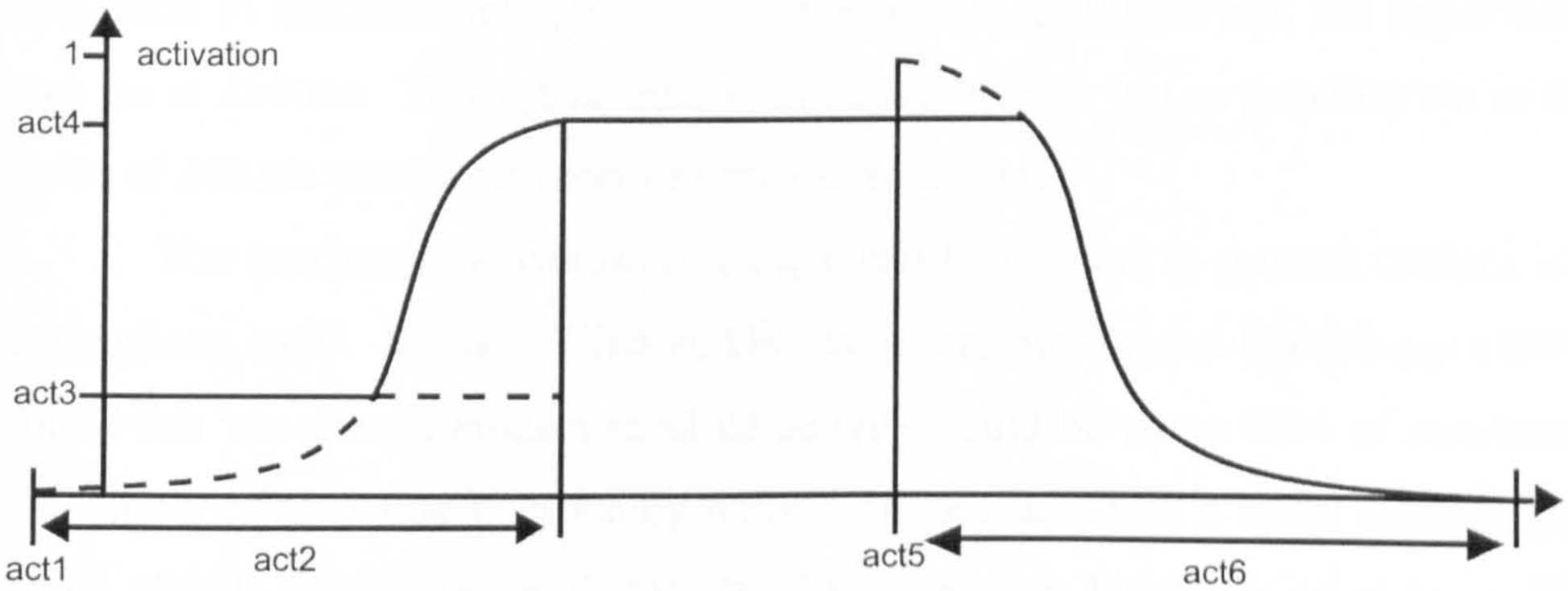

Figure 7.3. Activation time histories for each joint.

act1 corresponded to the time of initial torque onset, act2 was the ramp time taken for the muscle to reach full activation act4, and act3 was the minimum activation level prior to time act5. act5 was the time the torque generator started to switch off and act6 was the time taken for the activation to fall to zero. After

time act5, the lower of the two activation levels was used to define the actual activation level.

Table 7.2 shows the lower and upper limits for the six variables. The upper and lower limits for act5 differ in the two simulations. Values for simulations for both height and distance respectively are therefore given.

Table 7.2. Upper and lower limits of the extensor / flexor activation variables.

variable	lower limit	upper limit
act1	-0.050 s	0.250 s
act2	0.100 s	0.250 s
act3	0.0	0.5
act4	0.6	1.0
act5	0.100 / 0.075 s	0.250 / 0.200 s
act6	0.100 s	0.200 s

Contraction duration times, measured from onset to peak torque have been found to be in the region of 100 ms (Freund and Budingen,1978; Bobbert and van Zandwijk, 1999). The minimum time for the torque generators to go from initial activation to maximal activation was therefore set at 100 ms and the upper limit was set at 250 ms. This upper limit could have been as big as possible but as the value of 250 ms was never reached this was sufficient.

The maximum activation a muscle can have prior to ground contact is a contentious issue. Kovacs, Tihanyi, Devita, Racz, Barrier and Hortobagyi (1999) found this pre-ground contact level of activity could be up to 80% of maximum activation. This value is probably quite high and therefore a more conservative value of 50% was chosen in this study. The minimum level was set at zero. The lower limit for time of initial onset was set at –50 ms so if the torque generators were activated at this time and the minimum ramp time was chosen the activation level at time zero would be no more than 50%.

In addition to these six variables, five further variables were needed to define the activation time histories of the flexor muscles (ankle, knee and hip), and the extensor muscles (shoulder and free hip) (Figure 7.4). Again, two quintic

functions were used to define the activation levels. The first defined the ramp down from 100% to 0% activation and the second defined the ramp back up to 100% activation. actf1 corresponded to the time deactivation was initiated, actf2 corresponded to the ramp time taken for the activation level to fall to 0% and actf3 corresponded to the maximum possible activation level of the flexors/extensors prior to time actf4.

The flexors / extensors were required to be switched on again towards the end of the simulation in order to prevent the joints from over extending or flexing. actf4 corresponded to the time the torque generators began ramping up again to maximum activation and actf5 was the ramp time. After time actf4, the higher of the two activation levels predicted by the two quintic functions defined the actual activation levels. Similar upper and lower limits were chosen for these five variables.

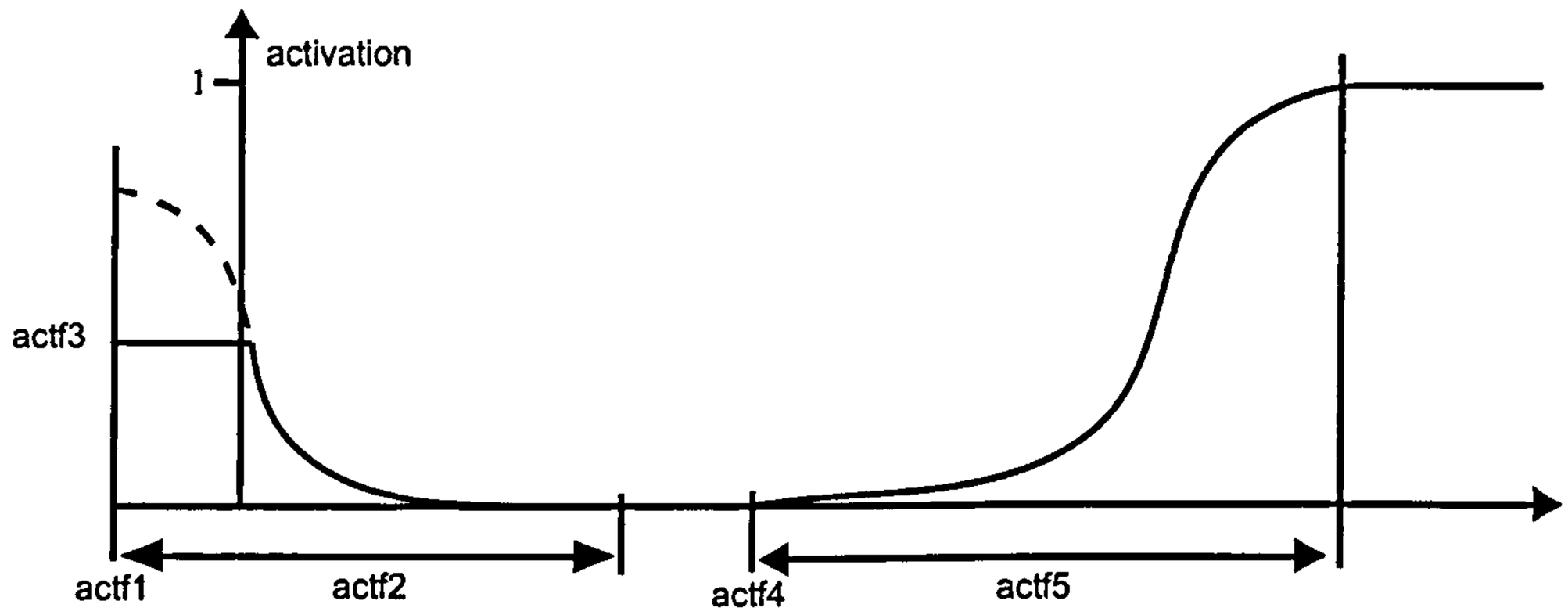

Figure 7.4. Torque generator activation profile for the knee and shoulder joints.

Table 7.3. Upper and lower limits of the flexor/extensor activation variables.

Variable	lower limit	upper limit
actf1	-0.100 s	0.100 s
actf2	0.100 s	0.250 s
actf3	0.0	0.5
actf4	0.100 / 0.075 s	0.250 / 0.200 s
actf5	0.100 s	0.250 s

Because the shoulder joint in the model represented the two shoulder joints, and the strength data collected using the isovelocity dynamometer was only for one shoulder, the maximum activation level of the shoulder muscles was set at 2.0 instead of 1.0. This meant the initial levels of activation, act3 and actf3 were given upper limits of 1.0 instead of 0.5.

In addition to the activation variables, certain initial conditions were allowed to be varied and optimised. These variables included the joint angular velocities of all joints (except the elbow and the free knee), and the trunk angular velocity. These initial angular velocities were allowed to vary by ± 50°s^{-1} from the actual values obtained from the image analysis. The ± 50°s^{-1} limits were decided upon after using different tightness of fit when splining the angle data. Using a different fit of the spline resulted in a marginal change in the angles but a change in the angular velocities at touchdown of up to 100°s^{-1}. The variables slipx and slipy were also allowed to vary in the same way as in the angle-driven models (Chapter 6).

Criteria for comparing actual and simulated

For the torque-driven model further criteria, in addition to those used in the angle-driven models (Chapter 6), needed to be included in the objective function. As the model was not angle-driven, criteria which matched joint angles at certain times during the simulation were needed. It was decided that matching the joint angles at takeoff and the minimum joint angles during the simulation were sufficient. For some angles, however, the joint did not reach a minimum, but either increased or decreased throughout the simulation, so in these cases only the angle at takeoff was used.

Angle-driven joints

At the beginning of the study, it was assumed that the movement of the free knee only affected overall performance marginally. Whilst evaluating the torque-driven model, however, it was realised that this was not the case. Small changes to the angular velocity of the free knee resulted in large changes in the overall performance. This may have been a result of the free knee being angle-driven, whilst all other joints (except the elbow) were torque-driven.

Predetermining the joint angle time histories of the free knee and elbow joints whilst at the same time allowing the other joint angle time histories to vary causes problems and a very poor simulation may result. Due to this sensitivity of the model to the free knee kinematics and errors incurred through digitisation, a sine series function and its first and second derivatives identical to the one used for the ankle, knee and hip joints in the angle-driven models (Chapter 4) was used at this joint in the torque-driven model. The values of these constants were varied between limits ($-0.5 < a_n < 0.5$, $n = 1,5$) in order to give the free knee some freedom. The initial knee angle still remained at the value from the actual performance. So that the match between the simulated joint angle time history and the actual joint angle time history was good, the minimum and final free knee angle were included in the objective function. Although the elbow joint did not seem to affect the performance as much as the free knee, the same procedure of allowing the angle time history to vary was implemented, with the elbow angle at takeoff also being included in the objective function.

Objective function and weightings

The objective function and weightings were the same as those used for the angle-driven models described in Chapter 6. The score for the additional criteria (the joint angles throughout the performance and the angle-driven joint angles), was calculated in the same way as the score for the orientation and configuration angles at takeoff. The additional criteria were included in the part of the objective function with the other configuration angles.

Penalties

In addition to the penalties included in the evaluation of the angle-driven model, extra penalties were needed in the evaluation of the torque-driven model. The first penalty was incurred if the knee angle extended beyond 180°. The second penalty resulted if the time of contact was greater than 10% longer than the actual time of contact. It was decided that the maximum flexion the free knee could achieve was to an angle of 20°. If during the simulation the free knee flexed more than this a penalty was incurred.

Results

Optimisations were run using the Simulated Annealing algorithm (Corana et al., 1987) until the closest possible match between actual performances and simulations was achieved. Problems associated with the Simulated Annealing algorithm, discussed in Chapter 2, include the algorithm finding a local and not a global minimum. Due to the number of variables used to find an optimal solution in this evaluation procedure there was a high risk that this would occur. In order to try and prevent this, different optimisations were run in which the variables were varied in different orders and the starting values of the variables were changed. This gave the algorithm more chance of finding the global optimum.

The best match between the actual performances and simulations for height and distance resulted in objective function scores of 6.4 and 15.6 respectively. The corresponding activation profiles for each of the joints for each simulation are shown in Figures 7.5 and 7.6. The following sections look at the individual parts of the objective function which resulted in these optimal solutions. Table 7.4 shows a comparison of the takeoff conditions between the actual performances and simulations. The orientation / configurations angles used in the evaluation procedure are shown in Table 7.5 and 7.6.

Table 7.4. Comparison of the take off conditions for actual performances and simulations using the torque-driven model.

		Trial 36	Trial 46
simulated	v_{cmx} (ms^{-1})	-1.88	-5.28
actual		-1.89	-5.31
simulated	v_{cmy} (ms^{-1})	3.24	3.49
actual		3.31	3.47
simulated	angular momentum ($kg.m^2.s^{-1}$)	4.8	6.5
actual		5.0	4.9
simulated	time of contact (s)	0.204	0.149
actual		0.205	0.155

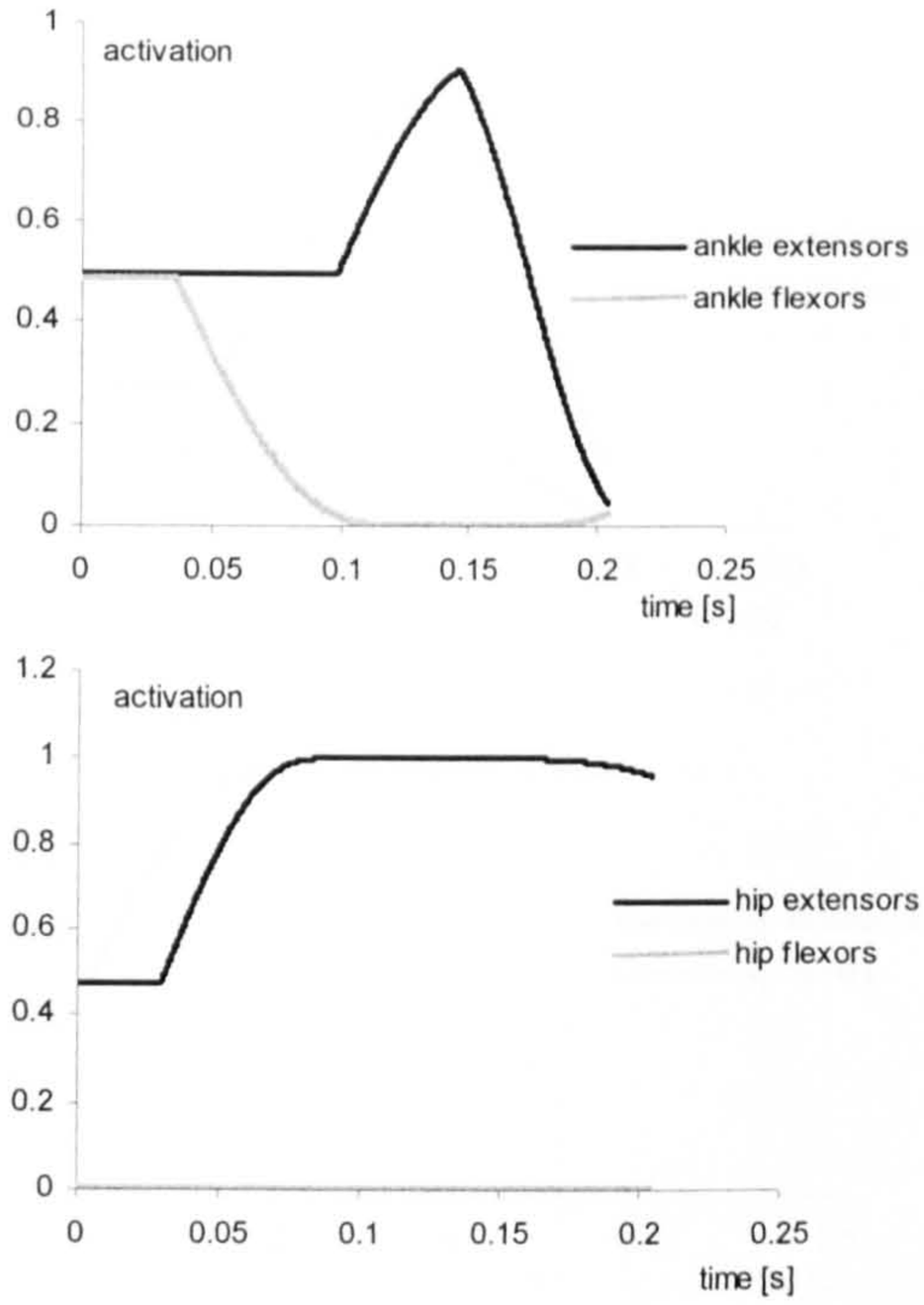

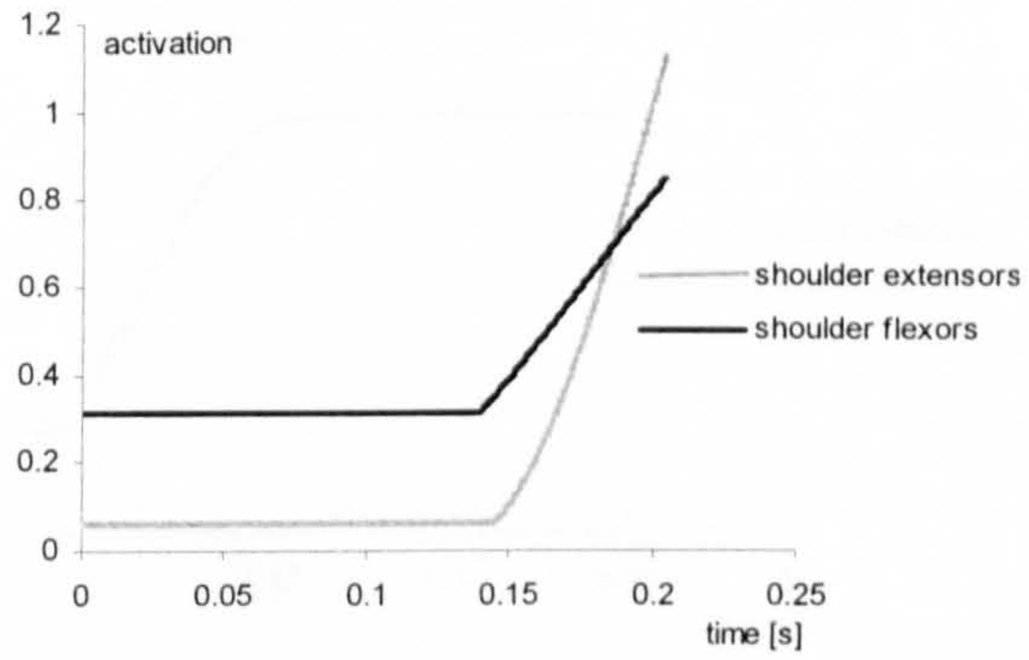

Figure 7.5. Torque generator activation profiles used in the simulation for height.

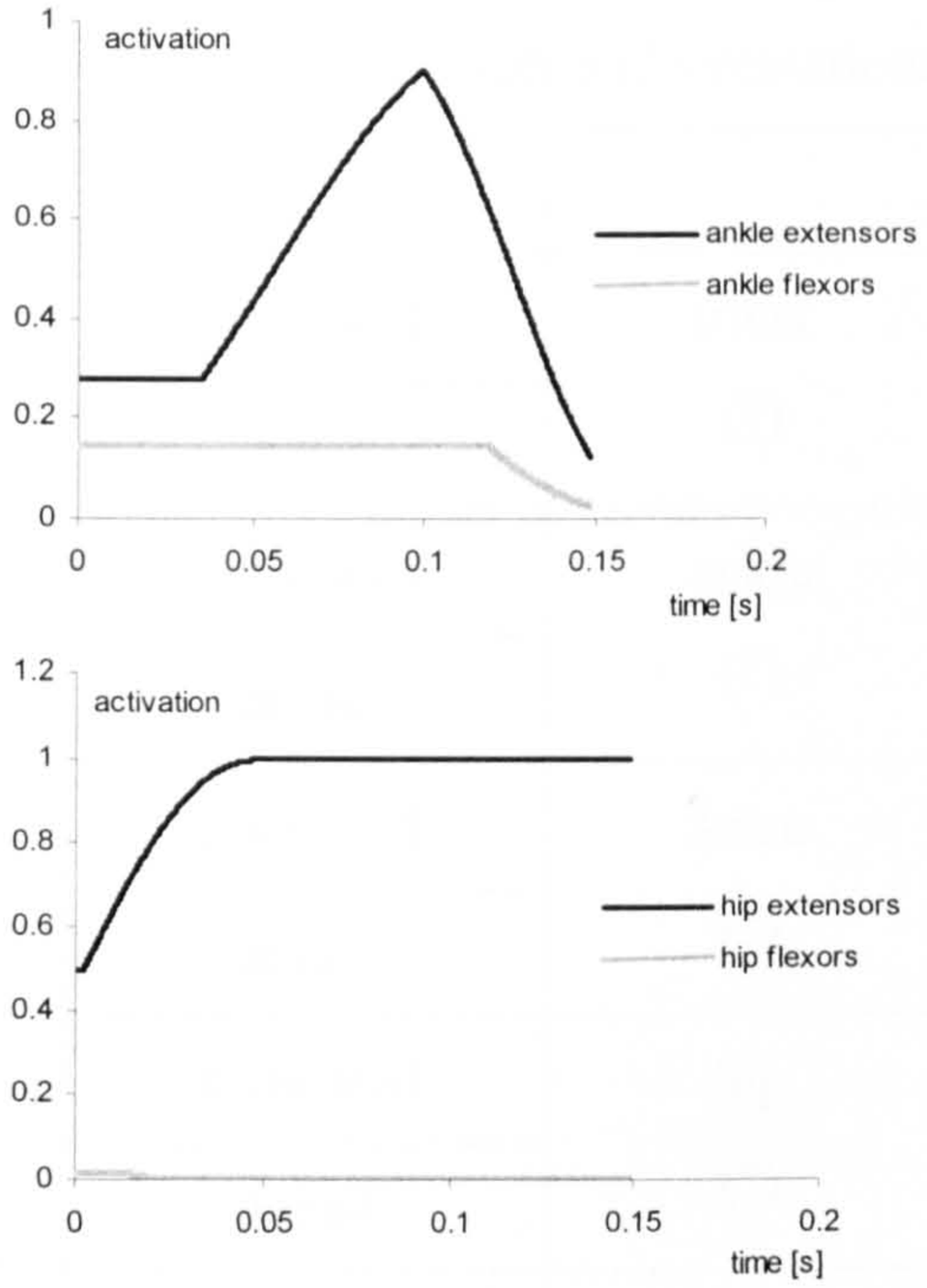

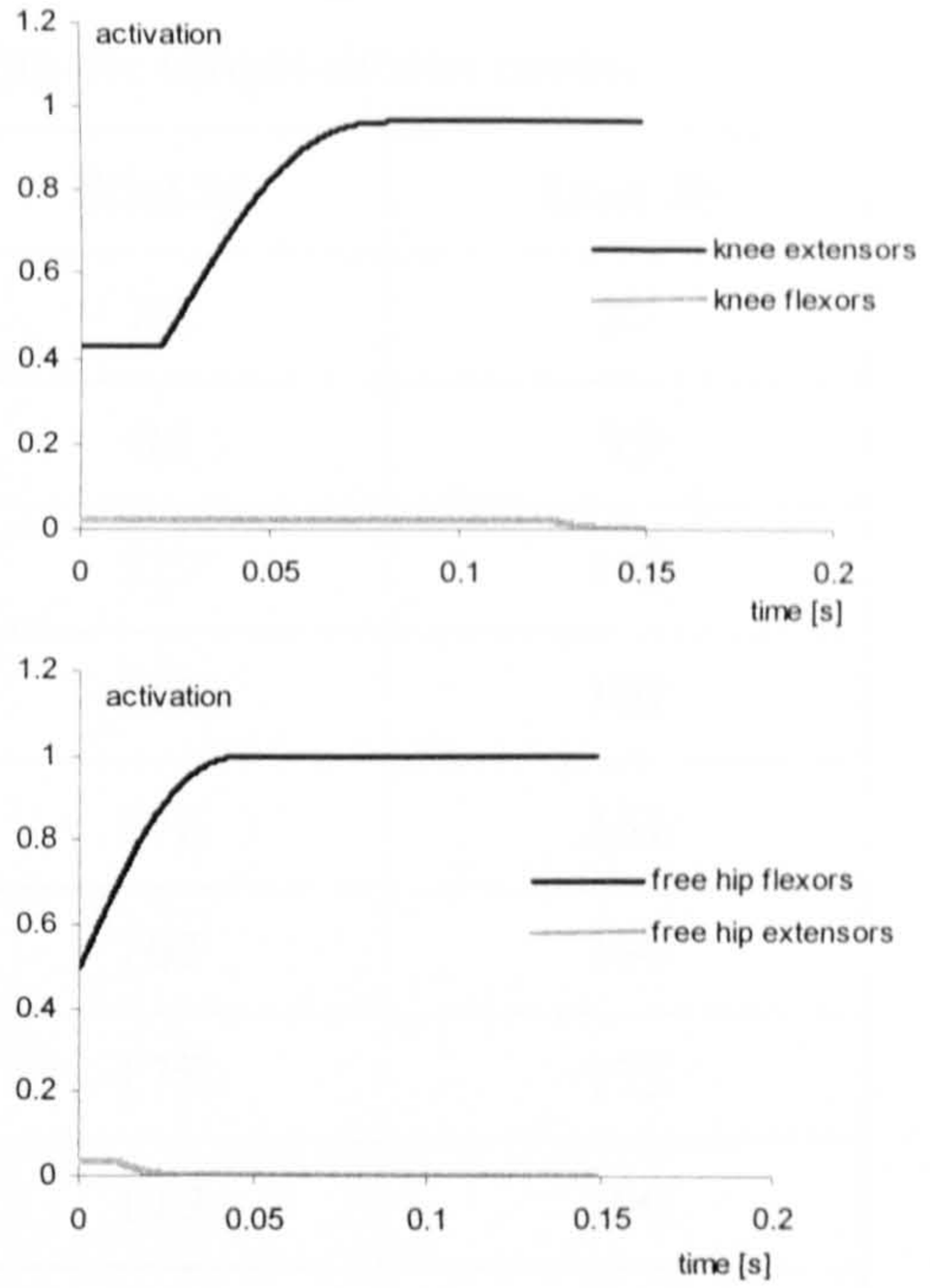

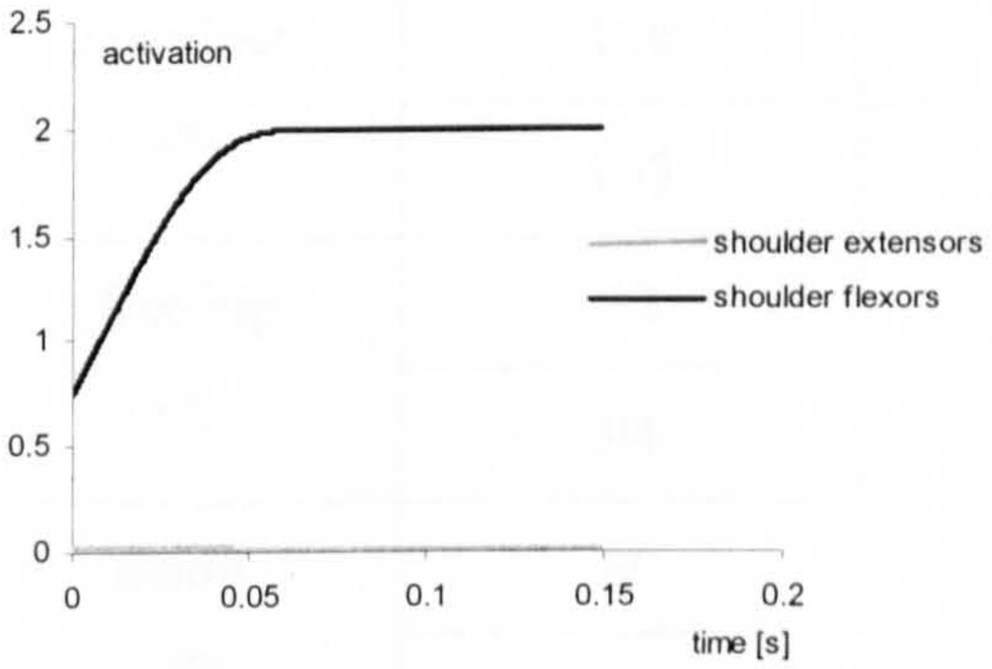

Figure 7.6. Torque generator activation profiles used in the simulation for distance.

Table 7.5. Comparison of the configuration orientation angles at take off for actual performances and simulations using the torque-driven model.

		Trial 36	Trial 46
simulated	trunk (°)	86	87
actual		86	93
simulated	ankle (°)	117	132
actual		106	101
simulated	knee (°)	170	151
actual		167	166
simulated	hip (°)	175	175
actual		179	190
simulated	shoulder (°)	106	101
actual		105	87
simulated	free hip (°)	93	123
actual		94	89
simulated	elbow (°)	80	70
actual		80	71
simulated	free knee (°)	96	65
actual		93	52

Table 7.6. Comparison of the minimum ankle, knee and hip angles during the actual performances and simulations using the torque-driven model.

		Trial 36	Trial 46
simulated	minimum ankle (°)	88	87
actual		78	68
simulated	minimum knee (°)	135	120
actual		132	133
simulated	minimum hip (°)	149	-
actual		148	-
simulated	minimum free knee (°)	59	20
actual		72	35

The scores for the individual parts of the objective function score are shown in Table 7.7.

Table 7.7. Individual objective function scores.

	Trial 36	Trial 46
orientation	0.1°	4.7°
configuration	6.4°	19.2°
angular momentum	0.33%	5.18%
linear momentum	1.45%	0.44%
time of contact	0.30%	3.81%
Force	14.33%	32.08%

The simulations which resulted in the best objective function score were used to determine the height or distance reached by the centre of mass. The height reached by the mass centre in the simulation for height was 1.80 m. The distance reached by the mass centre in the simulation for distance was 4.55 m. As the difference in linear momentum between the actual performances and the

simulations for height and distance was only 1.45% and 0.44% respectively, these heights/distances reached by the centre of mass were very close to those achieved in the actual performances. Graphical sequences of the actual performances along with the simulations of the performances for height and distance which match the actual performances most closely are shown in Figures 7.7 and 7.8 respectively. In the next section the heights reached, and the distances travelled by the centre of mass will be maximised.

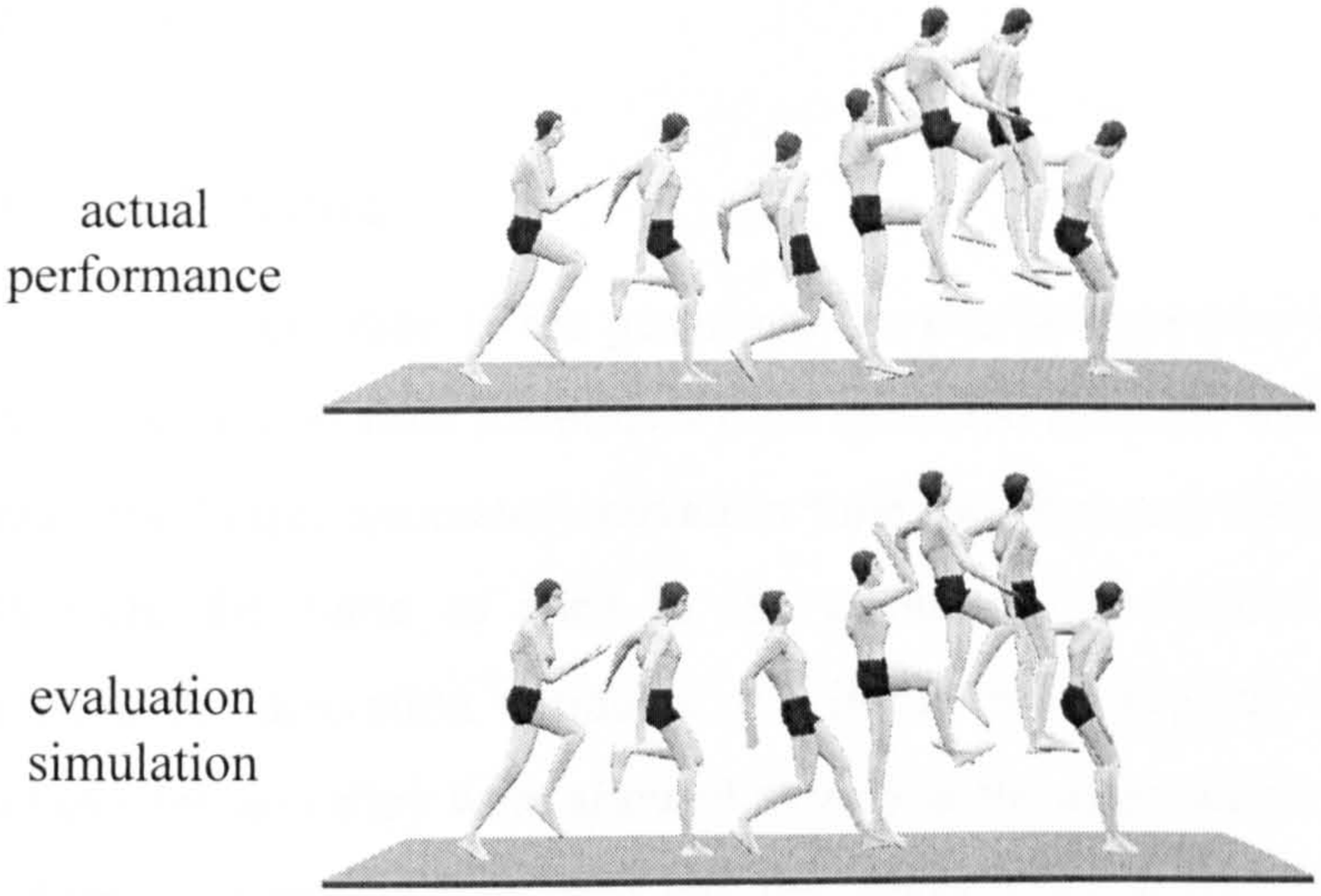

Figure 7.7. Computer graphics sequences of the actual performance and evaluation simulation for height.

Figure 7.8. Computer graphics sequences of actual performance and evaluation simulation for distance.

Optimisation

Introduction

In this section the method used to optimise running jumps for height and distance using the evaluated torque-driven simulation model will be described. Optimising the performances for both maximum height and maximum distance involved maximising an objective function which defined the success of a performance.

Objective function

The optimisation of the performances was achieved by varying the torque generator activation time histories within specified sensible limits. The variables defining the torque generator activation time histories and their upper and lower limits were the same as used in the evaluation procedure. In addition to optimising the activation variables, the initial joint angular velocities and the variables slipx and slipy were allowed to vary in the same way as in the evaluation procedure, as were the free knee and the elbow joint angle time histories. This resulted in the initial joint angles of the free knee and elbow being the same as in the actual performance but the joint angular velocities being allowed to vary from the actual values. The approach characteristics and the initial configuration and orientation angles used in the optimisation were obtained from the actual performances and these were not allowed to vary.

The objective function used to optimise the jumps for height and distance was simply a measure of the success of the performance. In the optimisation for maximum height, the objective function was the sum of the vertical height of the mass centre at takeoff plus the vertical height reached by the mass centre during the flight phase, determined using an equation of constant acceleration (equation 7.1).

$$s = \frac{v^2}{2g} \tag{7.1}$$

Where:

s = distance (height) travelled

v = vertical velocity of the mass centre at takeoff

g = acceleration due to gravity

In the optimisation for maximum distance the objective function was defined as the horizontal distance travelled by the mass centre during the flight phase determined by equations of constant acceleration. An assumption as to the height of the mass centre at landing had to be made and this was determined by looking at the recorded image analysis. A height of 0.6 m was chosen.

All the penalties included in the evaluation procedure were included in the optimisation of performance in order that the height or distance were maximised without the performance being anatomically / physically impossible. A few additions penalties were, however, required. The angular momentum at takeoff was restricted to be within ± 2.5 $kg.m^2.s^{-1}$ of the angular momentum in the actual performances so the performance was sensible and over rotation did not occur. If the angular momentum was outside these limits a penalty was incurred. Additional penalties limited the angles of the free hip, free knee, shoulder and elbow joints at takeoff. Each angle was given a fairly large range within which to vary, but outside these limits a penalty was incurred.

Results

Varying the activation time histories resulted in the height reached by the mass centre in the simulation for height increasing from 1.80 m to 2.01 m, an increase of 12%. This height of 2.01 m was the same height reached by the mass centre in the actual high jumping trial performed by the subject (Chapter 5). In the simulation for distance the distance travelled by the mass centre increased from 4.55 m to 5.19 m, an increase of 14%. Activation profiles used to obtain these optimal solutions are shown in Figures 7.9 and 7.10.

Graphics of the simulations for maximum height and maximum distance are shown in Figures 7.11 and 7.12 respectively.

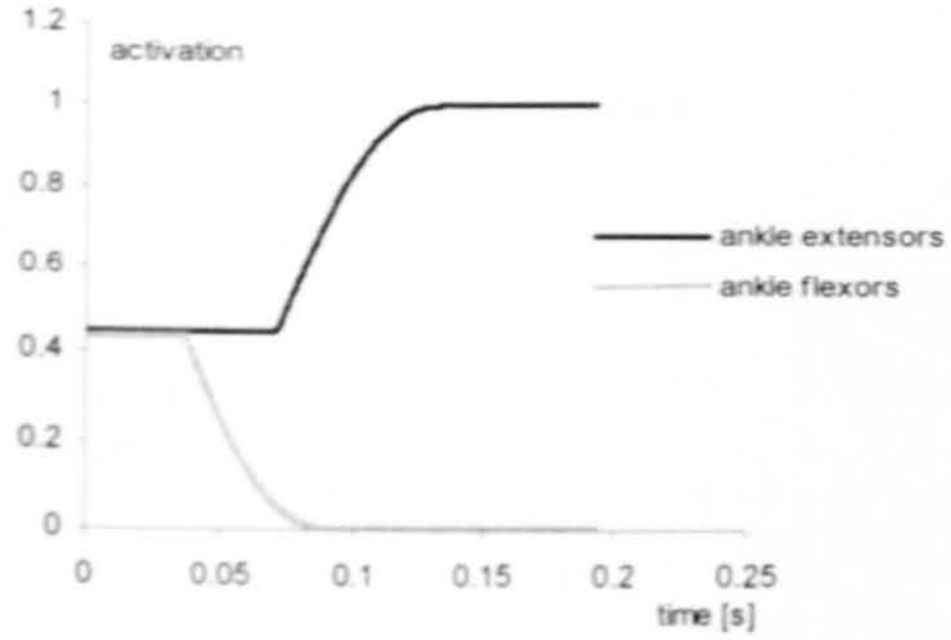

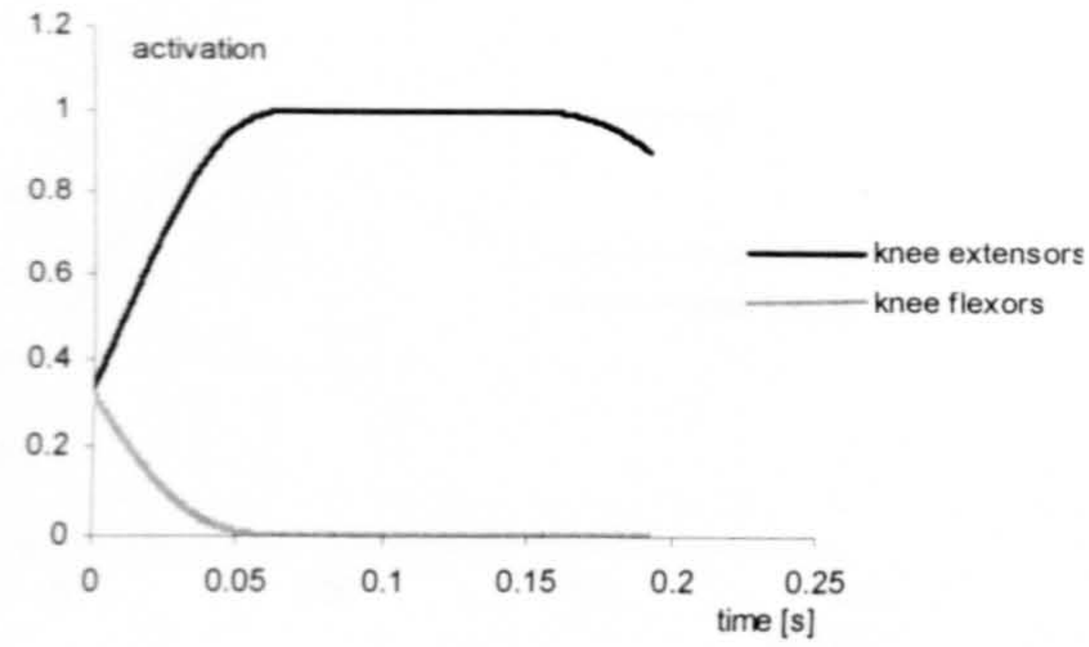

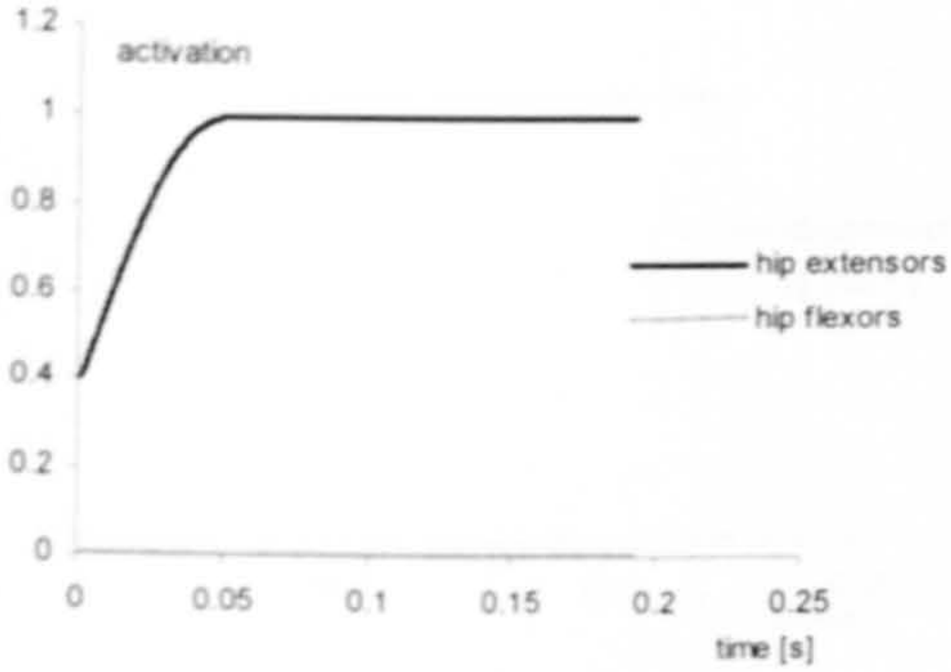

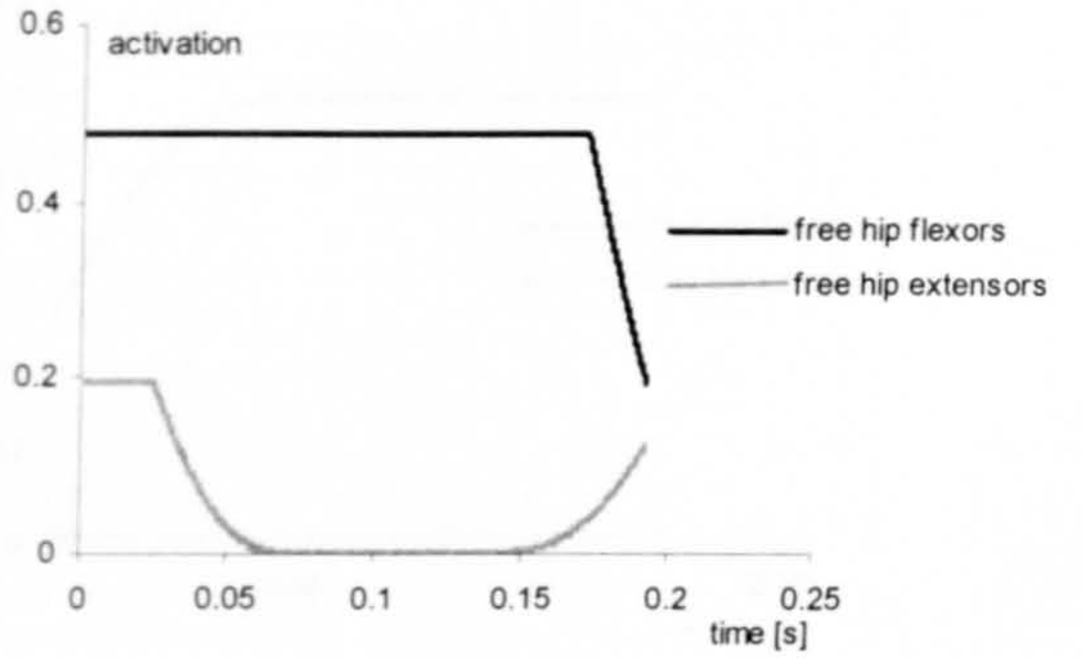

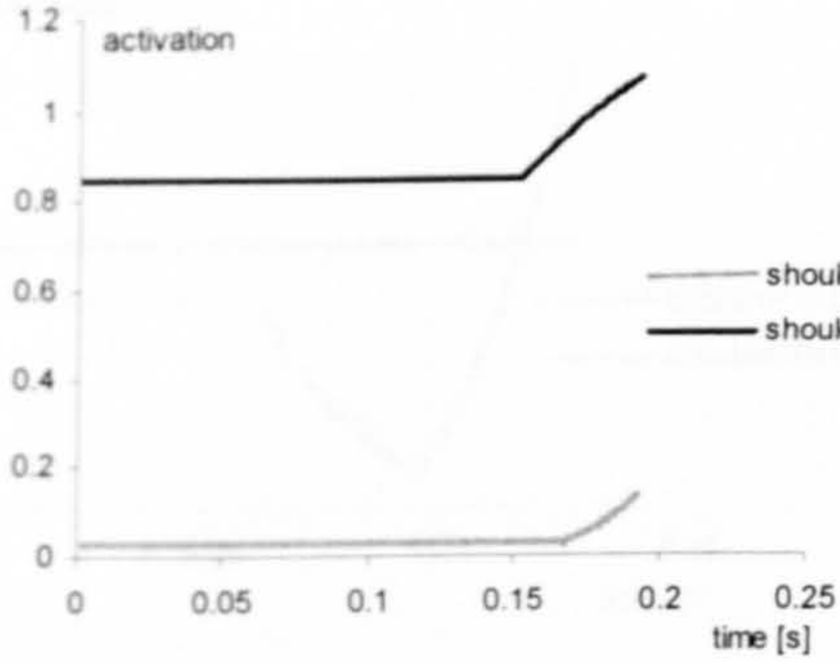

Figure 7.9. Torque generator activation profiles used in the simulation for maximum height.

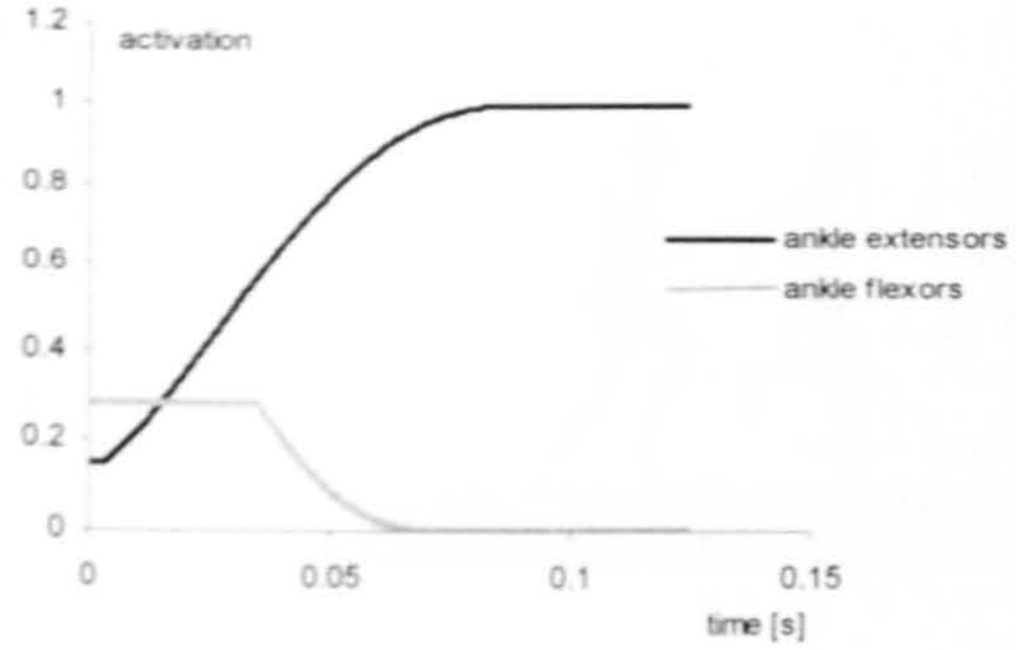

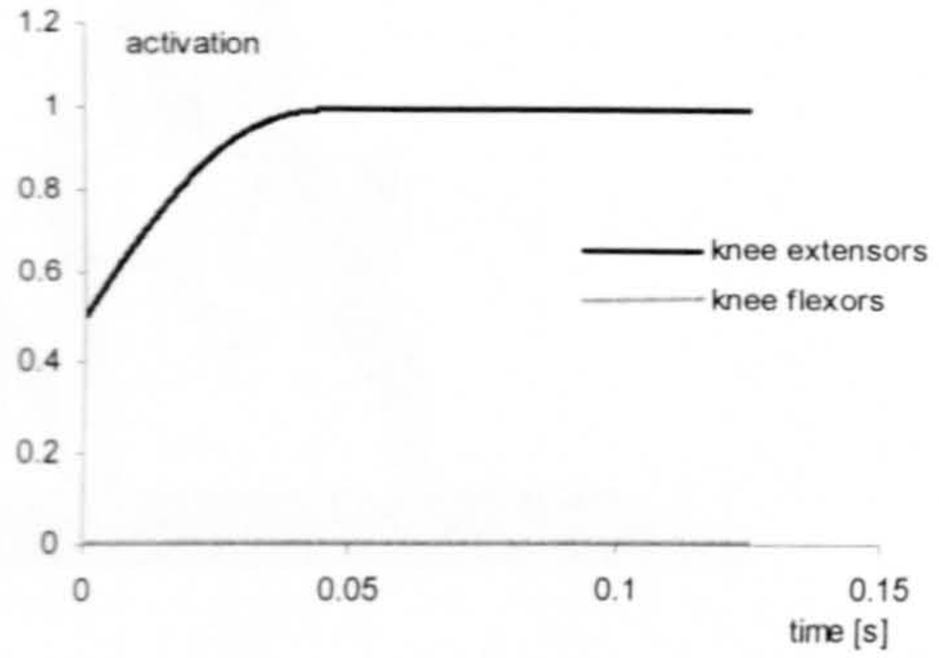

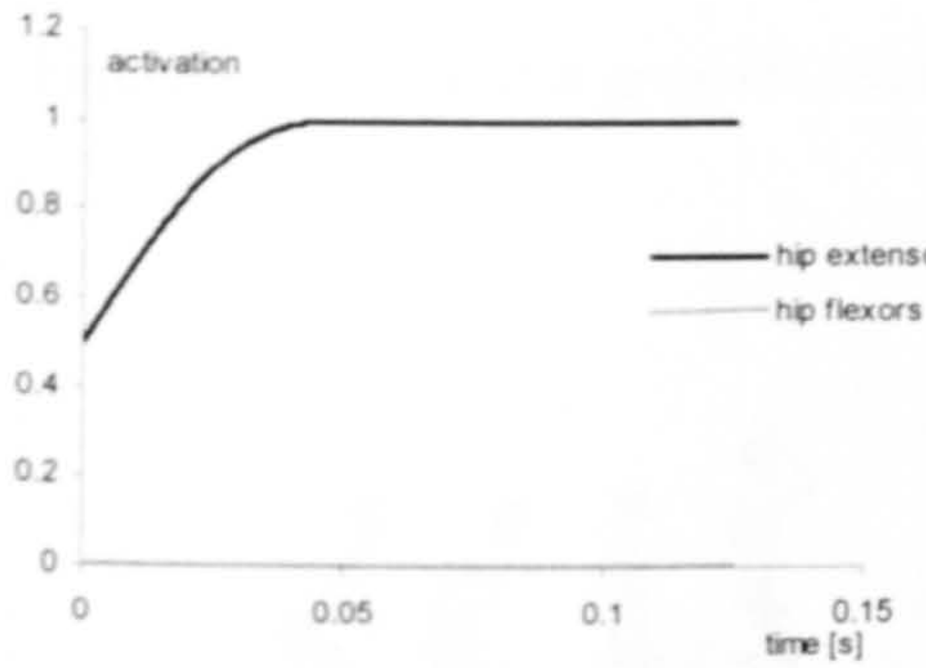

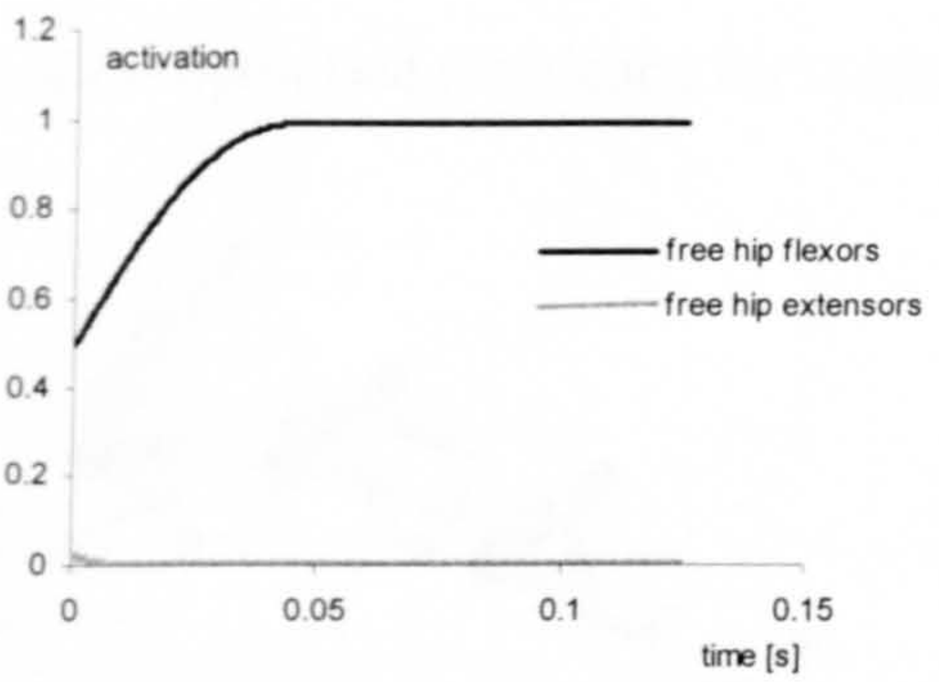

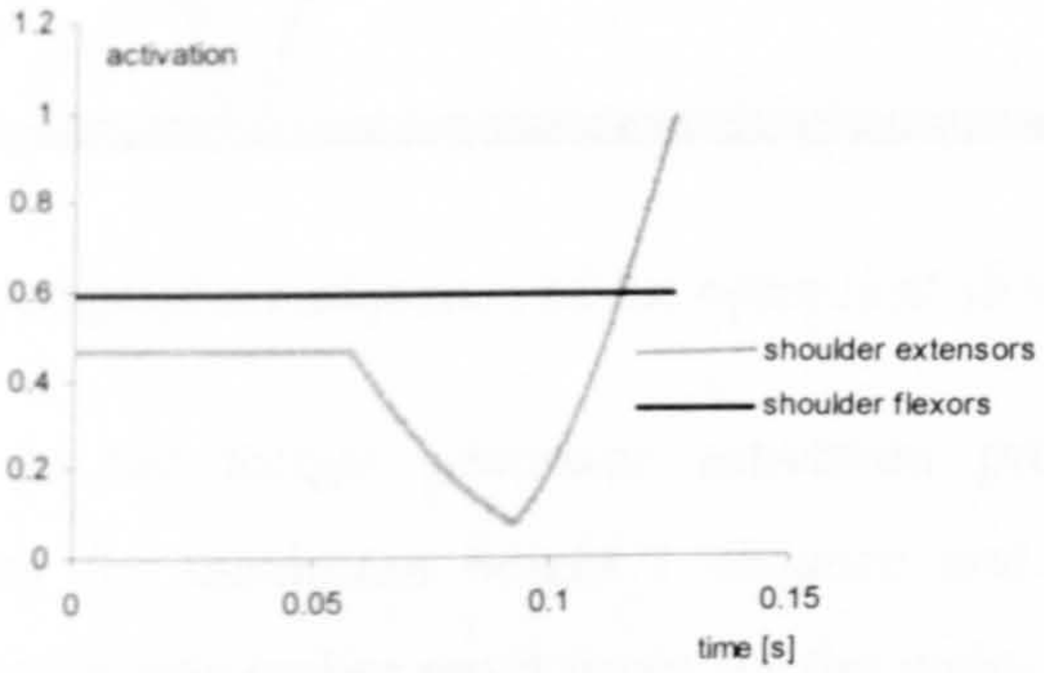

Figure 7.10. Torque generator activation profiles used in the simulation for maximum distance.

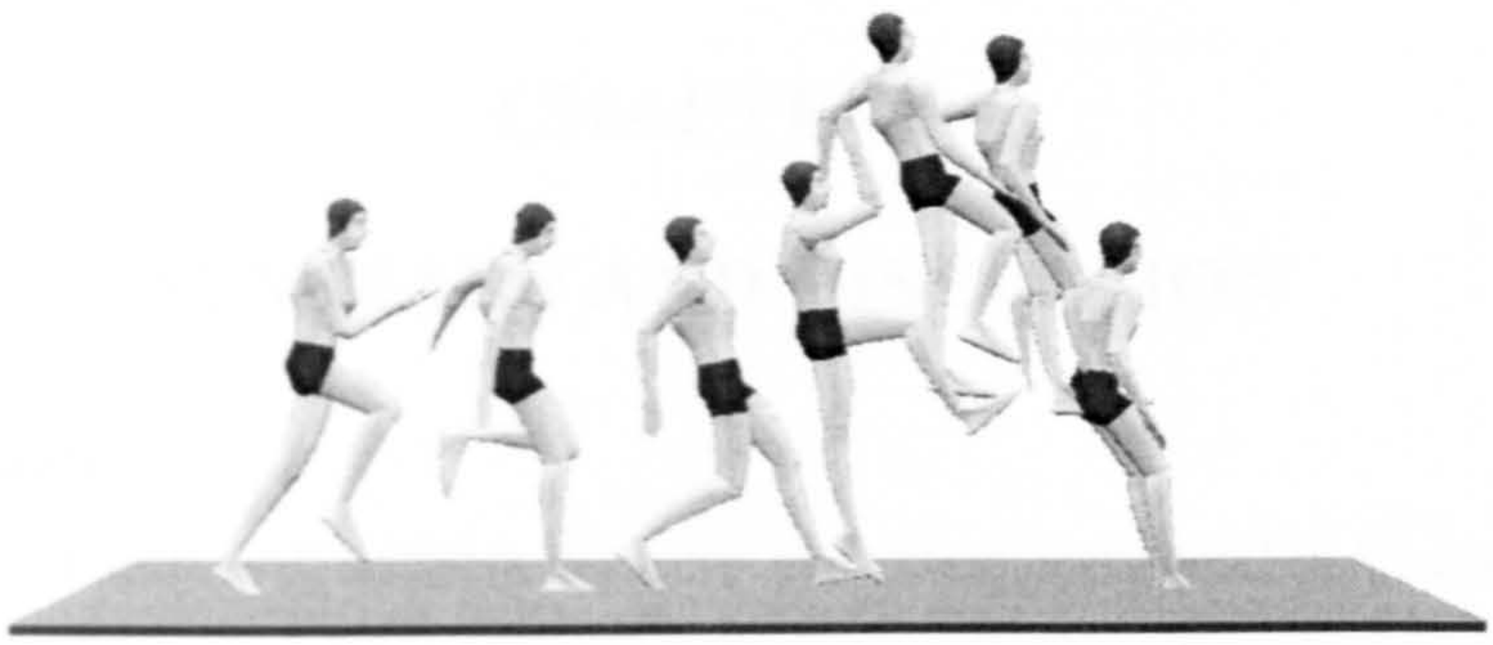

Figure 7.11. Computer graphics sequence of the optimised simulation for height.

Figure 7.12. Computer graphics sequence of the optimised simulation for distance.

Differences in the torque generator activation profiles between the optimum simulations for maximum height / distance and the corresponding matching simulations include earlier onset times for the majority of the joints and less antagonist muscle action.

Summary

The evaluation of the torque-driven model was relatively successful producing objective function score values of 6.4% and 15.6% in the simulations for height and distance respectively. By varying the torque generator activation time histories, the optimum solutions resulted in jump heights and distances considerably better than those achieved in the actual performances.

CHAPTER 8

SUMMARY AND DISCUSSION

Introduction

This Chapter will address the aims and questions posed in Chapter 1. The limitations and improvements to the techniques used in this study will then be considered followed by any future applications of the study.

Aims addressed

Mechanics of jumping / elements of a simulation model

This study set out to address some aims and questions regarding simulation modelling, the mechanics of dynamic jumping and factors affecting jumping performances (Chapter 1).

The three aims were as follows:

(i) To gain an understanding of the mechanics of dynamic jumping

(ii) To identify what elements are needed in a computer simulation model of jumping in order to provide an accurate representation

(iii) To apply such a model to the optimisation of jumping

The following sections will look at the individual aspects of the simulation model / performance in order to address aims (i) and (ii) and the questions posed in Chapter 1. Aim (iii) will then be addressed separately.

Torque generator activation profiles

Using the torque generator activation profiles which resulted in the optimum performances for maximum height and distance (2.01 m and 5.19 m respectively) the activation onset times were delayed by 20 ms at each joint individually and the effect of this in terms of jump height or jump distance was investigated (Table 8.1)

Table 8.1. The effect of delayed onset on jump height and distance.

joint	jump for height (m)	jump for distance (m)
optimal performance	2.01	5.19
ankle	1.93	5.14
knee	1.61	4.93
hip	1.95	5.02
free hip	2.01	5.15
shoulder	2.01	5.19

It is clear that the model / performances are sensitive to the activation timings. These results highlight that the knee joint is the most sensitive and therefore probably contributes the most to jumping performances.

Free limbs

Investigations into the effect of the free limb movement in the simulations of jumps for both height and distance were carried out by fixing the angle of the elbow and free knee joint in separate simulations. Table 8.2 shows the height and distances reached by the centre of mass in the two separate simulations compared to a height of 2.01 m and a distance of 5.19 m achieved in the optimal simulations. The results highlight that the movements of the free limbs, especially that of the free leg, do contribute to performances and therefore are necessary in a simulation model of jumping. The underlying mechanics are related to the velocity of the free limbs, resulting in a smaller vertical velocity of the hip, slower concentric conditions of the leg muscles and therefore a larger force exerted by the feet on the ground (Dapena et al., 1999).

Table 8.2. The effect of free limb effect on jump height and distance.

	jump for height (m)	jump for distance (m)
optimal performance	2.01	5.19
fixed elbow	1.90	4.98
fixed free knee	1.89	2.96

Wobbling masses

Wobbling masses are an important factor in the simulation modelling of dynamic movements with impacts. In reality the body does not behave as a rigid body. Rather each body segment consists of rigid part (bone) and a non-rigid part (muscle, fat etc.). During an impact the skeletal structures of the body experience high accelerations, whereas the soft tissue movement is delayed, initiating vibration of the soft tissue relative to the bone. The potential errors associated with rigid body models leads to the conclusion that the approximation of the human body with rigid segments is justified only for movements that are not too rapid (Denoth et al., 1984). The inclusion of wobbling masses in a model has only a small influence on the kinematic behaviour but a large affect on torques and forces during an impact phase. The angle-driven model (model 2) was able to simulate jumps for both height and distance. Using the simulations which matched the actual performances most closely, the springs attaching the wobbling masses to the corresponding rigid segment were made stiff so that little movement of the wobbling masses relative to the rigid segments occurred, hence making the model a rigid segment model. Figure 8.1 shows a comparison of the vertical ground reaction force in the jump for height with and without wobbling mass movement respectively. When no movement of the wobbling masses takes place the ground reaction force is very different to the actual force exerted highlighting the need for wobbling masses in the simulation model. Also highlighted is the unrealistically large initial peak in the ground reaction force which is characteristic of simulations when the soft tissue movement of the human body is not modelled

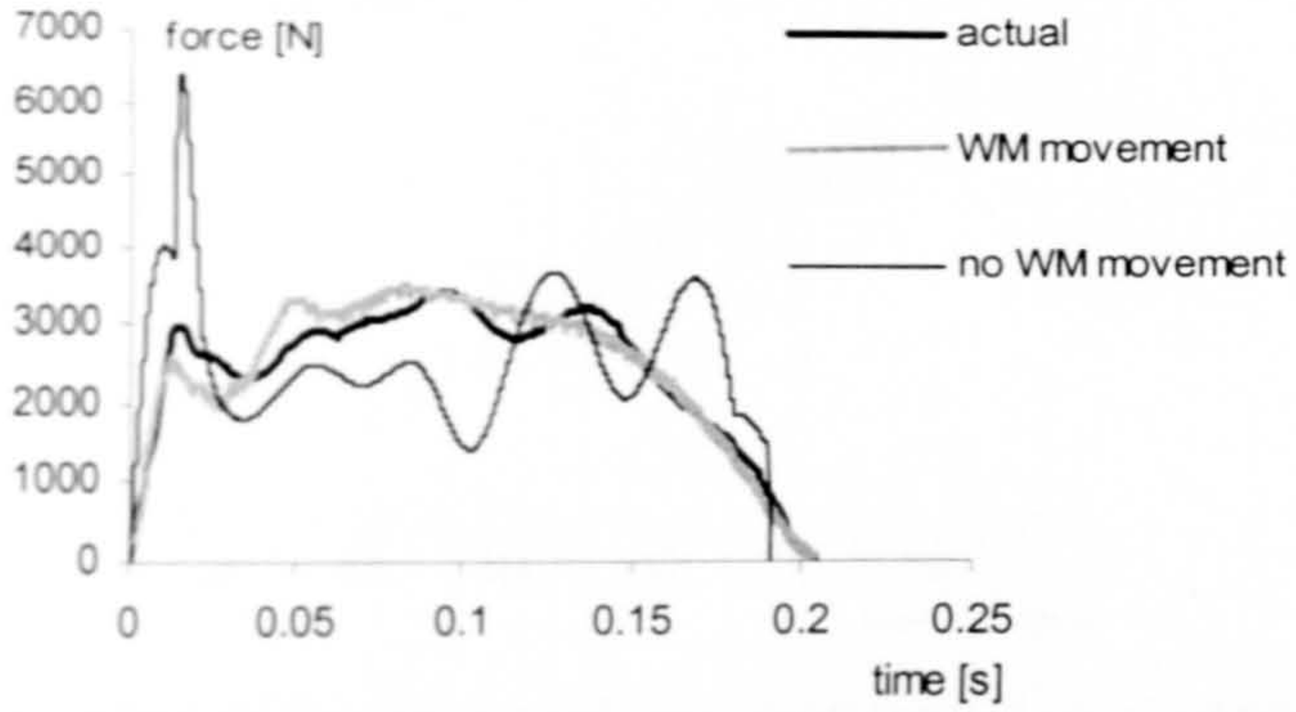

Figure 8.1. Comparison of vertical ground reaction force in actual performance and simulations with and without wobbling mass movement.

Foot-ground interface

Spring-damper system equations were required for the foot-ground interface in models 2 and 3 in order to model the impact successfully. A z^2 factor was needed to model the horizontal force at both the toe and the heel as without it a poor match between actual and simulated force resulted (Chapter 4). Including a z^2 factor makes sense as this mimics the vertical force and the more vertical depression there is the more difficult it is for the foot to move horizontally. This term also forces the horizontal ground reaction force to fall to zero as the vertical ground reaction force does so at the end of a simulation both vertical and horizontal forces are zero. Without this factor present the horizontal ground reaction force may have a large value at takeoff which in reality is not the case.

Approach conditions

Using the two-segment model (Chapter 3), a linear relationship between knee angle and jump height was identified (Figure 8.2) which was in agreement with Greig and Yeadon (2000).

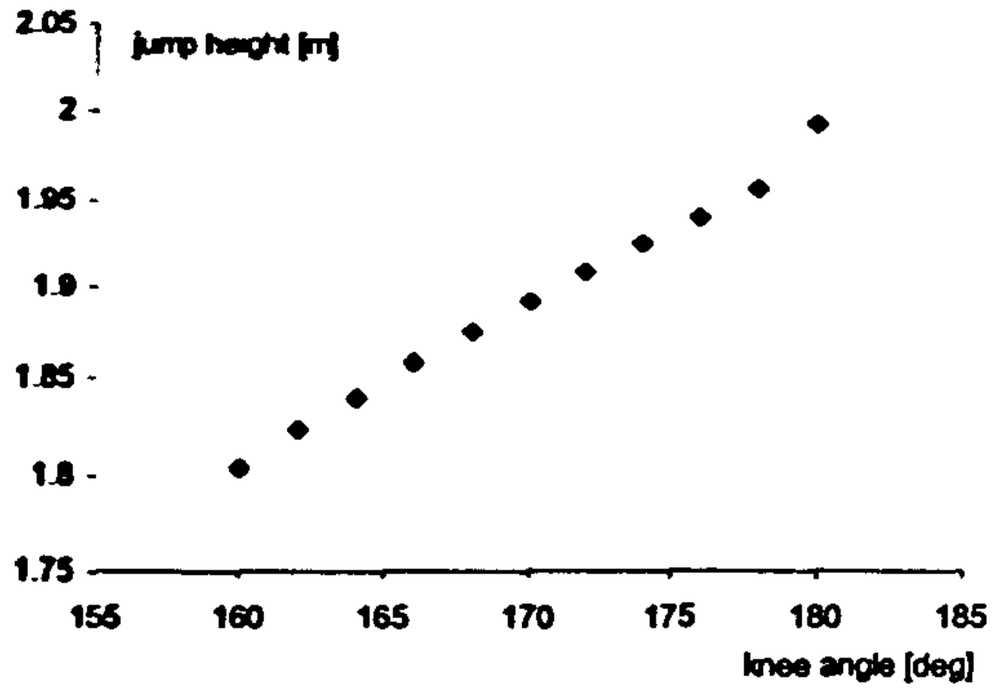

Figure 8.2. The effect of the knee angle on jump height (two-segment model).

Using the eight-segment torque-driven model (model 3) the effects of approach speed, leg plant angle and initial knee angle on jump height / distance were investigated.

The approach speed in the simulation of a jump for height was varied between 3.4 and 10.4 ms^{-1} in 1.0 ms^{-1} intervals, where 4.4 ms^{-1} was the actual approach speed. An approach speed of 6.6 ms^{-1}, used by the subject in the actual high jumping trial performed outdoors was also included (Figure 8.3). Similarly the approach speed in the simulation of a jump for distance was varied between 5.87 and 12.87 ms^{-1} in 1.0 ms^{-1} where 6.87 ms^{-1} was the actual approach speed used (Figure 8.4). The activation timings for all simulations were kept the same as in the two optimised solutions.

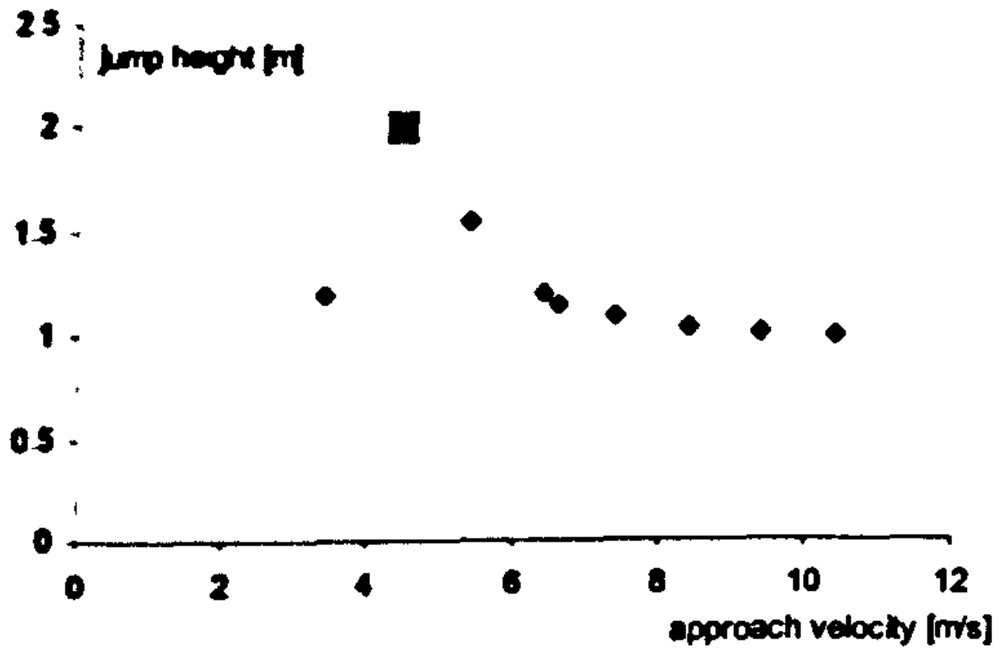

Figure 8.3. The effect of approach speed on jump height.

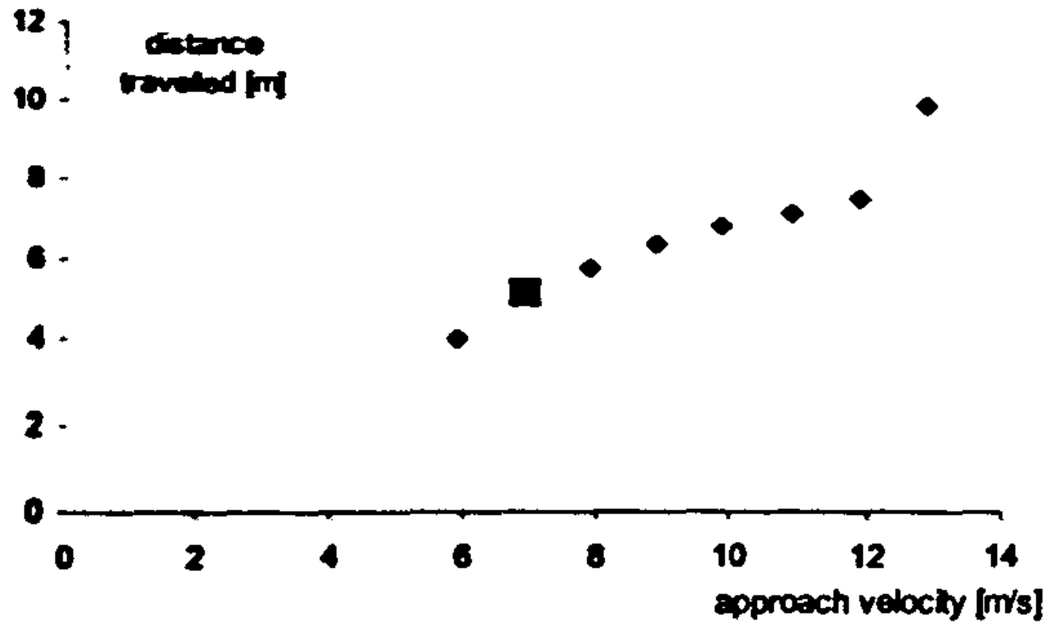

Figure 8.4. The effect of approach speed on distance travelled.

In the jump for distance, as expected the faster the approach speed the further the distance travelled by the centre of mass. In the simulation for height, however, this was not the case. It may initially appear surprising that any increase in approach velocity resulted in a poorer performance, however, the torque generator activation time histories had been optimised for an approach speed of 4.4 ms^{-1}. If any other approach speed is used the activation time histories will not be optimal and an over flexion of the knee occurs. In order to investigate properly the effect of increased approach speed on jump height and distance, the torque generator activation time histories would need to be re-optimised. The simulations of jumps for distance are obviously not as sensitive to changes in the activation time histories as the simulations of jumps for height.

As with the approach velocity, the knee angle at touchdown and the plant angle between the leg and the horizontal were varied from the values used in the actual performances (157° and 58° in the jump for height and 151° and 59° in the jump for distance). In the simulation of the jump for height both increasing and decreasing the plant angle led to a decrease in jump height (Figure 8.5), similarly with the knee angle no change in its initial value led to an increase in jump height (Figure 8.6). Again this is primarily because the torque generator activation timings have not been re-optimised. If they had been it would be expected that an increase in knee angle would result in an increase in jump height as shown using the two-segment model. In the simulation of the jump for distance increasing the knee angle resulted in a slight increase in distance reached by the mass centre followed by a decrease (Figure 8.7). Varying the plant angle, however, resulted in no increase in the distance reached (Figure 8.8).

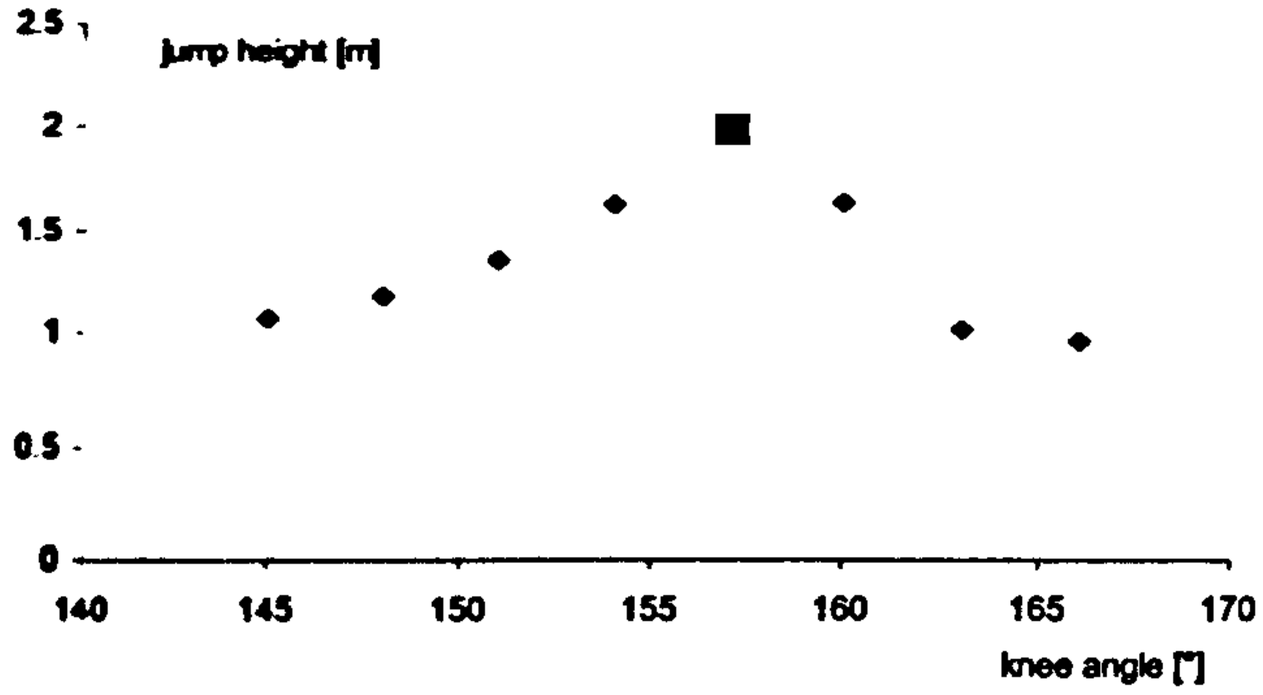

Figure 8.5. The effect of knee angle on jump height.

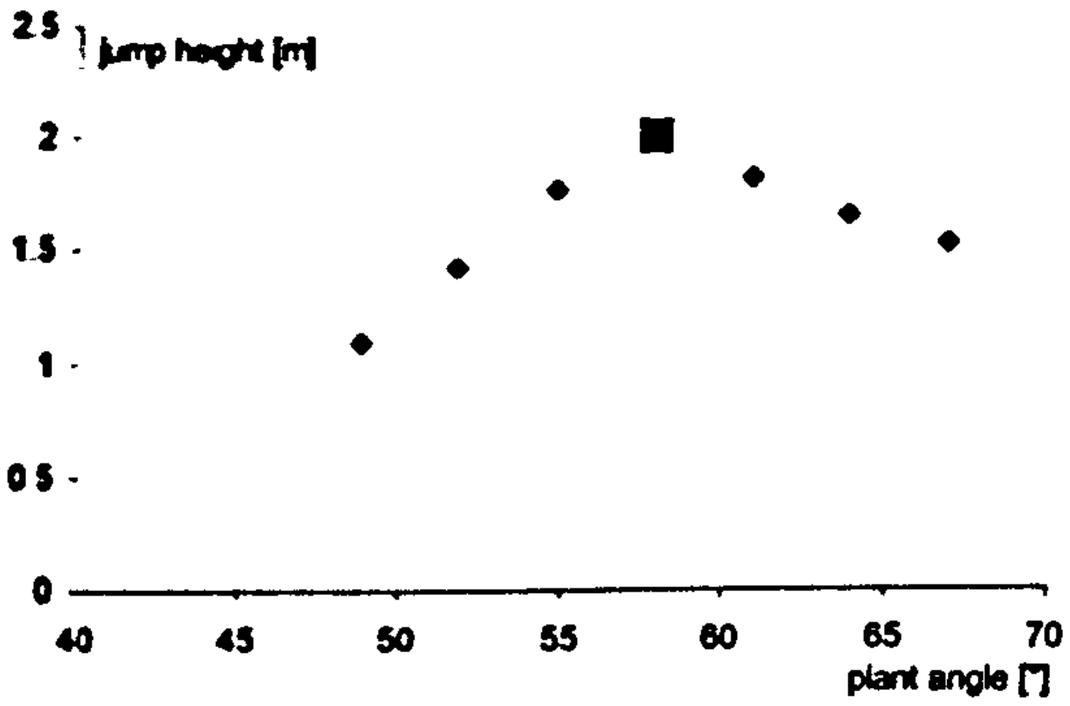

Figure 8.6. The effect of plant angle on jump height.

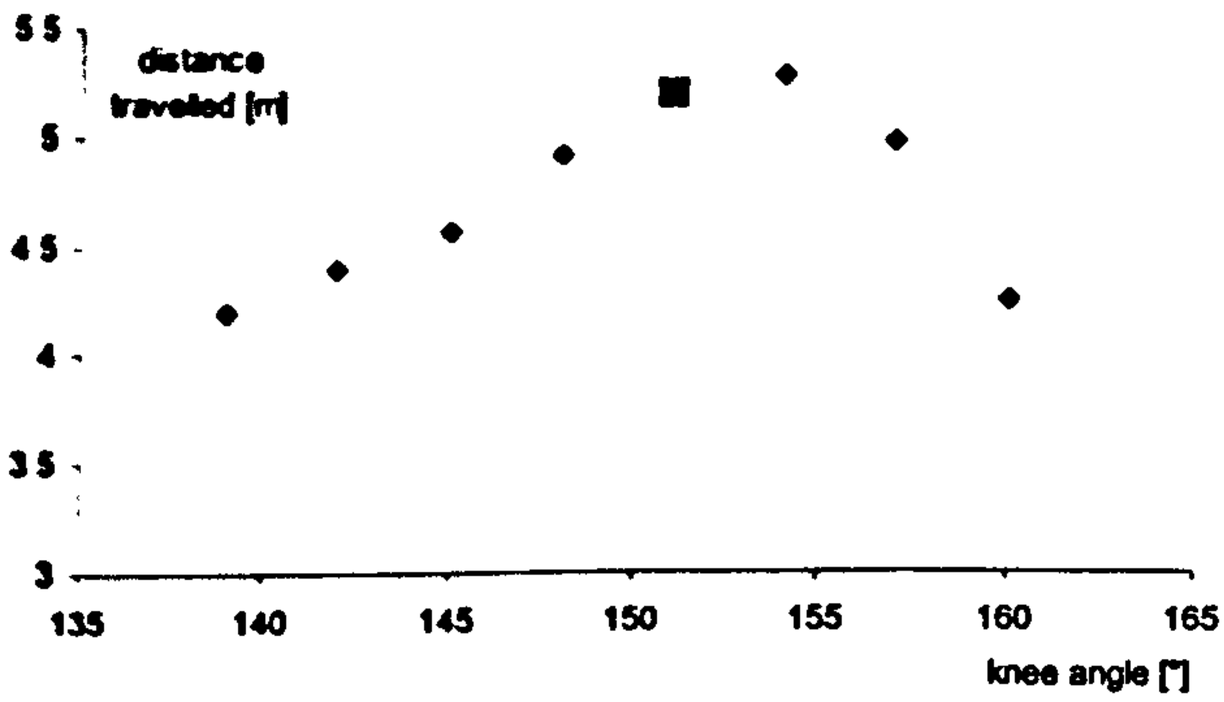

Figure 8.7. The effect of knee angle on distance travelled.

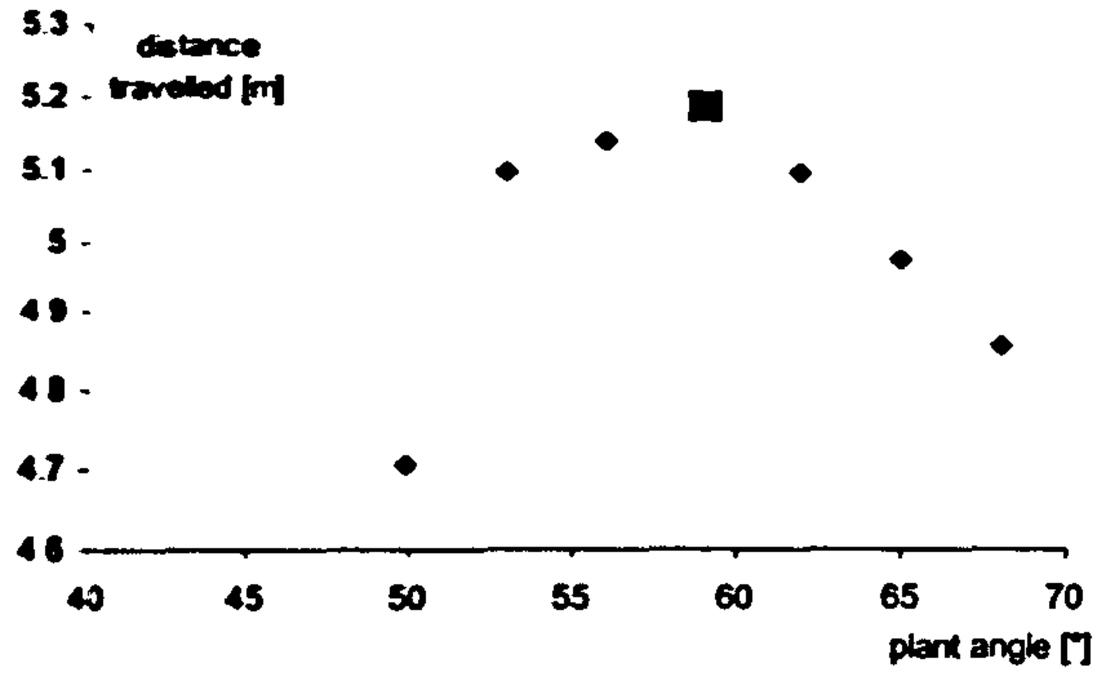

Figure 8.8. The effect of plant angle on distance travelled.

It is clear that the simulations are extremely sensitive to the torque generator activation timings and in order to fully investigate the effect of changes in parameter values, these activation timings need to be re-optimised.

Optimal performances

By varying the torque generator activation time histories only, and keeping the initial conditions the same as in the actual performances, the simulation model was used to optimise performance, i.e maximise height reached by the mass centre in the jump for height and maximise distance travelled by the mass centre in the jump for distance.

The maximum height reached by the mass centre was 2.01 m. This was 0.21 m higher than in the matching simulation of the actual performance, which was an increase of 12%. The maximum distance travelled by the mass centre was 5.19 m. This was 0.64 m further than in the matching simulation of the actual performance, which was an increase of 14%.

By allowing only the activation time histories to vary the simulations resulted in considerably better performances. If the initial conditions, i.e the configuration angles at touchdown and the approach characteristics, were also allowed to vary an even better performance would likely result.

Limitations and Improvements

Areas to be looked at in this section will be; data collection / image analysis, parameter determination, simulation modelling and evaluation.

Data collection/ Image analysis

Video and Coda

The data collection in this study was considered to have been reasonably successful. The high speed camera recording at 200 Hz was sufficient although the quality of the pictures was quite poor and in order that the pictures were bright enough extra lighting was required. However, this caused problems with the Coda system. Using a combination of both CODA and high speed video was found to be a problem. A clearer picture would have resulted in the digitised data being more accurate. It was also concluded that a faster video camera may have been useful for the initial impact where joint angles were changing rapidly.

The Coda data were not used in the study due to the movement of the markers during the impact which was a result of the markers having significant mass. A passive system in which the markers have insignificant mass may have lead to better data being collected.

EMG

EMG data were not collected for the two trials used in this study due to the limitations imposed by the wires attaching the electrodes to the amplifier. Using a remote EMG system would solve this problem. If such a system were available EMG data would be collected so information regarding muscle activation time histories could be obtained.

Force

The original horizontal force data collected simultaneously with the video data were not able to be used as the x,y gain range was set too low for the subject and the activity being performed. This resulted in the force being truncated at a level below the maximum that was exerted by the subject. A second data collection was performed in order to obtain some horizontal force data. The subject was asked to perform the same trials as in the initial data collection. Although the trials for the two data collections were similar in terms of the vertical force produced and the time of contact, the horizontal forces produced in the second trial may not have been close to those in the original trial. These may

have caused problems when the forces were used in the angle-driven model. This underlines that it is advisable to perform pilot studies to highlight these problems before the main data collection is carried out.

Parameter determination

Muscle parameters

Muscle parameters values were determined using the method discussed in Chapter 6. The subject performed concentric-eccentric and isometric actions on an isovelocity dynamometer at all joints which required muscle parameters in the simulation model. The protocol used appeared to be successful, although certain changes would be made if it were to be carried out again including trials at more angular velocities for a given joint in order to give more points to fit the torque-angular velocity function to. The use of goniometers at the joints being tested restricted the subject's movement to a certain extent. In future it may be more suitable to use video or an automatic system to determine the joint angles instead.

Series elastic component parameter values were determined using data from the literature. In future it may be possible to estimate series elastic parameters from experimental testing (e.g. Hof, 1998).

Wobbling mass to rigid body ratios

The wobbling mass to rigid body mass ratios were determined using data from the literature and anthropometric measurements and percentage body fat measurements taken on the subject. Although the ratios determined were considered to be good approximations, it may be possible to determine more accurate data experimentally in the future. Taking a Dexa scan of the subject may provide the relevant information to be able to determine the ratios solely from data on the subject.

Spring parameters

The spring parameters for the spring-damper systems representing both the wobbling masses and the foot-ground interface were determined using the angle-driven model and an optimisation procedure whereby an objective function was minimised using the Simulated Annealing algorithm (Chapter 6). This was

achieved by varying the stiffness and damping parameter values. This resulted in values of the spring parameters which gave a good match between the actual performances and simulations. If the kinematics had been more accurate, the movement of the foot could have been included in the objective function which may have resulted in stiffness and damping parameters which gave a better match between simulations and actual performances.

Simulation Modelling

In this study, three eight-segment models were developed as well as simple one and two-segment models. The limitations of the one and two segment models have already been addressed (Chapter 3) and will therefore will not be further discussed in this Chapter. The eight-segment models are almost identical in structure. The limitations of the models are therefore very similar and will not be discussed separately.

One segment foot

Perhaps the biggest limitation of the models which has been identified is the use of one segment to represent the foot. During the takeoff phase in high jumping or long jumping the foot flexes and extends at the ball. Relatively successful attempts were made to overcome the problems caused by this simplification. These involved applying some of the vertical force (produced at the toe) at the heel and varying the percentage of force as the heel came further off the ground (Chapter 4). This helped in placing the centre of pressure in the correct place. However, problems relating to the geometry of the foot were not overcome with this solution. In reality, when the heel has come off the ground the ball of the foot remains in contact. Using this model, when the heel comes off the ground only the end of the toes are still in contact putting the ankle further away from the toes than in reality.

One arm representing left and right arms

In the eight-segment simulation models the arm was modelled as two segments representing the upper and lower arms which simulated the action of both the left and right arms. In long jumping the arms are generally used together

during the contact phase, and in the jump for distance performed in the laboratory this was also the case. In the high jump trial the subject performed in the laboratory both arms also followed a very similar path. Although this simplification is able to model the general pattern of the arms throughout the contact phase, it is possible that modelling the arms individually may lead to a small improvement in the optimal performance.

Constrained joint angles

For all joints in the angle-driven models and for the elbow and free knee joints in the torque-driven model, the joint angle time histories were constrained to those determined from the video data. Any digitising errors incurred during the image analysis will have resulted in errors in the joint angles. The joint angle time histories of the ankle, knee and hip joints were varied using a sine series function (described in Chapter 4). This function allowed the joint angles and angular velocities a small amount of deviation from the specified time histories, determined from the actual performances, to overcome the effect of any errors in the data. These errors may have still resulted in difficulties in matching the actual performances and simulations. Similarly, when optimising performance using the torque-driven model, the free knee and elbow angle time histories were allowed to vary from the actual angle time history by an amount determined by the same sine series function. Although this allowed the two joints some freedom in their movement, the joint angle time histories were restricted, and may not have been optimal.

In this study the elbow and free knee angle were not torque-driven as they were not considered greatly important in the overall performance and it was thought that driving them with angles would be adequate. It has been identified, however, that having joints which are angle-driven and joints which are torque-driven in the same model can cause problems. This was particularly highlighted at the free knee joint. In future models the free knee and perhaps the elbow would be torque-driven.

Wobbling mass spring parameters

The wobbling mass stiffness and damping parameter values were optimised using the angle-driven models. In this optimisation it was assumed that the spring stiffness were the same at each end of the wobbling mass as well as the same horizontally and vertically. Making the assumption that they have the same value horizontally and vertically may have limited the model's ability to match actual performances.

Evaluation

The evaluation of simulation models is an extremely important part of the model development process and one which is often overlooked. In this study the angle-driven simulation model has been used to compare and match the actual performances with simulations. The evaluation of the torque-driven model has been performed by again matching the actual performances and simulations.

Performances for both maximum height and maximum distance have been compared. Good agreement was found between simulation and performance for both trials using the angle-driven models. The weakness of model 2 was in matching the ground reaction forces. Factors considered to be responsible for the differences were the foot being modelled using a single segment and the horizontal force data used to compare the force from the simulations not being the forces produced during the actual performances. The horizontal force was obtained from different trials to those used to evaluate the model (Chapter 5). In additional to these, the assumption regarding the wobbling mass spring parameters may also have been responsible for the wobble which occurred in the simulated forces. The simulations of jumps for both height and distance were matched to the actual performances to within 6.6% and 9.9% respectively. These percentages were considered good considering the tough challenge of matching both kinetic and kinematic variables.

With the torque-driven model, again, matching the ground reaction forces proved to be problematic. The simulations of jumps for both height and distance were matched to the actual performances to within 6.4% and 15.6% respectively. When only kinematic variables were used to match the actual performances and simulations, scores of 1.6% and 7.9% were achieved. As already stated, trying to

match both kinetic and kinematic variables is a tough challenge. There are a number of reasons, in addition to the ones discussed above, why it is hard to match the ground reaction forces using the model developed in this study and these are mainly related to the simplification of the model. Both the elasticity in the model and the movement of the soft tissue have been modelled in a very basic way. Although kinematically this is not a problem, from a kinetic point of view this is a highly simplified view of the human body which may have lead to discrepancies in the actual and simulated performances. A more complex model, incorporating more sophisticated representations of the wobbling masses and foot-ground interface, is needed in order to match both kinetic and kinematic variables more successfully. Obtaining percentages errors of 1.6% and 7.9% can be considered an indication of a successful model.

The Simulated Annealing algorithm used in the evaluation of the simulation models has limitations discussed in both Chapter 2 and Chapter 6. The chances of finding a local and not a global optima, with the number of variables needed to evaluate the models in this study, are fairly high. Although attempts were made to try and prevent this, there is a chance the solutions found were not optimal.

Future directions

The torque-driven simulation model developed in this study has been successfully evaluated and used to optimise performance by varying the torque generator activation time histories. In the future the model could be used to optimise performance by varying other parameters such as the approach conditions, and / or input parameters. The approach speed observed in the actual high jumping trial performed by the subject may be used as an initial value. This again would involve maximising an objective function which defines the success of a performance by optimising the torque generator activation time histories.

The individual contributions of different factors to performance could also be investigated, including the strength of the torque generators and anthropometric parameters such as leg length.

Finally, investigating the sensitivity of the model to changes in model parameter values could also be addressed. Such parameter values investigated could include, among others, the series elastic stiffness and the inertia parameters.

Although optimal solutions have been identified in this study, these performances may have overestimated what can practically be achieved. If the solutions are sensitive to small changes in parameter values then they are not robust. For a solution to be considered robust, small perturbations in parameter values, which result in an "optimal performance", should result in a near optimal performance. Harris and Wolpert (1998) presented a minimum-variance theory which proposed that the time profile of the neural command is selected so as to minimise the endpoint error in targetted movements. That is, the solution chosen is one which is insensitive to changes in parameter values with any changes resulting in an essentially unchanged optimal neural profile. For a more complete understanding of jumping technique a measure of robustness should be included as part of the objective function when optimising jumping performance.

REFERENCES

Abdel-Aziz, Y. I. and Karara, H. M. (1971). Direct linear transformation from comparator coordinates into object-space coordinates. ASP symposium on Close-Range Phoyogrammetry, Falls Church, VA, American Society of Photogrammetry.

Alexander, R. McN. (1990). Optimum take-off techniques for high jumps and long jumps. Philosophical Transactions of the Royal Society of London B 329: 3-10.

Alexander, R. McN. (1992). Simple models of walking and jumping. Human Movement Science 11: 3-9.

Alexander, R. McN. (1995). Simple models of human movement. Applied Mechanics Review 48(8): 461-469.

Allard, P., Stokes, I. A. F. and Blanchi, J. (1995). Three-dimensional analysis of human movement. Champaign: Human Kinetics.

Angulo, R. M. and Dapena, J. (1992). Comparison of film and video techniques for estimating three-dimensional coordinates within a large field. International Journal of Sport Biomechanics 8: 145-151.

Atha, J. (1984). Current techniques for measuring motion. Applied Ergonomics 15(4): 245-257.

Auckland, T. R., Henson, P. W. and Bailey, D. A. (1988). The uniform density assumption: Its effect upon the estimation of body segment inertial parameters. International Journal of Sport Biomechanics 4: 146-155.

Audu, M. L. and Davy, D. T. (1985). The influence of muscle model complexity in musculoskeletal motion modelling. Journal of Biomechanical Engineering 107: 147-157.

Baca, A. (1996). Precise determination of anthropometric dimensions by means of image processing methods for estimating human body segment parameter values. Journal of Biomechanics 29(4): 563-567.

Bartlett, R. (1992). Biomechanical analysis of performance in sport. British Association of Sport Science.

Bartlett, R. (1999). Sports Biomechanics. Reducing injury and improving performance. London: E & F.N.Spon.

Basmajian, J. V. (1974). Muscles alive: their functions revealed by electromyography. Baltimore: Waverly Press.

Bedi, J. F. and Cooper, J. M. (1977). Take off in the long jump - angular momentum considerations. Journal of Biomechanics 10: 541-548.

Blake, G. M. and Fogelman, I. (1997). Technical principles of dual energy X-ray absorptiometry. Seminars in Nuclear Medicine XXVII(3): 210-228.

Bobbert, M. F. (1988). Vertical jumping - a study of muscle function and coordination. Doctoral Dissertation, University of Amsterdam.

Bobbert, M. F. and Bruin, E. D. (1994). Strength and coordination in vertical jumping and implications for training. In Blankevoort, L. and Kooloos, S.G.M. (Eds.) Abtracts, Volume II of the Second World Congress of Biomechanics. Nijmegan Netherlands (p. 133).

Bobbert, M. F., Huijing, P. A. and van Ingen Schenau, G. J. (1986). A model of the human triceps surae muscle-tendon complex applied to jumping. Journal of Biomechanics 19(11): 887-898.

Bobbert, M. F. and Schamhardt, H. C. (1990). Accuracy of determining the point of force application with piezoelectric force plates. Journal of Biomechanics 23(7): 705-710.

Bobbert, M. F. and van Ingen Schenau, G. J. (1988). Coordination in vertical jumping. Journal of Biomechanics 21(3): 249-462.

Bobbert, M. F. and van Zandwijk, J. P. (1999). Dynamics of force and muscle stimulation in human vertical jumping. Medicine and Science in Sports and Exercise 31(2): 3030-310.

Brooks, C. B. and Jacobs, A. M. (1975). The gamma mass scanning technique for inertial anthropometric measurement. Medicine and Science in Sports 7(4): 290-294.

Burden, A. and Bartlett, R. (1997). Electromyography. In Bartlett, R.(Ed.), Biomechanical analysis of movement in sport and exercise (pp. 37-52). BASES.

Casius, L. J. R. and van Soest, A. J. (1999). Parallel genetic algorithms fro optimisation in musculoskeletal modelling. In Proceedings of the VIIth International Symposium of Computer Simulation in Biomechanics, Calgary, Canada (pp. 5-7).

Cavagna, G. A., Dusman, B. and Margaria, R. (1968). Positive work done by a previously stretched muscle. Journal of Applied Physiology 24(1): 21-32.

Challis, J. H. (1991). Estimating individual muscle forces in human movement, Unpublished Doctoral Dissertation. Loughborough University.

Challis, J. H., Bartlett, R. and Yeadon, M. R. (1997). Low frequency image-based motion analysis. In Bartlett, R. (Ed.), Biomechanics analysis of movement in sports and exercise (pp. 7-30). BASES.

Challis, J. H. and Kerwin, D. G. (1992). Calculating upper limb inertial parameters. Journal of Sports Sciences 10(3): 275-284.

Chandler, R. F., Clauser, C. E., McConville, J. T., Reynolds, H. M. and Young, J. W. (1975). Investigation of inertial properties of the human body. AMRL-TR-74-137, AD-A016-484, DOT-HS-801-430. Aerospace Medical Research Laboratories, Wright-Patterson Air Force Base, OH.

Chao, E. Y. and Rim, K. (1973). Application of optimisation principles in determining the applied moments in human leg joints during gait. Journal of Biomechanics 6: 497-510.

Chapman, A. E. (1985). The mechanical properties of human muscle. Exercise and Sport Science Review 13: 443-501.

Clarys, J. P. (2000). Electromyography in sports and occupational settings: an update of its limits and possibilities. Ergonomics 43(10): 1750-1762.

Clarys, J. P. and Cabri, J. (1993). Electromyography and the study of sports movements: a review. Journal of Sports Sciences 11(5): 379-448.

Clarys, J. P. and Marfell-Jones, M. J. (1986). Anthropometric prediction of component tissue masses in the minor limb segments of the human body. Human Biology 58(5): 761-769.

Clarys, J. P., Martin, A. D. and Drinkwater, D. T. (1984). Gross tissue weights in the human body by cadaver dissection. Human Biology 56(3): 459-473.

Clauser, C. E., McConville, J. T. and Young, J. W. (1969). Weight, volume and center of mass of segments of the human body (AMRL TR 69-70). Dayton, OH: Wright-Patterson Air Force Base.

Cole, G. K., van den Bogert, A. J., Herzog, W. and Gerritsen, K. G. (1996). Modelling of force production in skeletal muscle undergoing stretch. Journal of Biomechanics 29(8): 1091-1104.

Corana, A., Marchesi, M., Martini, C. and Ridella, S. (1987). Minimising multimodal functions of continuous variables with the "simulated annealing" algorithm. ACM Transactions on Mathematical Software 13(3): 262-280.

Cross, R. (1999). Standing, walking, running and jumping on a force plate. American Journal of Physics 67(4): 304-309.

Dapena, J. (1980). Mechanics of translation in the fosbury-flop. Medicine and Science in Sports and Exercise 12(1): 37-44.

Dapena, J. (1988). Biomechanical analysis of the fosbury flop. Track Technique 104: 3307-3317;3333-3350.

Dapena, J. (1992). Biomechanical studies in the high jump and the implications to coaching. Track and Field Quarterly Review 92(2): 34-38.

Dapena, J. (1993). Biomechanical studies in the high jump and the implications to coaching. Modern Athlete and Coach 31(4): 7-12.

Dapena, J. (1996). A biomechanical scientific support program for high jumpers. In Abrantes, J.M.C.S. (Ed.), Abstracts of the International Society of Biomechanics in Sport (pp. 54-55).

Dapena, J. (1999). A biomechanical explanation of the effect of arm actions on the vertical velocity of a standing vertical jump. In Herzog, W. and Jinha, A. (eds.), Abstracts of the XVIIth International Society of Biomechanics Congress, Calgary, Canada (p. 100).

Dapena, J. and Chung, C. S. (1988). Vertical and radial motions of the body during the take-off phase of high jumping. Medicine and Science in Sports and Exercise 20(3): 290-302.

Dapena, J., McDonald, C. and Cappaert, J. (1990). A regression analysis of high jumping technique. International Journal of Sport Biomechanics 6(3): 246-261.

De Luca, C. J. (1997). The use of surface electrodes in biomechanics. Delsys Incorporated.

Dempster, W. T. (1955). Space requirements of the seated operator (WADC TR 55-159). Dayton, OH: Wright-Patterson Air Force Base.

Denoth, J., Gruber, K., Ruder, H. and Keppler, M. (1985). Forces and torques during sport activities with high accelerations. In Perren, S.M. and Schneider, E. (Eds.), Biomechanics: Current interdisciplinary research (pp. 663-668). Dordrect: Mertinus Nijhoff Publishers.

Dessureault, J. and Lafortune, M. A. (1981). Biomechanical features of two styles of high jumping. In Morecki, K., Fidelus, K., Kedzior, K. and Witt, A. (Eds.), Biomechanics VIIBA (pp. 264-276). Warsaw: Polish Human Kinetics.

De Zee, M. and Voigt, M. (2001). Moment dependency of the series elastic stiffness in the human plantar flexors measured in vivo. Journal of Biomechanics 34(11): 1399-1406.

Drillis, R., Contini, R. and Bluestein, M. (1964). Body segment parameters. Artificial Limbs 8: 44-66.

Dyson, G. (1977). The mechanics of athletics (7th Ed.). New York: Holmes and Meier.

Edman, K. A. (1976). Non-hyperbolic force-velocity relationship in single muscle fibres. Acta Physiologica Scandinavica 98: 143-156.

Edman, K. A. (1988). Double-hyperbolic force-velocity relation in frog muscle fibres. Journal of Physiology 404: 301-321.

Edman, K. A. (1992). Contractile performance of skeletal muscle fibres. In Komi, P. V. (Ed.), Strength and power in sport (pp.96-114). Oxford: Blackwell Science Ltd.

Elliott, B. C. and Chivers, L. (1988). A three dimensional cinematographic analysis of the penalty corner hit in field hockey. In de Groot, G., Hollander, A. P., Huijing, P. A., van Ingen Schenau, G. J. and Schenau, I (Eds.), Biomechanics XI-B. Amsterdam: Free University Press.

Elliott, B. C., Marsh, T. and Blanksby, B. (1986). A three-dimensional cinematographic analysis of the tennis serve. International Journal of Sport Biomechanics 2(4): 260-271.

Ettema, G. J. and Huijing, P. A. (1989). Properties of the tendinous structures and series elastic component of EDL muscle-tendon complex of the rat. Journal of Biomechanics 22(11-12): 1209-1215.

Fenn, W. O. and Marsh, B. S. (1935). Muscular force at three different speeds of shortening. Journal of Physiology 85: 277-297.

Freund, H. J. and Budingen, H. J. (1978). The relationship between speed and amplitude of the fastest contractions of human arm muscles. Experimental Brain Research 31(1): 1-12.

Froese, E. A. and Houston, M. E. (1985). Torque-velocity characteristics and muscle fiber type in human vastus lateralis. Journal of Applied Physiology 59(2): 309-314.

Fuller, N. J., Laskey, M. A. and Elia, M. (1992). Assessment of the composition of major body regions by dual-energy X-ray absorptiometry (DEXA), with special reference to limb muscle mass. Clinical Physiology 12: 253-266.

Gerritsen, K. G., van den Bogert, A. J. and Nigg, B. M. (1995). Direct dynamics simulation of the impact phase in heel-toe running. Journal of Biomechanics 28(6): 661-668.

Gilchrist, L. A. and Winter, D. A. (1996). A two-part, viscoelastic foot model for use in gait simulations. Journal of Biomechanics 29(6): 795-798.

Goffe, W. L., Ferrier, G. D. and Rogers, J. (1994). Global optimisation of statistical functions with simulated annealing. Journal of Econometrics 60: 65-99.

Greig, M. P. and Yeadon, M. R. (2000). The influence of touchdown parameters on the performance of a high jumper. Journal of Applied Biomechanics 16(4): 367-378.

Grieve, D. W. (1975). Techniques for the analysis of human movement. Lepus Books.

Gruber, K., Ruder, H., Denoth, J. and Schneider, K. (1998). A comparative study of impact dynamics: wobbling mass model versus rigid body models. Journal of Biomechanics 31(5): 439-444.

Gruen, A. (1997). Fundamentals of videogrammetry - A review. Human Movement Science 16: 155-187.

Hall, M. G., Flemming, H. E., Dolan, M. J., Millbank, S. F. D. and Paul, J. P. (1996). Static in situ calibration of force plates. Journal of Biomechanics 29(5): 659-665.

Harman, E. A., Rosenstein, M. T., Frykman, P. N. and Rosenstein, R. M. (1990). The effect of arms and countermovement on vertical jumping. Medicine and Science in Sports and Exercise 22(6): 825-833.

Harris, C. M. and Wolpert, D. M. (1998). Signal-dependent noise determines motor planning. Nature 394(20): 780-784.

Harry, J. D., Ward, A. W., Heglund, N. C., Morgan, D. L. and McMahon, T. A. (1990). Cross-bridge cycling theories cannot explain high-speed lengthening behaviour in frog muscle. Biophysical Journal 57: 201-208.

Hatze, H. (1980). A mathematical model for the computational determination of parameter values of anthropometric segments. Journal of Biomechanics 13: 833-843.

Hatze, H. (1981). A comprehensive model for human motion simulation and it's application to the take-off phase of the long jump. Journal of Biomechanics 14(3): 135-142.

Hay, J. G. (1975). Biomechanical aspects of jumping. Exercise and Sport Science Review 3: 135-161.

Hay, J. G. (1981). Fundamental mechanics of jumping. In Gambetta, V.(ed.), Track and field coaching manual (pp. 148-154). New York: Leisure Press.

Hay, J. G. (1985). Issues in sports biomechanics. In Perren, S. M. and Schneider, E. (Eds.), Biomechanics: Current interdisciplinary research (pp. 49-60). Dordrecht: Martinus Nijhoff Publishers.

Hay, J. G., Miller, J. A. and Canterna, R. W. (1986). The techniques of elite male long jumpers. Journal of Biomechanics 19(10): 855-866.

Hay, J. G. and Nohara, H. (1990). Techniques used by male long jumpers in preparation for takeoff. Journal of Biomechanics 23(3): 229-239.

Herzog, W. (1988). The relation between the resultant moments at a joint and the moments measured by an isokinetic dynamometer. Journal of Biomechanics 21(1): 5-12.

Herzog, W. (2000). Mechanical properties and performance in skeletal muscles. In Zatsiorsky, V. (Ed.), Biomechanics in sport (pp. 21-32). Oxford: Blackwell Science Ltd.

Hicks, C. R. (1982). Fundamental concepts in the design of experiments. New York: Holt, Rinehart and Winston.

Hill, A. V. (1938). The heat of shortening and the dynamic constants of muscle. Proceedings of the Royal Society Series B 126: 136-195.

Hinrichs, R. N. (1975). Regression equations to predict segmental moments of inertia from anthropometric measurements: An extension of the data of Chandler et al. Journal of Biomechanics 18(8): 621-624.

Hof, A. L. (1998). In vivo measurement of the series elastic elasticity release curve of human triceps surae muscle. Journal of Biomechanics 31: 793-800.

Hubbard, M. (1993). Computer simulation in sport and industry. Journal of Biomechanics 26 Supplement 1: 53-61.

Huxley, A. F. (1957). Muscle structure and theories of contraction. Progress in Biophysics and Biophysical chemistry 7: 225-318.

IAAF (1990). Scientific research project at the games of the XXIVth Olympiad., Seoul.

Iossifidou, A. N. and Baltzopoulos, V. (1998). Inertial effects on the assessment of performance in isokinetic dynamometry. International Journal of Sports Medicine 19: 567-573.

Jacobs, R., Bobbert, M. F. and van Ingen Schenau, G. J. (1996). Mechanical output from individual muscles during explosive leg extensions: The role of biarticular muscles. Journal of Biomechanics 29(4): 513-523.

Jacoby, E. and Fraley, B. (1995). Complete book of jumps. Leeds: Human Kinetics.

James, C., Sacco, P., Hurley, M. V. and Jones, D. A. (1994). An evaluation of different protocols for measuring the force-velocity relationship of the human quadriceps muscle. European Journal of Applied Physiology 68(1): 41-47.

John, J. A. and Quenouille, M. H. (1977). Experiments: Design and analysis. London: Griffin.

Johnson, M. D. and Buckley, J. G. (2001). Muscle power patterns in the mid-acceleration phase of sprinting. Journal of Sports Sciences 19(4): 263-272.

Kane, T. R. and Levinson, D. A. (1996). Dynamics online: Theory and implementations with AUTOLEV. Sunnyvale: Online Dynamics Inc.

Karara, H. M. (1980). Non-metric cameras. In Aktinson, K. B. (Ed.), Developments in close range photogrammetry –1 (pp. 63-80). London: Applied Science Publishers.

Katz, B. (1939). The relation between force and speed in muscular contraction. Journal of Physiology 96: 45-64.

Kerwin, D. G. (1995). Apex / Target high resolution video digitising system. In Proceedings of the Biomechanics Section (pp. 1-4). Leeds Metropolitan University, BASES.

Kerwin, D. G. (1997). Force plate analyses of human jumping. Unpublished Doctoral Thesis, Loughborough University.

King, M. A. (1998). Contributions to performance in dynamic jumps. Unpublished Doctoral Thesis, Loughborough University.

King, M. A. and Yeadon, M. R. (2002). Determining subject-specific torque parameters for use in a torque-driven simulation model of dynamic jumping. Journal of Applied Biomechanics 18(3): 207-217.

Koh, T. J. and Hay, J. G. (1990). Landing leg motion and performance in the horizontal jumps I: The long jump. International Journal of Sport Biomechanics 6: 343-360.

Krazhev, V. D., Strizhah, A. P., Popov, G. I. and Bobrovnik, V. I. (1990). A biomechanical analysis of the technique of the world's top female high jumpers. Soviet Sports Review 25(2): 64-65.

Lease, D. (1994). Field athletics. London: Blandford.

Lees, A., Graham-Smith, P. and Fowler, N. (1994). A biomechanical analysis of the last stride, touchdown, and take-off characteristics of the women's long jump. Journal of Applied Biomechanics 10: 61-78.

Lieber, R. L. (1992). Skeletal muscle structure and function: Implications for rehabilitation and sports medicine. Baltimore, Md: Williams and Wilkins.

Linthorne, N. P. and Kemble, B. A. (1998). Take-off technique in the high jump. In Proceedings of the XVI International Symposium on Biomechanics in Sport, Konstanz, Germany (pp. 356-359).

Maganaris, C. N. and Paul, J. P. (2002). Tensile properties of the in vivo human gastrocnemius tendon. Journal of Biomechanics 35(12): 1639-1646.

Miller, D. I. (1979). Modelling in biomechanics: An overview. Medicine and Science in Sports 11(2): 115-122.

Misevich, K. W. and Cavagna, P. R. (1984). Material aspects of modelling shoe/foot interaction. In Fredrick, E. C. (Ed.), Sport and playing surfaces (pp. 47-75). Champaign: Human Kinetics.

Mungiole, M. and Martin, P. E. (1990). Estimating segment inertial properties: Comparison of magnetic resonance imaging with existing methods. Journal of Biomechanics 23(10): 1039-1046.

Muramatsu, T., Muraoka, T., Takeshita, D., Kawakami, Y., Hirano, Y. and Fukunaga, T. (2001). Mechanical properties of tendon and aponeurosis of human gastrocnemius muscle in vivo. Journal of Applied Physiology 90: 1671-1678.

Muraoka, T., Kawakami, Y., Tachi, M. and Fukunaga, T. (2001). Muscle fiber and tendon length changes in the human vastus lateralis during slow pedaling. Journal of Applied Physiology 91: 2035-2040.

Nagano, A. and Gerritsen, K. G. (2001). Effects of neuromuscular strength training on vertical jumping performance - A computer simulation study. Journal of Applied Biomechanics 17(2): 113-128.

Nagano, A., Gerritsen, K. G. and Fukashiro, S. (2000). A sensitivity analysis of the calculation of mechanical output through inverse dynamics: a computer simulation study. Journal of Biomechanics 33(10): 1313-1318.

Nelder, J. A. and Mead, R. (1965). A simplex method for function minimization. Computer Journal 7: 308-313.

Nigg, B. M. (1999). Mathematically determinate systems. In Nigg, B. M. and Herzog, W.(Eds.), Biomechanics of the musculo-skeletal system (pp. 458-532). Chichester: John Wiley and Sons Ltd.

Nigg, B. M., Cole, G. K. and Bruggeman, G. P. (1995). Impact forces during heel toe running. Journal of Applied Biomechanics 11(4): 407-432.

Nigg, B. M. and Liu, W. (1999). The effect of muscle stiffness and damping on simulated impact force peaks during running. Journal of Biomechanics 32(8): 849-856.

O'Connor, B. J., Yack, H. J. and White, S. C. (1995). Reducing errors in kinetic calculations: Improved synchronisation of video and ground reaction force records. Journal of Applied Biomechanics 11(2): 216-223.

Pain, M. T. G. (1999). An analysis of human soft tissue. Unpublished Doctoral Thesis, Penn State University.

Pain, M. T. G. and Challis, J. H. (2001). The role of the heel pad and shank soft tissue during impacts: a further resolution of a paradox. Journal of Biomechanics 34: 327-333.

Pandy, M. G. and Zajac, F. E. (1991). Optimal muscular coordination strategies for jumping. Journal of Biomechanics 24(1): 1-10.

Pandy, M. G., Zajac, F. E., Sim, E. and Levine, W. S. (1990). An optimal control model for maximum-height human jumping. Journal of Biomechanics 23(12): 1185-1198.

Pearsall, D. J. and Reid, J. G. (1994). The study of human body segment parameters in biomechanics. Sports Medicine 18(2): 126-140.

Pierrynowski, M. R. (1995). In Allard, P., Stokes, I. A. F. and Blanchi, J. (Eds.), Three-dimensional analysis of human movement. Champaign: Human Kinetics.

Press, W. H., Flannery, B. P., Teukolsky, S. A. and Vetterling, W. T. (1986). Numerical recipes: The art of scientific programming. Cambridge: Cambridge University Press.

Richards, J. G. (1999). The measurement of human motion: A comparison of commercially available systems. Human Movement Science 18: 589-602.

Ridderikhoff, A., Batelaan, J. H. and Bobbert, M. F. (1999). Jumping for distance: Control of the external force in squat jumps. Medicine and Science in Sports and Exercise 31(8): 1196-1204.

Roubenoff, R., Kehayias, J. J., Dawson-Hughs, B. and Heymsfield, S. B. (1993). Use of dual-energy x-ray absorpiometry in body-composition studies: Not yet a "gold standard". American Journal of Clinical Nutrition 58: 589-591.

Sapega, A. A., Nicholas, J. A., Sokolow, D. and Saranti, A. (1982). The nature of torque "overshoot" in Cybex isokinetic dynamometry. Medicine and Science in Sports and Exercise 14(5): 368-375.

Schaechter, D. B., Levinson, D. A. and Kane, T. R. (1991). Autolev User's Manual (Version 2). Sunnyvale, CA: Online Dynamics Inc.

Schutte, L. and Risher, D. (1994). An inverse dynamics approach to dynamic optimisation: Applications to a trajectory matching problem. In proceedings of the

Eighth Biennial Conference, Canadian Society of Biomechanics, Calgary (pp. 210-211).

Shorten, M.R. (1987). Muscle elasticity and human performance. Medicine and Sports Science 25: 1-8.

Sorenson, H., Simonsen, E. B. and van den Bogert, A. J. (1999). A simulation model of the long jump takeoff. In Proceedings of the VIIth International Symposium on Computer Simulation in Biomechanics, Calgary, Canada (pp.34-37).

Tan, J. (1997). The mechanics of the curved approach in high jumping. Unpublished Doctoral Thesis, Loughborough University.

Taylor, N. A. S., Sanders, R. H., Howick, E. I. and Stanley, S. N. (1991). Static and dynamic assessment of the Biodex dynamometer. European Journal of Applied Physiology 62: 180-188.

Teel, B. (1981). The long jump. In Gambetta, V. (Ed.), Track and field coaching manual (pp. 155-165). New York: Leisure Press.

van den Bogert, A. J. and Nigg, B. M. (1999). Simulation. In Nigg, B. M. and Herzog, W. (Eds.), Biomechanics of the musculo-skeletal system (pp. 594-616). Chichester: John Wiley & Sons Ltd.

Van Ghelwe, B. (1981). A biomechanical simulation model for airbourne twist in backward somersaults. Journal of Human Movement Studies 7: 1-22.

van Soest, A. J. (1992). Jumping from structure to control - A simulation study of explosive movements. Doctoral Dissertation, University of Amsterdam.

van Soest, A. J., Schwab, A. L., Bobbert, M. F. and van Ingen Schenau, G. J. (1993). The influence of the biarticularity of the gastrocnemius muscle on vertical-jumping achievement. Journal of Biomechanics 26(1): 1-8.

Vaughan, C. L. (1984). Computer simulation of human motion in sports biomechanics. Exercise and Sport Science Review 12: 373-416.

Vaughan, C. L. (1989). Biomechanics in sport. Boca Raton: CRC Press.

Ward-Smith, A. J. (1983). The influence of aerodynamic and biomechanical factors on long jump performance. Journal of Biomechanics 16(8): 655-658.

Ward-Smith, A. J. (1984). Calculation of long jump performance by numerical integration of the equation of motion. Journal of Biomechanical Engineering 106(3): 244-248.

Westing, S. H., Seger, J. Y., Karlson, E. and Ekblom, B. (1988). Eccentric and concentric torque-velocity characteristics of the quadriceps femoris in man. European Journal of Applied Physiology 58(1-2): 100-104.

Westing, S. H., Seger, J. Y. and Thorstensson, A. (1990). Effects of electrical stimulation on eccentric and concentric torque-velocity relationships during knee extension in man. Acta Physiologica Scandinavica 140(1): 17-22.

Wilkie, D. R. (1968). Muscle. London: Edward Arnold Ltd.

Williams, M. and Lissner, H. R. (1977). Biomechanics of human motion. Saunders.

Winter, D. A. (1990). Biomechanics and motor control of human movement. New York: John Wiley & Sons, Inc.

Winter, D. A., Wells, R. P. and Orr, G. W. (1981). Errors in the use of isokinetic dynamometers. European Journal of Applied Physiology and Occupational Physiology 46(4): 397-408.

Winters, J. M. (1995). How detailed should muscle models be to understand multi-joint movement coordination. Human Movement Science 14: 401-442.

Wood, G. A. and Jennings, L. S. (1979). On the use of spline functions for data smoothing. Journal of Biomechanics 12: 447-479.

Yeadon, M. R. (1989). A method for obtaining three-dimensional data on ski jumping using pan and tilt cameras. International Journal of Sport Biomechanics 5(2): 238-247.

Yeadon, M. R. (1990a). The simulation of aerial movement-I. The determination of orientation angles from film data. Journal of Biomechanics 23(1): 59-66.

Yeadon, M. R. (1990b). The simulation of aerial movement-II. A mathematical inertia model of the human body. Journal of Biomechanics 23(1): 67-74.

Yeadon, M. R. (1990c). The simulation of aerial movement-III. The determination of the angular momentum of the human body. Journal of Biomechanics 23(1): 75-83.

Yeadon, M. R., Atha, J. and Hales, F. D. (1990d). The simulation of aerial movement-IV. A computer simulation model. Journal of Biomechanics 23(1): 85-89.

Yeadon, M. R. and Challis, J. H. (1994). The future of performance-related sports biomechanics research. Journal of Sports Sciences 12(1): 3-32.

Yeadon, M. R., Challis, J. H. and Ng, R. (1993). Personalised segmental inertia parameters. In Proceedings of the XIVth International Society of Biomechanics Congress, Paris, France (pp. 1494-1495).

Yeadon, M. R. and Hiley, M. J. (2000). The mechanics of the backward giant circle on the high bar. Human Movement Science 19: 153-173.

Yeadon, M. R. and King, M. A. (1999). A method for synchronising digitised video data. Journal of Biomechanics 32(9): 983-986.

Yeadon, M. R. and King, M. A. (2002). Evaluation of a torque-driven simulation model of tumbling. Journal of Applied Biomechanics 18(3): 195-206.

Yeadon, M. R. and Morlock, M. (1989). The appropriate use of regression equations for the estimation of segmental inertia parameters. Journal of Biomechanics 22(6/7): 683-689.

Zatsiorsky, V. and Seluyanov, V. (1983). The mass and inertia characteristics of the main segments of the human body. In Matsui, H. and Kobayashi, K. (Eds.), Biomechanics VIII-B (pp. 1152-1159). Champaign: Human Kinetics.

APPENDIX 1

SIMULATION MODELS DEVELOPED USING AUTOLEV

Appendix 1a Autolev commands used for the two-segment model of jumping

Appendix 1b Autolev commands used for the eight-segment angle-driven model

Appendix 1c Autolev commands used for the eight-segment torque-driven model

Appendix 1a

Autolev commands used for the two-segment model of jumping

```
% 2 SEGMENT MODEL OF JUMPING
%TWO SEGMENTS USED TO REPRESENT THE LEG
%FORWARD DYNAMICS MODEL WITH TORQUE GENERATOR
%
%-------------------------
%Physical declarations
NEWTONIAN N
FRAMES A
BODIES B,C
POINTS O,P1,P2,CM
PARTICLES P3
%
%---------------------------------
%Mathematical Declarations
MASS B=MB, C=MC, P3=MP3
INERTIA B, 0,IB,IB
INERTIA C, 0,IC,IC
VARIABLES U{4}'
VARIABLES Q1',Q2',Q3',Q4'
VARIABLES RX,RY
VARIABLES KANG, KANGVEL, TOR1
CONSTANTS KNETOR, HILL, KANGVELMAX
CONSTANTS L{4}
CONSTANTS K{4}
CONSTANTS G
%
%---------------------------------
%Geometry relating unit vectors
SIMPROT(N,B,3,Q3)
SIMPROT(N,C,3,Q4)
%
%---------------------------------
%Position Vectors
P_O_P1>=Q1*N1> + Q2*N2>
P_P1_BO>=L1*B1>
P_P1_P2>=L2*B1>
P_P2_CO>=L3*C1>
P_P2_P3>=L4*C1>
%Position of points relative to O
P_O_BO>=P_O_P1>+P_P1_BO>
P_O_P2>=P_O_P1>+P_P1_P2>
P_O_CO>=P_O_P2>+P_P2_CO>
P_O_P3>=P_O_P2>+P_P2_P3>
%
%---------------------------------
%Position of points in x-y coordinates
POP1X=DOT(P_O_P1>,N1>)
POP1Y=DOT(P_O_P1>,N2>)
POP2X=DOT(P_O_P2>,N1>)
POP2Y=DOT(P_O_P2>,N2>)
POP3X=DOT(P_O_P3>,N1>)
POP3Y=DOT(P_O_P3>,N2>)
```

```
%
%--------------------------------
%Position vector of the bodies b and c from o
P_O_CM>=CM(O)
POCMX=DOT(P_O_CM>,N1>)
POCMY=DOT(P_O_CM>,N2>)
%
%--------------------------------
%Kinematical differential equations
Q1'=U1
Q2'=U2
Q3'=U3
Q4'=U4
%
%Angular velocities and accelerations
W_B_N>=Q3'*N3>
W_C_N>=Q4'*N3>
ALF_B_N>=DT(W_B_N>,N)
ALF_C_N>=DT(W_C_N>,N)
%
%--------------------------------
%Linear velocities and accelerations
V_O_N>=0>
V_P1_N>=DT(P_O_P1>,N)
V_BO_N>=DT(P_O_BO>,N)
V_P2_N>=DT(P_O_P2>,N)
V_CO_N>=DT(P_O_CO>,N)
V_P3_N>=DT(P_O_P3>,N)
V_CM_N>=DT(P_O_CM>,N)
VOCMX=DOT(V_CM_N>,N1>)
VOCMY=DOT(V_CM_N>,N2>)
%
A_O_N>=0>
A_P1_N>=DT(V_P1_N>,N)
A_BO_N>=DT(V_BO_N>,N)
A_P2_N>=DT(V_P2_N>,N)
A_CO_N>=DT(V_CO_N>,N)
A_P3_N>=DT(V_P3_N>,N)
%
%--------------------------------
%Joint angles
KANG=180+Q3-Q4
KANGVEL=U3-U4
%
%--------------------------------
%Generalised forces (gravity, extensor torques)
TOR1=T*KNETOR*HILL*KANGVELMAX
TORQUE(C/B,TOR1*B3>)
GRAVITY(G*N2>)
RX=-K1*Q1-K2*U1
RY=-K3*Q2-K4*U2
FORCE(P1,RX*N1>+RY*N2>)
%
%--------------------------------
%Equations of motion
ZERO = FR() + FRSTAR()
KANE()
%
%--------------------------------
%Inputs
```

```
INPUT TINITIAL=0.0, TFINAL=5.0, INTEGSTP=0.001
INPUT ABSERR=1.0E-08, RELERR=1.0E-07
INPUT L1=0.25, L2=0.5, L3=0.25, L4=0.5
INPUT IB=10.0, IC=10.0, MB=1, MC=1, MP3=68
INPUT G=-9.81
INPUT KNETOR=1000, HILL=3, KANGVELMAX=35
%
%------------------------------
%OUTPUT
OUTPUT T, POP1X, POP1Y, POP2X, POP2Y, POP3X, POP3Y
OUTPUT T, Q1, U1, Q2, U2, Q3, U3, Q4, U4, KANG, KANGVEL, VOCMX, VOCMY
OUTPUT T, RX, RY
%
%------------------------------
%Units
UNITS L1=M, L2=M, L3=M, L4=M
UNITS POP1X=M, POP1Y=M, POP2X=M, POP2Y=M, POP3X=M, POP3Y=M
UNITS Q1=M, Q2=M, Q3=DEG, Q4=DEG, U1=M/S, U2=M/S
UNITS U3=DEG/S, U4=DEG/S
UNITS IB=KG.M^2, IC=KG.M^2, MB=KG, MC=KG, MP3=KG, T=S, G=M/S^2
UNITS KANG=DEG, KANGVEL=DEG/S, KNETOR=N.M, KANGVELMAX=DEG/S
%
CODE DYNAMICS() C:\AL\CASSIE\JUMP2SEG.FOR, SUBS
```

Appendix 1b

Autolev commands used for the eight-segment angle-driven model

```
% INVDYN.AL
% 8 SEGMENT MODEL OF JUMPING
% CONTAINS WOBBLING MASSES AT THE SHANK,THIGH AND TRUNK
% FORWARD DYNAMICS MODEL WHICH CALCULATES JOINT TORQUE
%Physical declarations
NEWTONIAN N
BODIES A,B,C,D,E,F,G,H,I,J,K
POINTS O,P1,P2,P3,P4,P5,P6,P7,P8,P9,P10,P11,P12,P13,P14,P15,P16,PW1,PW2,PW3,PW4,
PW5,PW6,CM
%
%--------------------------------
%Mathematical Declarations
%length constraints: L1 is length to from O to segment 1 CM, L2 is the length
%from O to the other end of segment 1 etc
%lengths are calculated from human anthropometrics
%9 generalised coordinates/speeds
MASS A=MA, B=MB, C=MC, D=MD, E=ME, F=MF, G=MG, H=MH, I=MI, J=MJ, K=MK
INERTIA A, 0,0,IA
INERTIA B, 0,0,IB
INERTIA C, 0,0,IC
INERTIA D, 0,0,ID
INERTIA E, 0,0,IE
INERTIA F, 0,0,IF
INERTIA G, 0,0,IG
INERTIA H, 0,0,IH
INERTIA I, 0,0,II
INERTIA J, 0,0,IJ
INERTIA K, 0,0,IK
VARIABLES U{19}'
VARIABLES Q1',Q2', Q3', Q4',Q5',Q6',Q7',Q8',Q9',Q10',Q11',Q12'
VARIABLES RX,RY,RX1,RY1,SWM1X,SWM1Y,SWM2X,SWM2Y,SWM3X,SWM3Y,
SWM4X,SWM4Y,SWM5X,SWM6X,SWM6Y
VARIABLES POP1X,POP1Y,POP2X,POP2Y,POP3X,POP3Y,POP4X,POP4Y,POP5X,POP5Y
VARIABLES POP6X,POP6Y,POP7X,POP7Y,POP8X,POP8Y,POP9X,POP9Y,POP10X,POP10Y
VARIABLES POP11X,POP11Y,POP12X,POP12Y,POP13X,POP13Y,POP14X,POP14Y,
POP15X,POP15Y,POP16X,POP16Y
VARIABLES POPW1X,POPW1Y,POPW2X,POPW2Y,POPW3X,POPW3Y,POPW4X,POPW4Y
,POPW5X,POPW5Y,POPW6X,POPW6Y
VARIABLES VOP1X,VOP1Y,VOP2X,VOP2Y,VOP3X,VOP3Y,VOP4X,VOP4Y,VOP5X,
VOP5Y
VARIABLES VOP6X,VOP6Y,VOP7X,VOP7Y,VOP8X,VOP8Y,VOP9X,VOP9Y,VOP10X,
VOP10Y
VARIABLES VOP11X,VOP11Y,VOP12X,VOP12Y,VOP13X,VOP13Y,VOP14X,VOP14Y,
VOP15X,VOP15Y,VOP16X,VOP16Y
VARIABLES VOPW1X,VOPW1Y,VOPW2X,VOPW2Y,VOPW3X,VOPW3Y,VOPW4X,
VOPW4Y,VOPW5X,VOPW5Y,VOPW6X,VOPW6Y
VARIABLES POCMX,POCMY,VOCMX,VOCMY
VARIABLES ANKANG,KNEANG,HIPANG,SHRANG,ELBANG,RHIPANG,RKNEANG
VARIABLES ANKW,KNEW,HIPW,SHRW,ELBW,RHIPW,RKNEW
VARIABLES TORANK,TORKNE,TORHIP,TORSHR,TORRHIP,TORELB,TORRKNE
VARIABLES KECM,KEA,KEB,KEC,KED,KEE,KEF,KEG,KEH,KEI,KEJ,KEK
VARIABLES PECM,PEA,PEB,PEC,PED,PEE,PEF,PEG,PEH,PEI,PEJ,PEK
```

```
VARIABLES PANK,PKNE,PHIP,PSHR,PRHIP
VARIABLES XMOM,YMOM,ZAMOM
CONSTANTS L{31}
CONSTANTS K{16}
CONSTANTS G,TOTMASS,HEIGHT
CONSTANTS R1, R2, R3, R4, R5, R6, R7
SPECIFIED AAB", ABC", ACD", ADE", AEF", ADG", AGH"
AAB = R1 + (R1*T^2)
ABC = R2 + (R2*T^2)
ACD = R3 + (R3*T^2)
ADE = R4 + (R4*T^2)
AEF = R5 + (R5*T^2)
ADG = R6 + (R6*T^2)
AGH = R7 + (R7*T^2)
%
ZEE_NOT = [TORANK, TORKNE, TORHIP, TORSHR, TORELB, TORRHIP, TORRKNE]
%--------------------------------
%
%Geometry relating unit vectors
SIMPROT(N,D,3,Q3)
SIMPROT(A,B,3,PI-AAB)
SIMPROT(B,C,3,ABC-PI)
SIMPROT(C,D,3,PI-ACD)
SIMPROT(D,E,3,PI-ADE)
SIMPROT(E,F,3,AEF-PI)
SIMPROT(G,D,3,2*PI-ADG)
SIMPROT(H,G,3,AGH-PI)
SIMPROT(B,I,3,Q4)
SIMPROT(C,J,3,Q7)
SIMPROT(D,K,3,Q10)
%
%--------------------------------
%Position Vectors
P_O_P1>=Q1*N1> + Q2*N2>
P_P1_AO>=L4*A1> + L5*A2>
P_P1_P2>=L2*A1>
P_P1_P3>=L1*A1> + L3*A2>
P_P3_BO>=L6*B1>
P_P3_P4>=L7*B1>
P_P4_CO>=L8*C1>
P_P4_P5>=L9*C1>
P_P5_DO>=L10*D1>
P_P5_P6>=L11*D1>
P_P6_EO>=L12*E1>
P_P6_P7>=L13*E1>
P_P7_FO>=L14*F1>
P_P7_P8>=L15*F1>
P_P5_GO>=L16*G1>
P_P5_P9>=L17*G1>
P_P9_HO>=L18*H1>
P_P9_P10>=L19*H1>
%
%Wobbling mass positions
%
P_P3_P11>=L20*B1>
P_P3_P12>=L21*B1>
P_P11_P12>=(L21-L20)*B1>
P_P11_PW1>=Q5*N1>+Q6*N2>
P_PW1_IO>=L22*I1>
P_PW1_PW2>=L23*I1>
```

```
%
P_P4_P13>=L24*C1>
P_P4_P14>=L25*C1>
P_P13_P14>=(L25-L24)*C1>
P_P13_PW3>=Q8*N1>+Q9*N2>
P_PW3_JO>=L26*J1>
P_PW3_PW4>=L27*J1>
%
P_P5_P15>=L28*D1>
P_P5_P16>=L29*D1>
P_P15_P16>=(L29-L28)*D1>
P_P15_PW5>=Q11*N1>+Q12*N2>
P_PW5_KO>=L30*K1>
P_PW5_PW6>=L31*K1>
%
%Position of points relative to O
P_O_AO>=P_O_P1>+P_P1_AO>
P_O_P2>=P_O_P1>+P_P1_P2>
P_O_P3>=P_O_P1>+P_P1_P3>
P_O_BO>=P_O_P3>+P_P3_BO>
P_O_P4>=P_O_P3>+P_P3_P4>
P_O_CO>=P_O_P4>+P_P4_CO>
P_O_P5>=P_O_P4>+P_P4_P5>
P_O_DO>=P_O_P5>+P_P5_DO>
P_O_P6>=P_O_P5>+P_P5_P6>
P_O_EO>=P_O_P6>+P_P6_EO>
P_O_P7>=P_O_P6>+P_P6_P7>
P_O_FO>=P_O_P7>+P_P7_FO>
P_O_P8>=P_O_P7>+P_P7_P8>
P_O_GO>=P_O_P5>+P_P5_GO>
P_O_P9>=P_O_P5>+P_P5_P9>
P_O_HO>=P_O_P9>+P_P9_HO>
P_O_P10>=P_O_P9>+P_P9_P10>
P_O_P11>=P_O_P3>+P_P3_P11>
P_O_P12>=P_O_P3>+P_P3_P12>
P_O_PW1>=P_O_P11>+P_P11_PW1>
P_O_PW2>=P_O_PW1>+P_PW1_PW2>
P_O_IO>=P_O_PW1>+P_PW1_IO>
P_O_P13>=P_O_P4>+P_P4_P13>
P_O_P14>=P_O_P4>+P_P4_P14>
P_O_PW3>=P_O_P13>+P_P13_PW3>
P_O_PW4>=P_O_PW3>+P_PW3_PW4>
P_O_JO>=P_O_PW3>+P_PW3_JO>
P_O_P15>=P_O_P5>+P_P5_P15>
P_O_P16>=P_O_P5>+P_P5_P16>
P_O_PW5>=P_O_P15>+P_P15_PW5>
P_O_PW6>=P_O_PW5>+P_PW5_PW6>
P_O_KO>=P_O_PW5>+P_PW5_KO>
%---------------------------------
%Position of points in x-y coordinates
POP1X=DOT(P_O_P1>,N1>)
POP1Y=DOT(P_O_P1>,N2>)
POP2X=DOT(P_O_P2>,N1>)
POP2Y=DOT(P_O_P2>,N2>)
POP3X=DOT(P_O_P3>,N1>)
POP3Y=DOT(P_O_P3>,N2>)
POP4X=DOT(P_O_P4>,N1>)
POP4Y=DOT(P_O_P4>,N2>)
POP5X=DOT(P_O_P5>,N1>)
POP5Y=DOT(P_O_P5>,N2>)
```

```
POP6X=DOT(P_O_P6>,N1>)
POP6Y=DOT(P_O_P6>,N2>)
POP7X=DOT(P_O_P7>,N1>)
POP7Y=DOT(P_O_P7>,N2>)
POP8X=DOT(P_O_P8>,N1>)
POP8Y=DOT(P_O_P8>,N2>)
POP9X=DOT(P_O_P9>,N1>)
POP9Y=DOT(P_O_P9>,N2>)
POP10X=DOT(P_O_P10>,N1>)
POP10Y=DOT(P_O_P10>,N2>)
POP11X=DOT(P_O_P11>,N1>)
POP11Y=DOT(P_O_P11>,N2>)
POP12X=DOT(P_O_P12>,N1>)
POP12Y=DOT(P_O_P12>,N2>)
POP13X=DOT(P_O_P13>,N1>)
POP13Y=DOT(P_O_P13>,N2>)
POP14X=DOT(P_O_P14>,N1>)
POP14Y=DOT(P_O_P14>,N2>)
POP15X=DOT(P_O_P15>,N1>)
POP15Y=DOT(P_O_P15>,N2>)
POP16X=DOT(P_O_P16>,N1>)
POP16Y=DOT(P_O_P16>,N2>)
%Of wobbling masses
POPW1X=DOT(P_O_PW1>,N1>)
POPW1Y=DOT(P_O_PW1>,N2>)
POPW2X=DOT(P_O_PW2>,N1>)
POPW2Y=DOT(P_O_PW2>,N2>)
POPW3X=DOT(P_O_PW3>,N1>)
POPW3Y=DOT(P_O_PW3>,N2>)
POPW4X=DOT(P_O_PW4>,N1>)
POPW4Y=DOT(P_O_PW4>,N2>)
POPW5X=DOT(P_O_PW5>,N1>)
POPW5Y=DOT(P_O_PW5>,N2>)
POPW6X=DOT(P_O_PW6>,N1>)
POPW6Y=DOT(P_O_PW6>,N2>)

%
POAOX=DOT(P_O_AO>,N1>)
POAOY=DOT(P_O_AO>,N2>)
POBOX=DOT(P_O_BO>,N1>)
POBOY=DOT(P_O_BO>,N2>)
POCOX=DOT(P_O_CO>,N1>)
POCOY=DOT(P_O_CO>,N2>)
PODOX=DOT(P_O_DO>,N1>)
PODOY=DOT(P_O_DO>,N2>)
POEOX=DOT(P_O_EO>,N1>)
POEOY=DOT(P_O_EO>,N2>)
POFOX=DOT(P_O_FO>,N1>)
POFOY=DOT(P_O_FO>,N2>)
POGOX=DOT(P_O_GO>,N1>)
POGOY=DOT(P_O_GO>,N2>)
POHOX=DOT(P_O_HO>,N1>)
POHOY=DOT(P_O_HO>,N2>)
POIOX=DOT(P_O_IO>,N1>)
POIOY=DOT(P_O_IO>,N2>)
POJOX=DOT(P_O_JO>,N1>)
POJOY=DOT(P_O_JO>,N2>)
POKOX=DOT(P_O_KO>,N1>)
POKOY=DOT(P_O_KO>,N2>)
%
```

```
%--------------------------------
%Position vector of the bodies b and c from o
P_O_CM>=CM(O)
POCMX=DOT(P_O_CM>,N1>)
POCMY=DOT(P_O_CM>,N2>)
%
%--------------------------------
%Kinematical differential equations
Q1'=U1
Q2'=U2
Q3'=U3
Q4'=U4
Q5'=U5
Q6'=U6
Q7'=U7
Q8'=U8
Q9'=U9
Q10'=U10
Q11'=U11
Q12'=U12
%
%Angular velocities and accelerations
W_D_N>=Q3'*N3>
W_A_B>=AAB'*N3>
W_C_B>=ABC'*N3>
W_C_D>=ACD'*N3>
W_D_E>=ADE'*N3>
W_F_E>=AEF'*N3>
W_G_D>=ADG'*N3>
W_G_H>=AGH'*N3>
W_I_B>=Q4'*N3>
W_J_C>=Q7'*N3>
W_K_D>=Q10'*N3>
%
%Use generalised speeds u13,U14,15,U16,U17,U18 and u19 to produce measure numbers
%for the joint torques
%
W_A_B> = W_A_B> + U13*B3>
W_C_B> = W_C_B> + U14*C3>
W_C_D> = W_C_D> + U15*D3>
W_D_E> = W_D_E> + U16*E3>
W_F_E> = W_F_E> + U17*F3>
W_G_D> = W_G_D> + U18*G3>
W_G_H> = W_G_H> + U19*H3>
%
ALF_D_N>=DT(W_D_N>,N)
ALF_A_B>=DT(W_A_B>,N)
ALF_C_B>=DT(W_C_B>,N)
ALF_C_D>=DT(W_C_D>,N)
ALF_D_E>=DT(W_D_E>,N)
ALF_F_E>=DT(W_F_E>,N)
ALF_G_D>=DT(W_G_D>,N)
ALF_G_H>=DT(W_G_H>,N)
ALF_I_B>=DT(W_I_B>,N)
ALF_J_C>=DT(W_J_C>,N)
ALF_K_D>=DT(W_K_D>,N)
%
%--------------------------------
%Linear velocities
V_O_N>=0>
```

```
V_P1_N>=DT(P_O_P1>,N)
V2PTS(N,A,P1,AO)
V2PTS(N,A,P1,P2)
V2PTS(N,A,P1,P3)
V2PTS(N,B,P3,BO)
V2PTS(N,B,P3,P4)
V2PTS(N,C,P4,CO)
V2PTS(N,C,P4,P5)
V2PTS(N,D,P5,DO)
V2PTS(N,D,P5,P6)
V2PTS(N,E,P6,EO)
V2PTS(N,E,P6,P7)
V2PTS(N,F,P7,FO)
V2PTS(N,F,P7,P8)
V2PTS(N,G,P5,GO)
V2PTS(N,G,P5,P9)
V2PTS(N,H,P9,HO)
V2PTS(N,H,P9,P10)
%
V2PTS(N,B,P3,P11)
V2PTS(N,B,P3,P12)
V2PTS(N,C,P4,P13)
V2PTS(N,C,P4,P14)
V2PTS(N,D,P5,P15)
V2PTS(N,D,P5,P16)
%
%Linear velocities of wobbling masses
%
V_PW1_N>=DT(P_O_PW1>,N)
V2PTS(N,I,PW1,PW2)
V2PTS(N,I,PW1,IO)
V_PW3_N>=DT(P_O_PW3>,N)
V2PTS(N,J,PW3,PW4)
V2PTS(N,J,PW3,JO)
V_PW5_N>=DT(P_O_PW5>,N)
V2PTS(N,K,PW5,PW6)
V2PTS(N,K,PW5,KO)
%
%Centre of mass velocities
%
V_CM_N>=DT(P_O_CM>,N)
VOCMX=DOT(V_CM_N>,N1>)
VOCMY=DOT(V_CM_N>,N2>)
%
VOP1X=DOT(V_P1_N>,N1>)
VOP1Y=DOT(V_P1_N>,N2>)
VOP2X=DOT(V_P2_N>,N1>)
VOP2Y=DOT(V_P2_N>,N2>)
VOP3X=DOT(V_P3_N>,N1>)
VOP3Y=DOT(V_P3_N>,N2>)
VOP4X=DOT(V_P4_N>,N1>)
VOP4Y=DOT(V_P4_N>,N2>)
VOP5X=DOT(V_P5_N>,N1>)
VOP5Y=DOT(V_P5_N>,N2>)
VOP6X=DOT(V_P6_N>,N1>)
VOP6Y=DOT(V_P6_N>,N2>)
VOP7X=DOT(V_P7_N>,N1>)
VOP7Y=DOT(V_P7_N>,N2>)
VOP8X=DOT(V_P8_N>,N1>)
VOP8Y=DOT(V_P8_N>,N2>)
```

```
VOP9X=DOT(V_P9_N>,N1>)
VOP9Y=DOT(V_P9_N>,N2>)
VOP10X=DOT(V_P10_N>,N1>)
VOP10Y=DOT(V_P10_N>,N2>)
VOP11X=DOT(V_P11_N>,N1>)
VOP11Y=DOT(V_P11_N>,N2>)
VOP12X=DOT(V_P12_N>,N1>)
VOP12Y=DOT(V_P12_N>,N2>)
VOP13X=DOT(V_P13_N>,N1>)
VOP13Y=DOT(V_P13_N>,N2>)
VOP14X=DOT(V_P14_N>,N1>)
VOP14Y=DOT(V_P14_N>,N2>)
VOP15X=DOT(V_P15_N>,N1>)
VOP15Y=DOT(V_P15_N>,N2>)
VOP16X=DOT(V_P16_N>,N1>)
VOP16Y=DOT(V_P16_N>,N2>)
VOPW1X=DOT(V_PW1_N>,N1>)
VOPW1Y=DOT(V_PW1_N>,N2>)
VOPW2X=DOT(V_PW2_N>,N1>)
VOPW2Y=DOT(V_PW2_N>,N2>)
VOPW3X=DOT(V_PW3_N>,N1>)
VOPW3Y=DOT(V_PW3_N>,N2>)
VOPW4X=DOT(V_PW4_N>,N1>)
VOPW4Y=DOT(V_PW4_N>,N2>)
VOPW5X=DOT(V_PW5_N>,N1>)
VOPW5Y=DOT(V_PW5_N>,N2>)
VOPW6X=DOT(V_PW6_N>,N1>)
VOPW6Y=DOT(V_PW6_N>,N2>)
%
VOAOX=DOT(V_AO_N>,N1>)
VOAOY=DOT(V_AO_N>,N2>)
VOBOX=DOT(V_BO_N>,N1>)
VOBOY=DOT(V_BO_N>,N2>)
VOCOX=DOT(V_CO_N>,N1>)
VOCOY=DOT(V_CO_N>,N2>)
VODOX=DOT(V_DO_N>,N1>)
VODOY=DOT(V_DO_N>,N2>)
VOEOX=DOT(V_EO_N>,N1>)
VOEOY=DOT(V_EO_N>,N2>)
VOFOX=DOT(V_FO_N>,N1>)
VOFOY=DOT(V_FO_N>,N2>)
VOGOX=DOT(V_GO_N>,N1>)
VOGOY=DOT(V_GO_N>,N2>)
VOHOX=DOT(V_HO_N>,N1>)
VOHOY=DOT(V_HO_N>,N2>)
VOIOX=DOT(V_IO_N>,N1>)
VOIOY=DOT(V_IO_N>,N2>)
VOJOX=DOT(V_JO_N>,N1>)
VOJOY=DOT(V_JO_N>,N2>)
VOKOX=DOT(V_KO_N>,N1>)
VOKOY=DOT(V_KO_N>,N2>)
%
%Linear accelerations
%
A_O_N>=0>
A_P1_N>=DT(V_P1_N>,N)
A_AO_N>=DT(V_AO_N>,N)
A_P2_N>=DT(V_P2_N>,N)
A_P3_N>=DT(V_P3_N>,N)
A_BO_N>=DT(V_BO_N>,N)
```

```
A_P4_N>=DT(V_P4_N>,N)
A_CO_N>=DT(V_CO_N>,N)
A_P5_N>=DT(V_P5_N>,N)
A_DO_N>=DT(V_DO_N>,N)
A_P6_N>=DT(V_P6_N>,N)
A_EO_N>=DT(V_EO_N>,N)
A_P7_N>=DT(V_P7_N>,N)
A_FO_N>=DT(V_FO_N>,N)
A_P8_N>=DT(V_P8_N>,N)
A_GO_N>=DT(V_GO_N>,N)
A_P9_N>=DT(V_P9_N>,N)
A_HO_N>=DT(V_HO_N>,N)
A_P10_N>=DT(V_P10_N>,N)
A_P11_N>=DT(V_P11_N>,N)
A_P12_N>=DT(V_P12_N>,N)
A_PW1_N>=DT(V_PW1_N>,N)
A_PW2_N>=DT(V_PW2_N>,N)
A_IO_N>=DT(V_IO_N>,N)
A_P13_N>=DT(V_P13_N>,N)
A_P14_N>=DT(V_P14_N>,N)
A_PW3_N>=DT(V_PW3_N>,N)
A_PW4_N>=DT(V_PW4_N>,N)
A_JO_N>=DT(V_JO_N>,N)
A_P15_N>=DT(V_P15_N>,N)
A_P16_N>=DT(V_P16_N>,N)
A_PW5_N>=DT(V_PW5_N>,N)
A_PW6_N>=DT(V_PW6_N>,N)
A_KO_N>=DT(V_KO_N>,N)
%
%-------------------------------
%Joint angles
ANKANG=AAB
KNEANG=ABC
HIPANG=ACD
SHRANG=ADE
ELBANG=AEF
RHIPANG=ADG
RKNEANG=AGH
%
ANKW=DT(ANKANG,N)
KNEW=DT(KNEANG,N)
HIPW=DT(HIPANG,N)
SHRW=DT(SHRANG,N)
ELBW=DT(ELBANG,N)
RHIPW=DT(RHIPANG,N)
RKNEW=DT(RKNEANG,N)
%
%-------------------------------
%Energy
%
KECM=KE(A,B,C,D,E,F,G,H,I,J,K)
KEA=KE(A)
KEB=KE(B)
KEC=KE(C)
KED=KE(D)
KEE=KE(E)
KEF=KE(F)
KEG=KE(G)
KEH=KE(H)
KEI=KE(I)
```

```
KEJ=KE(J)
KEK=KE(K)
PECM=-1*TOTMASS*G*POCMY
PEA=-1*MA*G*POAOY
PEB=-1*MB*G*POBOY
PEC=-1*MC*G*POCOY
PED=-1*MD*G*PODOY
PEE=-1*ME*G*POEOY
PEF=-1*MF*G*POFOY
PEG=-1*MG*G*POGOY
PEH=-1*MH*G*POHOY
PEI=-1*MI*G*POIOY
PEJ=-1*MJ*G*POJOY
PEK=-1*MK*G*POKOY
%
%Angular and linear momentum
%
AMOM>=MOMENTUM(ANGULAR,CM)
ZAMOM=DOT(AMOM>,N3>)
LMOM>=MOMENTUM(LINEAR)
XMOM=DOT(LMOM>,N1>)
YMOM=DOT(LMOM>,N2>)
%
%Forces
%
TORQUE(B/A,TORANK*N3>)
TORQUE(B/C,TORKNE*N3>)
TORQUE(D/C,TORHIP*N3>)
TORQUE(E/D,TORSHR*N3>)
TORQUE(F/E,TORELB*N3>)
TORQUE(G/D,TORRHIP*N3>)
TORQUE(G/H,TORRKNE*N3>)
GRAVITY(G*N2>)
RX=-K1*Q1-K2*U1
RY=-K3*Q2-K4*U2
FORCE(P1,RX*N1>+RY*N2>)
RX1=-K5*POP2X-K6*VOP2X
RY1=-K7*POP2Y-K8*VOP2Y
FORCE(P2,RX1*N1>+RY1*N2>)
SWM1X=-K9*Q5-K10*U5
SWM1Y=-K11*Q6-K12*U6
FORCE(P11/PW1,SWM1X*N1>+SWM1Y*N2>)
SWM2X=-K13*(POPW2X-POP12X)-K14*(VOPW2X-VOP12X)
SWM2Y=-K15*(POPW2Y-POP12Y)-K16*(VOPW2Y-VOP12Y)
FORCE(P12/PW2,SWM2X*N1>+SWM2Y*N2>)
SWM3X=-K9*Q8-K10*U8
SWM3Y=-K13*Q9-K12*U9
FORCE(P13/PW3,SWM3X*N1>+SWM3Y*N2>)
SWM4X=-K13*(POPW4X-POP14X)-K14*(VOPW4X-VOP14X)
SWM4Y=-K15*(POPW4Y-POP14Y)-K16*(VOPW4Y-VOP14Y)
FORCE(P14/PW4,SWM4X*N1>+SWM4Y*N2>)
SWM5X=-K9*Q11-K10*U11
SWM5Y=-K11*Q12-K12*U12
FORCE(P15/PW5,SWM5X*N1>+SWM5Y*N2>)
SWM6X=-K13*(POPW6X-POP16X)-K14*(VOPW6X-VOP16X)
SWM6Y=-K15*(POPW6Y-POP16Y)-K16*(VOPW6Y-VOP16Y)
FORCE(P16/PW6,SWM6X*N1>+SWM6Y*N2>)
%
%AUXILIARY[1]=U13
%AUXILIARY[2]=U14
```

```
%AUXILIARY[3]=U15
%AUXILIARY[4]=U16
%AUXILIARY[5]=U17
%AUXILIARY[6]=U18
%AUXILIARY[7]=U19
AUXILIARY[1]=DOT(W_A_B>,A3>) - AAB'
AUXILIARY[2]=DOT(W_C_B>,B3>) - ABC'
AUXILIARY[3]=DOT(W_C_D>,D3>) - ACD'
AUXILIARY[4]=DOT(W_D_E>,E3>) - ADE'
AUXILIARY[5]=DOT(W_F_E>,E3>) - AEF'
AUXILIARY[6]=DOT(W_G_D>,D3>) - ADG'
AUXILIARY[7]=DOT(W_G_H>,H3>) - AGH'
%
CONSTRAIN(AUXILIARY[U13,U14,U15,U16,U17,U18,U19])
%---------------------------------
%Equations of motion
ZERO = FR() + FRSTAR()
KANE(TORANK,TORKNE,TORHIP,TORSHR,TORELB,TORRHIP,TORRKNE)
%
%---------------------------------
%Inputs
INPUT TINITIAL=0.0, TFINAL=5.0, INTEGSTP=0.001, PRINTINT=5
INPUT ABSERR=1.0E-08, RELERR=1.0E-07
INPUT Q1=0,Q2=0,Q3=90.0,Q4=0.0,Q5=0.0,Q6=0.0,Q7=0.0,Q8=0.0,Q9=0.0,Q10=0.0,
Q11=0.0
INPUT MA=3,MB=5,MC=7,MD=13,ME=5,MF=3,MG=10,MH=10,MI=5,MJ=7,MK=13
INPUT IA=0.1,IB=0.1,IC=0.1,ID=0.1,IE=0.1,IF=0.1,IG=0.1,IH=0.1,II=0.1,IJ=0.1,
IK=0.1
INPUT L1=0.2,L2=0.25,L3=0.1,L4=0.15,L5=0.04,L6=0.25,L7=0.5,L8=0.3,L9=0.6,
L10=0.35,L11=0.7
INPUT L12=0.15,L13=0.3,L14=0.1,L15=0.2,L16=0.3,L17=0.6,L18=0.28,L19=0.56,
L20=0.05,L21=0.45
INPUT L22=0.2,L23=0.4,L24=0.05,L25=0.55,L26=0.25,L27=0.5,L28=0.05,L29=0.65,
L30=0.3,L31=0.6
INPUT G=-9.81
INPUT R1=110, R2=160, R3=150, R4=100, R5=120, R6=120, R7=100
INPUT K1=150000,K2=10000,K3=150000,K4=10000
INPUT K5=150000,K6=10000,K7=150000,K8=10000
INPUT K9=75000,K10=1000,K11=75000,K12=1000
INPUT K13=75000,K14=1000,K15=75000,K16=1000
%
%---------------------------------
%OUTPUT
OUTPUT T,POP1X,POP1Y,POP2X,POP2Y,POP3X,POP3Y,POP4X,POP4Y,POP5X,POP5Y,
POP6X,POP6Y,POP7X,POP7Y,POP8X,POP8Y,POP7X,POP7Y,POP6X,POP6Y,POP5X,POP5Y,
POP9X,POP9Y,POP10X,POP10Y,POCMX,POCMY
OUTPUT T,VOP1X,VOP1Y,VOP2X,VOP2Y,VOP3X,VOP3Y,VOP4X,VOP4Y,VOP5X,VOP5Y
,VOP6X,VOP6Y,VOP7X,VOP7Y,VOP8X,VOP8Y,VOP9X,VOP9Y,VOP10X,VOP10Y,VOCMX
,VOCMY
OUTPUT T,POAOX,POAOY,POBOX,POBOY,POCOX,POCOY,PODOX,PODOY,POEOX,
POEOY,POFOX,POFOY,POGOX,POGOY,POHOX,POHOY,POIOX,POIOY,POJOX,POJOY,P
OKOX,POKOY,POCMX,POCMY
OUTPUT T,VOAOX,VOAOY,VOBOX,VOBOY,VOCOX,VOCOY,VODOX,VODOY,VOEOX
,VOEOY,VOFOX,VOFOY,VOGOX,VOGOY,VOHOX,VOHOY,VOCMX,VOCMY
OUTPUT T,Q1,U1,Q2,U2,Q3,U3,Q4,U4,Q5,U5,Q6,U6,Q7,U7,Q8,U8,Q9,U9,Q10,U10,Q11,U11,
Q12,U12,AAB,AAB',ABC,ABC',ACD,ACD',ADE,ADE',AEF,AEF',ADG,ADG',AGH,AGH'
OUTPUT T,ANKANG,ANKW,KNEANG,KNEW,HIPANG,HIPW,SHRANG,SHRW,ELBANG,
ELBW,RHIPANG,RHIPW,RKNEANG,RKNEW
OUTPUT T,TORANK,TORKNE,TORHIP,TORSHR,TORELB,TORRHIP,TORRKNE,RX,RY,
```

```
RX1,RY1,SWM1X,SWM1Y,SWM2X,SWM2Y,SWM3X,SWM3Y,SWM4X,SWM4Y,SWM5X,S
WM5Y,SWM6X,SWM6Y
OUTPUT T,KECM,KEA,KEB,KEC,KED,KEE,KEF,KEG,KEH,KEI,KEJ,KEK
OUTPUT T,PECM,PEA,PEB,PEC,PED,PEE,PEF,PEG,PEH,PEI,PEJ,PEK
OUTPUT T,ZAMOM,XMOM,YMOM
%
%--------------------------------
%Units
UNITS [K1,K3,K5,K7,K9,K11,K13,K15]=N/M, [K2,K4,K6,K8,K10,K12,K14,K16]=N/M/S
UNITS [L1,L2,L3,L4,L5,L6,L7,L8,L9,L10,L11,L12,L13,L14,L15,L16,L17,L18,L19]=M
UNITS [L20,L21,L22,L23,L24,L25,L26,L27,L28,L29,L30,L31]=M
UNITS TOTMASS=KG, T=S, G=M/S^2
UNITS POP1X=M,POP1Y=M,POP2X=M,POP2Y=M,POP3X=M,POP3Y=M,POP4X=M,
POP4Y=M,POP5X=M,POP5Y=M
UNITS POP6X=M,POP6Y=M,POP7X=M,POP7Y=M,POP8X=M,POP8Y=M,POP9X=M,
POP9Y=M,POP10X=M,POP10Y=M
UNITS [POP11X,POP11Y,POP12X,POP12Y,POP13X,POP13Y,POP14X,POP14Y,POP15X,
POP15Y, POP16X,POP16Y]=M
UNITS [POPW1X,POPW1Y,POPW2X,POPW2Y,POPW3X,POPW3Y,POPW4X,POPW4Y,
POPW5X,POPW5Y, POPW6X,POPW6Y]=M
UNITS Q1=M, Q2=M, Q3=DEG, Q4=DEG, Q5=M, Q6=M, Q7=DEG, Q8=M, Q9=M,
Q10=DEG, Q11=M, Q12=M
UNITS AAB=DEG, ABC=DEG, ACD=DEG, ADE=DEG, AEF=DEG, ADG=DEG, AGH=DEG
UNITS U1=M/S, U2=M/S, U3=DEG/S, U4=DEG/S, U5=M/S, U6=M/S, U7=DEG/S, U8=M/S,
U9=M/S, U10=DEG/S, U11=M/S, U12=M/S
UNITS AAB'=DEG/S, ABC'=DEG/S, ACD'=DEG/S, ADE'=DEG/S, AEF'=DEG/S,
ADG'=DEG/S, AGH'=DEG/S
UNITS [R1,R2,R3,R4,R5,R6,R7]=DEG
UNITS [IA,IB,IC,ID,IE,IF,IG,IH,II,IJ,IK]=KG.M^2
UNITS [MA,MB,MC,MD,ME,MF,MG,MH,MI,MJ,MK]=KG
UNITS [RX,RY,RX1,RY1]=N
UNITS [TORANK,TORKNE,TORHIP,TORSHR,TORELB,TORRHIP,TORRKNE]=Nm
UNITS [SWM1X,SWM1Y,SWM2X,SWM2Y,SWM3X,SWM3Y,SWM4X,SWM4Y,SWM5X,
SWM5Y,SWM6X,SWM6Y] =N
UNITS [KECM,KEA,KEB,KEC,KED,KEE,KEF,KEG,KEH,KEI,KEJ,KEK,PECM,PEA,PEB,
PEC,PED,PEE ,PEF,PEG,PEH,PEI,PEJ,PEK]=J
UNITS [XMOM,YMOM]=KG.M/S, ZAMOM=KG.M^2/S
%
CODE DYNAMICS() C:\AL\CASSIE\INVDYN.FOR, SUBS
SAVE C:\AL\CASSIE\INVDYN.ALL
```

Appendix 1c

Autolev commands used for the eight-segment torque-driven model

```
% 8SEGWM.AL
% 8 SEGMENT MODEL OF JUMPING
% CONTAINS WOBBLING MASSES AT THE SHANK,THIGH AND TRUNK
%-------------------------
%Physical declarations
NEWTONIAN N
BODIES A,B,C,D,E,F,G,H,I,J,K
POINTS
O,P1,P2,P3,P4,P5,P6,P7,P8,P9,P10,P11,P12,P13,P14,P15,P16,PW1,PW2,PW3,PW4,PW5,PW6,C
M
%
AUTOZ ON
%-------------------------------
%Mathematical Declarations
%length constraints: L1 is length to seg1 CM, L2
%is to the other end of seg 1 etc
%lengths are calculated from human anthropometrics
%9 generalised coordinates/speeds
MASS A=MA, B=MB, C=MC, D=MD, E=ME, F=MF, G=MG, H=MH, I=MI, J=MJ, K=MK
INERTIA A, 0,0,IA
INERTIA B, 0,0,IB
INERTIA C, 0,0,IC
INERTIA D, 0,0,ID
INERTIA E, 0,0,IE
INERTIA F, 0,0,IF
INERTIA G, 0,0,IG
INERTIA H, 0,0,IH
INERTIA I, 0,0,II
INERTIA J, 0,0,IJ
INERTIA K, 0,0,IK
VARIABLES U{19}'
VARIABLES Q1',Q2',Q3',Q4',Q5',Q6',Q7',Q8',Q9',Q10',Q11',Q12',Q13',Q14',
Q15',Q16',Q17'
VARIABLES
RX,RY,RX1,RY1,SWM1X,SWM1Y,SWM2X,SWM2Y,SWM3X,SWM3Y,SWM4X,SWM4Y
,SWM5X,SWM6X,SWM6Y
VARIABLES POP1X,POP1Y,POP2X,POP2Y,POP3X,POP3Y,POP4X,POP4Y,POP5X,POP5Y
VARIABLES POP6X,POP6Y,POP7X,POP7Y,POP8X,POP8Y,POP9X,POP9Y,POP10X,POP10Y
VARIABLES POP11X,POP11Y,POP12X,POP12Y,POP13X,POP13Y,POP14X,POP14Y,
POP15X,POP15Y,POP16X,POP16Y
VARIABLES
POPW1X,POPW1Y,POPW2X,POPW2Y,POPW3X,POPW3Y,POPW4X,POPW4Y,
POPW5X,POPW5Y,POPW6X,POPW6Y
VARIABLES
VOP1X,VOP1Y,VOP2X,VOP2Y,VOP3X,VOP3Y,VOP4X,VOP4Y,VOP5X,VOP5Y
VARIABLES
VOP6X,VOP6Y,VOP7X,VOP7Y,VOP8X,VOP8Y,VOP9X,VOP9Y,VOP10X,VOP10Y
VARIABLES VOP11X,VOP11Y,VOP12X,VOP12Y,VOP13X,VOP13Y,VOP14X,VOP14Y,
VOP15X,VOP15Y,VOP16X,VOP16Y
VARIABLES
VOPW1X,VOPW1Y,VOPW2X,VOPW2Y,VOPW3X,VOPW3Y,VOPW4X,VOPW4Y,
VOPW5X,VOPW5Y,VOPW6X,VOPW6Y
VARIABLES POCMX,POCMY,VOCMX,VOCMY
```

```
VARIABLES ANKANG,KNEANG,HIPANG,SHRANG,ELBANG,RHIPANG,RKNEANG
VARIABLES ANKW,KNEW,HIPW,SHRW,ELBW,RHIPW,RKNEW
VARIABLES TORANK,TORKNE,TORHIP,TORSHR,TORRHIP,TORELB,TORRKNE
VARIABLES KECM,KEA,KEB,KEC,KED,KEE,KEF,KEG,KEH,KEI,KEJ,KEK
VARIABLES PECM,PEA,PEB,PEC,PED,PEE,PEF,PEG,PEH,PEI,PEJ,PEK
VARIABLES PANK,PKNE,PHIP,PSHR,PRHIP
VARIABLES XMOM,YMOM,ZAMOM
CONSTANTS ANKTOR,KNETOR,HIPTOR,SHRTOR,RHIPTOR
CONSTANTS L{31}
CONSTANTS K{16}
CONSTANTS G,TOTMASS,HEIGHT
CONSTANTS R1, R2
SPECIFIED AEF", AGH"
AEF = R1 + (R1*T^2)
AGH = R2 + (R2*T^2)
%
ZEE_NOT = [TORELB, TORRKNE]
%--------------------------------
%
%Geometry relating unit vectors
SIMPROT(N,A,3,Q3)
SIMPROT(N,B,3,Q4)
SIMPROT(N,C,3,Q5)
SIMPROT(N,D,3,Q6)
SIMPROT(N,E,3,Q7)
SIMPROT(F,E,3,PI-AEF)
SIMPROT(N,G,3,Q8)
SIMPROT(G,H,3,PI-AGH)
SIMPROT(B,I,3,Q11)
SIMPROT(C,J,3,Q14)
SIMPROT(D,K,3,Q17)
%
%--------------------------------
%Position Vectors
P_O_P1>=Q1*N1> + Q2*N2>
P_P1_AO>=L4*A1> + L5*A2>
P_P1_P2>=L2*A1>
P_P1_P3>=L1*A1> + L3*A2>
P_P3_BO>=L6*B1>
P_P3_P4>=L7*B1>
P_P4_CO>=L8*C1>
P_P4_P5>=L9*C1>
P_P5_DO>=L10*D1>
P_P5_P6>=L11*D1>
P_P6_EO>=L12*E1>
P_P6_P7>=L13*E1>
P_P7_FO>=L14*F1>
P_P7_P8>=L15*F1>
P_P5_GO>=L16*G1>
P_P5_P9>=L17*G1>
P_P9_HO>=L18*H1>
P_P9_P10>=L19*H1>
%
%Wobbling mass positions
%
P_P3_P11>=L20*B1>
P_P3_P12>=L21*B1>
P_P11_P12>=(L21-L20)*B1>
P_P11_PW1>=Q9*N1>+Q10*N2>
P_PW1_IO>=L22*I1>
```

```
P_PW1_PW2>=L23*I1>
%
P_P4_P13>=L24*C1>
P_P4_P14>=L25*C1>
P_P13_P14>=(L25-L24)*C1>
P_P13_PW3>=Q12*N1>+Q13*N2>
P_PW3_JO>=L26*J1>
P_PW3_PW4>=L27*J1>
%
P_P5_P15>=L28*D1>
P_P5_P16>=L29*D1>
P_P15_P16>=(L29-L28)*D1>
P_P15_PW5>=Q15*N1>+Q16*N2>
P_PW5_KO>=L30*K1>
P_PW5_PW6>=L31*K1>
%
%Position of points relative to O
P_O_AO>=P_O_P1>+P_P1_AO>
P_O_P2>=P_O_P1>+P_P1_P2>
P_O_P3>=P_O_P1>+P_P1_P3>
P_O_BO>=P_O_P3>+P_P3_BO>
P_O_P4>=P_O_P3>+P_P3_P4>
P_O_CO>=P_O_P4>+P_P4_CO>
P_O_P5>=P_O_P4>+P_P4_P5>
P_O_DO>=P_O_P5>+P_P5_DO>
P_O_P6>=P_O_P5>+P_P5_P6>
P_O_EO>=P_O_P6>+P_P6_EO>
P_O_P7>=P_O_P6>+P_P6_P7>
P_O_FO>=P_O_P7>+P_P7_FO>
P_O_P8>=P_O_P7>+P_P7_P8>
P_O_GO>=P_O_P5>+P_P5_GO>
P_O_P9>=P_O_P5>+P_P5_P9>
P_O_HO>=P_O_P9>+P_P9_HO>
P_O_P10>=P_O_P9>+P_P9_P10>
P_O_P11>=P_O_P3>+P_P3_P11>
P_O_P12>=P_O_P3>+P_P3_P12>
P_O_PW1>=P_O_P11>+P_P11_PW1>
P_O_PW2>=P_O_PW1>+P_PW1_PW2>
P_O_IO>=P_O_PW1>+P_PW1_IO>
P_O_P13>=P_O_P4>+P_P4_P13>
P_O_P14>=P_O_P4>+P_P4_P14>
P_O_PW3>=P_O_P13>+P_P13_PW3>
P_O_PW4>=P_O_PW3>+P_PW3_PW4>
P_O_JO>=P_O_PW3>+P_PW3_JO>
P_O_P15>=P_O_P5>+P_P5_P15>
P_O_P16>=P_O_P5>+P_P5_P16>
P_O_PW5>=P_O_P15>+P_P15_PW5>
P_O_PW6>=P_O_PW5>+P_PW5_PW6>
P_O_KO>=P_O_PW5>+P_PW5_KO>
%---------------------------------
%Position of points in x-y coordinates
POP1X=DOT(P_O_P1>,N1>)
POP1Y=DOT(P_O_P1>,N2>)
POP2X=DOT(P_O_P2>,N1>)
POP2Y=DOT(P_O_P2>,N2>)
POP3X=DOT(P_O_P3>,N1>)
POP3Y=DOT(P_O_P3>,N2>)
POP4X=DOT(P_O_P4>,N1>)
POP4Y=DOT(P_O_P4>,N2>)
POP5X=DOT(P_O_P5>,N1>)
```

POP5Y=DOT(P_O_P5>,N2>)
POP6X=DOT(P_O_P6>,N1>)
POP6Y=DOT(P_O_P6>,N2>)
POP7X=DOT(P_O_P7>,N1>)
POP7Y=DOT(P_O_P7>,N2>)
POP8X=DOT(P_O_P8>,N1>)
POP8Y=DOT(P_O_P8>,N2>)
POP9X=DOT(P_O_P9>,N1>)
POP9Y=DOT(P_O_P9>,N2>)
POP10X=DOT(P_O_P10>,N1>)
POP10Y=DOT(P_O_P10>,N2>)
POP11X=DOT(P_O_P11>,N1>)
POP11Y=DOT(P_O_P11>,N2>)
POP12X=DOT(P_O_P12>,N1>)
POP12Y=DOT(P_O_P12>,N2>)
POP13X=DOT(P_O_P13>,N1>)
POP13Y=DOT(P_O_P13>,N2>)
POP14X=DOT(P_O_P14>,N1>)
POP14Y=DOT(P_O_P14>,N2>)
POP15X=DOT(P_O_P15>,N1>)
POP15Y=DOT(P_O_P15>,N2>)
POP16X=DOT(P_O_P16>,N1>)
POP16Y=DOT(P_O_P16>,N2>)
%Of wobbling masses
POPW1X=DOT(P_O_PW1>,N1>)
POPW1Y=DOT(P_O_PW1>,N2>)
POPW2X=DOT(P_O_PW2>,N1>)
POPW2Y=DOT(P_O_PW2>,N2>)
POPW3X=DOT(P_O_PW3>,N1>)
POPW3Y=DOT(P_O_PW3>,N2>)
POPW4X=DOT(P_O_PW4>,N1>)
POPW4Y=DOT(P_O_PW4>,N2>)
POPW5X=DOT(P_O_PW5>,N1>)
POPW5Y=DOT(P_O_PW5>,N2>)
POPW6X=DOT(P_O_PW6>,N1>)
POPW6Y=DOT(P_O_PW6>,N2>)

%
POAOX=DOT(P_O_AO>,N1>)
POAOY=DOT(P_O_AO>,N2>)
POBOX=DOT(P_O_BO>,N1>)
POBOY=DOT(P_O_BO>,N2>)
POCOX=DOT(P_O_CO>,N1>)
POCOY=DOT(P_O_CO>,N2>)
PODOX=DOT(P_O_DO>,N1>)
PODOY=DOT(P_O_DO>,N2>)
POEOX=DOT(P_O_EO>,N1>)
POEOY=DOT(P_O_EO>,N2>)
POFOX=DOT(P_O_FO>,N1>)
POFOY=DOT(P_O_FO>,N2>)
POGOX=DOT(P_O_GO>,N1>)
POGOY=DOT(P_O_GO>,N2>)
POHOX=DOT(P_O_HO>,N1>)
POHOY=DOT(P_O_HO>,N2>)
POIOX=DOT(P_O_IO>,N1>)
POIOY=DOT(P_O_IO>,N2>)
POJOX=DOT(P_O_JO>,N1>)
POJOY=DOT(P_O_JO>,N2>)
POKOX=DOT(P_O_KO>,N1>)
POKOY=DOT(P_O_KO>,N2>)

```
%
%--------------------------------
%Position vector of the bodies b and c from o
P_O_CM>=CM(O)
POCMX=DOT(P_O_CM>,N1>)
POCMY=DOT(P_O_CM>,N2>)
%
%--------------------------------
%Kinematical differential equations
Q1'=U1
Q2'=U2
Q3'=U3
Q4'=U4
Q5'=U5
Q6'=U6
Q7'=U7
Q8'=U8
Q9'=U9
Q10'=U10
Q11'=U11
Q12'=U12
Q13'=U13
Q14'=U14
Q15'=U15
Q16'=U16
Q17'=U17
%
%Angular velocities and accelerations
W_A_N>=Q3'*N3>
W_B_N>=Q4'*N3>
W_C_N>=Q5'*N3>
W_D_N>=Q6'*N3>
W_E_N>=Q7'*N3>
W_F_E>=AEF'*N3>
W_G_N>=Q8'*N3>
W_H_G>=AGH'*N3>
W_I_N>=(Q4'+Q11')*N3>
W_J_N>=(Q5'+Q14')*N3>
W_K_N>=(Q6'+Q17')*N3>
%
%Use generalised speeds u9 and u10 to produce measure numbers
%for the joint torques
%
W_F_N> = W_F_N> + U18*F3>
W_H_N> = W_H_N> + U19*H3>
%
ALF_A_N>=DT(W_A_N>,N)
ALF_B_N>=DT(W_B_N>,N)
ALF_C_N>=DT(W_C_N>,N)
ALF_D_N>=DT(W_D_N>,N)
ALF_E_N>=DT(W_E_N>,N)
ALF_F_E>=DT(W_F_E>,N)
ALF_G_N>=DT(W_G_N>,N)
ALF_H_G>=DT(W_H_G>,N)
ALF_I_N>=DT(W_I_N>,N)
ALF_J_N>=DT(W_J_N>,N)
ALF_K_N>=DT(W_K_N>,N)
%
%--------------------------------
%Linear velocities
```

```
V_O_N>=0>
V_P1_N>=DT(P_O_P1>,N)
V2PTS(N,A,P1,AO)
V2PTS(N,A,P1,P2)
V2PTS(N,A,P1,P3)
V2PTS(N,B,P3,BO)
V2PTS(N,B,P3,P4)
V2PTS(N,C,P4,CO)
V2PTS(N,C,P4,P5)
V2PTS(N,D,P5,DO)
V2PTS(N,D,P5,P6)
V2PTS(N,E,P6,EO)
V2PTS(N,E,P6,P7)
V2PTS(N,F,P7,FO)
V2PTS(N,F,P7,P8)
V2PTS(N,G,P5,GO)
V2PTS(N,G,P5,P9)
V2PTS(N,H,P9,HO)
V2PTS(N,H,P9,P10)
%
V2PTS(N,B,P3,P11)
V2PTS(N,B,P3,P12)
V2PTS(N,C,P4,P13)
V2PTS(N,C,P4,P14)
V2PTS(N,D,P5,P15)
V2PTS(N,D,P5,P16)
%
%Linear velocities of wobbling masses
%
V_PW1_N>=DT(P_O_PW1>,N)
V2PTS(N,I,PW1,PW2)
V2PTS(N,I,PW1,IO)
V_PW3_N>=DT(P_O_PW3>,N)
V2PTS(N,J,PW3,PW4)
V2PTS(N,J,PW3,JO)
V_PW5_N>=DT(P_O_PW5>,N)
V2PTS(N,K,PW5,PW6)
V2PTS(N,K,PW5,KO)
%
%Centre of mass velocities
%
V_CM_N>=DT(P_O_CM>,N)
VOCMX=DOT(V_CM_N>,N1>)
VOCMY=DOT(V_CM_N>,N2>)
%
VOP1X=DOT(V_P1_N>,N1>)
VOP1Y=DOT(V_P1_N>,N2>)
VOP2X=DOT(V_P2_N>,N1>)
VOP2Y=DOT(V_P2_N>,N2>)
VOP3X=DOT(V_P3_N>,N1>)
VOP3Y=DOT(V_P3_N>,N2>)
VOP4X=DOT(V_P4_N>,N1>)
VOP4Y=DOT(V_P4_N>,N2>)
VOP5X=DOT(V_P5_N>,N1>)
VOP5Y=DOT(V_P5_N>,N2>)
VOP6X=DOT(V_P6_N>,N1>)
VOP6Y=DOT(V_P6_N>,N2>)
VOP7X=DOT(V_P7_N>,N1>)
VOP7Y=DOT(V_P7_N>,N2>)
VOP8X=DOT(V_P8_N>,N1>)
```

```
VOP8Y=DOT(V_P8_N>,N2>)
VOP9X=DOT(V_P9_N>,N1>)
VOP9Y=DOT(V_P9_N>,N2>)
VOP10X=DOT(V_P10_N>,N1>)
VOP10Y=DOT(V_P10_N>,N2>)
VOP11X=DOT(V_P11_N>,N1>)
VOP11Y=DOT(V_P11_N>,N2>)
VOP12X=DOT(V_P12_N>,N1>)
VOP12Y=DOT(V_P12_N>,N2>)
VOP13X=DOT(V_P13_N>,N1>)
VOP13Y=DOT(V_P13_N>,N2>)
VOP14X=DOT(V_P14_N>,N1>)
VOP14Y=DOT(V_P14_N>,N2>)
VOP15X=DOT(V_P15_N>,N1>)
VOP15Y=DOT(V_P15_N>,N2>)
VOP16X=DOT(V_P16_N>,N1>)
VOP16Y=DOT(V_P16_N>,N2>)
VOPW1X=DOT(V_PW1_N>,N1>)
VOPW1Y=DOT(V_PW1_N>,N2>)
VOPW2X=DOT(V_PW2_N>,N1>)
VOPW2Y=DOT(V_PW2_N>,N2>)
VOPW3X=DOT(V_PW3_N>,N1>)
VOPW3Y=DOT(V_PW3_N>,N2>)
VOPW4X=DOT(V_PW4_N>,N1>)
VOPW4Y=DOT(V_PW4_N>,N2>)
VOPW5X=DOT(V_PW5_N>,N1>)
VOPW5Y=DOT(V_PW5_N>,N2>)
VOPW6X=DOT(V_PW6_N>,N1>)
VOPW6Y=DOT(V_PW6_N>,N2>)
%
VOAOX=DOT(V_AO_N>,N1>)
VOAOY=DOT(V_AO_N>,N2>)
VOBOX=DOT(V_BO_N>,N1>)
VOBOY=DOT(V_BO_N>,N2>)
VOCOX=DOT(V_CO_N>,N1>)
VOCOY=DOT(V_CO_N>,N2>)
VODOX=DOT(V_DO_N>,N1>)
VODOY=DOT(V_DO_N>,N2>)
VOEOX=DOT(V_EO_N>,N1>)
VOEOY=DOT(V_EO_N>,N2>)
VOFOX=DOT(V_FO_N>,N1>)
VOFOY=DOT(V_FO_N>,N2>)
VOGOX=DOT(V_GO_N>,N1>)
VOGOY=DOT(V_GO_N>,N2>)
VOHOX=DOT(V_HO_N>,N1>)
VOHOY=DOT(V_HO_N>,N2>)
VOIOX=DOT(V_IO_N>,N1>)
VOIOY=DOT(V_IO_N>,N2>)
VOJOX=DOT(V_JO_N>,N1>)
VOJOY=DOT(V_JO_N>,N2>)
VOKOX=DOT(V_KO_N>,N1>)
VOKOY=DOT(V_KO_N>,N2>)
%
%Linear accelerations
%
A_O_N>=0>
A_P1_N>=DT(V_P1_N>,N)
A_AO_N>=DT(V_AO_N>,N)
A_P2_N>=DT(V_P2_N>,N)
A_P3_N>=DT(V_P3_N>,N)
```

```
A_BO_N>=DT(V_BO_N>,N)
A_P4_N>=DT(V_P4_N>,N)
A_CO_N>=DT(V_CO_N>,N)
A_P5_N>=DT(V_P5_N>,N)
A_DO_N>=DT(V_DO_N>,N)
A_P6_N>=DT(V_P6_N>,N)
A_EO_N>=DT(V_EO_N>,N)
A_P7_N>=DT(V_P7_N>,N)
A_FO_N>=DT(V_FO_N>,N)
A_P8_N>=DT(V_P8_N>,N)
A_GO_N>=DT(V_GO_N>,N)
A_P9_N>=DT(V_P9_N>,N)
A_HO_N>=DT(V_HO_N>,N)
A_P10_N>=DT(V_P10_N>,N)
A_P11_N>=DT(V_P11_N>,N)
A_P12_N>=DT(V_P12_N>,N)
A_PW1_N>=DT(V_PW1_N>,N)
A_PW2_N>=DT(V_PW2_N>,N)
A_IO_N>=DT(V_IO_N>,N)
A_P13_N>=DT(V_P13_N>,N)
A_P14_N>=DT(V_P14_N>,N)
A_PW3_N>=DT(V_PW3_N>,N)
A_PW4_N>=DT(V_PW4_N>,N)
A_JO_N>=DT(V_JO_N>,N)
A_P15_N>=DT(V_P15_N>,N)
A_P16_N>=DT(V_P16_N>,N)
A_PW5_N>=DT(V_PW5_N>,N)
A_PW6_N>=DT(V_PW6_N>,N)
A_KO_N>=DT(V_KO_N>,N)
%
%-------------------------------
%Joint angles
ANKANG=180-Q3+Q4
KNEANG=180-Q5+Q4
HIPANG=180-Q5+Q6
SHRANG=180-Q6+Q7
ELBANG=AEF
RHIPANG=180-Q8+Q6
RKNEANG=AGH
%
ANKW=DT(ANKANG,N)
KNEW=DT(KNEANG,N)
HIPW=DT(HIPANG,N)
SHRW=DT(SHRANG,N)
ELBW=DT(ELBANG,N)
RHIPW=DT(RHIPANG,N)
RKNEW=DT(RKNEANG,N)
%
%-------------------------------
%Generalised forces (gravity, extensor torques)
TORANK=ANKTOR*T
TORKNE=KNETOR*T
TORHIP=HIPTOR*T
TORSHR=SHRTOR*T
TORRHIP=RHIPTOR*T
%
%Energy
%
KECM=KE(A,B,C,D,E,F,G,H,I,J,K)
KEA=KE(A)
```

```
KEB=KE(B)
KEC=KE(C)
KED=KE(D)
KEE=KE(E)
KEF=KE(F)
KEG=KE(G)
KEH=KE(H)
KEI=KE(I)
KEJ=KE(J)
KEK=KE(K)
PECM=-1*TOTMASS*G*POCMY
PEA=-1*MA*G*POAOY
PEB=-1*MB*G*POBOY
PEC=-1*MC*G*POCOY
PED=-1*MD*G*PODOY
PEE=-1*ME*G*POEOY
PEF=-1*MF*G*POFOY
PEG=-1*MG*G*POGOY
PEH=-1*MH*G*POHOY
PEI=-1*MI*G*POIOY
PEJ=-1*MJ*G*POJOY
PEK=-1*MK*G*POKOY
%
%Joint powers
%
PANK=TORANK*ANKW
PKNE=TORKNE*KNEW
PHIP=TORHIP*HIPW
PSHR=TORSHR*SHRW
PRHIP=TORRHIP*RHIPW
%
%Angular and linear momentum
%
AMOM>=MOMENTUM(ANGULAR,CM)
ZAMOM=DOT(AMOM>,N3>)
LMOM>=MOMENTUM(LINEAR)
XMOM=DOT(LMOM>,N1>)
YMOM=DOT(LMOM>,N2>)
%
%Forces
%
TORQUE(B/A,TORANK*A3>)
TORQUE(B/C,TORKNE*B3>)
TORQUE(D/C,TORHIP*C3>)
TORQUE(E/D,TORSHR*D3>)
TORQUE(E/F,TORELB*F3>)
TORQUE(G/D,TORRHIP*G3>)
TORQUE(G/H,TORRKNE*H3>)
GRAVITY(G*N2>)
RX=-K1*Q1-K2*U1
RY=-K3*Q2-K4*U2
FORCE(P1,RX*N1>+RY*N2>)
RX1=-K5*POP2X-K6*VOP2X
RY1=-K7*POP2Y-K8*VOP2Y
FORCE(P2,RX1*N1>+RY1*N2>)
SWM1X=-K9*Q9-K10*U9
SWM1Y=-K11*Q10-K12*U10
FORCE(P11/PW1,SWM1X*N1>+SWM1Y*N2>)
SWM2X=-K13*(POPW2X-POP12X)-K14*(VOPW2X-VOP12X)
SWM2Y=-K15*(POPW2Y-POP12Y)-K16*(VOPW2Y-VOP12Y)
```

```
FORCE(P12/PW2,SWM2X*N1>+SWM2Y*N2>)
SWM3X=-K9*Q12-K10*U12
SWM3Y=-K13*Q15-K12*U13
FORCE(P13/PW3,SWM3X*N1>+SWM3Y*N2>)
SWM4X=-K13*(POPW4X-POP14X)-K14*(VOPW4X-VOP14X)
SWM4Y=-K15*(POPW4Y-POP14Y)-K16*(VOPW4Y-VOP14Y)
FORCE(P14/PW4,SWM4X*N1>+SWM4Y*N2>)
SWM5X=-K9*Q15-K10*U15
SWM5Y=-K11*Q16-K12*U16
FORCE(P15/PW5,SWM5X*N1>+SWM5Y*N2>)
SWM6X=-K13*(POPW6X-POP16X)-K14*(VOPW6X-VOP16X)
SWM6Y=-K15*(POPW6Y-POP16Y)-K16*(VOPW6Y-VOP16Y)
FORCE(P16/PW6,SWM6X*N1>+SWM6Y*N2>)
%
%AUXILIARY[1]=DOT(W_F_E>,N3>) - AEF'
%AUXILIARY[2]=DOT(W_H_G>,N3>) - AGH'
AUXILIARY[1]=U18
AUXILIARY[2]=U19
%
CONSTRAIN(AUXILIARY[U18,U19])
%---------------------------------
%Equations of motion
ZERO = FR() + FRSTAR()
KANE(TORELB,TORRKNE)
%
%---------------------------------
%Inputs
INPUT TINITIAL=0.0, TFINAL=5.0, INTEGSTP=0.001, PRINTINT=5
INPUT ABSERR=1.0E-08, RELERR=1.0E-07
INPUT Q1=0,Q2=0,Q3=0.0,Q4=80.0,Q5=65.0,Q6=90.0,Q7=140.0,Q8=250.0,Q9=0.0
,Q10=0.0,Q11=0.0,Q12=0.0,Q13=0.0,Q14=0.0,Q15=0.0,Q16=0.0,Q17=0.0
INPUT MA=3,MB=5,MC=7,MD=13,ME=5,MF=3,MG=10,MH=10,MI=5,MJ=7,MK=13
INPUT IA=0.1,IB=0.1,IC=0.1,ID=0.1,IE=0.1,IF=0.1,IG=0.1,IH=0.1,II=0.1, IJ=0.1,IK=0.1
INPUT L1=0.2,L2=0.25,L3=0.1,L4=0.15,L5=0.04,L6=0.25,L7=0.5,L8=0.3,L9=
0.6,L10=0.35,L11=0.7
INPUT L12=0.15,L13=0.3,L14=0.1,L15=0.2,L16=0.3,L17=0.6,L18=0.28,L19=
0.56,L20=0.05,L21=0.45
INPUT L22=0.2,L23=0.4,L24=0.05,L25=0.55,L26=0.25,L27=0.5,L28=0.05,L29=
0.65,L30=0.3,L31=0.6
INPUT G=-9.81
INPUT R1=130, R2=160
INPUT ANKTOR=550,KNETOR=500,HIPTOR=600,SHRTOR=300,RHIPTOR=600
INPUT K1=150000,K2=10000,K3=150000,K4=10000
INPUT K5=150000,K6=10000,K7=150000,K8=10000
INPUT K9=75000,K10=1000,K11=75000,K12=1000
INPUT K13=75000,K14=1000,K15=75000,K16=1000
%
%---------------------------------
%OUTPUT
OUTPUT T,POP1X,POP1Y,POP2X,POP2Y,POP3X,POP3Y,POP4X,POP4Y,POP5X,POP5Y,
POP6X,POP6Y,POP7X,POP7Y,POP8X,POP8Y,POP7X,POP7Y,POP6X,POP6Y,POP5X,POP5Y,
POP9X,POP9Y,POP10X,POP10Y,POCMX,POCMY
OUTPUT
T,VOP1X,VOP1Y,VOP2X,VOP2Y,VOP3X,VOP3Y,VOP4X,VOP4Y,VOP5X,VOP5Y,
VOP6X,VOP6Y,VOP7X,VOP7Y,VOP8X,VOP8Y,VOP9X,VOP9Y,VOP10X,VOP10Y,VOCMX,
VOCMY
OUTPUT
T,POAOX,POAOY,POBOX,POBOY,POCOX,POCOY,PODOX,PODOY,POEOX,POEOY,
POFOX,POFOY,POGOX,POGOY,POHOX,POHOY,POIOX,POIOY,POJOX,POJOY,POKOX,P
OKOY,POCMX,POCMY
```

```
OUTPUT
T,VOAOX,VOAOY,VOBOX,VOBOY,VOCOX,VOCOY,VODOX,VODOY,VOEOX,VOEOY,
VOFOX,VOFOY,VOGOX,VOGOY,VOHOX,VOHOY,VOCMX,VOCMY
OUTPUT T,Q1,U1,Q2,U2,Q3,U3,Q4,U4,Q5,U5,Q6,U6,Q7,U7,Q8,U8,Q9,U9,Q10,U10,
Q11,U11,Q12,U12,Q13,U13,Q14,U14,Q15,U15,Q16,U16,Q17,U17,AEF,AEF',AGH,AGH'
OUTPUT
T,ANKANG,ANKW,KNEANG,KNEW,HIPANG,HIPW,SHRANG,SHRW,ELBANG,ELBW,
RHIPANG,RHIPW,RKNEANG,RKNEW
OUTPUT
T,TORANK,TORKNE,TORHIP,TORSHR,TORRHIP,RX,RY,RX1,RY1,SWM1X,SWM1Y,
SWM2X,SWM2Y,SWM3X,SWM3Y,SWM4X,SWM4Y,SWM5X,SWM5Y,SWM6X,SWM6Y
OUTPUT T,TORELB,TORRKNE
OUTPUT T,KECM,KEA,KEB,KEC,KED,KEE,KEF,KEG,KEH,KEI,KEJ,KEK
OUTPUT T,PECM,PEA,PEB,PEC,PED,PEE,PEF,PEG,PEH,PEI,PEJ,PEK
OUTPUT T,PANK,PKNE,PHIP,PSHR,PRHIP,ZAMOM,XMOM,YMOM
%
%---------------------------------
%Units
UNITS [K1,K3,K5,K7,K9,K11,K13,K15]=N/M, [K2,K4,K6,K8,K10,K12,K14,K16]=N/M/S
UNITS [L1,L2,L3,L4,L5,L6,L7,L8,L9,L10,L11,L12,L13,L14,L15,L16,L17,L18, L19]=M
UNITS [L20,L21,L22,L23,L24,L25,L26,L27,L28,L29,L30,L31]=M
UNITS TOTMASS=KG, T=S, G=M/S^2
UNITS
POP1X=M,POP1Y=M,POP2X=M,POP2Y=M,POP3X=M,POP3Y=M,POP4X=M,POP4Y=M,
POP5X=M,POP5Y=M
UNITS
POP6X=M,POP6Y=M,POP7X=M,POP7Y=M,POP8X=M,POP8Y=M,POP9X=M,POP9Y=M,
POP10X=M,POP10Y=M
UNITS [POP11X,POP11Y,POP12X,POP12Y,POP13X,POP13Y,POP14X,POP14Y,POP15X,
POP15Y,POP16X,POP16Y]=M
UNITS
[POPW1X,POPW1Y,POPW2X,POPW2Y,POPW3X,POPW3Y,POPW4X,POPW4Y,POPW5X,
POPW5Y,POPW6X,POPW6Y]=M
UNITS Q1=M, Q2=M, Q3=DEG, Q4=DEG, Q5=DEG, Q6=DEG, Q7=DEG, Q8=DEG, Q9=M,
Q10=M
UNITS Q11=DEG, Q12=M, Q13=M, Q14=DEG, Q15=M, Q16=M, Q17=DEG, AEF=DEG,
AGH=DEG
UNITS U1=M/S, U2=M/S, U3=DEG/S, U4=DEG/S, U5=DEG/S, U6=DEG/S, U7=DEG/S,
U8=DEG/S, U9=M/S, U10=M/S
UNITS U11=DEG/S, U12=M/S, U13=M/S, U14=DEG/S, U15=M/S, U16=M/S, U17=DEG/S,
AEF'=DEG/S, AGH'=DEG/S
UNITS [R1,R2]=DEG
UNITS [IA,IB,IC,ID,IE,IF,IG,IH,II,IJ,IK]=KG.M^2
UNITS [MA,MB,MC,MD,ME,MF,MG,MH,MI,MJ,MK]=KG
UNITS [ANKTOR,KNETOR,HIPTOR,SHRTOR,RHIPTOR]=Nm,[RX,RY,RX1,RY1]=N
UNITS [TORANK,TORKNE,TORHIP,TORSHR,TORELB,TORRHIP,TORRKNE]=Nm
UNITS
[SWM1X,SWM1Y,SWM2X,SWM2Y,SWM3X,SWM3Y,SWM4X,SWM4Y,SWM5X,SWM5Y,
SWM6X,SWM6Y]=N
UNITS [KECM,KEA,KEB,KEC,KED,KEE,KEF,KEG,KEH,KEI,KEJ,KEK,PECM,PEA,PEB,
PEC,PED,PEE,PEF,PEG,PEH,PEI,PEJ,PEK]=J
UNITS [PANK,PKNE,PHIP,PSHR,PRHIP]=W
UNITS [XMOM,YMOM]=KG.M/S, ZAMOM=KG.M^2/S
%
CODE DYNAMICS() C:\AL\CASSIE\8SEGWM.FOR, SUBS
SAVE C:\AL\CASSIE\8SEGWM.ALL
```

APPENDIX 2

CALCULATIONS OF WOBBLING MASS AND SERIES ELASTIC COMPONENT PARAMETERS

Appendix 2a

Determination of SEC stiffness

Ratio of mass / leg length / height between subject and literature

Jacobs et al. (1996):

Leg length = 0.898 m

Mass = 77.8 kg

r^2 = 77.8/0.898 = 86.637

r = 9.308

Subject:

leg length = 0.889 m

mass = 81.9 kg

r^2 = 81.9/0.889 = 92.126

r = 9.598

Ratio of moments arms between literature and subject = 9.598/9.308 = **1.0312**

Allard et al. (1992):

Height = 1.78 m

Subject in study:

height = 1.86 m

Ratio of SEC lengths between literature and subject = 1.86/1.78 = **1.045**

SEC lengths

Using data from Allard et al, 1992:

Example calculation:

Soleus:

$\theta = 26°$

lb = 129 mm

lf = 49 mm

lt = 227 mm

Where: θ = pennation angle, lb = muscle belly length, lf = muscle fibre length, lt = tendon length.

SEC length = 227 + (49×cos26) = 312 mm

Table 2a.1. SEC lengths before scaling to subject

muscle group	θ [°]	Lb [mm]	Lf [mm]	Lt [mm]	SEC length [mm]
soleus	26	129	49	227	312
gastrocnemius	13	237	78	217	377
tibialis anterior	9	117	99	217	236
rectus femoris	10	302	88	186	401
vasti	11	273	110	138	301
hamstrings	10	255	125	142	273
gluteus	5	111	104	73	81

Moment arms (Jacobs et al., 1996) and lengths of series elastic component (Allard et al., 1992) which are scaled to the subject are shown in Table 2. The hamstrings and rectus femoris muscles act at both the knee and the hip joints. Their moment arms at these two joint are different and both values are shown in Table 2.

Table 2a.2. SEC lengths and moment arms after scaling to the subject

muscle group	SEC length [mm]	moment arm [mm]
soleus	326	47
gastrocnemius	394	47
tibialis anterior	247	42
rectus femoris	419	43 / 36
vasti	315	43
hamstrings	285	27 / 79
gluteus	85	64

Calculation of stiffness values

Using SEC lengths and moment arm lengths determined using data from the literature and scaling to the subject SEC, and assuming a 5% stretch of the SEC, stiffness values were determined for each joint as follows:

Example calculation:

Ankle Plantar flexion:

Muscles producing plantar flexion are the soleus and the gastrocnemius.

Ratio of cross-sectional area taken from Allard et al. (1992):

Soleus:Gastrocnemius

6167:11868

Ratio of moment arm:

1:1

Therefore ratio of torque:

6167:11868

Maximum isometric ankle plantar flexion torque = 702.43 Nm

Soleus torque = 702.43×(11868/(11868+6167)) = 462.24 Nm

Gastrocnemius torque = 702.43×(6167/(6167+11868)) = 240.19 Nm

Soleus:

Tendon length = 326 mm

Moment arm = 47 mm

$\Delta l = 0.326 \times 0.05 = 0.0163$

$\Delta\theta = 0.0163/0.047 = 0.3468$

$k(\text{stiffness}) = 462.24/0.3468 = 1332.10\ \text{Nm.rad}^{-1}$

Gastrocnemius:

Tendon length = 394 mm

Moment arm = 47 mm

$\Delta l = 0.394 \times 0.05 = 0.0197$

$\Delta\theta = 0.0197/0.047 = 0.419$

k(stiffness) = 240.19/0.419 = 573.35 $Nm.rad^{-1}$

Stiffness of SEC of ankle plantar flexors = 1905 $Nm.rad^{-1}$

Appendix 2b

Wobbling mass parameter determination

Wobbling mass to rigid ratio

Table 2b.1. Total mass of limbs (from *Clarys and Marfell-Jones, 1986*).

segment	mass (kg)	mass for 2 limbs (kg)
Arm	1.5603	3.1206
forearm	0.7644	1.5288
Hand	0.3453	0.6905
Thigh	7.7785	15.5569
Shank	2.1363	4.2725
Foot	0.8878	1.7755
Total	13.4724	26.9448

Total body mass = 64.3 kg

Therefore trunk mass = 37.4 kg

Table 2b.2. Bone mass (from Clarys and Marfell-Jones, 1986).

segment	mass for 2 limbs (kg)
arm	0.4362
forearm	0.2434
hand	0.1930
thigh	1.4050
shank	0.9269
foot	0.5314
total	3.7359

From Clarys et al. (1984) the body is made up of 13.4% bone

Therefore total bone mass = 64.3×0.134 = 8.6162 kg

Bone in trunk = 4.8803 kg which as a percentage of trunk mass = 13.0646%

From Clarys et al. (1984) total body fat is 34.6%

Total body fat = 64.3×0.346 = 22.2478 kg

Table 2b.3. Fat mass (from Clarys and Marfell-Jones, 1986).

segment	mass for 2 limbs (kg)
arm	1.1734
forearm	0.3622
hand	0.1545
thigh	6.6322
shank	1.2297
foot	0.4988
total	10.0508

Trunk

Fat in trunk = 12.197 kg which as a percentage of trunk mass = 32.65%

Therefore percentage of muscle in trunk = 54.28%

Percentage fat in subject's trunk = 9×(32.65/34.6) = 8.493142

Percentage of fat left to redistribute = 32.65 – 8.493142 = 24.16%

Thigh

Total mass = 7.77845

Mass of bone = 0.7025

Mass of fat = 3.3161

Percentage bone = 9.03%

Percentage fat = 42.63% which as a fraction of total body fat = 1.232

Percentage muscle = 48.34%

Percentage fat in subjects thigh = 9×1.232 = 11.08922

Percentage of fat left to re-distribute = 31.54%

Shank

Total mass = 2.13625

Mass of bone = 0.46345

Mass of fat = 0.61485

Percentage bone = 21.69%

Percentage of fat = 28.78% which as a fraction of total body fat is 0.8318

Percentage muscle = 49.5237

Percentage fat in subjects shank = 9×0.8318 = 7.4866

Percentage fat left to re-distribute = 21.295

Re-distributing of excess fat

1. All to muscle

Trunk:

Bone	13.06%
Wobbling	86.94%

Thigh:

Bone	9.03%
Wobbling	90.97%

Shank:

Bone	21.69%
Wobbling	78.31%

2. Keeping muscle to bone ratio constant

Trunk:

With no fat, bone = 19.40%

With fat at 3.1726 kg (using subjects percentage), bone = 17.23%

Bone	17.23%
Wobbling	82.77%

Thigh:

With no fat, bone = 15.74%

With fat at 0.86257 kg (using subject's percentage), bone = 13.19%

Bone	13.19%
Wobbling	86.81%

Shank:

With no fat, bone = 30.46%

With fat at 0.1599 kg (using subject's percentage), bone = 27.56%

Bone	27.56%
Wobbling	72.44%

APPENDIX 3

INFORMED CONSENT

INFORMED CONSENT FORM (SUBJECTS)

PURPOSE
To obtain kinematic data during sports movements.

PROCEDURES
The kinematic data of sports movements will be obtained using:

- Video and cinematographic recordings typically using two cameras

A number of trials will be requested with suitable breaks to minimise fatigue and boredom.

During the measurements two researchers will be present, at least one of whom will be of the same sex as you.

QUESTIONS
The researchers will be pleased to answer any questions you may have at any time.

WITHDRAWAL
You are free to withdraw from the study at any stage, without having to give any reasons. An opportunity will be provided in this event for you to discuss privately your wish to withdraw.

CONFIDENTIALITY
Your identity will remain confidential in any material resulting from this work.

I have read the outline of the procedures which are involved in this study, and I understand what will be required by me. I have had the opportunity to ask for further information and for clarification of the demands of each of the procedures and understand what is entailed. I am aware that I have the right to withdraw from the study at any time with no obligation to give reasons for my decision. As far as I am aware I do not have any injury or infirmity which would be affected by the procedures outlined.

Name .....

Signed ..... (subject) Date .....

In the presence of:

Name .....

Signed ..... (coach) Date .....